COMPUTATIONAL ANALYSIS OF DIFFUSER PERFORMANCE

FOR THE SUBSONIC AERODYNAMIC RESEARCH

LABORATORY WIND TUNNEL

By

CHRISTOPHER DAVID KING

DR. SEMIH M. ÖLÇMEN, COMMITTEE CHAIR
DR. MUHAMMAD ALI ROB SHARIF
DR. JOHN BAKER

A THESIS

Submitted in partial fulfillment of the requirements
for the degree of Master of Science
in the Department of Aerospace Engineering and Mechanics
in the Graduate School of
The University of Alabama

TUSCALOOSA, ALABAMA

2012

ABSTRACT

The Air Force has expressed interest in improving the efficiency of the Subsonic Aerodynamic Research Laboratory (SARL) wind tunnel. In a previous analysis of losses throughout the tunnel, it was found that approximately thirty percent of pressure losses through the tunnel occurred at the exit of the tunnel (Britcher, 2011). The use of alternative diffuser geometries in reducing pressure losses at the exit of the tunnel and the computation of their efficiency improvement with respect to the original tunnel geometry and with respect to each other for the SARL wind tunnel are the focus of this research.

Three different diffuser geometries were evaluated numerically using both the SolidWorks Flow Simulation add-on, and ANSYS FLUENT. For each of these geometries, a scaled down model was manufactured to be used for experimental validation in future work. Both the full size and small scale numerical models were evaluated with an inlet velocity of sixty meters per second. As the nature of the flow at this point in the wind tunnel is not known, both a uniform and fully developed turbulent flow profiles were evaluated for each design, both for the small scale models and the full size models, to determine pressure losses with respect to the varying flow types entering the diffusers. This research seeks to determine the effects of these different geometries on the flow downstream of the exit, and the possible energy savings associated with each design. In addition, it seeks to compare the numerical results obtained from both SolidWorks Flow Simulation and ANSYS FLUENT.

LIST OF ABBREVIATIONS AND SYMBOLS

γ	Specific Gravity of Fluid
δ_{ij}	Kronecker Delta Function (equal to unity when $i=j$, zero otherwise)
ε	Turbulent dissipation
θ	Diffuser Half Apex Angle
η	Diffuser Efficiency
λ	Section Skin Friction Coefficient
μ	Dynamic Viscosity of Fluid
μ_t	Turbulent Dynamic Viscosity of Fluid
ρ	Density of Fluid
τ_{ii}	Normal Stress
τ_{ij}	Shear Stress
ν	Kinematic Viscosity of Fluid
υ_T	Turbulent Kinematic Viscosity of Fluid
σ_k	Computational constant for turbulent kinetic energy
σ_ε	Computational constant for turbulent dissipation
a	Speed of Sound, $a \equiv \sqrt{\gamma RT}$
AR	Diffuser Aspect Ratio, $AR = \frac{A_2}{A_1}$
A_{ts}	SARL tunnel Test Section Area

C_μ	Computational constant for dynamic viscosity
$C_{\varepsilon 1}$	Empirical computational constant for turbulent dissipation
$C_{\varepsilon 2}$	Empirical computational constant for turbulent dissipation
$C_{\varepsilon 3}$	ANSYS FLUENT constant term relating turbulent dissipation to buoyancy
CFD	Computational Fluid Dynamics
$\vec{F}$	ANSYS FLUENT External Body Forces Term
f_μ	SolidWorks Flow Simulation Turbulent Viscosity Factor
ft	Feet
G_b	ANSYS FLUENT Turbulence Production due to Buoyancy
G_k	ANSYS FLUENT Turbulence Kinetic Energy Production Term
h	Thermal Enthalpy
h	Elevation
H	Total Enthalpy, $H = h + \frac{u^2}{2}$
H_{L1}	Head loss associated with diffuser
H_{L2}	Head loss associated with exit flow
I	Unit Tensor
in	Inches
k	Turbulent kinetic energy
k	Thermal conductivity
K	Local Total Pressure Loss

K_0	Section Total Pressure Loss
L	Characteristic Length
m	Meter
M	Mach Number
M_T	Turbulent Mach Number
P	Static Pressure
P	Turbulent production parameter
$\overline{P}$	Average Static Pressure
P_{local}	Static Pressure at a specified location within the SARL tunnel
P_0	Total Pressure
ΔP_0	Change in Total Pressure across a given location
P_B	Turbulent production due to buoyancy forces
Pr	Prandtl Number
q	Dynamic Pressure, $q = P + \frac{\rho V^2}{2}$
q_i	Diffusive Heat Flux
Q_H	SolidWorks Flow Simulation Term for Heat Source/Sink per unit volume
$\bar{q}$	Average Dynamic Pressure, $\bar{q} = \overline{P} + \frac{\rho \bar{V}^2}{2}$
q_{local}	Dynamic Pressure at a specified location within the SARL tunnel, $q_{local} = P_{local} + \frac{\rho V_{local}^2}{2}$
q_{ts}	Dynamic Pressure at the Test Section of the SARL tunnel

R	Specific Gas Constant for Air
Re	Reynolds Number
s	Seconds
S_ε	SolidWorks Flow Simulation Turbulent Dissipation Source Term
S_k	SolidWorks Flow Simulation Turbulent Kinetic Energy Source Term
S_i	SolidWorks Flow Simulation Term for Mass-Distributed External Force
S_m	ANSYS FLUENT Mass Source Term
SARL	Subsonic Aerodynamic Research Laboratory
T	Absolute Temperature of Fluid
u	Velocity in the x-direction
u_i	Velocity in the i-direction, where i is a Cartesian component
v	Velocity in the y-direction
V	Velocity Magnitude
$\bar{V}$	Average Velocity Magnitude
V_{local}	Velocity Magnitude at a specified location within the SARL tunnel
V_{ts}	Velocity Magnitude at the Test Section of the SARL tunnel
w	Velocity in the z-direction
x_i	Vector in the i-direction, where i is a Cartesian component
y	Distance from wall
Y_M	ANSYS FLUENT Dilitation Dissipation Term

ACKNOWLEDGEMENTS

I would like to express my gratitude to my advisor, Dr. Semih Ölçmen for all of his guidance, encouragement, direction and patience with me through my time as a graduate student at The University of Alabama. In addition, I would also like to thank the members of my thesis committee, Dr. Muhammad Ali Rob Sharif and Dr. John Baker for all of their guidance and input during the research process. In addition, I would also like to thank Mr. Chase Leibenguth from the Department of Aerospace Engineering and Mechanics for his recommendations in the use of ANSYS FLUENT, as I had essentially no experience in this program prior to this research.

Finally, I would like to extend my utmost gratitude to my family and friends, who have supported and encouraged me during my time as a student at The University of Alabama. I would like to especially thank my fiancé and my parents for their unwavering support, as I would not be where I am today without them.

CONTENTS

LIST OF TABLES

LIST OF FIGURES

CHAPTER 1

INTRODUCTION

This chapter provides a brief overview of the motivation behind this research, and a review of relevant information pertaining to previous work analyzing losses through the tunnel. It also discusses previous research on jet velocity reduction methods through the use of diffusers. The last section of this chapter focuses on the basic methods used in CFD, as well as specific information pertaining to each of the solvers used in this research, SolidWorks Flow Simulation and ANSYS FLUENT.

1.1 SARL Information

The SARL wind tunnel was approved for construction in 1983. The SARL wind tunnel is designed to operate between Mach Numbers of 0 to 0.5. It is driven by a 20,000 HP engine, located approximately 15 ft. outside the exit of the tunnel. It has a forty-six foot by fifty foot inlet, with a contraction ratio of 35:1 at the test section. Honeycombs were installed to reduce turbulence intensity in the test section to 0.05% and below. **Figure 1** provides a schematic drawing of the SARL wind tunnel, while **Figure 2** provides a drawing of the fan duct and diffuser section being considered in this research.

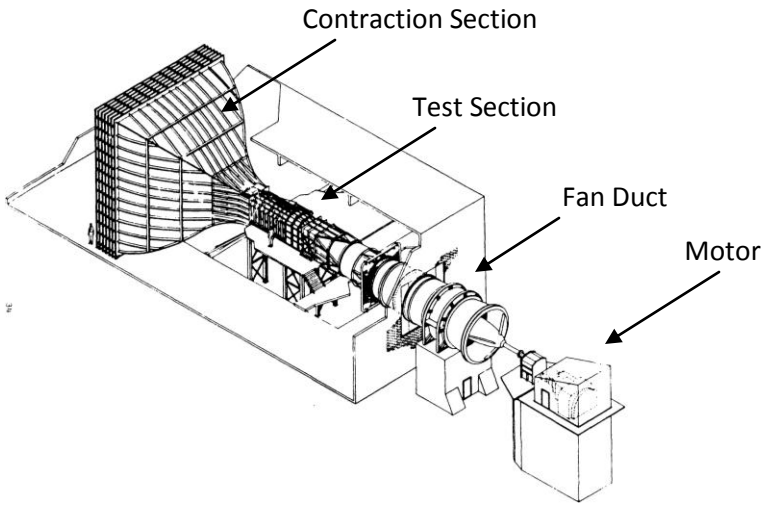

Figure 1 - Schematic Drawing with Labels of the SARL Wind Tunnel (Wright-Patterson AFB, 1992)

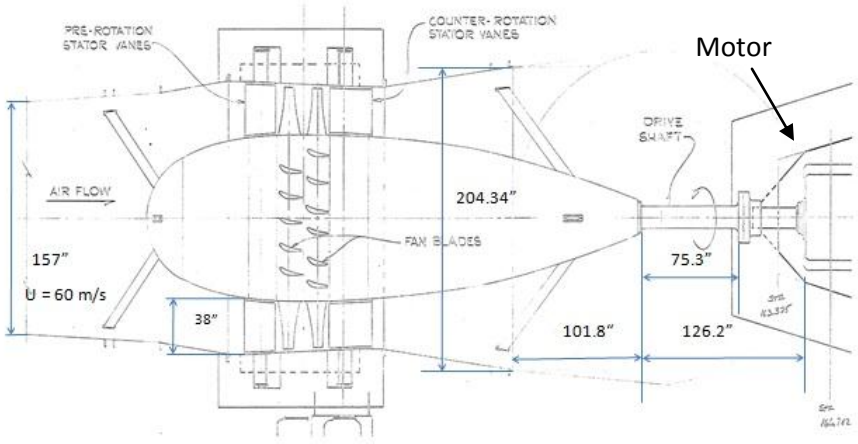

Figure 2 - Drawing of Fan Duct and Exit Diffuser Section of the SARL Wind Tunnel (Ölçmen, 2011)

The tunnel was designed to provide low turbulence flow for flow visualization and precision measurements at low-cost efficient operation (Wright-Patterson AFB, 1992). It is unique in that it was designed from conception as a tunnel for flow simulation, as it allows for a 360 degree line-of-sight of the model in the test section.

1.2 Motivation

The Air Force, which operates the SARL wind tunnel, has expressed interest in improving the efficiency of the tunnel. Improving the efficiency of the tunnel will result in monetary savings, as the power needed to run the tunnel during tests will be reduced. Previous analysis of cumulative losses throughout the tunnel identified that approximately thirty percent of all losses in the tunnel occurred at the tunnel exit (Britcher, 2011). The Air Force is interested in minimizing the losses in this section of the tunnel by modifying the diffuser and by adding additional diffuser geometries.

To reduce losses in the diffuser and exit sections of the tunnel, several varying diffuser geometries required identification and evaluation for effectiveness in reduction of losses. While experimental verification was the desired result, it was not feasible to design, create and test a multitude of diffuser geometries for the tunnel. In addition, the exit diameter of the tunnel is approximately 204 in, which can neither be easily manufactured, nor tested in most wind tunnels due to its size. Experimental models, with a size ratio of 1:98.393, were constructed for experimental verification as a result, and are also evaluated computationally in this study. However, it should be noted that the experimental study itself is beyond the scope of this thesis.

However, the experimental results of the small scale models need to be related to the full size geometries in application. To do this, a comparison between the computational results for the small scale models and the full size models will be used to generate an approximate relation between the experimental results and application to the full size geometries.

1.3 Literature Review

Prior to reviewing previous studies in reducing jet velocity with diffusers, it is relevant to first summarize recent research involving the SARL tunnel in relation to losses through the tunnel.

In a previous study of the power losses through the tunnel at varying locations set of losses within each stage of the tunnel was compiled (Britcher, 2011). In that work, the geometry of the entire tunnel was considered. The local total pressure loss coefficient is defined as

$$K = \frac{\Delta p_0}{q_{local}} \tag{1.3.1}$$

In relation to the test section of the tunnel, the section total pressure loss coefficient is defined as

$$K_0 = \frac{\Delta p_0}{q_{ts}} = K\frac{q_{local}}{q_{ts}} = K\left(\frac{V_{local}}{V_{ts}}\right)^2 \tag{1.3.2}$$

Finally, the circuit energy ratio, or the ratio of actual drive power to the test section energy flux, can be expressed in terms of the loss coefficients as

$$ER = \frac{\frac{1}{2}\rho V_{ts}^3 A_{ts}}{\sum losses} = \frac{1}{\sum K_0} \tag{1.3.3}$$

Following these equations, **Figure 3** below provides a graphical summation of the results of the study, showing the cumulative power loss coefficient versus the position within the tunnel. For reference, **Figure 4** shows the static pressure distribution versus position within the tunnel.

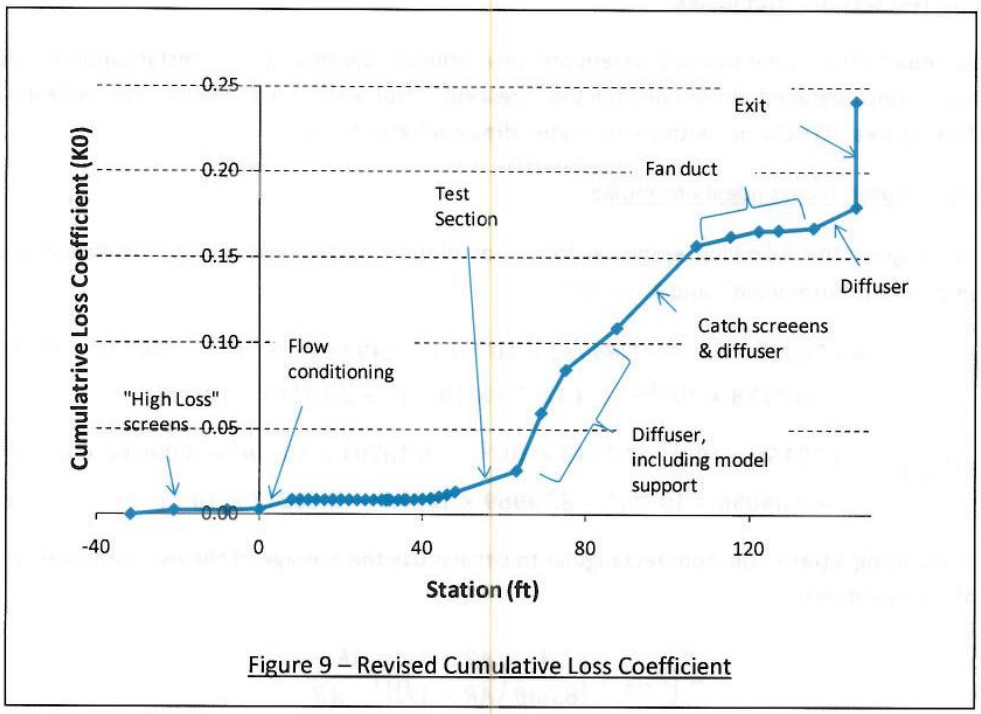

Figure 3 - SARL Cumulative Power Loss Coefficient Analysis (Old Dominion University, Britcher, 2011)

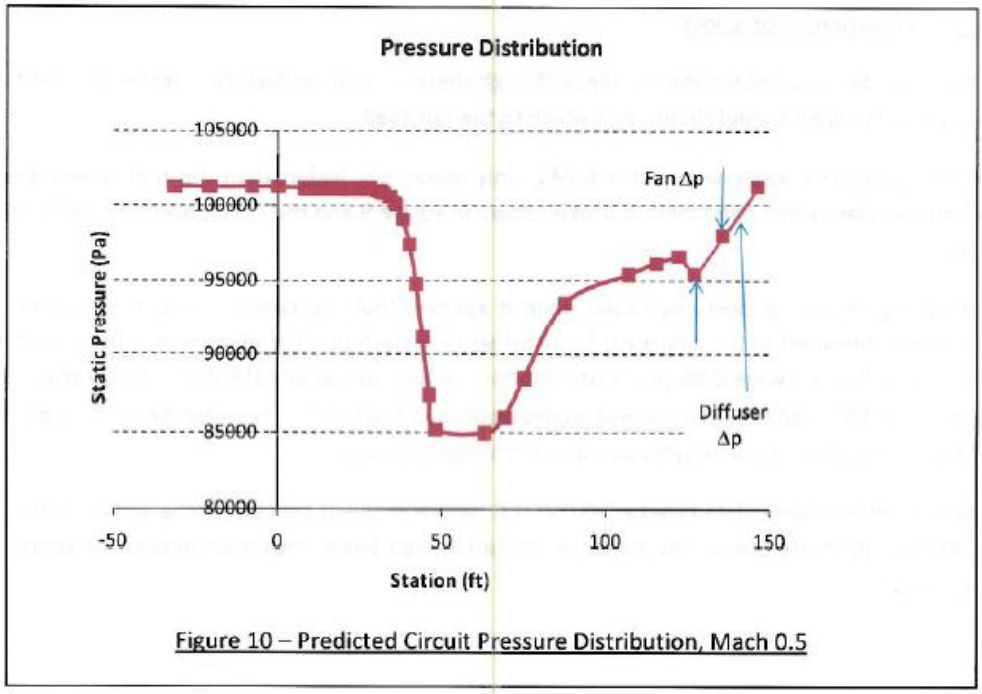

Figure 4 - SARL Static Pressure Analysis (Old Dominion University, Britcher, 2011)

In **Figure 3**, the data points starting at "Fan Duct" and extending to "Exit" represent the portion of the tunnel that is being analyzed in this thesis. In a preliminary study, the cumulative loss coefficient through the tunnel was found to be 0.237. However, revised methods were applied to the high loss sections, such as the test section strut losses, and to the diffuser section ahead of the fan duct. The revised cumulative loss coefficient was then found to be 0.245, which implied that the facility was underperforming. The study concluded that the circuit losses were "dominated" by the diffuser and exit sections of the tunnel. If the exit loss coefficient could be reduced, a significant reduction in losses could be observed for the entire tunnel, up to

approximately 16% reduction based on analytical study and approximately 13% reduction from experimental data obtained by Schmidt (1986) (Britcher, 2011).

As the results of the previous study indicated that significant reduction in losses could be achieved through the use of a diffuser at the exit of the tunnel, it is appropriate to review the concept and use of diffusers in aerospace applications. Diffusers are used as devices to recover kinetic energy of a flow, thus resulting in a rise in static pressure (Japikse, 2008). Generally speaking, there are three types of diffuser geometries, a two-dimensional rectangular geometry, a conical geometry and an annular geometry, illustrated in **Figure 5**.

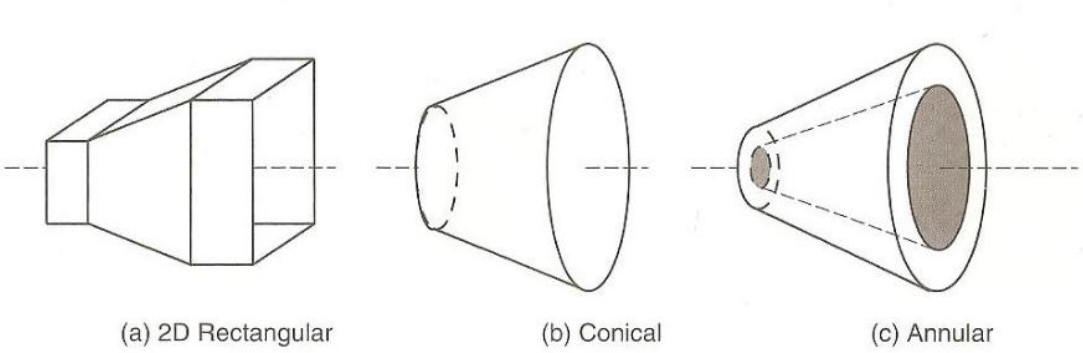

Figure 5 - Schematic drawing of subsonic diffuser types with straight centerline (Farokhi, 2009)

For a subsonic diffuser, where state "1" represents the inlet of the diffuser and state "2" represents the outlet of the diffuser, several statements about the flow at each point can be determined. First, there is a rise in static pressure ($P_2 > P_1$) as the flow is slowed down due to the

expansion of the diffuser geometry. Secondly, as the static pressure has increased, due to the equation of state:

$$P = \rho RT \tag{1.3.4}$$

the temperature will also increase across the diffuser ($T_2 > T_1$). As the velocity decreases across the diffuser, the kinetic energy, related proportionally to the square of the velocity, also decreases. For an adiabatic diffuser, this is a constant total temperature process. However, there is a change in the total pressure across the diffuser ($P_{02} < P_{01}$), leading to a change in entropy Δs. **Figure 6** below is a T-s diagram depicting the static and stagnation states in a diffuser.

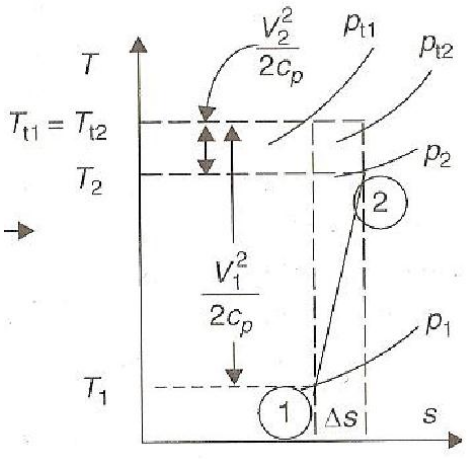

Figure 6 - T-s Diagram of a Diffuser (Farokhi, 2009)

For an ideal diffuser, considering quasi-1D flow, the Bernoulli equation

$$P + \frac{1}{2}\rho V^2 + \rho g h = constant \tag{1.3.5}$$

can be applied between states 1 and 2, and combined with the continuity equation for ideal quasi-1D flow

$$\rho A_1 V_1 = \rho A_2 V_2 \tag{1.3.6}$$

to obtain the ideal static pressure recovery coefficient (Farokhi, 2009), $C_{PR_{ideal}}$:

$$C_{PR_{ideal}} = \frac{q_1 - q_2}{q_1} = 1 - \left(\frac{A_1}{A_2}\right)^2 = 1 - \frac{1}{AR^2} \tag{1.3.7}$$

where q_1 and q_2 are the dynamic pressures at the inlet and exit, respectively. It can be seen that for the ideal case, as the exit area increases relative to the inlet area, the static pressure recovery coefficient will increase as well. However, this term, as it only considers ideal flow, neglects the

effects of viscosity and boundary layers. The static pressure recovery coefficient for non-ideal flow is defined as:

$$C_{PR} = \frac{p_2 - p_1}{\bar{q}_1} = \frac{\Delta p}{\rho_1 \bar{V}_1^2/2} \tag{1.3.8}$$

This term represents the static pressure contribution to the total pressure loss coefficient term shown in Equation 1.3.1. Another diffuser performance parameter is the diffuser efficiency, η.

$$\eta = \frac{C_{PR}}{C_{PR_{ideal}}} \tag{1.3.9}$$

As it can be seen from a very basic level how the diffuser geometry can impact efficiency even for an ideal case, Equations 1.3.1 and 1.3.2 should be considered again. These equations, while effective for a preliminary investigation, were refined (Eckert et al., 1976) for diffusers to include both expansion and friction losses within the duct. This refined representation for the total pressure loss coefficient was found to be:

$$K = \left[K_{exp} + \left(\frac{\lambda}{8\sin\theta}\frac{AR+1}{AR-1}\right)\right]\left(\frac{AR-1}{AR}\right)^2 \quad (1.3.10)$$

Here, the loss coefficient due to expansion, K_{exp}, was calculated numerically using one of the following three equations for a conical diffuser, dependent on the diffuser cone angle.

$$K_{exp} = 1.70925 \times 10^{-1} - 5.84932 \times 10^{-2}(2\theta) + 8.14936 \times 10^{-3}(2\theta)^2 + 1.34777 \times 10^{-4}(2\theta)^3 - 5.67258 \times 10^{-5}(2\theta)^4 - 4.15879 \times 10^{-7}(2\theta)^5 + 2.10219 \times 10^{-7}(2\theta)^6 \quad (1.3.11)$$

$$K_{exp} = 1.03395 \times 10^{-1} - 1.19465 \times 10^{-2}(2\theta) \quad (1.3.12)$$

$$K_{exp} = -9.66135 \times 10^{-2} + 2.336135 \times 10^{-2}(2\theta) \quad (1.3.13)$$

For these three equations, where θ is the diffuser half apex angle, Equation 1.3.11 is used for ranges of $3° \leq 2\theta \leq 10°$, Equation 1.3.12 is used for ranges of $0° \leq 2\theta \leq 3°$, and Equation 1.3.13 is used for ranges of $2\theta > 10°$.

The value of θ, the diffuser half apex angle, plays a major part in the efficiency of a diffuser. For each of the three major types of diffusers mentioned earlier, with high Reynolds

numbers and with small inlet blockage, the optimum performance of each has been correlated with θ (Sovran and Klomp, 1963, as cited by Farokhi, 2009). From this correlation, a general rule of thumb has been established that the optimum wall inclination angle for a planar diffuser should be approximately 4°. However, for optimum pressure recovery, it is recommended that this angle reach 5°, while for optimum flow steadiness it should be around 2.5° (Mehta, 1977). As flow unsteadiness would lend to unsteadiness in the efficiency of the diffuser, it would be desired to reach an optimal inclination angle between 2.5° and 5°. According to Townsend (1976), the maximum angle for 2D "unidirectional, self-preserving, fully developed flow" to be possible without boundary layer control is 4.3° (as cited by Mehta, 1977). Considering a conical diffuser, this angle shifts slightly. From the correlation determined by Sovran and Klomp, the apex angle, 2θ, for optimum pressure recovery should be approximately 7° for a conical diffuser (as cited by Lefebvre, 2010). Lastly, the use of a diffuser with splitter plates or cones will create, in essence, a series of parallel diffusers, which effectively creates a short diffuser of a large area ratio (Farokhi, 2009). This provides potential benefits of improving performance by preventing flow separation, without increasing the overall length of the diffuser.

With these recommendations in mind, several widely varying diffuser geometries were developed by Dr. Ölçmen to be evaluated for effectiveness in reducing losses for the SARL tunnel.

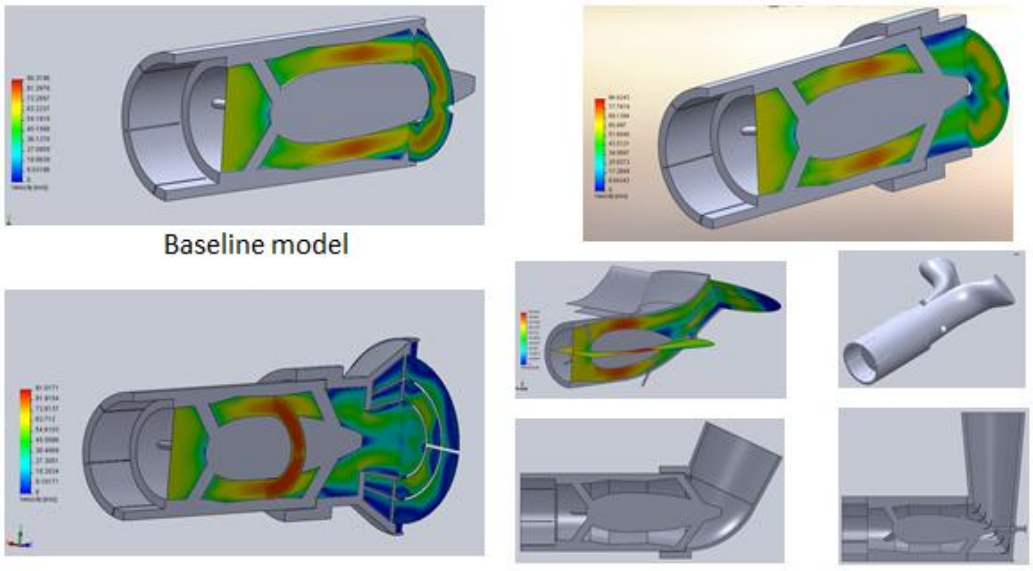

Figure 7 - SARL Example Diffuser Designs Tested by Dr. Ölçmen in 2011 Study (Ölçmen, 2011)

Over seventy different diffuser geometries were tested during this study, with **Figure 7** illustrating a few examples of the geometries considered. Due to the engine casing's close proximity to the exit of the tunnel of 177.1 in, all designs had their lengths restricted to be less than 14 ft, as the diffuser had to fit between the tunnel exit and the engine casing. Each design was modeled in SolidWorks. A preliminary computational analysis of each of the models was completed using the SolidWorks Flow Simulation solver. The computational results identified two specific diffuser geometries that achieved the greatest reduction in losses. In both cases, the existing diffuser was replaced with a new diffuser with a smaller wall incident angle of 3.5°,

named as “3.5 Base Tunnel.” This reduced wall incidence angle can be seen in **Figure 8** below for comparison.

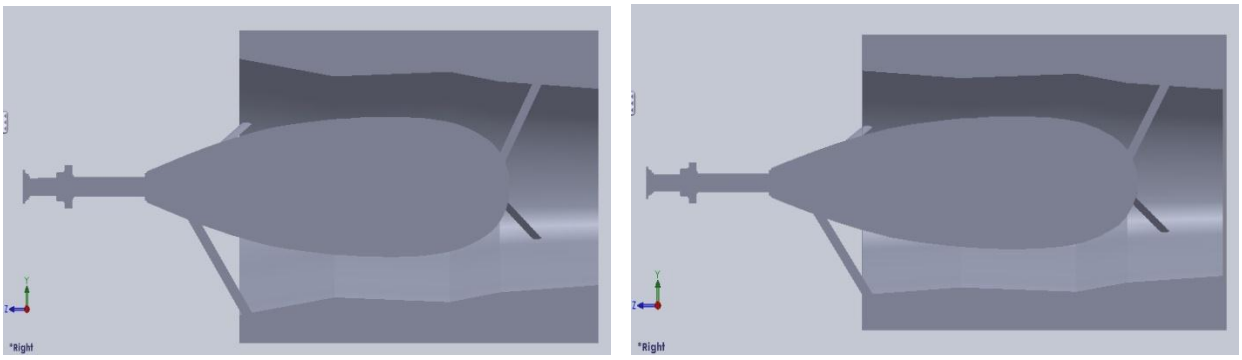

Figure 8 - Comparison of "7.5 Base Tunnel" Diffuser (Left) to "3.5 Base Tunnel" Diffuser (Right) Cross-Sectional Views

The first selected design simply added a second constant-area conical diffuser to the end of the new diffuser, named as “3.5 + Flat.” The reported improvement compared to the current SARL diffuser configuration was 19.3%. The second selected design added another extended diffuser as well, but made use of two conical sections to split the flow exiting the diffuser, while also having a greater aspect ratio, named as “3.5 + Flat + Conical.” The reported improvement compared to the current SARL diffuser configuration was 20.3% in this case. For these designs, the estimated improvement in tunnel efficiency was approximately 6% (Ölçmen, 2011). The two

geometries identified in this study are the focus for computational analysis in this thesis. It should be noted at this time, that due to size limitations, geometrically similar support spars for the engine nacelle cannot be manufactured. As a result, the small scale experimental models used in this research will make use of enlarged support spars, to allow these models to be manufactured and tested in a different project. **Figure 9** and **Figure 10** provide a comparison of the general geometries of each of the diffuser designs being tested in this thesis. For additional information concerning the dimensions of each diffuser model, please see Appendix C.

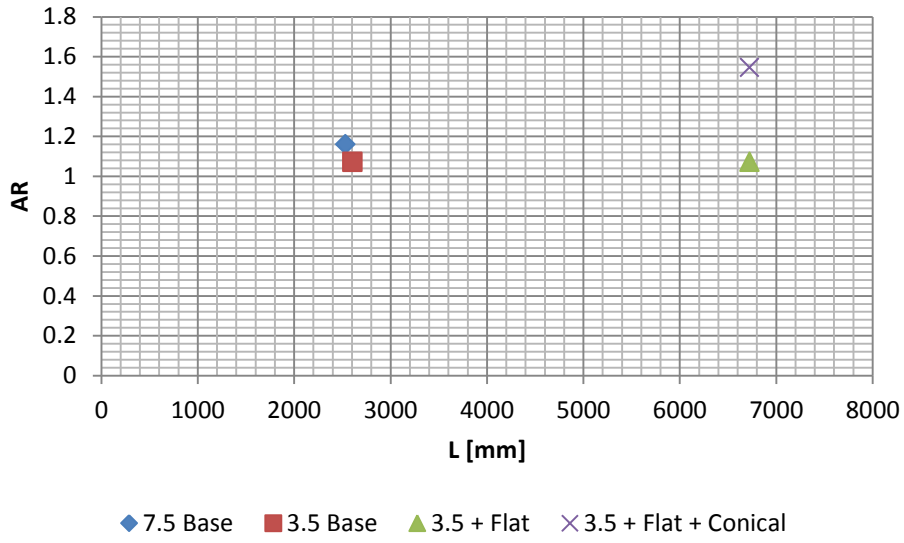

Figure 9 - Aspect Ratio versus Diffuser Length for Full Size Models

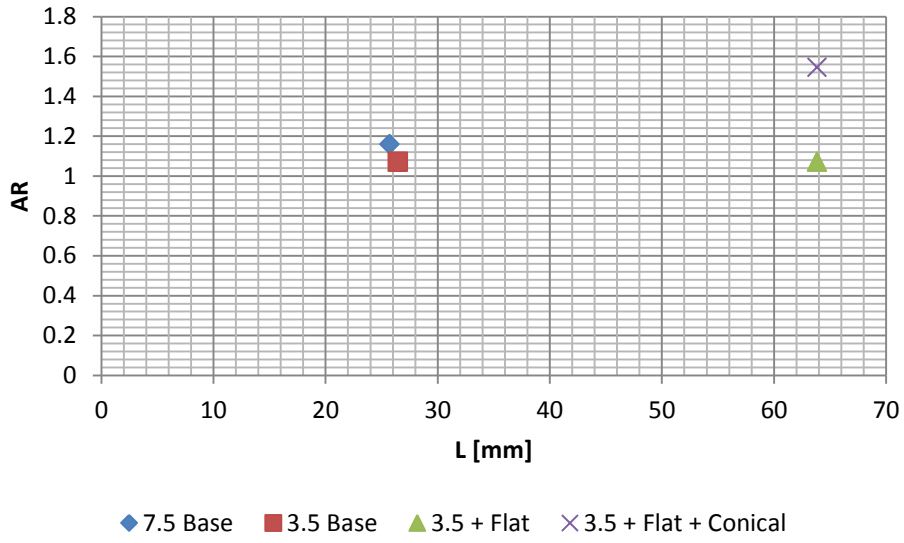

Figure 10 - Aspect Ratio versus Diffuser Length for Small Scale Models

CHAPTER 2

OVERVIEW OF CFD METHODS

2.1 Finite Difference Method and General Governing Equations

The use of CFD has become increasingly prominent in calculating the solution of complex fluid dynamics problems in recent years, due in part to the increasing capability of computers to handle larger computational loads. The physical characteristics of fluid motion can be described through several fundamental mathematical equations, typically expressed as partial differential equations. These fundamental equations are known as the governing equations. To solve these governing equations, finite differencing methods are applied to the equations to discretize the equations in such a way that they can be expressed as an algebraic approximation that are calculated over a number of varying locations in the flow. To solve these discretized governing equations over a computational domain containing fluid and solid bodies, the domain must be separated into small elements, creating what is known as a mesh or grid. Finite differencing allows for higher order approximations on these grids, thus resulting in a greater level of accuracy in the solution. To briefly discuss the process of obtaining finite difference approximations for the governing equations, a simple example for calculating the first-order derivative of an arbitrary flow field variable, $f(x)$, will be discussed. The function $f(x)$ is analytical, and as a result, $f(x+\Delta x)$ can be expanded through the use of a Taylor series.

$$f(x+\Delta x) = f(x) + (\Delta x)\frac{\partial f}{\partial x} + \frac{(\Delta x)^2}{2!}\frac{\partial^2 f}{\partial x^2} + \frac{(\Delta x)^3}{3!}\frac{\partial^3 f}{\partial x^3} + \cdots \tag{2.4.1}$$

$$= f(x) + \sum_{n=1}^{\infty} \frac{(\Delta x)^n}{n!}\frac{\partial^n f}{\partial x^n}$$

From this, the equation for $\frac{\partial f}{\partial x}$ can be found to be

$$\frac{\partial f}{\partial x} = \frac{f(x+\Delta x) - f(x)}{\Delta x} - \frac{\Delta x}{2!}\frac{\partial^2 f}{\partial x^2} - \frac{(\Delta x)^2}{3!}\frac{\partial^3 f}{\partial x^3} + \cdots \tag{2.4.2}$$

To obtain the first-order approximation for $\frac{\partial f}{\partial x}$, all terms with factors of Δx and higher are summed into a representative function, H(Δx). This results in the first-order forward approximation for $\frac{\partial f}{\partial x}$ (Hoffman et al., 1993).

$$\frac{\partial f}{\partial x} = \frac{f(x+\Delta x) - f(x)}{\Delta x} + H(\Delta x) \tag{2.4.3}$$

Similarly, second-order and higher-order approximations are obtained by included factors of Δx^2 and higher, respectively, in this equation. With a basic introduction to finite difference approximations, the governing equations that describe fluid flow will be discussed.

The governing equations for such a fluid element in steady, laminar flow are comprised of the equations for conservation of mass, momentum and energy, shown below in Cartesian coordinates, respectively.

$$\frac{\partial}{\partial x}(\rho u) + \frac{\partial}{\partial y}(\rho v) + \frac{\partial}{\partial z}(\rho w) = 0 \tag{2.1.4}$$

$$\rho \frac{Du_i}{Dt} = -\gamma \frac{\partial h}{\partial x_i} - \frac{\partial P}{\partial x_i} + \frac{\partial}{\partial x_j}\left[\mu\left(\frac{\partial u_j}{\partial x_i} + \frac{\partial u_i}{\partial x_j}\right)\right] - \frac{2}{3}\frac{\partial}{\partial x_i}\left(\mu \frac{\partial u_m}{\partial x_m}\right) \tag{2.1.5}$$

$$\begin{aligned}\rho \frac{DE}{Dt} = {} & \frac{\partial}{\partial x}\left[k\frac{\partial T}{\partial x}\right] + \frac{\partial}{\partial y}\left[k\frac{\partial T}{\partial y}\right] + \frac{\partial}{\partial z}\left[k\frac{\partial T}{\partial z}\right] - \frac{\partial (uP)}{\partial x} - \frac{\partial (vP)}{\partial y} - \frac{\partial (wP)}{\partial z} + \frac{\partial (u\tau_{xx})}{\partial x} \\ & + \frac{\partial (v\tau_{yy})}{\partial y} + \frac{\partial (w\tau_{zz})}{\partial z} + \frac{\partial (v\tau_{xy})}{\partial x} + \frac{\partial (v\tau_{yy})}{\partial y} + \frac{\partial (v\tau_{zy})}{\partial z} + \frac{\partial (w\tau_{xz})}{\partial x} \\ & + \frac{\partial (w\tau_{yz})}{\partial y} + \frac{\partial (w\tau_{zz})}{\partial z}\end{aligned} \tag{2.1.6}$$

Here, *h* is the elevation, and *k* is the thermal conductivity. These governing equations are capable of describing laminar fluid flows. However, for this research, the flow travelling through the fan duct and diffuser sections is not necessarily laminar, and is most likely turbulent. As a result, what is known as a turbulence model must be used to take into account the effects of turbulence on the solution to the fluid flow problem. A wide variety of turbulence models exist,

such as k-ε, k-ω and the Reynolds Stress Model. For this thesis, the standard k-ε turbulence model was used in both the SolidWorks Flow Simulation solver and the ANSYS FLUENT solver. When the velocity terms are separated into an average term and a fluctuating term, and then simplified using the Reynolds stress tensor, a set of new equations known as the Reynolds-Averaged Navier-Stokes (RANS) equations are obtained. To solve these equations, it is necessary to make use of a turbulence model. In this case, the standard k-ε turbulence model is used. Note that these equations are those representing 2D, incompressible, turbulent flow (Tu et al., 2008).

$$\frac{\partial \bar{u}}{\partial x} + \frac{\partial \bar{v}}{\partial y} = 0 \tag{2.1.8}$$

$$\frac{D\bar{u}}{Dt} = -\frac{1}{\rho}\frac{\partial \bar{p}}{\partial x} + \frac{\partial}{\partial x}\left(\vartheta \frac{\partial \bar{u}}{\partial x}\right) + \frac{\partial}{\partial y}\left(\vartheta \frac{\partial \bar{u}}{\partial y}\right) + \frac{\partial}{\partial x}\left(\vartheta \frac{\partial \bar{u}}{\partial x}\right) + \frac{\partial}{\partial y}\left(\vartheta \frac{\partial \bar{v}}{\partial x}\right) - \left[\frac{\partial(\overline{u'u'})}{\partial x} + \frac{\partial(\overline{v'v'})}{\partial y}\right] \tag{2.1.9}$$

$$\frac{D\bar{v}}{Dt} = -\frac{1}{\rho}\frac{\partial \bar{p}}{\partial y} + \frac{\partial}{\partial x}\left(\vartheta \frac{\partial \bar{v}}{\partial x}\right) + \frac{\partial}{\partial y}\left(\vartheta \frac{\partial \bar{v}}{\partial y}\right) + \frac{\partial}{\partial x}\left(\vartheta \frac{\partial \bar{u}}{\partial y}\right) + \frac{\partial}{\partial y}\left(\vartheta \frac{\partial \bar{v}}{\partial y}\right) - \left[\frac{\partial(\overline{u'v'})}{\partial x} + \frac{\partial(\overline{v'v'})}{\partial y}\right] \tag{2.1.10}$$

$$\frac{\partial \bar{T}}{\partial t}+\frac{\partial(\overline{uT})}{\partial x}+\frac{\partial(\overline{vT})}{\partial y}=\frac{\partial}{\partial x}\left(\frac{k}{\rho C_P}\frac{\partial \bar{T}}{\partial x}\right)+\frac{\partial}{\partial y}\left(\frac{k}{\rho C_P}\frac{\partial \bar{T}}{\partial y}\right)-\left[\frac{\partial \overline{u'T'}}{\partial x}+\frac{\partial \overline{v'T'}}{\partial y}\right] \quad (2.1.11)$$

In these equations, $\bar{u}$, $\bar{v}$, $\bar{p}$ and $\bar{T}$ are mean values, while u', v', p' and T' represent the turbulent fluctuations in these quantities. It can be observed that three additional unknowns have been added to these equations, while for the 3D case, nine additional unknowns are added. To solve these equations, the standard k-ε turbulence model is applied. Defining k, the turbulent kinetic energy, and ε, the turbulent dissipation,

$$\mathrm{k}=\frac{1}{2}u'_i u'_i, \qquad \text{for } i=1,2,3 \quad (2.1.12)$$

$$\varepsilon=\vartheta_T\overline{\left(\frac{\partial u'_i}{\partial x_j}\right)\left(\frac{\partial u'_i}{\partial x_j}\right)}, \qquad \text{for } i=1,2,3 \quad (2.1.13)$$

The value of ϑ_T, the turbulent viscosity, can be calculated from the values of k and ε:

$$\vartheta_T=\frac{C_\mu \mathrm{k}^2}{\varepsilon} \quad (2.1.14)$$

Here, $C_\mu = 0.09$ (Launder et al., 1974). Finally, expressions for the Reynolds stresses are substituted into the RANS equations, resulting in the non-conservative form of the governing equations (Tu et al., 2008).

$$\frac{\partial u}{\partial x} + \frac{\partial v}{\partial y} = 0 \tag{2.1.15}$$

$$\frac{Du}{Dt} = -\frac{1}{\rho}\frac{\partial p}{\partial x} + \frac{\partial}{\partial x}\left([\vartheta + \vartheta_T]\frac{\partial u}{\partial x}\right) + \frac{\partial}{\partial y}\left([\vartheta + \vartheta_T]\frac{\partial u}{\partial y}\right) + \frac{\partial}{\partial x}\left([\vartheta + \vartheta_T]\frac{\partial u}{\partial x}\right) + \frac{\partial}{\partial y}\left([\vartheta + \vartheta_T]\frac{\partial v}{\partial x}\right) \tag{2.1.16}$$

$$\frac{Dv}{Dt} = -\frac{1}{\rho}\frac{\partial p}{\partial y} + \frac{\partial}{\partial x}\left([\vartheta + \vartheta_T]\frac{\partial v}{\partial x}\right) + \frac{\partial}{\partial y}\left([\vartheta + \vartheta_T]\frac{\partial v}{\partial y}\right) + \frac{\partial}{\partial x}\left([\vartheta + \vartheta_T]\frac{\partial u}{\partial y}\right) + \frac{\partial}{\partial y}\left([\vartheta + \vartheta_T]\frac{\partial v}{\partial y}\right) \tag{2.1.17}$$

$$\frac{DT}{Dt} = \frac{\partial}{\partial x}\left(\left[\frac{\vartheta}{Pr} + \frac{\vartheta_T}{Pr_T}\right]\frac{\partial T}{\partial x}\right) + \frac{\partial}{\partial y}\left(\left[\frac{\vartheta}{Pr} + \frac{\vartheta_T}{Pr_T}\right]\frac{\partial T}{\partial y}\right) \tag{2.1.18}$$

Here, Pr_T is the turbulent Prandtl number. Lastly, the transport equations for k and ε can be written in a non-conservative form:

$$\frac{D\mathrm{k}}{Dt} = \frac{\partial}{\partial x}\left(\frac{\vartheta_T}{\sigma_k}\frac{\partial \mathrm{k}}{\partial x}\right) + \frac{\partial}{\partial y}\left(\frac{\vartheta_T}{\sigma_k}\frac{\partial \mathrm{k}}{\partial y}\right) + P - D \tag{2.1.19}$$

$$\frac{D\varepsilon}{Dt} = \frac{\partial}{\partial x}\left(\frac{\vartheta_T}{\sigma_\epsilon}\frac{\partial \epsilon}{\partial x}\right) + \frac{\partial}{\partial y}\left(\frac{\vartheta_T}{\sigma_\epsilon}\frac{\partial \epsilon}{\partial y}\right) + \frac{\epsilon}{\mathrm{k}}(C_{\epsilon 1}P - C_{\epsilon 2}D) \tag{2.1.20}$$

Here, P is the turbulent production term, and D is the dissipation of turbulent dissipation term. The values selected for the constants $C_\mu, \sigma_k, \sigma_\epsilon, C_{\epsilon 1}$ and $C_{\epsilon 2}$ vary by solver package. However, Launder and Spalding (1974) obtained values for these constants for a range of turbulent flows with $C_\mu = 0.09$, $\sigma_k = 1.0, \sigma_\epsilon = 1.3, C_{\epsilon 1} = 1.44$ and $C_{\epsilon 2} = 1.92$ (cited by Tu et al., 2008). *P*, the turbulent production, is defined as

$$P = 2\vartheta_T\left(\left[\frac{\partial u}{\partial x}\right]^2 + \left[\frac{\partial v}{y}\right]^2\right) + \vartheta_T\left(\frac{\partial u}{\partial y} + \frac{\partial v}{\partial x}\right)^2 \tag{2.1.21}$$

With a review of finite difference methods, the governing equations for CFD and the standard k-ε turbulence model finished the specifics of the governing equations and constants used by SolidWorks Flow Simulation and ANSYS FLUENT can be discussed.

2.2 SolidWorks Flow Simulation Governing Equations

SolidWorks Flow Simulation does not allow for user input as to what methods to use outside of enabling or disabling certain models. The governing equations employed by the SolidWorks Flow Simulation solver are as follows (COSMOS, 2008). It should be noted that this solver makes use of the Favre-averaged Navier-Stokes equations.

$$\frac{\partial \rho}{\partial t} + \frac{\partial}{\partial x_i}(\rho u_i) = 0 \tag{2.2.1}$$

$$\frac{\partial \rho u_i}{\partial t} + \frac{\partial}{\partial x_j}\left(\rho u_i u_j\right) + \frac{\partial p}{\partial x_i} = \frac{\partial}{\partial x_j}\left(\tau_{ij} + \tau_{ij}^R\right) + S_i, \qquad i = 1,2,3, \ldots \tag{2.2.2}$$

$$\frac{\partial \rho H}{\partial t} + \frac{\partial \rho u_i H}{\partial x_i} = \frac{\partial}{\partial x_i}\left(u_j\left[\tau_{ij} + \tau_{ij}^R\right] + q_i\right) + \frac{\partial p}{\partial t} - \tau_{ij}^R \frac{\partial u_i}{\partial x_i} + \rho\epsilon + S_i u_i + Q_H \tag{2.2.3}$$

$$H = h + \frac{u^2}{2} \tag{2.2.4}$$

Here, S_i is a mass-distributed external force per unit mass due to a porous media resistance ($S_{i,porous}$), a buoyancy ($S_{i,gravity} = -\rho g_i$, where g_i is the gravitational acceleration component along

the *i-th* coordinate direction), and the rotation of the coordinate system ($S_{i,rotation}$), i.e., $S_i = S_{i,porous} + S_{i,gravity} + S_{i,rotation}$ (COSMOS, 2008). In addition, the shear stress tensor for a Newtonian fluid, and the Reynolds-stress tensor are defined in SolidWorks as:

$$\tau_{ij} = \mu\left(\frac{\partial u_i}{\partial x_j} + \frac{\partial u_j}{\partial x_i} - \frac{2}{3}\delta_{ij}\frac{\partial u_k}{\partial x_k}\right) \tag{2.2.5}$$

$$\tau_{ij}^{R} = \mu_T\left(\frac{\partial u_i}{\partial x_j} + \frac{\partial u_j}{\partial x_i} - \frac{2}{3}\delta_{ij}\frac{\partial u_k}{\partial x_k}\right) - \frac{2}{3}\rho\delta_{ij} \tag{2.2.6}$$

Finally, considering the k-ε turbulence model,

$$\mu_T = f_\mu \frac{C_\mu \rho \mathrm{k}^2}{\epsilon} \tag{2.2.7}$$

$$f_\mu = [1 - e^{-0.025R_y}]^2 \times \left(1 + \frac{20.5}{R_T}\right) \tag{2.2.8}$$

$$R_T = \frac{\rho \mathrm{k}^2}{\mu\epsilon}, \qquad R_y = \frac{\rho\sqrt{\mathrm{k}}y}{u}$$

$$\frac{\partial \rho k}{\partial t} + \frac{\partial}{\partial x_i}(\rho u_i \mathrm{k}) = \frac{\partial}{\partial x_i}\left(\left[\mu + \frac{\mu_T}{\sigma_k}\right]\frac{\partial \mathrm{k}}{\partial x_i}\right) + S_k \tag{2.2.9}$$

$$\frac{\partial \rho \epsilon}{\partial t} + \frac{\partial}{\partial x_i}(\rho u_i \epsilon) = \frac{\partial}{\partial x_i}\left(\left[\mu + \frac{\mu_T}{\sigma_\epsilon}\right]\frac{\partial \epsilon}{\partial x_i}\right) + S_\epsilon \tag{2.2.10}$$

$$S_k = \tau_{ij}^R \frac{\partial u_i}{\partial x_j} - \rho\epsilon + \mu_T P_B \tag{2.2.11}$$

$$S_\epsilon = C_{\epsilon 1}\frac{\epsilon}{\mathrm{k}}\left(f_1 \tau_{ij}^R \frac{\partial u_i}{\partial x_j} + \mu_T C_B P_B\right) - C_{\epsilon 2} f_2 \frac{\rho \epsilon^2}{\mathrm{k}} \tag{2.2.12}$$

The values of all of the constants used in these equations are as follows: $C_\mu = 0.09, C_{\epsilon 1} = 1.44, C_{\epsilon 2} = 1.92, C_\epsilon = 1.3, \sigma_k = 1, \sigma_C = 0.9$, and Pr is the Prandtl number. The turbulent generation term, P_B, is defined as

$$P_B = -\frac{g_i}{\sigma_B}\frac{1}{\rho}\frac{\partial \rho}{\partial x_i} \tag{2.2.13}$$

Here, $\sigma_B = 0.9$. Finally, the terms f_1 and f_2 are written

$$f_1 = 1 + (\frac{0.05}{f_\mu})^3 \tag{2.2.14}$$

$$f_2 = 1 - e^{-R_T^2} \tag{2.2.15}$$

This concludes the definition of the governing equations used by the SolidWorks Flow Simulation Solver (COSMOS, 2008).

2.3 ANSYS FLUENT Governing Equations

The ANSYS FLUENT solver allows a greater deal of choices in selecting what models to use in its calculations. However, the standard k-ε turbulence model was selected for this solver as well. The governing equations used by the ANSYS FLUENT solver are as follows:

$$\frac{\partial \rho}{\partial t} + \nabla \cdot (\rho \vec{v}) = S_m \tag{2.3.1}$$

$$\frac{\partial}{\partial t}(\rho \vec{v}) + \nabla \cdot (\rho \vec{v} \vec{v}) = -\nabla p + \nabla \cdot (\tau) + \rho \vec{g} + \vec{F} \tag{2.3.2}$$

$$\tau = \mu\left(\left[\nabla\vec{v} + \nabla\overrightarrow{v^T}\right] - \frac{2}{3}\nabla\cdot\vec{v}I\right) \tag{2.3.3}$$

Here, *I* is the unit tensor. The turbulence model equations for k and ε are defined in ANSYS FLUENT as:

$$\frac{\partial}{\partial t}(\rho\mathrm{k}) + \frac{\partial}{\partial x_i}(\rho\mathrm{k}u_i) = \frac{\partial}{\partial x_j}\left[\left(\mu + \frac{\mu_T}{\sigma_k}\right)\frac{\partial\mathrm{k}}{\partial x_j}\right] + G_k + G_B - \rho\epsilon - Y_M + S_k \tag{2.3.4}$$

$$\frac{\partial}{\partial t}(\rho\epsilon) + \frac{\partial}{\partial x_i}(\rho\epsilon u_i) = \frac{\partial}{\partial x_j}\left[\left(\mu + \frac{\mu_T}{\sigma_\epsilon}\right)\frac{\partial\epsilon}{\partial x_j}\right] + C_{\epsilon1}\frac{\epsilon}{\mathrm{k}}(G_k + C_{\epsilon3}G_b) - C_{\epsilon2}\rho\frac{\epsilon^2}{\mathrm{k}} + S_\epsilon \tag{2.3.5}$$

where, for an ideal gas,

$$G_k = -\rho\overline{u_i'u_j'}\frac{\partial u_j}{\partial x_i} \tag{2.3.6}$$

$$G_b = -g_i\frac{\mu_t}{\rho Pr_T}\frac{\partial\rho}{\partial x_i} \tag{2.3.7}$$

$$Y_M = 2\rho\epsilon M_T^2 \tag{2.3.8}$$

$$M_T = \sqrt{\frac{k}{a^2}}, \tag{2.3.9}$$

$$a \equiv \sqrt{\gamma RT}$$

Here, G_k is the production of turbulent kinetic energy in ANSYS FLUENT, G_b is the production of turbulence due to buoyancy, Y_M is the dilatation dissipation term, M_T is the turbulent Mach number and a is the speed of sound. The definition for turbulent viscosity, μ_T, is calculated in the same manner as previously shown for the SolidWorks Flow Simulation solver. The constants for the ANSYS FLUENT turbulence model are as follows: $C_{\epsilon 1} = 1.44, C_{\epsilon 2} = 1.92, C_\mu = 0.09, \sigma_k = 1.0$ and $\sigma_\epsilon = 1.3$, the same as those identified by Launder and Spalding (1974).

CHAPTER 3

CFD SETUP

Prior to reviewing the results of the computations, it is necessary to represent the setup of the computational methods, the grid settings and boundary conditions used in this research. As both the SolidWorks Flow Simulator and ANSYS FLUENT solvers were used, setups for both cases will be reviewed.

3.1 Computational Method Selection

For SolidWorks Flow Simulation and ANSYS FLUENT, the manner of computational method must be determined prior to computation. This selection process differs between both solvers, and the selected choices for both will be explained in this section.

SolidWorks Flow Simulation does not offer a selection of equations or turbulence models to choose from, they are a set of defaults for the solver. The equations and models used by SolidWorks Flow Simulation have been discussed in greater detail in Section 2.2. However, a few choices can be made by the user regarding what equations and models to activate or ignore. For this study, the setup selected for each case has been compiled into **Table 1** below. Of particular note, the "Laminar and Turbulent" method has been enabled, thus using the k-ε turbulence model.

Table 1 - SolidWorks Flow Simulation Solver Setup Conditions

Analysis Type	Internal
Exclude Cavities without Flow Conditions	Yes
Physical Features	
Heat Conduction in Solids	No
Radiation	No
Time-Dependent	No
Gravity	-9.81 m/s^2 in Y Plane
Rotation	No
Fluid Type	Air
Flow Characteristics	
Flow Type	Laminar and Turbulent
Humidity	No
Wall Conditions	
Wall Thermal Condition	Adiabatic
Roughness	0.5 micrometer
Initial Conditions	
Pressure	101325 Pa
Pressure Potential	Yes
Temperature	293.2 K
Velocity in X-Direction	0 m/s
Velocity in Y-Direction	0 m/s
Velocity in Z-Direction	0 m/s
Turbulence Intensity	2%
Turbulence Length	0.000749121903 m

ANSYS FLUENT allows for a greater degree of choice in the use of varying equations and models in its solutions that SolidWorks Flow Simulation. A detailed description of the models selected for use with ANSYS FLUENT has been discussed in greater detail in Section 2.3. **Table 2** below contains the setup conditions used for all ANSYS FLUENT computations.

Table 2 - ANSYS FLUENT Solver Setup Conditions

General	
Solver Type:	Pressure-Based
Velocity Formulation:	Absolute
Time:	Steady
Gravity:	-9.81 m/s2 in Y
Models	
Viscous	Standard k-ε, Standard Wall Fn
Materials	
Fluid	Air
Solid	Aluminum
Dynamic Mesh	
Dynamic Mesh	Disabled
Solution Methods	
Scheme	SIMPLE
Gradient	Least Squares Cell Based
Pressure	Standard
Momentum	Second-Order Upwind
Turbulent Kinetic Energy	Second-Order Upwind
Turbulent Dissipation Rate	Second-Order Upwind
Under-Relaxation Factors	
Pressure	0.3
Density	1
Body Forces	1
Momentum	0.7
Turbulent Kinetic Energy	0.8
Turbulent Dissipation Rate	0.8
Turbulent Viscosity	1

3.2 Grid Design and Grid Independence

To solve the governing equations detailed in Chapter 2, it is necessary to apply a mesh to each of the diffuser geometries to be studied. Both SolidWorks Flow Simulation and ANSYS FLUENT contain an internal package for developing a mesh for a given geometry. SolidWorks Flow Simulation uses an automatic method which applies a rectangular element mesh to differentiate between solid and fluid regions within the computational domain. As the flow at the exit of the diffuser was desired, a rectangular computational domain enclosing the interior of the diffuser and fan duct was applied to the models. From this, the mesh could be refined. Mesh refinement is the process of splitting existing cells within the mesh into smaller, similarly-shaped cells. For SolidWorks Flow Simulation, mesh refinement splits the existing cells into smaller parallelepiped-shaped elements using the model geometry, so as to obtain a better representation of the solid and fluid regions within the domain (COSMOS, 2008). The more refined the mesh, the greater the number of elements within the mesh, the more accurate the results. However, with more elements in a mesh, the computational resources necessary to complete the calculation increase. SolidWorks Flow Simulation does not provide the user with a method to apply mesh controls to specific regions of the geometry. Instead, it makes use of varying "levels" of grid refinement, spanning from 1 to 8, with 1 being the coarsest mesh, and 8 the most refined. As SolidWorks does not recommend using any setting for mesh settings below level 3, only settings

above this level were considered. **Figure 11** below provides an example of a level 6 mesh applied to the original diffuser geometry.

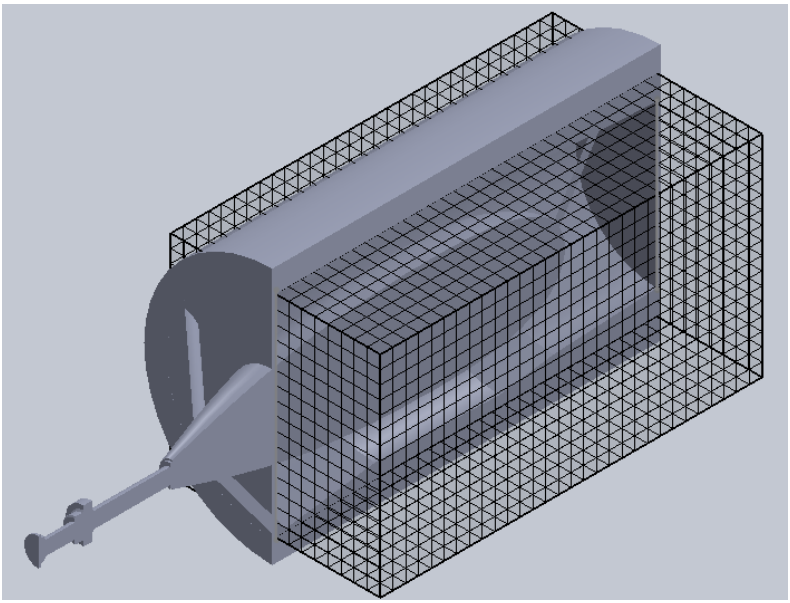

Figure 11 – Sample of Level 6 Mesh applied to Original Geometry with Cross-Sectional View in SolidWorks Flow Simulation

ANSYS FLUENT has an internal meshing package that will also automatically generate a mesh for the model geometry. However, as opposed to SolidWorks Flow Simulation, the computational domain is not defined by the solver, but rather by the geometry itself. That is to say, a "fluid" body representing all regions that governing equations for the fluid will be

calculated must be the geometry used by the model. Any boundaries, whether an opening to atmosphere, an inlet flow or a solid surface, are not included in the geometry and thus are excluded from the computational domain. It should be noted that designing a "fluid body" was accomplished through the use of the "Create Fluid Body" tool contained with SolidWorks Flow Simulation, which was imported into ANSYS FLUENT for computation. With the computational domain geometry imported into FLUENT, the ANSYS meshing tool was used to generate a mesh. The ANSYS mesh tool allows the user a great deal of control over the mesh and its design. While a great number of different mesh design philosophies can be applied for developing a mesh within ANSYS, a design using an unstructured grid was used for all FLUENT geometries. An unstructured grid is one in which elements of non-uniform shapes and sizes are used throughout the domain, as opposed to a structured grid in which each element is identical in size and shape to the other elements in the grid. Unstructured grids are particularly useful for computations considering complex geometries such as those in this research (Tu et al, 2008). The use of an unstructured grid also allows for the solution of large and complex problems in a shorter period of time than if a structured grid had been used (Wyman, 2001). An example of such a complex problem was a study in which the calculation of the axial thrust, convective and radiative wall heat fluxes for liquid rocket engine nozzles was analyzed using CFD. In this study, an unstructured grid was used over a previously designed structured grid due to increasing requirements for parallel computing efficiency and the need for faster grid generation (Wang, 2004). To briefly describe the design philosophy for the ANSYS FLUENT meshes, the solid bodies, that is, the outer diffuser and fan duct wall and the engine nacelle and support spars, had

a “face sizing” mesh control applied to their surfaces, with a slow smoothing method applied to the domain from these locations. This created an unstructured grid that had the highest mesh refinement near the actual diffuser geometry, which was necessary due to its complexity, slowly became coarser farther away from these surfaces. This philosophy helped to reduce the computational expense of each run, while maintaining the greatest level of accuracy around the locations of importance, i.e., the diffuser geometry. **Figures 12 and 13** provide an example of the meshing design used for the diffuser geometries.

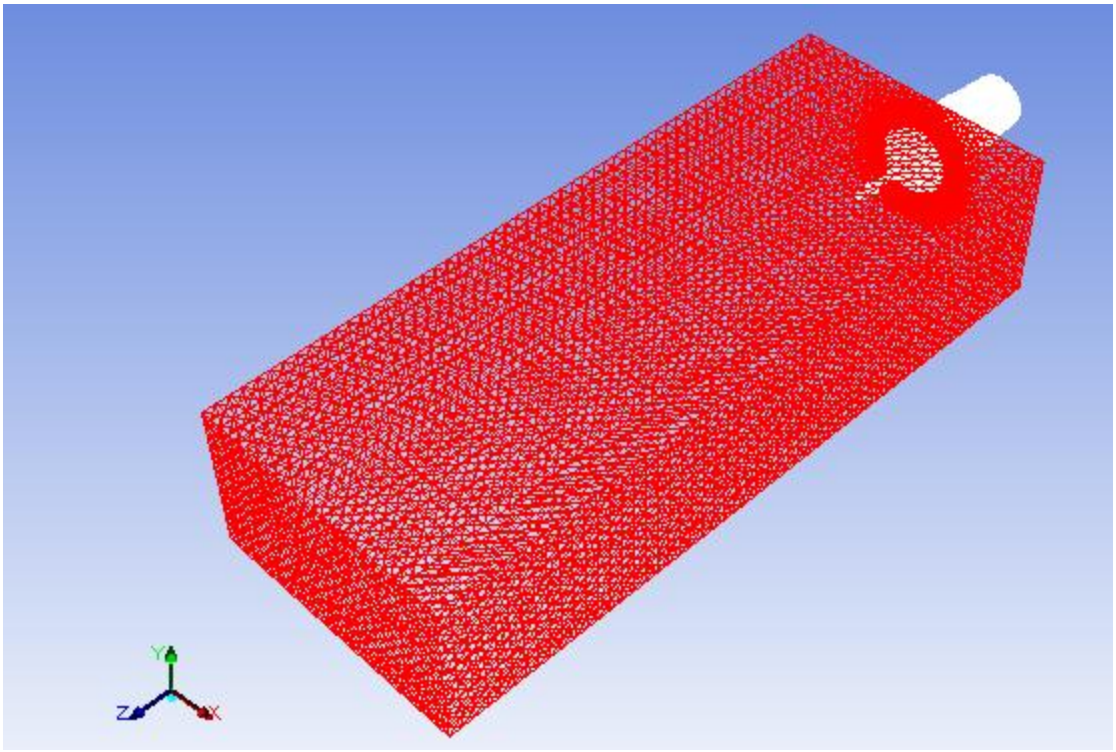

Figure 12 - Sample Mesh of Base Diffuser Geometry for Entire Computational Domain for Full Size 7.5 Base Tunnel in ANSYS FLUENT

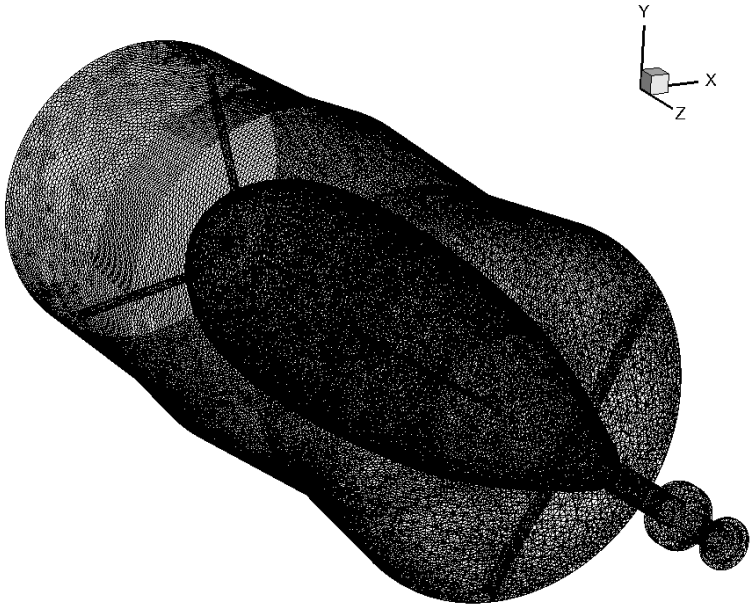

Figure 13 - Sample Mesh of Base Diffuser Geometry showing Surface Meshing for Full Size 7.5 Base Tunnel in ANSYS FLUENT

Additional information concerning the mesh controls applied to the ANSYS FLUENT models can be found in Appendix A.

To obtain the most accurate results with minimal computational time, a grid independence study is used. This is an iterative process of applying a coarse mesh to the geometry, solving the governing equations for that mesh, and then refining the mesh and solving again. The results between the coarse mesh and the refined mesh are compared, and if there is a notable difference between the results, the process is repeated after refining the mesh once more.

This process of refining the mesh and comparing the results is repeated until differences between the results for both meshes are found to be essentially negligible. This condition, when the results of the computation are independent of any further refinement to the mesh, is known as grid independence, and is required to maximize the accuracy of the results while minimizing the computational time. Grid independence studies were conducted for both SolidWorks Flow Simulation and ANSYS FLUENT. **Figures 14 and 15** provide examples of the results of grid independence studies for SolidWorks Flow Simulation and ANSYS FLUENT, respectively, for the original full size diffuser geometry.

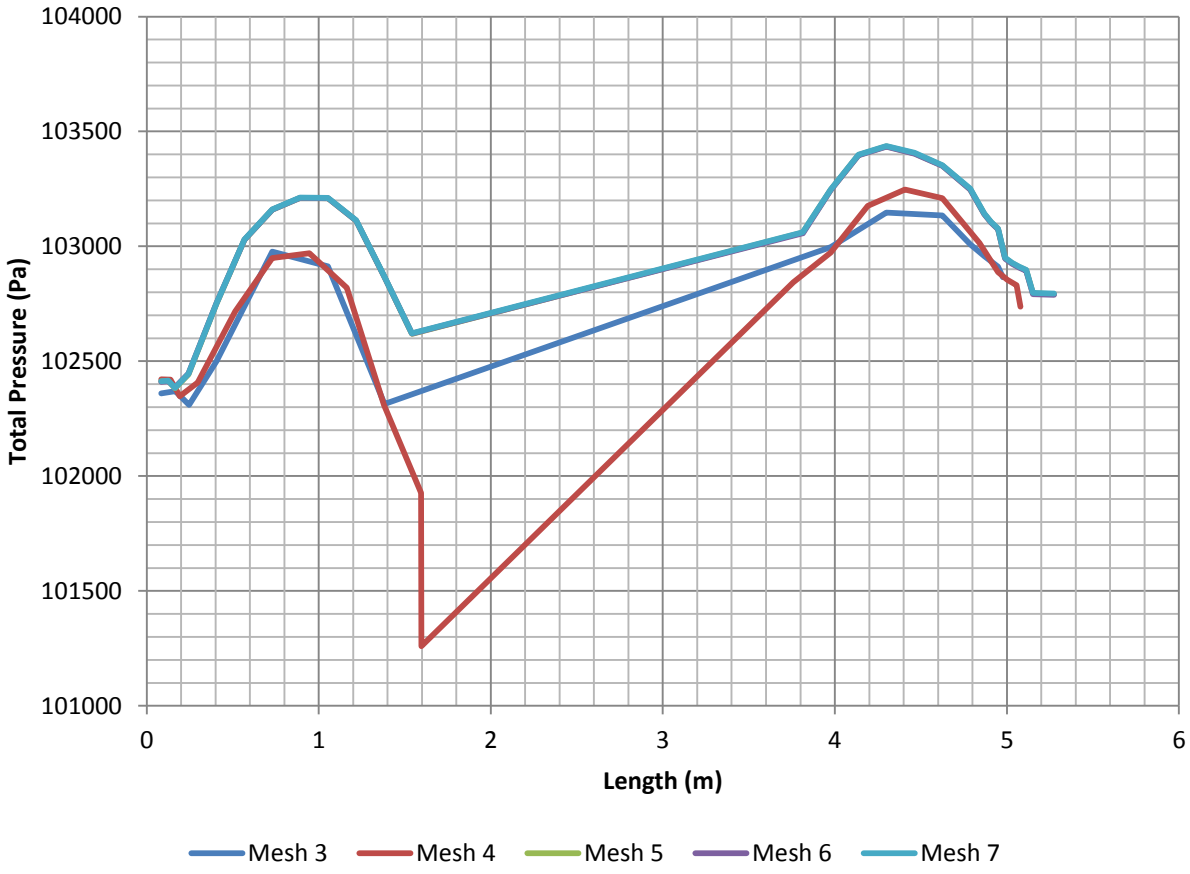

Figure 14 - Grid Independence Study for SolidWorks Flow Simulation for Full Size 7.5 Base Tunnel Configuration using Total Pressure as Parameter

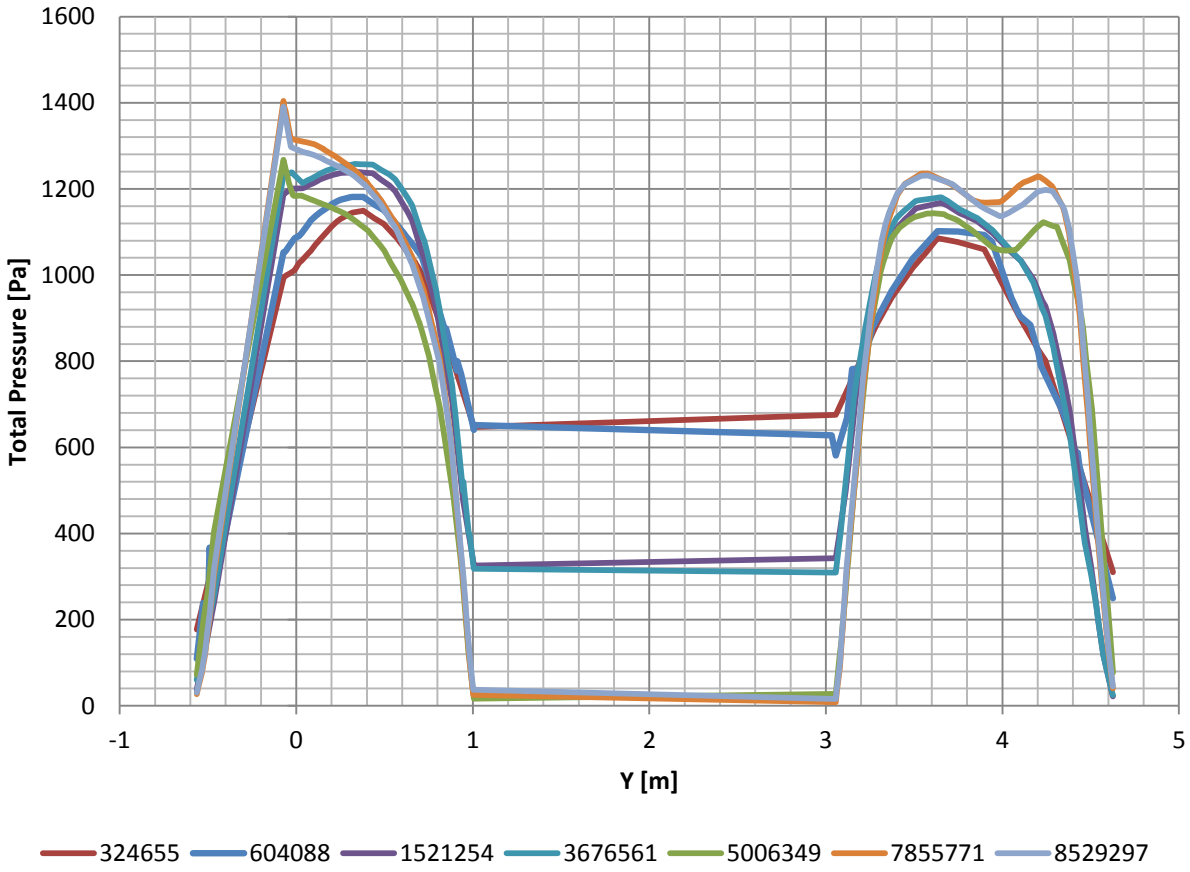

Figure 15 - Grid Independence Study for ANSYS FLUENT for Full Size 7.5 Base Tunnel Configuration using Total Pressure as Parameter

Once grid independence was established for the original diffuser geometry, the same mesh settings were applied to the other geometries, as the changes in their geometries were

relatively small. One exception to this was the diffuser geometry that made use of conical sections to split the flow at the exit of the diffuser. This geometry had a separate grid independence study applied to it, and thus, uses as different level of mesh refinement for its calculations. Appendix A contains the results of all grid independence studies for all models of all sizes for reference.

3.3 Boundary Conditions

To solve the governing equations discussed in Section 2.1, it was necessary to apply boundary conditions to the models. The method of application of these boundary conditions for SolidWorks Flow Simulation and ANSYS FLUENT differed slightly. SolidWorks Flow Simulation recognized all solid bodies as solids, and applied a "wall" boundary condition to each of these surfaces. Aside from this, an outlet pressure at atmospheric conditions was applied to the outlet of the diffusers, and an inlet velocity was supplied at the inlet of each of the geometries. SolidWorks Flow Simulation has an option to enable both uniform and fully developed flow conditions, and thus, was used for both inlet boundary conditions.

ANSYS FLUENT required that each zone in the model be defined, including surface bodies. Certain default conditions were applied to each of these zones as their boundary conditions. However, for the edges of the computational domain outside of the diffuser geometry, an outlet pressure at atmospheric conditions was applied. At the inlet of the fan duct section, an inlet velocity boundary condition was supplied. For the uniform flow case, FLUENT contained a method to apply a uniform flow automatically. However, no fully developed flow

option was available as it was in SolidWorks Flow Simulation. Thus, a profile defining a fully developed turbulent flow entering the fan duct had to be defined. To accomplish this, the entrance length necessary to achieve fully developed turbulent flow was calculated for both full size and small scale geometries. The entrance length for turbulent flow is defined as a function of Reynolds number (Engineering Toolbox, 2012).

$$EI = 4.4Re^{1/6} \tag{3.3.1}$$

where

$$Re = \frac{VD}{\upsilon} \tag{3.3.2}$$

In these equations, D is the duct inlet diameter. Substituting in the known values of inlet velocity, viscosity of air and inlet diameter, a Reynolds number of 1.647×10^7 for the full size model and 1.674×10^5 for the small scale model can be calculated. Using these values for the Reynolds number, the entrance length for both sizes of model was calculated. To make use of this entrance length, another definition of the entrance length was used (Engineering Toolbox, 2012):

$$EI = \frac{l_e}{D} \tag{3.3.3}$$

By substituting in the known values of entrance length, EI, and inlet diameter, D, the total length to attain fully developed flow, l_e, was calculated. Next, two new geometries were designed in ANSYS, both of pipes of constant diameter. Each model had a diameter corresponding to the inlet diameter for the full size and small scale models, and a length equal to the previously calculated length to attain fully developed flow for each case. Then, a mesh was applied to each geometry. A uniform inlet velocity of 60 m/s was given for each pipe, open to atmospheric conditions at the exit. Each case was calculated, and the velocity distribution at the exit of the pipes saved as a profile within FLUENT. This velocity distribution at the exit of each pipe represented the velocity distribution of a fully developed turbulent flow. Thus, for each of the fully developed flow cases in FLUENT, these profiles were loaded as the inlet boundary condition, for the full size and small scale models, accordingly, and are shown in **Figure 16** below.

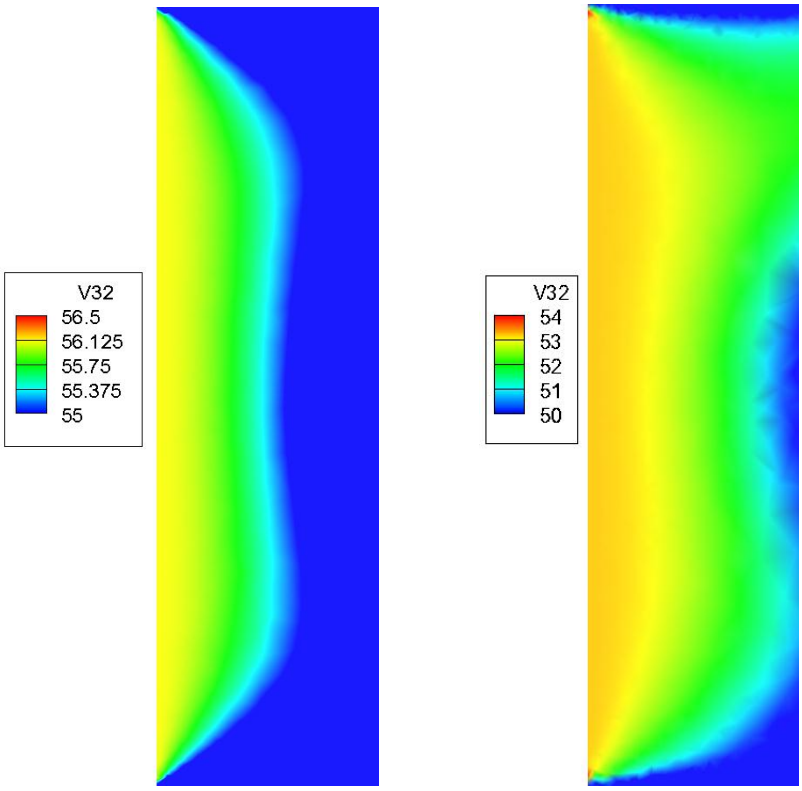

Figure 16 - Fully Developed Turbulent Flow Velocity Magnitude Profiles for Full Size (Left) and Small Scale (Right) Models in ANSYS FLUENT Solver

3.4 Computational Test Configurations

For this research, four different geometries were evaluated. The first geometry was the original tunnel diffuser configuration. The second geometry was essentially the same geometry as the original tunnel diffuser configuration, with the exception that instead of a wall inclination half-angle of 7.5°, the wall inclination angle was reduced to 3.5°, to satisfy the recommendations given in previous research (Sovran and Klomp, 1963, as cited by Farokhi, 2009). The third and

fourth geometries were those identified in previous analysis performed by Dr. Ölçmen (2011), which added an additional constant-area diffuser to the third geometry, and an increased aspect ratio diffuser with conical sections added to the fourth geometry. Each of these models had a full size and small scale model to be tested. For each of these models, both uniform and fully developed inlet flow conditions were used. Both SolidWorks Flow Simulation and ANSYS FLUENT were used to calculate the flow field for each of the given configurations listed in. **Table 3**.

Table 3 - Full Matrix of Computations by Model, Boundary Conditions and Solver

	SolidWorks - 3D Full Size	**SolidWorks - 3D Small Scale**
Grid Independence	Base Tunnel 7.5 3.5 + Flat + Conical	Base Tunnel 7.5 3.5 + Flat + Conical
Uniform Flow	Base Tunnel 7.5 Base Tunnel 3.5 3.5 + Flat + Conical 3.5 + Flat	Base Tunnel 7.5 Base Tunnel 3.5 3.5 + Flat + Conical 3.5 + Flat
Fully Developed Flow	Base Tunnel 7.5 Base Tunnel 3.5 3.5 + Flat + Conical 3.5 + Flat	Base Tunnel 7.5 Base Tunnel 3.5 3.5 + Flat + Conical 3.5 + Flat
	FLUENT - 3D Full Size	**FLUENT - 3D Small Scale**
Grid Independence	Base Tunnel 7.5 3.5 + Flat + Conical	Base Tunnel 7.5 3.5 + Flat + Conical
Uniform Flow	Base Tunnel 7.5 Base Tunnel 3.5 3.5 + Flat + Conical	Base Tunnel 7.5 Base Tunnel 3.5 3.5 + Flat + Conical

	3.5 + Flat	3.5 + Flat
Fully Developed Flow	Base Tunnel 7.5	Base Tunnel 7.5
	Base Tunnel 3.5	Base Tunnel 3.5
	3.5 + Flat + Conical	3.5 + Flat + Conical
	3.5 + Flat	3.5 + Flat

CHAPTER 4

RESULTS

This chapter contains the compiled results from both solvers, SolidWorks Flow Simulation and ANSYS FLUENT. Section 3.1 contains a compilation of all SolidWorks Flow Simulation results, and a comparison of the results obtained by that solver. Section 3.2 contains a compilation of all ANSYS FLUENT results and a comparison of the results obtained by that solver. Section 3.3 contains a comparison of results between both solvers.

3.1 SolidWorks Flow Simulation Results

This section provides a summary of the results obtained by the SolidWorks Flow Simulation solver. The results obtained for the full size models will be discussed first, followed by the results for the small scale models. Finally, the results of both size models will be compared.

The primary variable of interest in these results is the total pressure of the flow, which accounts for both the static pressure and the dynamic pressure of the flow. The total pressure distribution at the entrance of the tunnel is of greatest interest, as this will define the losses through the fan duct and diffuser, specifically through the change in the total pressure across the diffuser. As a result, it is relevant to consider the total pressure distribution through the entire tunnel, to consider the possibility of effects such as separation of the flow. For the first consideration, contour plots for the original tunnel configuration, labeled the "7.5 Base Tunnel," have been illustrated in **Figure 17, 18 and 19**.

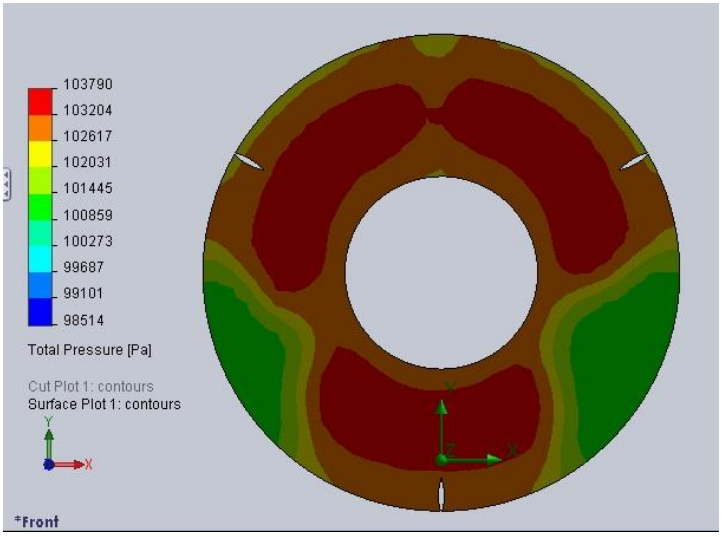

Figure 17 - SolidWorks Flow Simulation Total Pressure Distribution at Exit for 7.5 Base Tunnel - Full Size - Uniform Flow

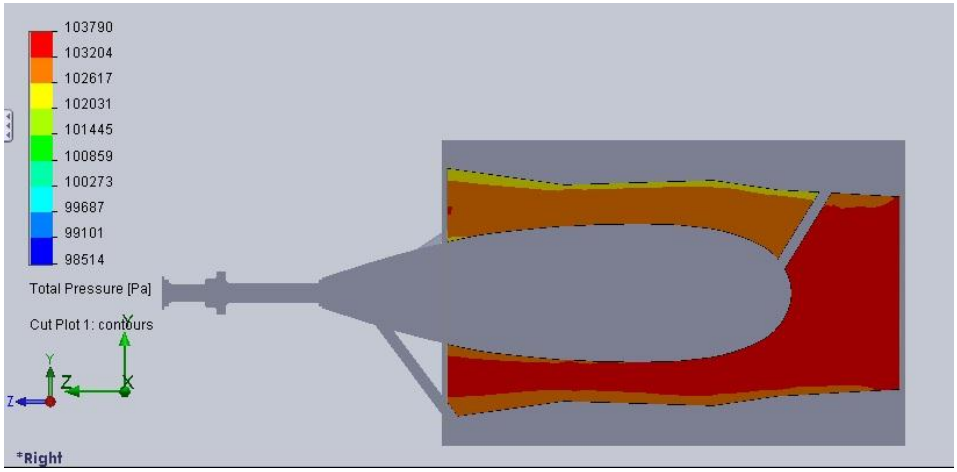

Figure 18 – SolidWorks Flow Simulation Total Pressure Distribution through Tunnel Cross-Section for 7.5 Base Tunnel - Full Size - Uniform Flow

From **Figure 17**, it would seem that there are two regions around 120° and 240° from the top of the exit where there is a much lower total pressure. This occurrence is indicative of flow separation induced by the 7.5° half-angle for this diffuser. To verify this, the velocity distribution at the exit was determined.

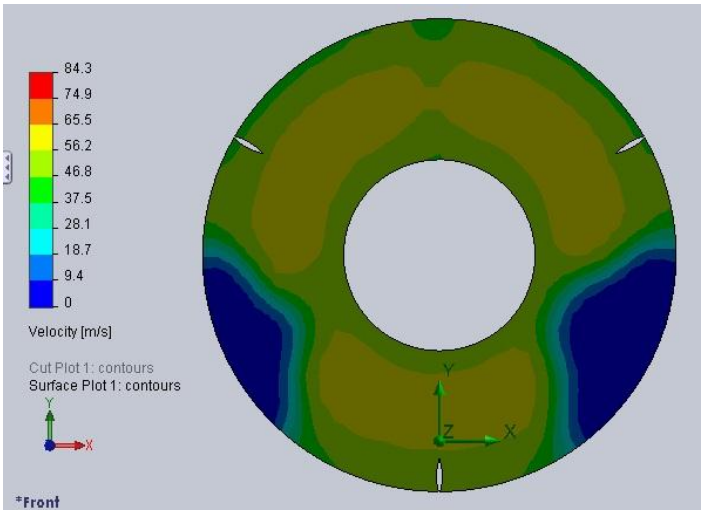

Figure 19 – SolidWorks Flow Simulation Velocity Distribution at Exit for 7.5 Base Tunnel - Full Size - Uniform Flow

It can be seen that two regions noted earlier contain a region of essentially zero velocity, a separation region. Such separation increases the losses in the tunnel, as discussed previously. For comparison, the total pressure distribution at the exit and along a mid-plane cross-section of this geometry for the fully developed flow case for this geometry is shown in **Figures 20 and 21**.

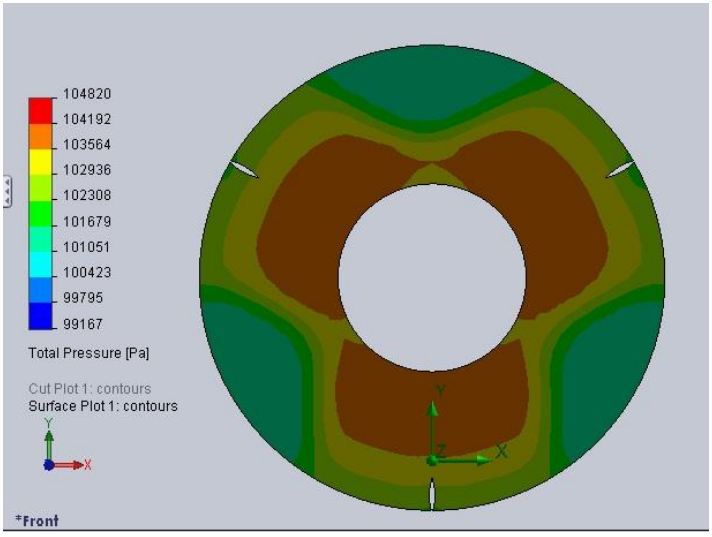

Figure 20 – SolidWorks Flow Simulation Total Pressure Distribution at Exit for 7.5 Base Tunnel - Full Size - Fully Developed Flow

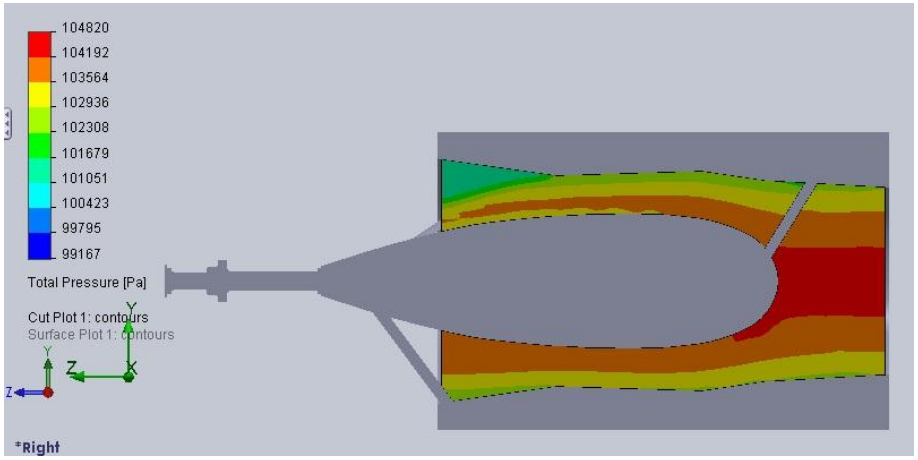

Figure 21 – SolidWorks Flow Simulation Total Pressure Distribution through Tunnel Cross-Section for 7.5 Base Tunnel – Full Size – Fully Developed Flow

Again, as with the uniform flow case, there are the two flow separation regions at 120° and 240°. However, in addition, a third region of separation has occurred at 0°. To verify this, a plot of the velocity through a cross-section of the geometry is shown in **Figure 22**.

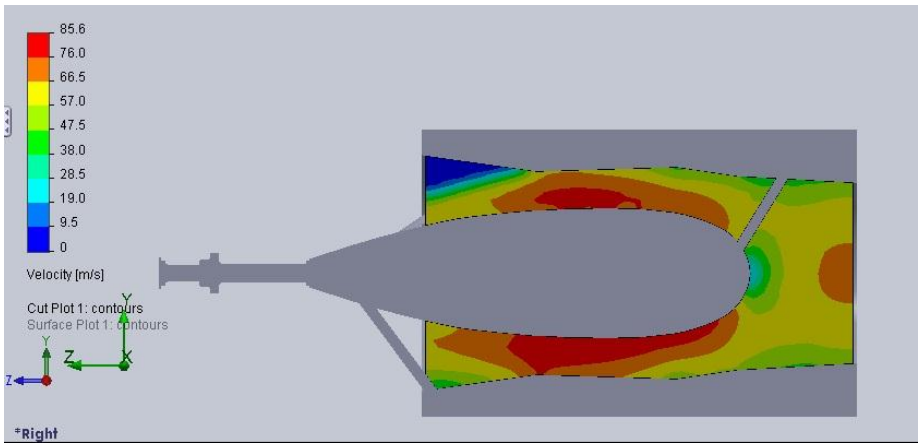

Figure 22 – SolidWorks Flow Simulation Velocity Distribution through tunnel Cross-Section for 7.5 Base Tunnel - Full Size - Fully Developed Flow

It can be seen that the flow separates at the beginning of the diffuser section where the 7.5° inclination angle occurs. From these results, the wall inclination angle for the diffuser is too wide, as expected by previous research discussed in Section 1.3. For the sake of comparison, the total pressure distribution at the exit of the tunnel and through a cross-section of the tunnel has

been provided in **Figure 23** and **Figure 24**, respectively, for the small scale model of this geometry as well.

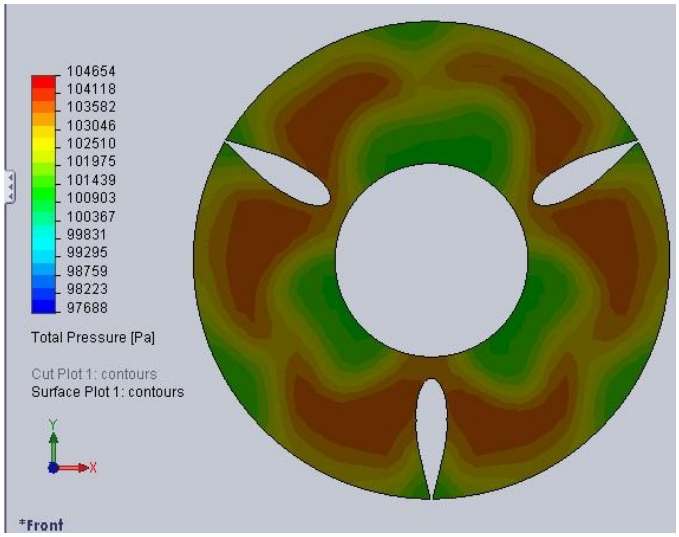

Figure 23 – SolidWorks Flow Simulation Total Pressure Distribution at Exit for 7.5 Base Tunnel - Small Scale - Uniform Flow

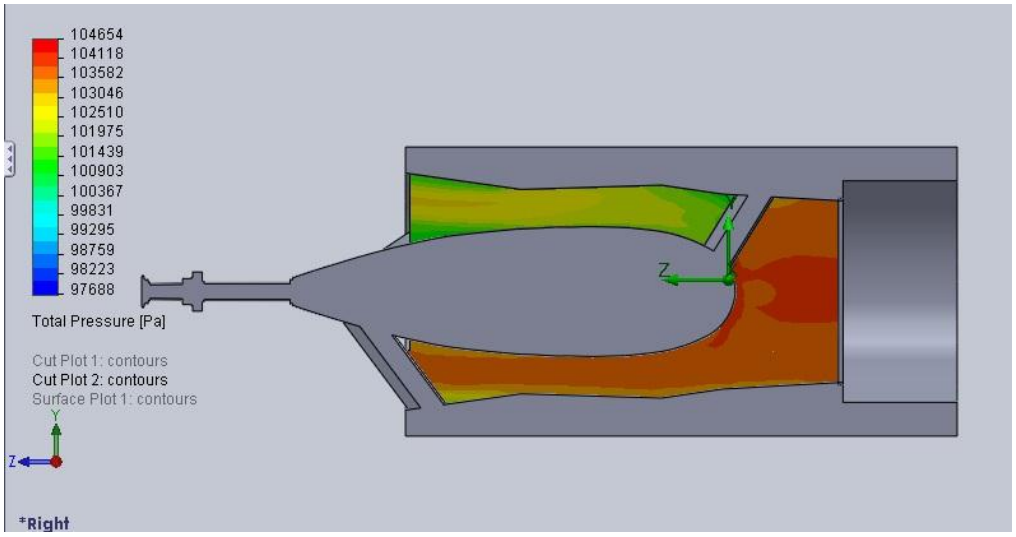

Figure 24 – SolidWorks Flow Simulation Total Pressure Distribution through tunnel Cross-Section for 7.5 Base Tunnel - Small Scale - Uniform Flow

The results for the small scale model differ from those of the full size model, as it can be seen that a very different total pressure distribution occurs at the exit. What appear to be separation regions along the engine nacelle have developed for this scale model, which is corroborated by the velocity distribution at the exit, shown in **Figure 25**.

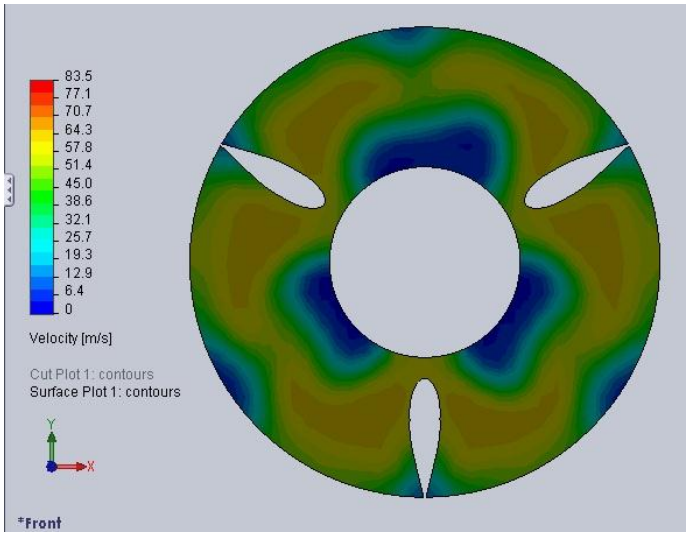

Figure 25 – SolidWorks Flow Simulation Velocity Distribution at Exit for 7.5 Base Tunnel - Small Scale - Uniform Flow

Finally, to consider all the cases for the "7.5 Base Tunnel" geometry, the total pressure distribution for the small scale model under a fully developed inlet flow is shown in **Figure 26**.

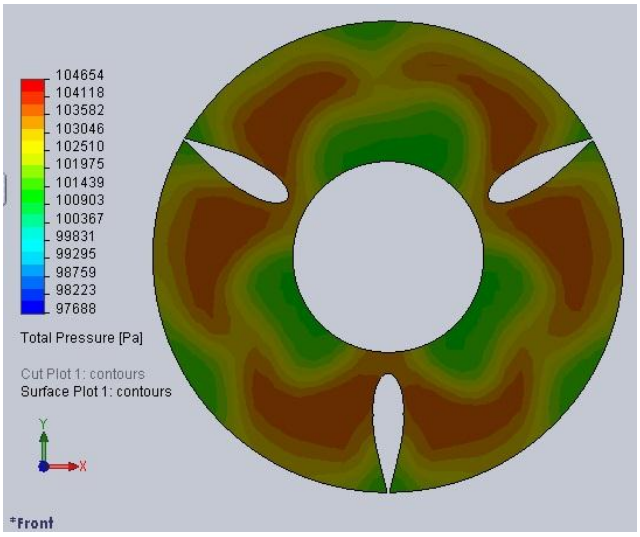

Figure 26 – SolidWorks Flow Simulation Total Pressure Distribution at Exit for 7.5 Base Tunnel - Small Scale - Fully Developed Flow

For the small scale cases, it can be seen that varying the inlet flow condition does not greatly vary the flow distribution at the exit of the diffuser. The separation regions present for the uniform flow case are still present for the fully developed flow case, and need to be minimized to reduce losses for the diffuser.

To define the losses through the diffuser, we begin by considering an Eulerian system, such as that illustrated in **Figure 27** below.

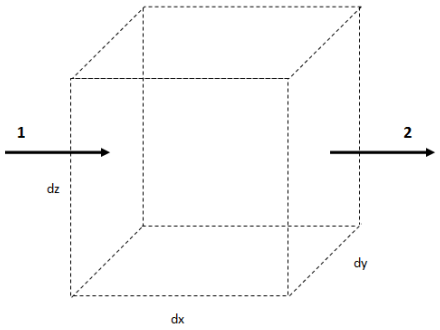

Figure 27 - Eulerian Fluid Element

Considering only the flow moving in the x-direction with no heat or work added, as shown in Figure 3, the total head loss coefficient through the element can be expressed as

$$h_L = \frac{(P_1 - P_2) + \frac{1}{2}\rho(V_1^2 - V_2^2)}{\rho g} \qquad 4.1.1$$

This relation is used to quantify the relative loss of power for the flow between two continuous locations in the tunnel. Reducing the value of this term would result in an increase in the efficiency of the tunnel. For the SARL tunnel, the power loss for the diffuser is considered in two parts: the power loss within the diffuser and the power loss of the flow exiting the diffuser. **Figure 28** below represents the locations for which these losses are associated.

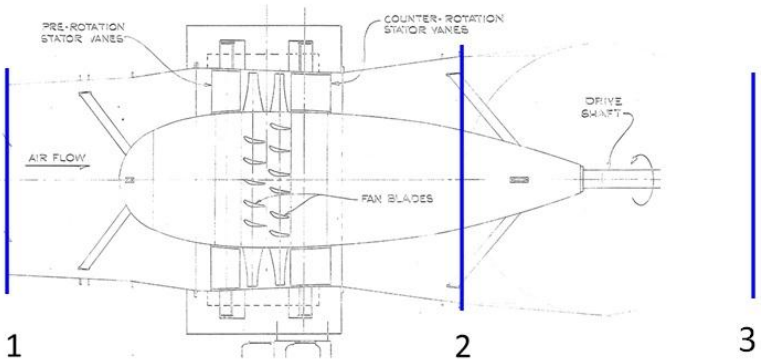

Figure 28 - General Locations for Power Loss Calculations relative to the SARL Wind Tunnel Fan Duct and Diffuser Sections

Here, location 3 represents a point outside the exit of the diffuser which is sufficiently far away that the velocity at this location has gone to essentially zero. Compiling both head losses for sections 1-2 and 2-3, the following equations are used:

$$h_{L_1} = \frac{(P_1 - P_2) + \frac{1}{2}\rho(V_1^2 - V_2^2)}{\rho g} \tag{4.1.2}$$

$$h_{L_2} = \frac{\frac{1}{2}V_2^2}{g} \tag{4.1.3}$$

$$h_{L_{total}} = h_{L_1} + h_{L_2} \tag{4.1.4}$$

Table 4 compiles all three head losses for each geometry, while **Table 5** compiles the percentage improvement in loss reduction for each geometry compared to the "7.5 Base Tunnel" geometry.

Table 4 – SolidWorks Flow Simulation Sum of Head Losses by Diffuser Geometry

	Small Scale Models		Full Size Models	
	Uniform Flow	Fully Developed Flow	Uniform Flow	Fully Developed Flow
7.5 Base Tunnel	204.1233549 m	200.1425428 m	168.6184703 m	177.0228342 m
3.5 Base Tunnel	203.9109048 m	195.2624509 m	155.3990003 m	161.1373806 m
3.5 + Flat	165.616222 m	159.5460778 m	116.804592 m	151.5131569 m
3.5 + Flat + Conical	165.3954211 m	150.4212555 m	121.9833666 m	143.0591271 m

Table 5 – SolidWorks Flow Simulation Percentage Improvement in Losses from 7.5 Base Tunnel Configuration

	Small Scale Models		Full Size Models	
	Uniform Flow	Fully Developed Flow	Uniform Flow	Fully Developed Flow
3.5 Base Tunnel	0.104079303	2.438308156	7.839870672	8.97367488
3.5 + Flat	18.86463845	20.28377601	30.72847131	14.41038803
3.5 + Flat + Conical	18.97280878	24.84293777	27.65717399	19.18605997

From these results, it can be seen that for the small scale models, the addition of the "3.5 + Flat + Conical" provides the greatest reduction in losses, with the "3.5 + Flat" geometry having slightly less marked improvement. As the exact type of flow condition entering the fan duct is not known, the improvement to be expected for these geometries will exist between the limits of the uniform flow and fully developed flow cases.

To consider the reduction in losses associated with the actual full size geometry, the exact diffuser geometry that is optimal varies with the nature of the flow entering the fan duct. For the uniform flow case, the "3.5 + Flat" diffuser geometry provides the optimal reduction of losses, with 30.73% improvement from the base tunnel configuration. However, for the fully developed

flow case, the “3.5 + Flat + Conical” diffuser geometry provides the optimal reduction of losses, with 19.19% improvement from the base tunnel configuration. As the actual nature of the inlet flow is not known, to determine which diffuser geometry is optimal, the average reduction in losses will be used as the determining factor. For the “3.5 + Flat” diffuser geometry, the average percentage improvement from the base tunnel geometry is 22.37%. However, for the “3.5 + Flat + Conical” diffuser geometry, the average percentage improvement from the base tunnel geometry is 23.32%. Thus, considering the average percentage improvement in diffuser efficiency, the “3.5 + Flat + Conical” geometry is the optimal design. To apply this to an efficiency gain for the entire tunnel, approximating that the fan duct and the exit losses account for approximately 35% of all losses for the tunnel, the “3.5 + Flat + Conical” design will offer approximately 6.72% to 9.68% improvement, with an average improvement of approximately 8.20%. The “3.5 + Flat” design will offer approximately 5.04% to 10.76% improvement, with an average improvement of approximately 7.89%.

One particularly notable trend in these results is the relative change in losses between the uniform flow case and fully developed flow cases for the small scale models compared with the full size models. For the small scale models, when the inlet flow is fully developed the sum of the head losses increases. In the reverse, for the full size models, when the inlet flow is fully developed, the sum of head losses decreases, with the exception to this being the “3.5 Base Tunnel” design. This is a particularly interesting result that seems to imply that boundary layer development in the small scale models will result in flow separation and thus increased losses,

while for the full size models; this boundary layer will remain attached and result in reduced losses.

Finally, the general effects of diffuser length and aspect ratio on the reduction of losses will be considered. While there are not enough data points to infer any direct correlations, a general report on the effects of diffuser length and aspect ratio on the head losses can be given. **Figure 29** represents the full size models under uniform flow conditions (Personal Communications with Dr. Ölçmen, 2012).

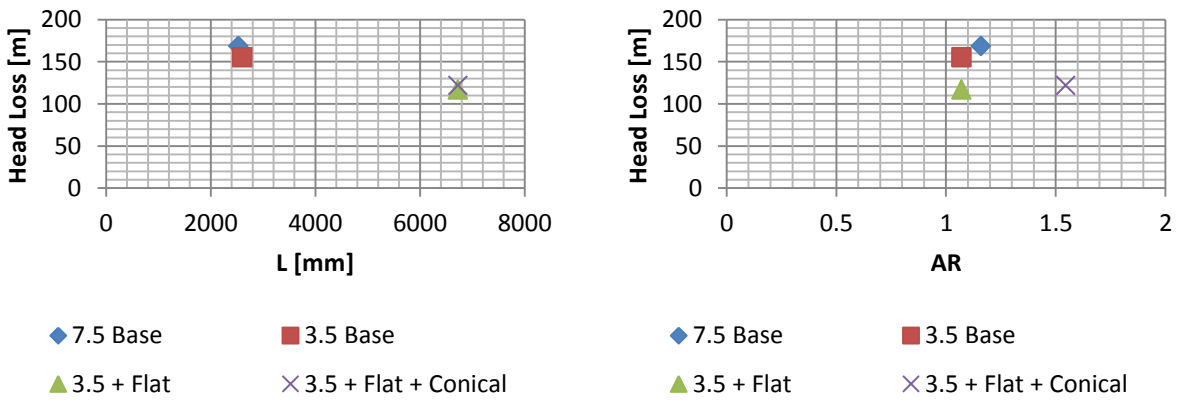

Figure 29 - Plots of Head Loss against Length and Aspect Ratio of Diffuser - Full Size - Uniform Flow

While the head losses for each model have been discussed previously, this provides a mean of observing the effects of diffuser length and aspect ratio on the head losses. Here, both models with an extended diffuser had reduced losses, with the effect of aspect ratio being dependent upon an increase in the length of the diffuser to reduce losses. Similar trends are also observed in the small scale uniform flow case, as shown in **Figure 30**.

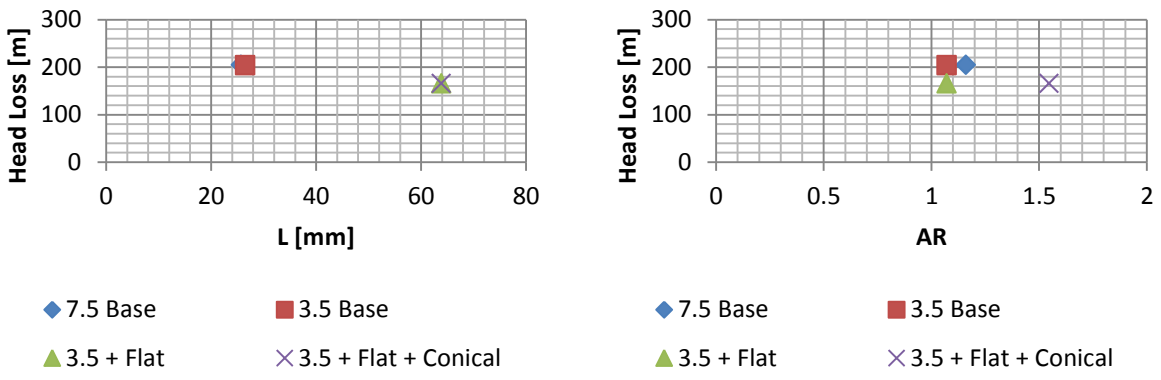

Figure 30 - Plots of Head Loss against Length and Aspect Ratio for Diffuser - Small Scale - Uniform Flow

Finally, considering the fully developed flow cases, similar trends of increasing length and aspect ratio leading to reduced losses can be observed, shown in **Figure 31** and **Figure 32**.

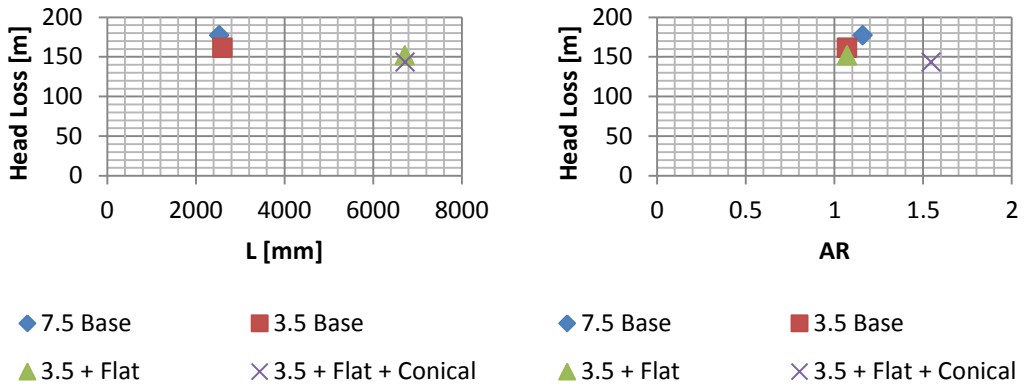

Figure 31 - Plots of Head Loss against Length and Aspect Ratio - Full Size – Fully Developed Flow

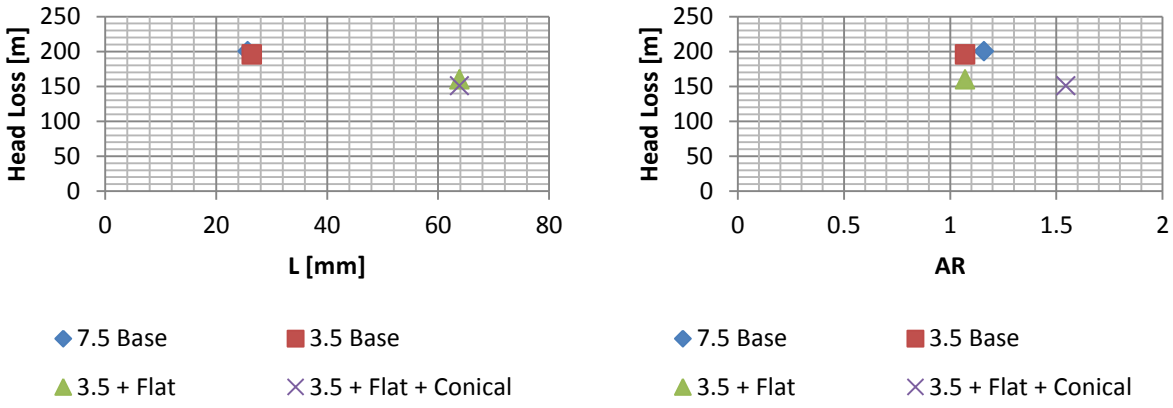

Figure 32 - Plots of Head Loss against Length and Aspect Ratio for Diffuser - Small Scale - Fully Developed Flow

4.2 ANSYS FLUENT Results

This section will discuss the results calculated by the ANSYS FLUENT solver. The small scale models will be considered first, then the full size models. Finally, the results for both the small scale and full size models will be compared, and the optimal diffuser geometry for minimizing losses will be determined.

Again, the primary variable of interest in these results is the total pressure of the flow. The total pressure distribution at the entrance of the tunnel is of greatest interest, as this defines the losses through the fan duct and diffuser. As the head losses are directly related to the change in the total pressure from the inlet to the exit of the diffuser, the total pressure distribution through the entire tunnel will be plotted, to visualize the possibility of effects such as separation of the flow. The results for the original tunnel configuration, the "7.5 Base Tunnel," are shown in **Figure 33**.

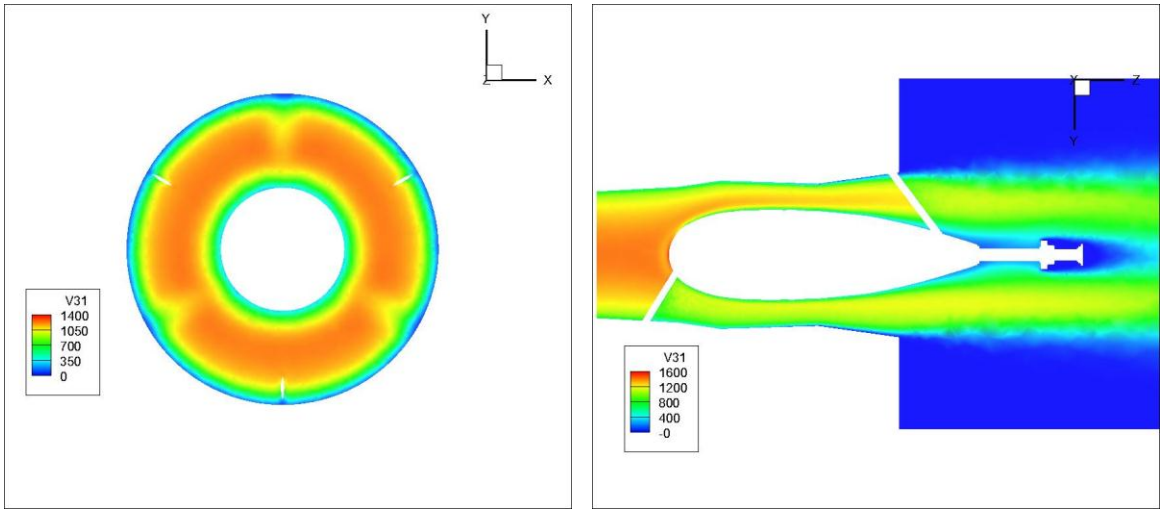

Figure 33 – ANSYS FLUENT Total Pressure Distribution through 7.5 Base Tunnel - Full Size - Uniform Flow

These contour plots, generated in TecPlot 360, are useful for visualizing the general ranges of total pressure existing through the tunnel. However, to visualize potential locations of flow separation and diffusion, contours of velocity distribution through the geometry are provided in **Figure 34**.

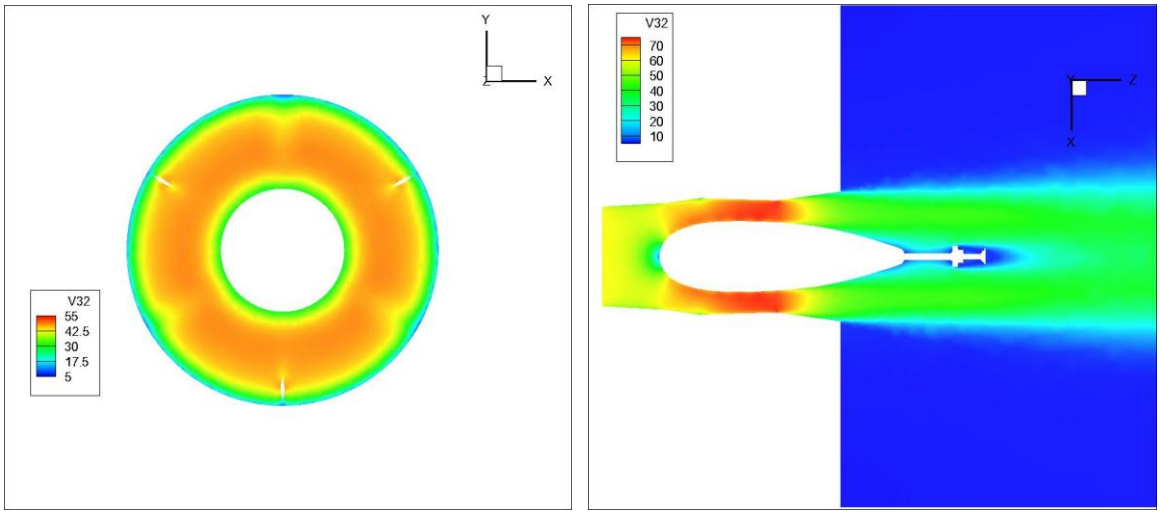

Figure 34 – ANSYS FLUENT Velocity Distribution through 7.5 Base Tunnel - Full Size - Uniform Flow

There are a few very small locations in which flow separation is occurring for this geometry. It can be seen that the flow does begin to slow significantly along the walls within the 7.5° angle diffuser section. However, the velocity distribution at the exit is otherwise generally uniform and symmetric. To compare this to the fully developed flow condition at the inlet, the distribution of the velocity through the model has been provided in **Figure 35**.

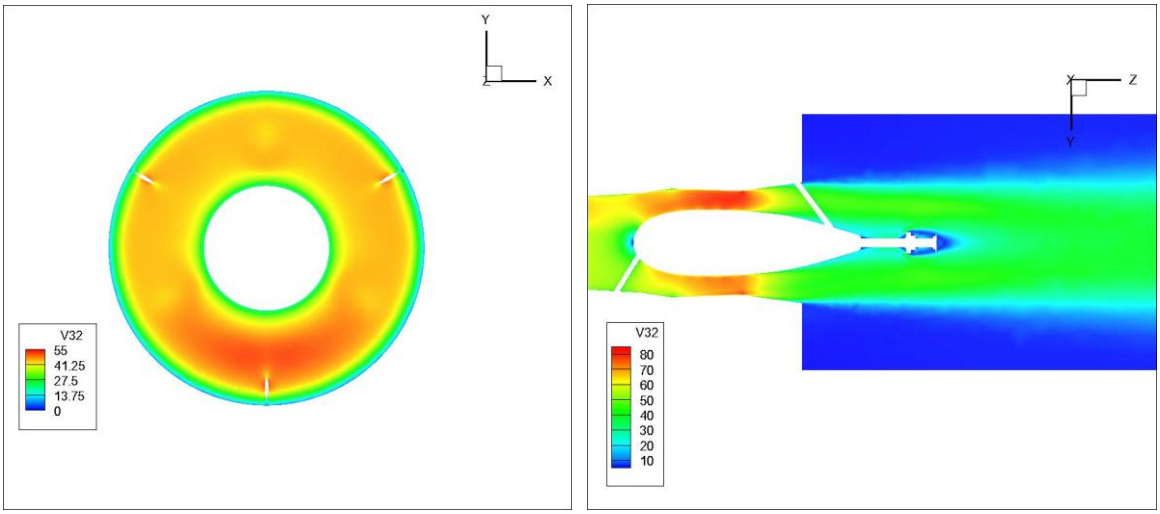

Figure 35 – ANSYS FLUENT Velocity Distribution through 7.5 Base Tunnel - Full Size - Fully Developed Flow

While the velocity distribution within the fan duct and diffuser does differ slightly from that of the uniform flow case, the velocity distribution at the exit does have one region of notable difference from the uniform case. While the velocity distribution at the exit of the 7.5 Base Tunnel for a fully developed flow is generally uniform between 240° and 60° from the top of the exit, it has a region of increased velocity along the bottom of the exit. This altered velocity distribution could be attributed to the flow remaining attached a greater distance for fully developed flow than for uniform flow within the diffuser, and without the interference of a support spar directly immediately upstream of the exit.

Next, the “3.5° Base Tunnel” geometry is considered. **Figure 36** represents the total pressure distribution through the model for the uniform inlet flow case, while the **Figure 37** represents the velocity distribution through the geometry.

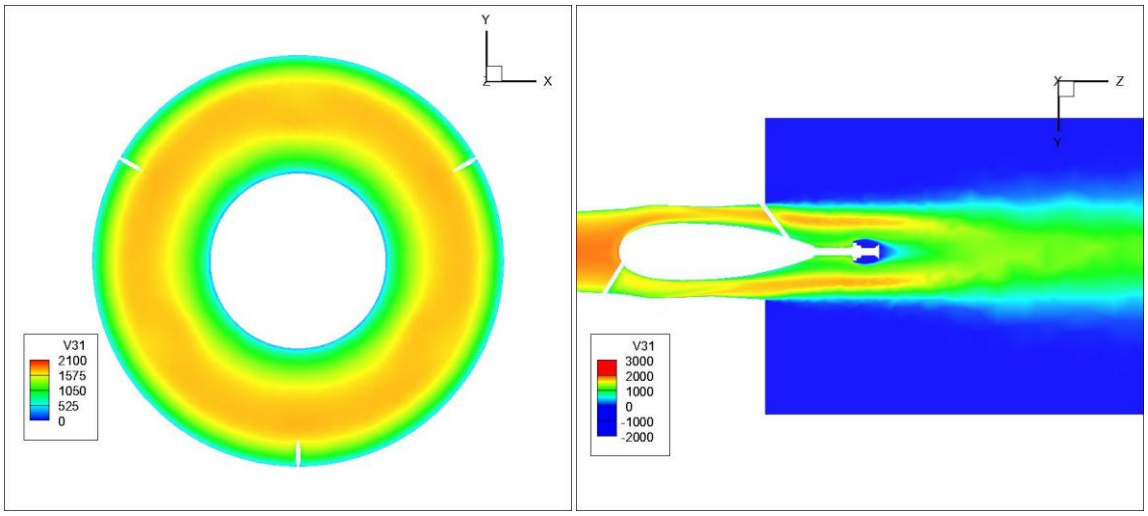

Figure 36 – ANSYS FLUENT Total Pressure Distribution through 3.5 Base Tunnel - Full Size - Uniform Flow

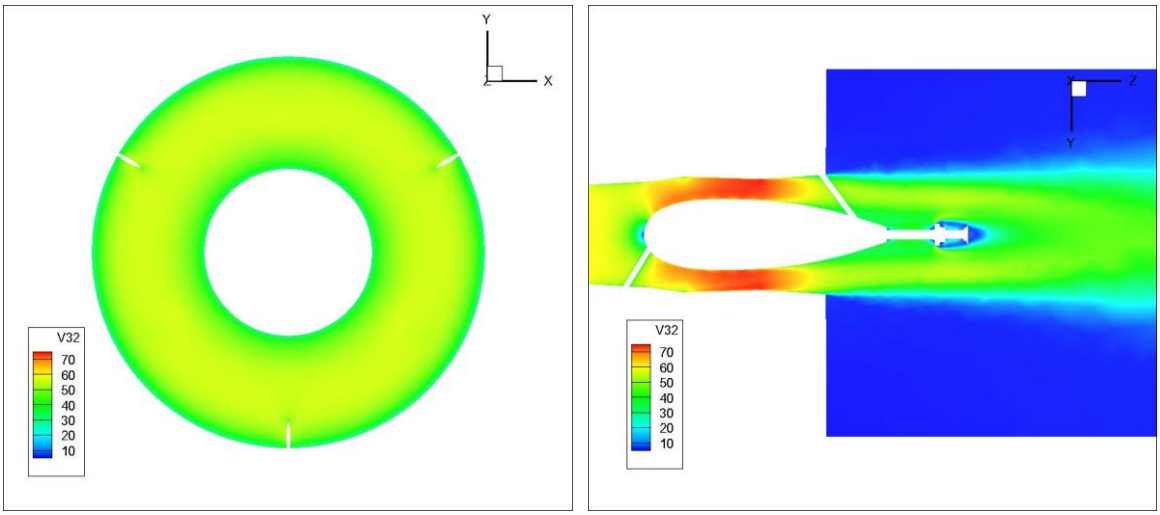

Figure 37 – ANSYS FLUENT Velocity Distribution through 3.5 Base Tunnel - Full Size - Uniform Flow

Compared to the distributions of total pressure and velocity observed in the "7.5 Base Tunnel" model, it seems that there is a greater degree of diffusion occurring in the flow near the exit of the "3.5 Base Tunnel" diffuser, which will likely lead to greater losses. To visualize the differences between the uniform flow and fully developed flow cases, **Figure 38** represents the velocity distribution through the full size "3.5 Base Tunnel" geometry for fully developed flow.

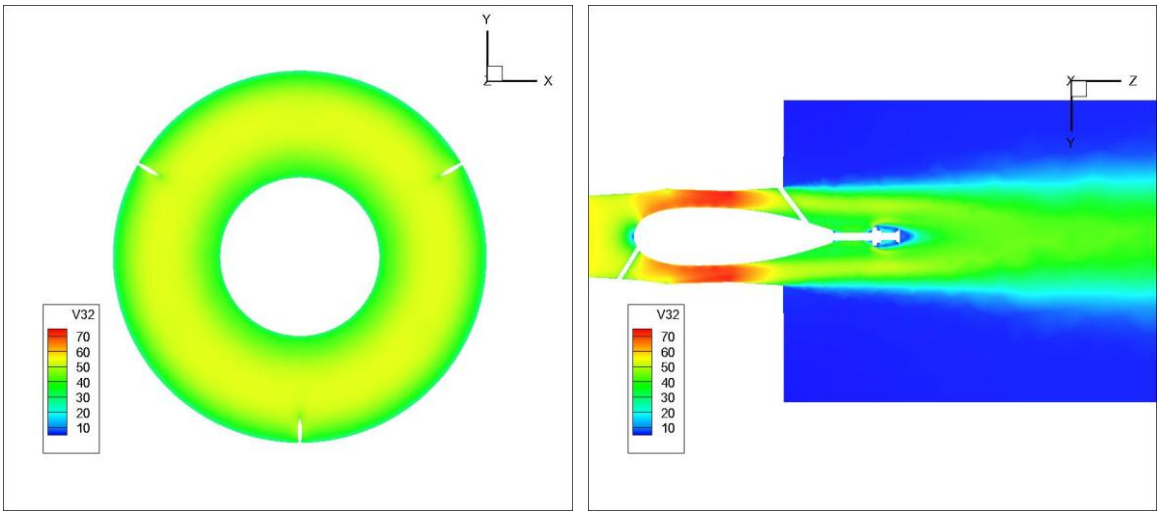

Figure 38 – ANSYS FLUENT Velocity Distribution through 3.5 Base Tunnel - Full Size - Fully Developed Flow

For both the uniform and fully developed flow cases, the flow travelling through the "3.5 Base Tunnel" geometry encounters the same diffusion as it nears the exit of the diffuser. As a result, it is likely that there will actually be greater losses associated with this diffuser geometry compared to that of the "7.5 Base Tunnel" configuration.

Similarly, a comparison of the total pressure and velocity distributions of the "3.5 + Flat" and "3.5 + Flat + Conical" models is necessary for comparison to the baseline geometry. **Figure 39** represents the total pressure distributions, while **Figure 40** represents the velocity distributions through the full size "3.5 + Flat" diffuser model under uniform flow conditions.

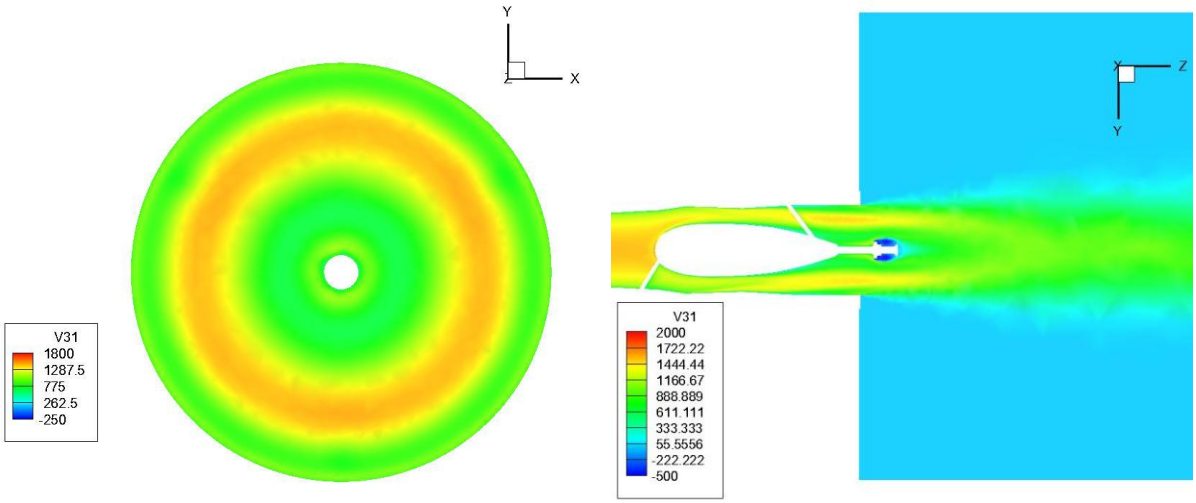

Figure 39 – ANSYS FLUENT Total Pressure Distribution through 3.5 + Flat - Full Size - Uniform Flow

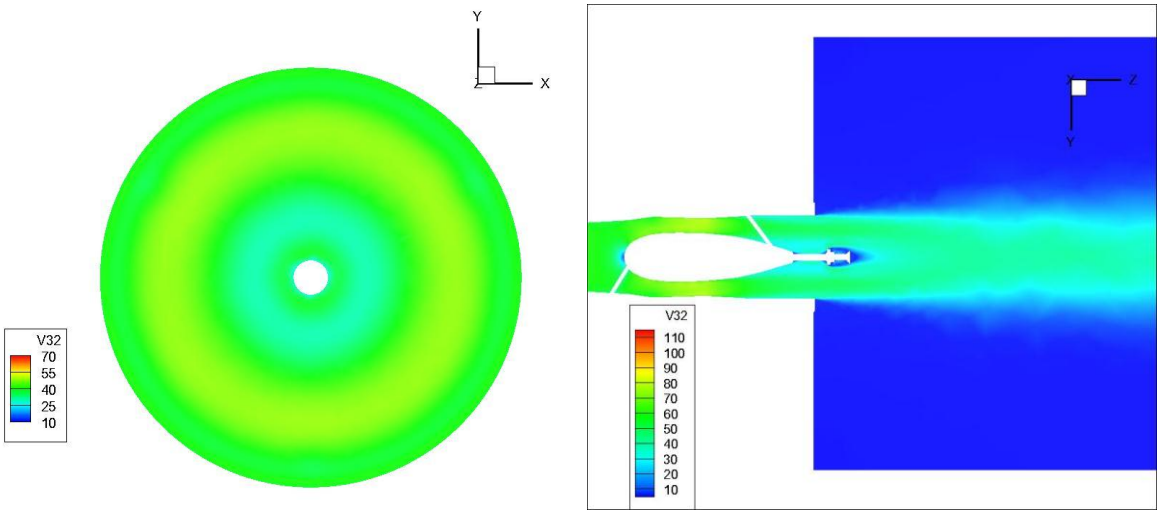

Figure 40 – ANSYS FLUENT Velocity Distribution through 3.5 + Flat - Full Size - Uniform Flow

Quickly looking at these figures, it can be seen that the velocity of the flow exiting the "3.5 + Flat" full size model is lower than that of the baseline geometry. In addition, the flow can be observed to slow following along the surface of the engine nacelle near the exit of the diffuser, compared to that of the "3.5 Base Tunnel," this reduction in velocity is not as pronounced, nor does it protrude into the flow. As a result, the losses associated with this geometry are likely to be lower than that of the baseline geometry, and the "3.5 Base Tunnel."

Figures 41 and 42 represent the total pressure and velocity distributions, respectively, of the full size "3.5 + Flat + Conical" diffuser geometry. As the SolidWorks previously predicted this geometry to offer the greatest percentage improvement in reduction of losses, it is expected that the velocity of the flow exiting this model will be the lowest of all four models.

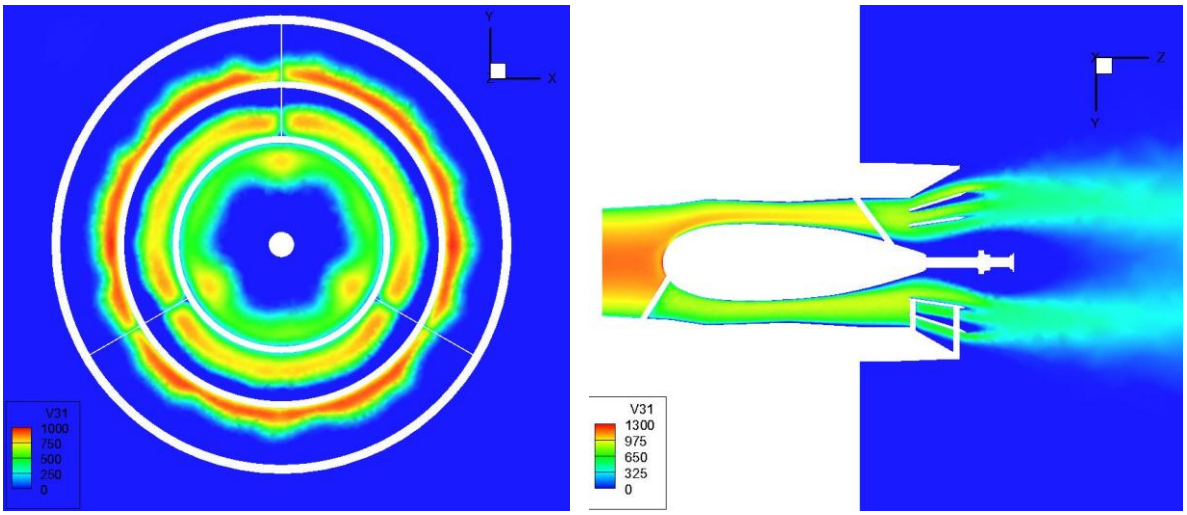

Figure 41 – ANSYS FLUENT Total Pressure Distribution through 3.5 + Flat + Conical - Full Size - Uniform Flow

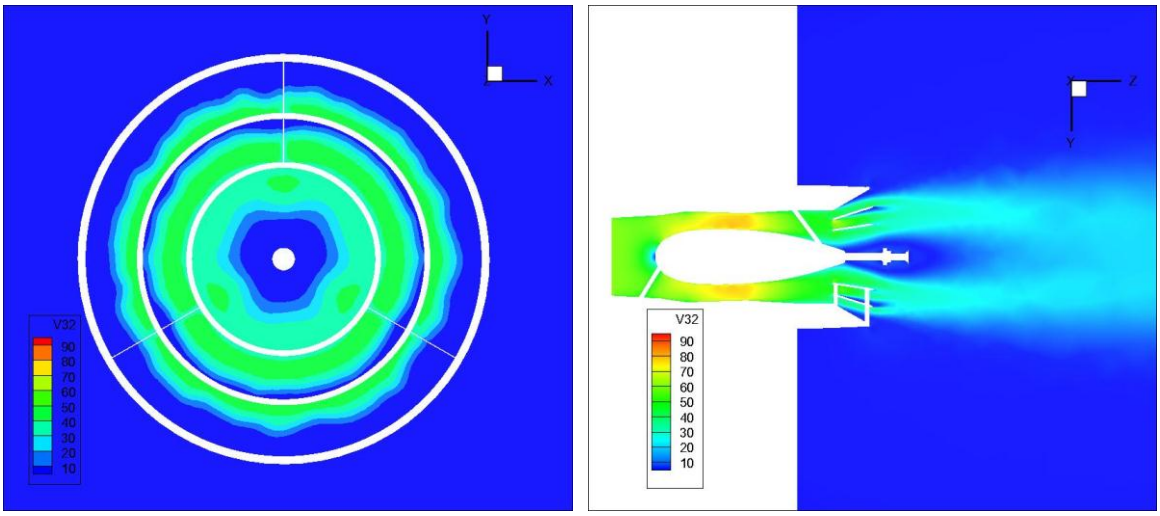

Figure 42 – ANSYS FLUENT Velocity Distribution through 3.5 + Flat + Conical - Full Size - Uniform Flow

The flow field associated with this geometry is particularly interesting. First, it should be noted that the total pressure exiting the diffuser is essentially at atmospheric conditions. Observing the velocity distribution through the cross-section of the model, the flow through the fan duct section is remarkably free of any kind of separation. Now, within the conical section region of the diffuser, flow separation occurs along the surfaces of the conical sections splitting the flow. The conical sections that are radially further from the center of the diffuser have the greatest level of separation occurring, while the middle sections have a lesser degree of flow separation occurring. In addition, the flow that is radially closest to the center of the diffuser is turned by the inner conical section, increasing the spreading rate of the jet exiting the tunnel. This has other potential benefits beyond simply pressure loss reduction. However, considering the total pressure distribution at the exit of this diffuser geometry, it is expected that the "3.5 + Flat + Conical" model will offer the greatest improvement in the reduction of losses. Additional contour plots of velocity, total pressure and static pressure for all models and boundary conditions tested can be found in Appendix C.

Now, compiling the head losses associated with the diffuser as calculated by Equations 4.1.1, 4.1.2 and 4.1.3, **Table 6** presents the head losses for each model considered in this research.

Table 6 - ANSYS FLUENT Head Losses by Diffuser Geometry

	Small Scale Models		Full Size Models	
	Uniform Flow	Fully Developed Flow	Uniform Flow	Fully Developed Flow
7.5 Base Tunnel	160.848472 m	126.8040263 m	113.0444985 m	106.2995676 m
3.5 Base Tunnel	198.9305041 m	159.0046268 m	153.7993301 m	136.1212656 m
3.5 + Flat	128.6798943 m	103.802302 m	108.2979733 m	94.53623618 m
3.5 + Flat + Conical	139.3758639 m	104.8927772 m	96.23651085 m	84.12098481 m

Upon initial inspection, it can be seen that for all cases, both full size and small scale, a fully developed inlet flow leads to a reduction in losses for the diffuser. This is quite different from the SolidWorks Flow Simulation results, which calculated that for the small scale models; fully developed flow would increase losses, while for the full size models it would decrease losses. In addition to this, there would appear to be a general correlation between the ratios of losses for the small scale full size models. To observe this, the ratios of small scale head losses over full size head losses have been compiled into **Table 7**.

Table 7 - ANSYS FLUENT Ratios of Small Scale Head Losses to Full Size Head Losses for Each Diffuser Geometry and Flow Type, $\frac{H_{L_{small}}}{H_{L_{full}}}$

	Uniform Flow	Fully Developed Flow
7.5 Base Tunnel	1.422877487	1.192893152
3.5 Base Tunnel	1.293441941	1.168110112
3.5 + Flat	1.188202238	1.098016022
3.5 + Flat + Conical	1.448263893	1.246927594

From **Table 7**, it can be seen that while an exact value relating the small scale model head losses to those of the full size models does not exist, a general range can be identified. For the uniform flow cases, the small scale models will generally have head losses approximately 1.2 to 1.4 times greater than those for the full size models. For the fully developed flow cases, the small scale cases will have head losses approximately 1.10 to 1.25 times greater than those for the full size models.

To more easily compare the reduction of losses associated with each diffuser model, the percentage improvement of each model relative to the "7.5 Base Tunnel" configuration has been compiled into **Table 8** below.

Table 8 - ANSYS FLUENT Percentage Improvement in Losses from 7.5 Base Tunnel Configuration

	Small Scale Models		Full Size Models	
	Uniform Flow	Fully Developed Flow	Uniform Flow	Fully Developed Flow
3.5 Base Tunnel	-23.6757189	-25.39398899	-36.05202564	-28.05439255
3.5 + Flat	19.99930573	18.13958513	4.198811322	11.06620818
3.5 + Flat + Conical	13.34958788	17.2796162	14.86847029	20.86422675

From these results, it can be seen that for the full size models, the "3.5 + Flat + Conical" diffuser geometry offers the greatest improvement to reducing losses. As the exact nature of the flow entering the fan duct is not known, the actual improvement will exist somewhere between the fully developed flow and uniform flow cases. Thus, the optimum improvement that could be seen by using the "3.5 + Flat + Conical" geometry for the full size tunnel would exist somewhere between 14.87% and 20.86%. Considering the entire tunnel, this translates to approximately a 5.20% to 7.30% improvement, with an average approximate improvement of 6.25%. The "3.5 + Flat" geometry also offer an improvement range of 4.20% to 11.07%, or 1.47% to 3.87% range for the entire tunnel, which, while not as efficient as the "3.5 + Flat + Conical" geometry, does offer an improvement. However, the "3.5 Base Tunnel" geometry actually increases the losses through the diffuser. This is most likely due to the separation noticed in the contour plots shown previously. Had this diffuser been extended, similar to the "3.5 + Flat" model, such flow separation would likely have been eliminated, making such a geometry viable. As a result, if the

base geometry was changed to include this new inclination angle of 3.5°, it would be necessary to implement one of the other two diffuser geometries to obtain improvement. This is an unusual result, as the results obtained by Sovran and Klomp (1963) would imply that this inclination angle would result in a more efficient diffuser design.

For the small scale models, a different trend is noticed. The "3.5 + Flat" diffuser geometry is actually the most efficient, offering a 18.4% to 20.0% improvement in the reduction of losses. This would prove misleading when using the small scale models in experimental testing, as while the "3.5 + Flat + Conical" is actually the most efficient for the full size tunnel; such a result would not be obtained. However, the "3.5 + Flat + Conical" design still offers an improvement to the pressure recovery across the diffuser for the small scale case. Finally, similar to the full size geometry, the "3.5 Base Tunnel" design results in an increase in losses. Thus, the recommendation from the ANSYS FLUENT results is that the "3.5 + Flat + Conical" diffuser geometry is optimal for pressure recovery in the full size tunnel, while results for the small scale experimental model would tend to indicate that the "3.5 + Flat" geometry is optimal. The "3.5 Base Tunnel" geometry results in an increase in losses, for both the full size and small scale geometries.

Finally, the impact of the length and aspect ratio of the diffusers on the head losses is considered. **Figures 33 and 34** show the head loss of the diffuser geometries with respect to their respective lengths and aspect ratios.

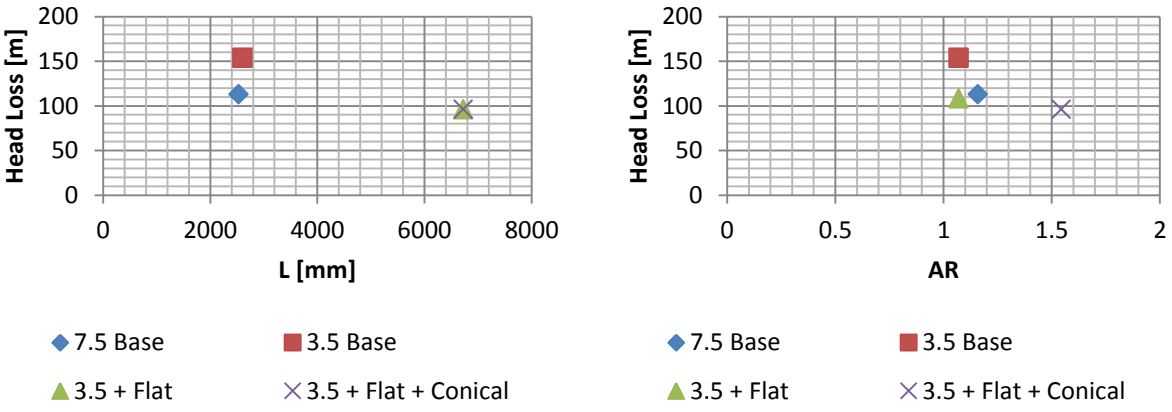

Figure 43 – ANSYS FLUENT Plots of Head Loss against Length and Aspect Ratio of Diffuser – Full Size – Uniform Flow

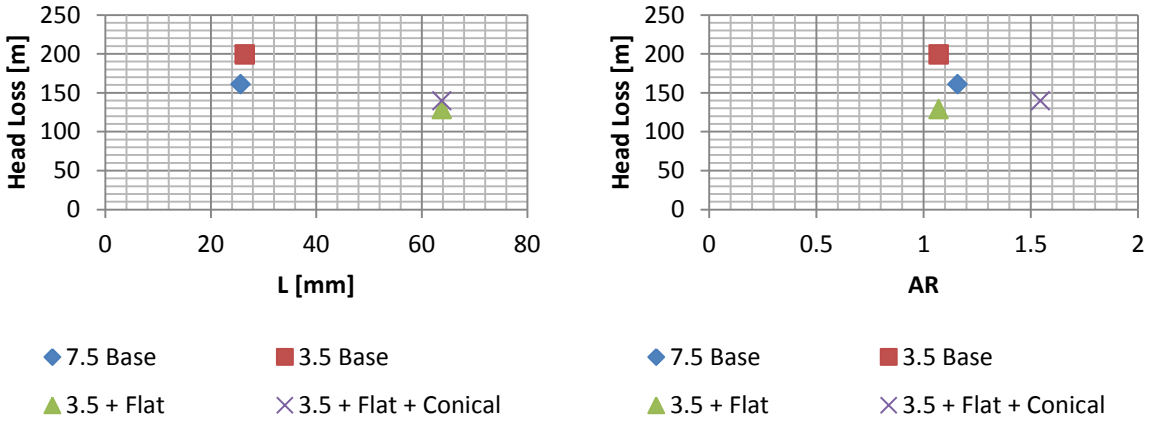

Figure 44 – ANSYS FLUENT Plots of Head Loss against Length and Aspect Ratio of Diffuser - Small Scale - Uniform Flow

As was seen in the SolidWorks Flow Simulation results, both of the extended diffusers had reduced head losses. However, the effects of aspect ratio on the reduction of losses are dependent upon the length of the diffuser to be effective. the losses are also decreased. These results are also similarly observed in the fully developed flow cases, shown in **Figures 45 and 46**.

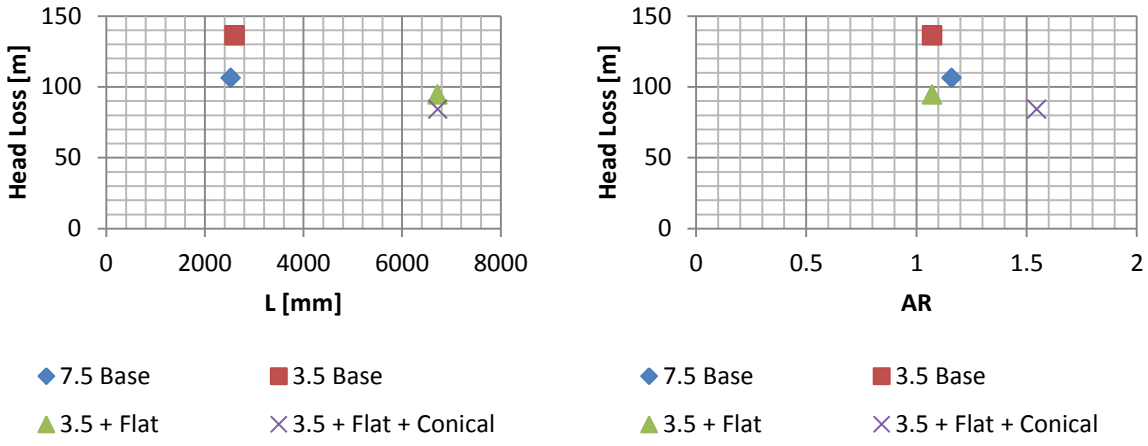

Figure 45 – ANSYS FLUENT Plots of Head Loss against Length and Aspect Ratio of Diffuser - Full Size - Fully Developed Flow

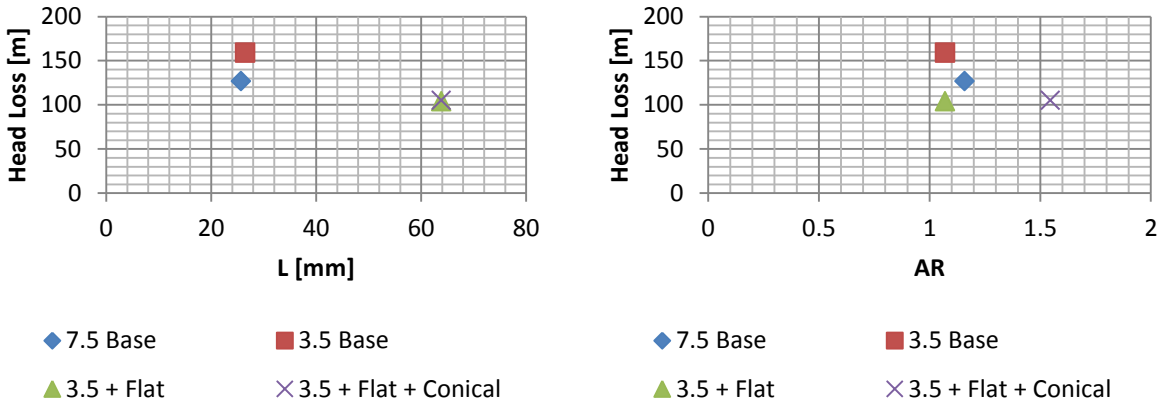

Figure 46 – ANSYS FLUENT Plots of Head Loss against Length and Aspect Ratio of Diffuser - Small Scale - Fully Developed Flow

4.3 Comparison of SolidWorks Flow Simulation and ANSYS FLUENT Results

While the main objective of this research was to identify the diffuser geometry offering the greatest reduction in pressure losses, it was also of interest to evaluate the differences between the two CFD solvers used. SolidWorks Flow Simulation is a very user-friendly solver that allows for the application of goals and boundary conditions through the use of the graphical UI. It can obtain numerical solutions for the flow field of a computational domain in a very short amount of time, with most run times spanning from as little as two minutes, to a maximum of one hour for this research. ANSYS FLUENT, on the other hand is not quite as user-friendly; there is a learning curve associated with the solver. However, FLUENT allows for greater control over the methods used to obtain the numerical solutions for fluid flow problems. It allows for far greater control of the mesh design as well, which is primarily responsible for the accuracy

of the solution. However, FLUENT computations require far greater processing power and CPU time to complete. Without access to a minimum of 8 GB of RAM, the computations would not have been capable of initializing. Furthermore, the time necessary to complete some of the computations in this research could take anywhere from two hours at the minimum, to over nine days at the maximum. With these considerations in mind, it would be more efficient to perform future computations using SolidWorks Flow Simulation due to lower computational expense. However, the SolidWorks solution must be accurate as well. As ANSYS FLUENT is considered a standard CFD solver, and makes use of greatly refined meshes, its results will be considered the "correct" results for the sake of comparison, due to the lack of experimental results to compare against. **Table 9** presents a relative percentage comparison of head losses between ANSYS FLUENT and SolidWorks Flow Simulation.

Table 9 - Relative Percentage Comparison of Head Losses for ANSYS FLUENT and SolidWorks Flow Simulation, $\frac{H_{L_{FLUENT}} - H_{L_{SolidWorks}}}{H_{L_{FLUENT}}}$

	Small Scale Models		Full Size Models	
	Uniform Flow	Fully Developed Flow	Uniform Flow	Fully Developed Flow
7.5 Base Tunnel	-26.90413059	-57.83611033	-49.16114666	-66.53203598
3.5 Base Tunnel	-2.50358824	-22.80299942	-1.04010214	-18.37781546
3.5 + Flat	-28.70403953	-53.70186854	-7.854827204	-60.26992719
3.5 + Flat + Conical	-18.66862492	-43.4047791	-26.75372941	-70.06354289

It is evident that in every case, the head losses calculated by ANSYS FLUENT are notably lower than those calculated by SolidWorks Flow Simulation. The variation in the percentage difference between the two solver solutions varies widely by diffuser geometry and flow type. Of particular note, the percentage difference in head losses for the models with a fully developed turbulent flow inlet condition is remarkably high. At the lowest, there is an 1.04% difference between the full size "3.5 Base Tunnel" geometry with uniform flow, while at the highest, there is a 70.06% difference between the full size "3.5 + Flat + Conical" geometry with fully developed flow. Such a large difference in calculated head losses between ANSYS FLUENT and SolidWorks is alarming. The most likely cause for such a large disparity between the solutions obtained by the two solvers is the difference in the refinement of the meshes for each solver. Appendix A contains full information containing the number of elements used in each mesh. To briefly summarize this information, the number of elements in the ANSYS FLUENT meshes was on the order of 10^6, while the number of elements in the SolidWorks Flow Simulation meshes was on the order of 10^4 or 10^5. The impact of this refinement can be further seen by comparing the total pressure distribution at the exit along the vertical centerline and total pressure contours at the exit of the diffusers, such as for the full size "7.5 Base Tunnel" geometry, shown in **Figures 47 and 48**, respectively.

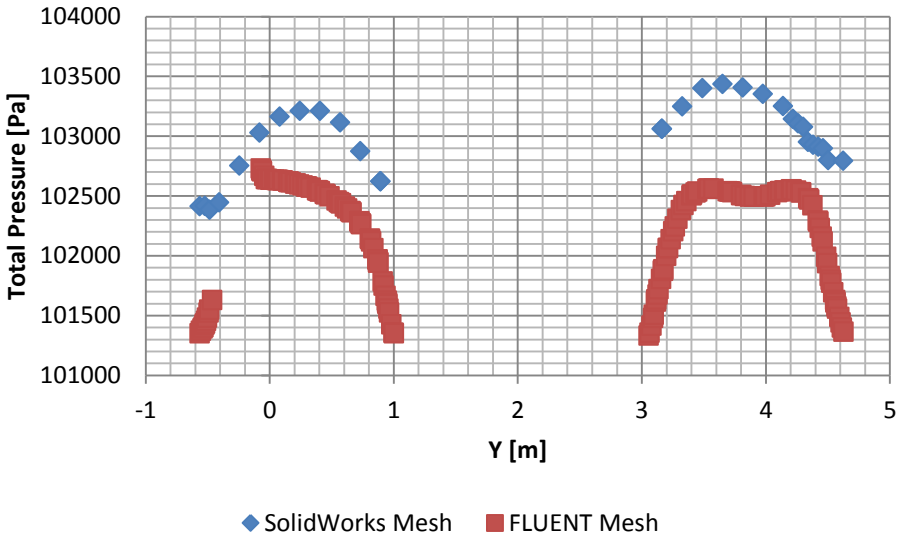

Figure 47 - Comparison of Total Pressure Distribution at 7.5 Base Tunnel Exit along Centerline for ANSYS FLUENT and SolidWorks Flow Simulation – Full Size – Uniform Flow

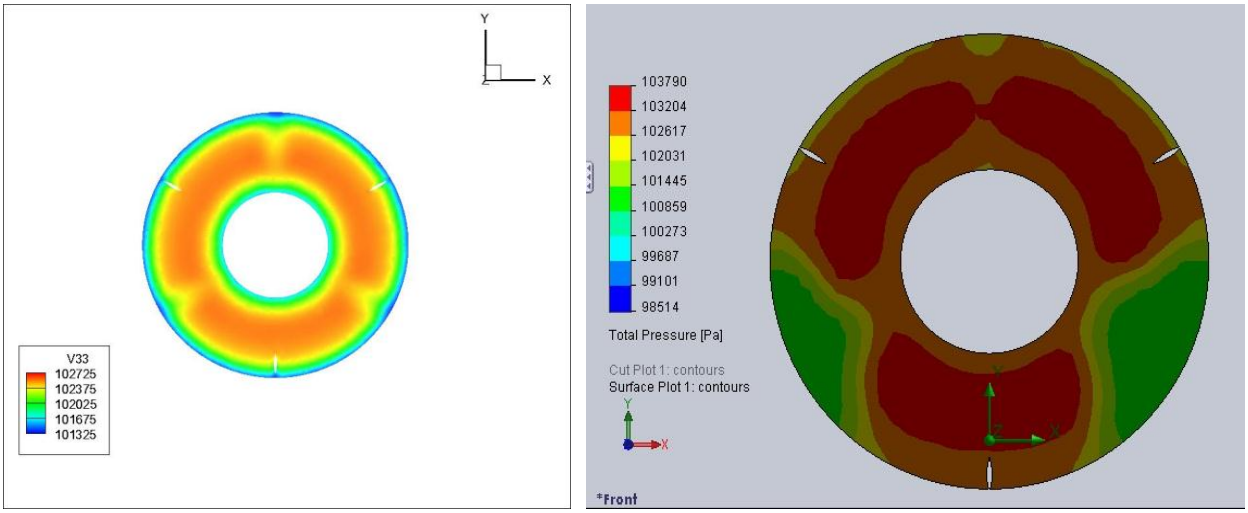

Figure 48 - Comparison of Total Pressure Contours at 7.5 Base Tunnel Exit - Full Size - Uniform Flow, ANSYS FLUENT Total Pressure (Left) and SolidWorks Flow Simulation Total Pressure (Right)

It can be seen that the total pressure distributions calculated by the two solvers vary greatly. SolidWorks Flow Simulation calculated two regions of flow separation at the exit of the diffuser, while ANSYS FLUENT did not. In addition, the total pressure distribution at the exit of the diffuser is closer to uniform for ANSYS FLUENT, when compared to the distribution observed in the SolidWorks Flow Simulation solver. For reference, the number of elements in the mesh used for SolidWorks Flow Simulation was 37997, while the number of elements in the mesh used for ANSYS FLUENT was 7855771. The plot of the total pressure distribution across the centerline of the diffuser exit reveals differences in the general trend of the total pressure

distribution in that region by solver as well. SolidWorks Flow Simulation calculated two parabolic regions, while ANSYS FLUENT calculated two generally parabolic regions, but with a lack of data associated with a spar supporting the engine nacelle intersecting with the computational domain, and with a region of decreased total pressure near the center of the flow along the top of the diffuser. During the grid independence study for ANSYS FLUENT for this particular model, shown in **Figure 15**, it was observed that similar trends in the total pressure distribution to that calculated by SolidWorks Flow Simulation, shown in **Figure 14**, occurred in the coarser meshes. This may indicate that the mesh used in SolidWorks Flow Simulation was not refined enough to consider the complexity of the geometry, nor all of the effects of the smaller turbulent eddies within the flow.

It was later determined that the root cause of this incorrect mesh independence observed in SolidWorks at Mesh Level 6 in each case was a result of how the nature of these levels changed within SolidWorks. While levels 3, 4 and 5 all do refine the mesh, going from Mesh Level 5 to 6, and from 6 to 7 does not actually result in further mesh refinement. Instead, the SolidWorks mesh generator selects a different algorithm for mesh generation. (Baker, 2012) The result of this unintuitive change in meshing caused essentially a “false positive” in the grid independence scheme. Had this been discovered in documentation prior, mesh refinement would have continued to Mesh Level 8, with additional refinement as necessary. This error resulted in solutions that were not grid independent, and thus cannot be used to properly compare ANSYS FLUENT to SolidWorks Flow Simulation.

CHAPTER 5

CONCLUSIONS

5.1 Conclusions

The primary goal of this research was to identify the diffuser geometry with the greatest reduction in pressure losses for the AFRL SARL tunnel. Previous analysis performed on the tunnel (Britcher, 2011), indicated that significant pressure recovery could be obtained by improving the diffuser geometry at the exit of the SARL tunnel. A wide variety of diffusers of varying shapes and sizes were evaluated in a preliminary computational study using SolidWorks Flow Simulation (Ölçmen, 2011), and two diffuser geometries were identified to provide optimal pressure recovery. These two geometries were evaluated, along with the original SARL diffuser and a modified version of the original SARL diffuser with reduced inclination angle, using the CFD software packages: SolidWorks Flow Simulation and ANSYS FLUENT. Both solvers used the standard k-ε turbulence model in calculating the solution for the flow field given a 60 m/s inlet velocity for both uniform flow and fully developed turbulent flow. Both full size models and small scale experimental models were evaluated. In addition, it was also of interest to determine the relative differences between the solutions obtained by SolidWorks Flow Simulation and ANSYS FLUENT, as ANSYS FLUENT is typically considered a standard CFD software package. Due to the reduced computational expense afforded by SolidWorks Flow

Simulation, it would be worthwhile to determine if its solution is within 10% of the solution obtained by ANSYS FLUENT for future computational studies.

To properly evaluate the calculated losses associated with each design, both a fully developed turbulent inlet velocity and uniform inlet velocity was applied to each model, as the exact nature of the flow in the SARL tunnel as this location is not known. However, the flow will range anywhere between these two cases, thus the losses of each design will represent the actual losses for the SARL tunnel within the range of losses calculated for the uniform and fully developed flow cases.

To determine the optimal diffuser geometry, the three modified diffuser geometries were compared against the original SARL diffuser geometry. Both the SolidWorks Flow Simulation and ANSYS FLUENT solutions identified that the "3.5 + Flat + Conical" diffuser geometry offered the greatest reduction in pressure losses, with SolidWorks calculating 19.19% to 27.66% improvement for the full size model, and ANSYS FLUENT calculating 14.87% to 20.86% improvement. When considering the improvement for the entire SARL tunnel, these ranges are approximately 6.72% to 9.68% from SolidWorks Flow Simulation and 5.20% to 7.30% from ANSYS FLUENT. The "3.5 + Flat" geometry also offered improvement in the reduction of losses, with SolidWorks calculating 14.41% to 30.73% improvement, while ANSYS FLUENT calculated 4.20% to 11.07% improvement. Considering the improvement for the entire SARL tunnel, these ranges are approximately 5.04% to 10.76% improvement from SolidWorks Flow Simulation and 1.47% to 3.77% improvement from ANSYS FLUENT. SolidWorks calculated

that the “3.5 Base Tunnel” geometry would offer minimal improvements, while ANSYS FLUENT calculated that this geometry would actually increase the losses, possibly due to the growth of the turbulent boundary layers observed in those calculations.

A comparison of the SolidWorks Flow Simulation and ANSYS FLUENT solvers was compiled for each model and case considered in this research. Using the head loss calculated for each model and inlet flow type, the percentage difference between the solution calculated by SolidWorks Flow Simulation and ANSYS FLUENT was found for each case. Unfortunately, it was not found that the percentage difference between the results obtained by the two solvers was less than or equal to 10% on average. Instead, the percentage difference varied widely by geometry and inlet flow type. The smallest percentage difference was 1.04% for the full size “3.5 Base Tunnel” geometry with uniform flow, while the greatest percentage difference was 70.06% for the full size “3.5 + Flat + Conical” geometry with fully developed flow. In general, the percentage difference for most cases was well above 10%, and thus, the SolidWorks Flow Simulation likely did not take into account some of the small intricacies of neither the diffuser geometries, nor the smaller turbulent eddies that exist within the flow. This conclusion was made through the observation of the refinement of the grid independent meshes obtained for both SolidWorks Flow Simulation and ANSYS FLUENT. FLUENT used meshes on the order of 10^6 elements, while SolidWorks Flow Simulation used meshes on the order of 10^4 and 10^5 elements. The huge difference in the refinement of these meshes was later discovered to be due to how Mesh Levels 5, 6 and 7 do not offer any refinement relative to one another, and is the primary cause for the differences in the solutions obtained by each of the solvers, as grid independence

was falsely obtained as a result. (Baker, 2012) Thus, the SolidWorks solutions do not offer a truly grid independent solution to the problem.

To answer the primary question addressed in this study, the optimal diffuser geometry for the full size SARL tunnel in the reduction of pressure losses was the "3.5 + Flat + Conical" diffuser geometry. The calculated percentage improvement in the reduction of head losses for this model were calculated to range from 14.87% to 20.86% over the current diffuser geometry implemented on the SARL tunnel. For the entire SARL tunnel, this translates to approximately a 5.20% to 7.30% improvement. Thus, a significant improvement in improving the efficiency of the SARL tunnel can be accomplished through the use of this improved diffuser geometry.

5.2 Future Work

This computational analysis can be extended to consider another improvement parameter as well. The Air Force is also interested in the possibility of reducing the aeroacoustic jet noise generated by running the SARL tunnel. However, CFD analysis of aeroacoustic jet noise would require large and long-term unsteady calculations (Kudo et al., 2009). However, using the ANSYS FLUENT CFD solver, the spreading of the flow exiting the diffuser could be calculated for various diffuser geometries, such as those considered in this research. This is of interest to reducing noise generation, as the nature of the velocity profile of the jet flow exiting the diffuser is related to the production of jet noise. "Normal" velocity profiles, where the inner jet has higher velocity, are noisier than "inverted" velocity profiles, where the inner jet has a lower velocity (Zaman, K et al., 2005).

Most importantly, however, an experimental analysis of the small scale models considered in this study is of utmost importance. This will allow for experimental verification of the computational results obtained in this research. These small scale models can be fabricated using a 3D printer, as the small scale models use enlarged support spars to allow for this fabrication. Velocity and static pressure measurements taken at the inlet and outlet of these models would allow for the calculation of head losses. To apply this experimental study to the full size models, the head losses calculated by ANSYS FLUENT for the full size and small scale models can be related, and used as a method for comparison to the full size tunnel. This will allow for an estimate of the actual losses that would be observed in application to the SARL tunnel.

REFERENCES

--, "Subsonic Aerodynamic Research Laboratory", Wright-Patterson Air Force Base, WL-TR-3053, Wright-Patterson AFB, Cleveland, OH, 1992.

--, "COSMOS 2008: COSMOSFloWorks Fundamentals", Penn State Personal Web Server: Jeremy Alan Hall [online], URL: http://www.personal.psu.edu/jah5420/Misc/SolidWorks/COSMOSFloWorks/FloWorks/lang/english/Docs/Fundamentals.pdf, Accessed 5/21/12.

--, "ANSYS 12.0: ANSYS FLUENT Theory Guide", SharcNet [online], URL: https://www.sharcnet.ca/Software/Fluent12/html/th/node3.htm

--, "Entrance Length and Developed Flow", Engineering Toolbox [online], URL: http://www.engineeringtoolbox.com/entrance-length-flow-d_615.html, Accessed: 3/22/12.

Britcher, Colin P., "Analysis of the AFRL SARL facility drive system", Old Dominion University, Department of Mechanical and Aerospace Engineering, Norfolk, VA, 2011.

Eckert, W.T., Mort, K.W., Jope, J., "Aerodynamic Design Guidelines and Computer Program for Estimation of Subsonic Wind Tunnel Performance", Ames Research Center and U.S. Army Air Mobility R&D Laboratory, NASA TN D-8243, Moffett Field, CA, 1976.

Farokhi, S., *Aircraft Propulsion*, John Wiley & Sons, Hoboken, NJ, 2009, pp. 227-235.

Hoffman, K.A., Chiang, S. T., *Computational Fluid Dynamics for Engineers – Volume I*, The Wichita State University, Wichita, Kansas, 1993.

Kudo, T., Maeda, K., Nishimura, M., "Techniques of Reducing Aerodynamic Noises in 3/4 Open-Jet Wind Tunnels", Journal of Environment and Engineering, Volume 4, No. 2, 2009, pp. 276 – 288.

Launder, B.E., Spalding, D.B., "The Numerical Computation of Turbulent Flows", Computer Methods in Applied Mechanics and Engineering, Volume 3, Issue 2, 1974, pp. 269-289.

Lefebvre, A. H., *Gas Turbine Combustion 2nd Edition.*, Taylor & Francis, Philadelphia, PA, 1999, pp. 77-78.

Mehta, R.D., "The Aerodynamic Design of Blow Tunnels with Wide-Angle Diffusers", *Progress in Aerospace Sciences*, Volume 18, 1977, pp. 59-120.

Nunn, R., *Intermediate Fluid Mechanics*, Hemisphere Publishing Corporation, New York, NY, 1989, pp. 167-178.

Ölçmen, S. M., "SARL Efficiency Improvement and Noise Reduction", Final Report as Summer Research Faculty supplied to WPAFB in Dayton, OH, 2011.

Schmidt, J., (May 19, 1989 data appended to:) Analysis of the Langley Eight-Foot Transonic Wind Tunnel Fan to be Used as the Drive Fan in the SARL Wind Tunnel, 1986.

Townsend, A.A., *The Structure of Turbulent Shear Flow*, Cambridge University Press, Cambridge, MA, 1976, p. 176.

Tu, J., Yeoh, G.H., Liu, C., *Computational Fluid Dynamics: A Practical Approach*, Elsevier, Oxford, UK, 2008.

Wang, T., "Multidimensional Unstructured-Grid Liquid Rocket Engine Nozzle Performance and Heat Transfer Analysis", AIAA-2004-4016, Huntsville, AL, 2004.

Wyman, N., "State of the Art in Grid Generation", CFD Review [online], URL: http://www.cfdreview.com/article.pl?sid=01/04/28/2131215, Accessed 5/23/12.

Zaman, K., Dahl, M., "Noise and Spreading of a Subsonic Coannular Jet – Comparison with Single Equivalent Jet", *43rd AIAA Aerospace Sciences Meeting and Exhibit*, AIAA-2005-0210, Reno, Nevada, 10-13 January 2005.

Personal Communication with Dr. Ölçmen, The University of Alabama, Tuscaloosa, AL, 2012.

Personal Communication with Dr. Baker, The University of Alabama, Tuscaloosa, AL, 2012.

APPENDIX A

GRID SETTINGS INFORMATION

SolidWorks Flow Simulation Grid Information

Table 10 – Mesh Information for SolidWorks Flow Simulation Models

		Total Cells	Fluid Cells	Solid Cells	Partial Cells	Trimmed Cells
7.5 Base Tunnel						
	Full Size	37997	19249	7766	10982	36
	Small Scale	39530	19794	7984	11752	10
3.5 Base Tunnel						
	Full Size	42814	23001	7609	12204	16
	Small Scale	104799	44573	24749	35477	82
3.5 + Flat						
	Full Size	98560	47090	21183	30287	44
	Small Scale	108850	49606	23917	35327	58
3.5 + Flat + Conical						
	Full Size	376497	210674	63084	102739	377
	Small Scale	115789	51346	23409	41034	209

Table 11 – Mesh Information for ANSYS FLUENT Models

		Number of Elements
7.5 Base Tunnel		
	Full Size	7855771
	Small Scale	6626599
3.5 Base Tunnel		
	Full Size	5811026
	Small Scale	4481456
3.5 + Flat		
	Full Size	6923648
	Small Scale	6759344
3.5 + Flat + Conical		
	Full Size	4670587
	Small Scale	5244412

SolidWorks Flow Simulation Grid Independence Results

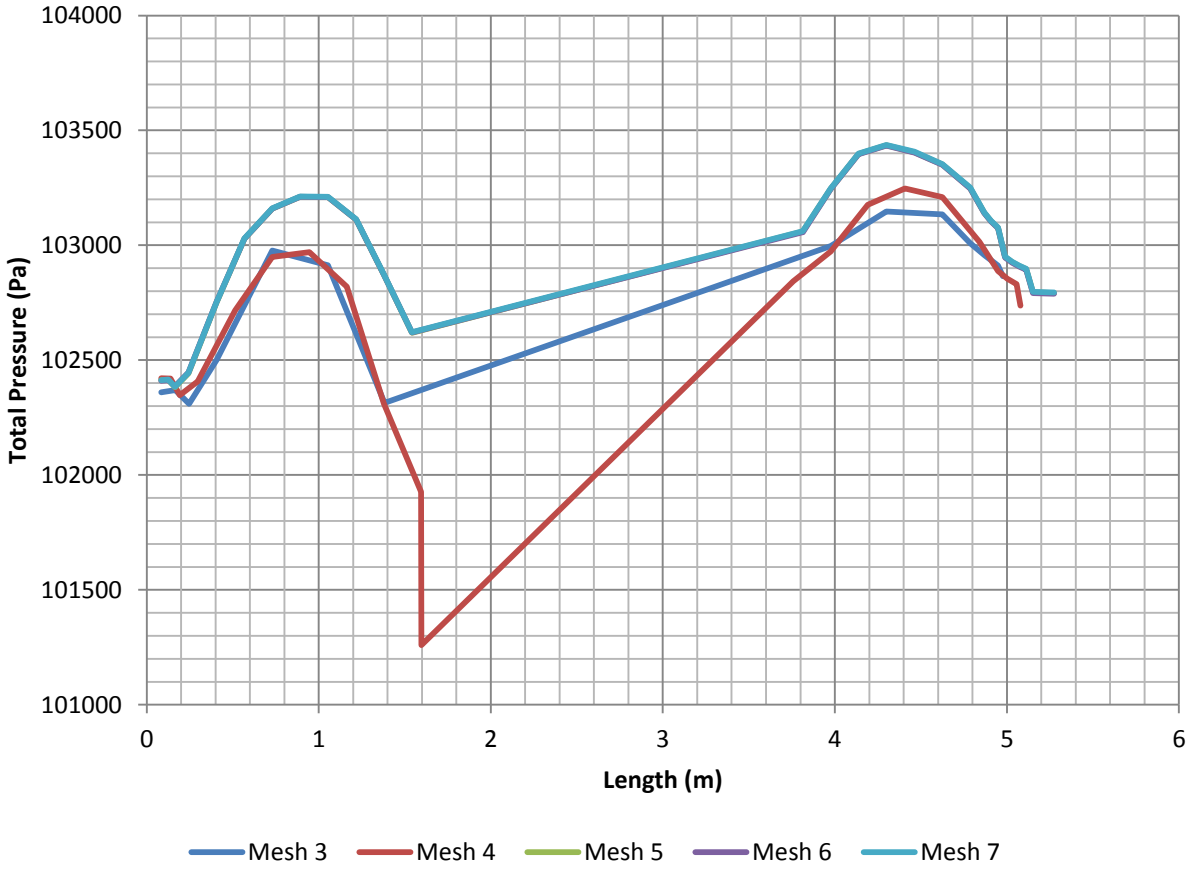

Figure 49 - SolidWorks Flow Simulation Grid Independence Study using Total Pressure Distribution at Diffuser Exit along Y Mid-Plane for 7.5 Base Tunnel - Full Size

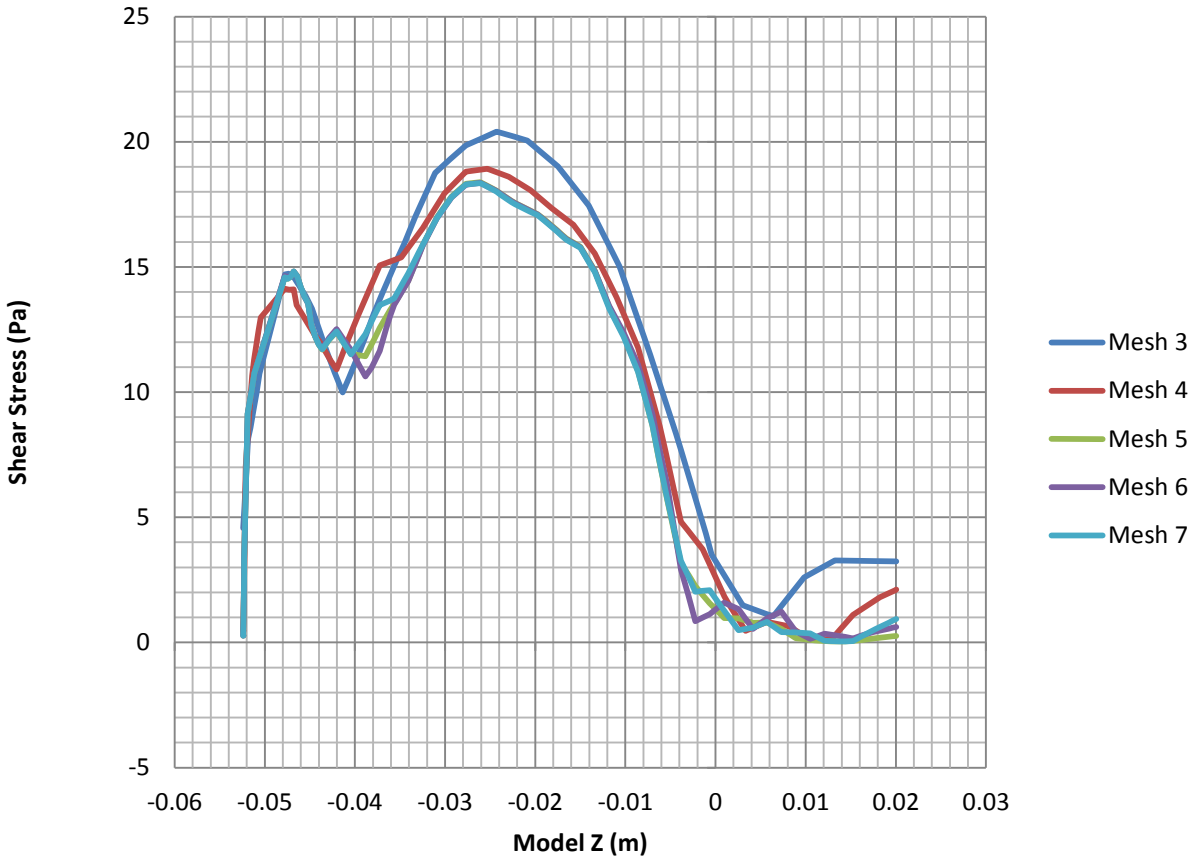

Figure 50 - SolidWorks Flow Simulation Grid Independence using Shear Stress along Top Surface of Engine Nacelle for 7.5 Base Tunnel - Small Scale

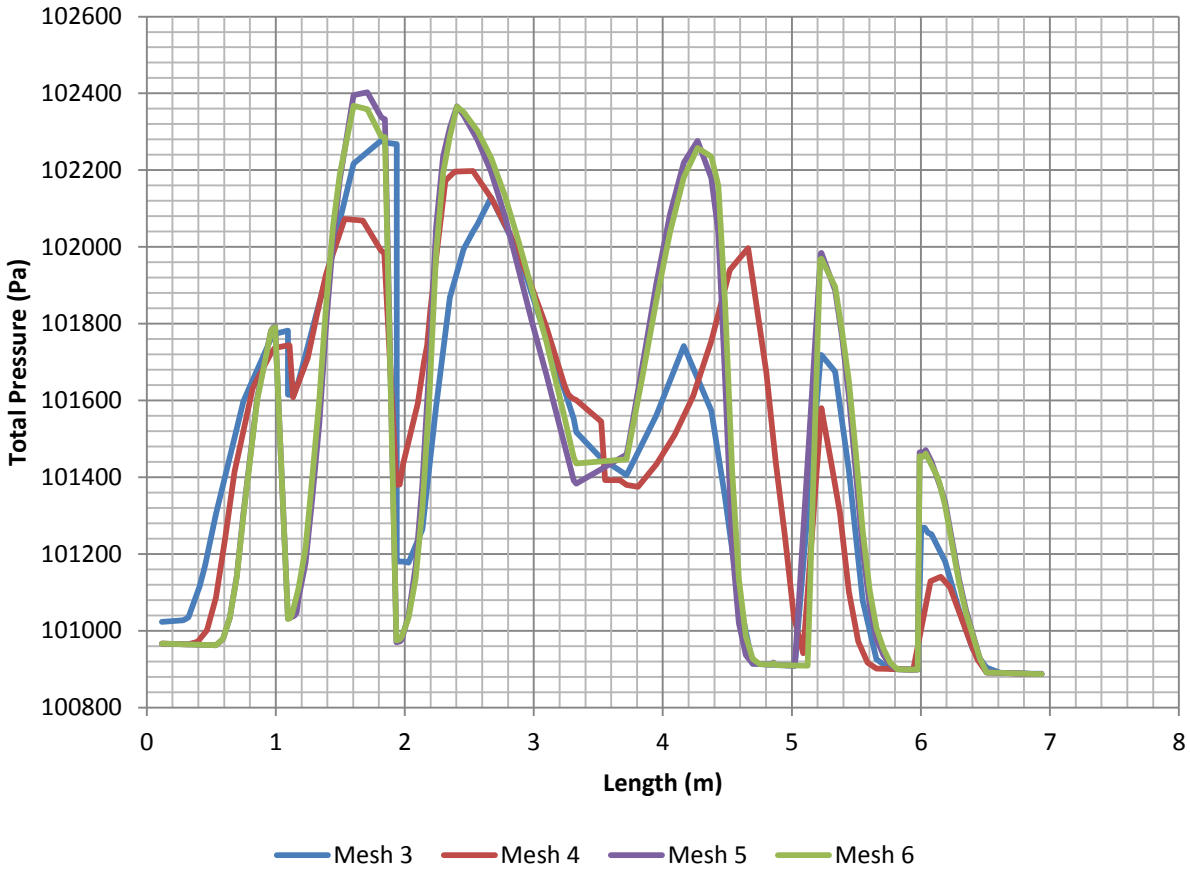

Figure 51 - SolidWorks Flow Simulation Grid Independence using Total Pressure Distribution at Diffuser Exit along Y Mid-Plane for 3.5 + Flat + Conical – Full Size

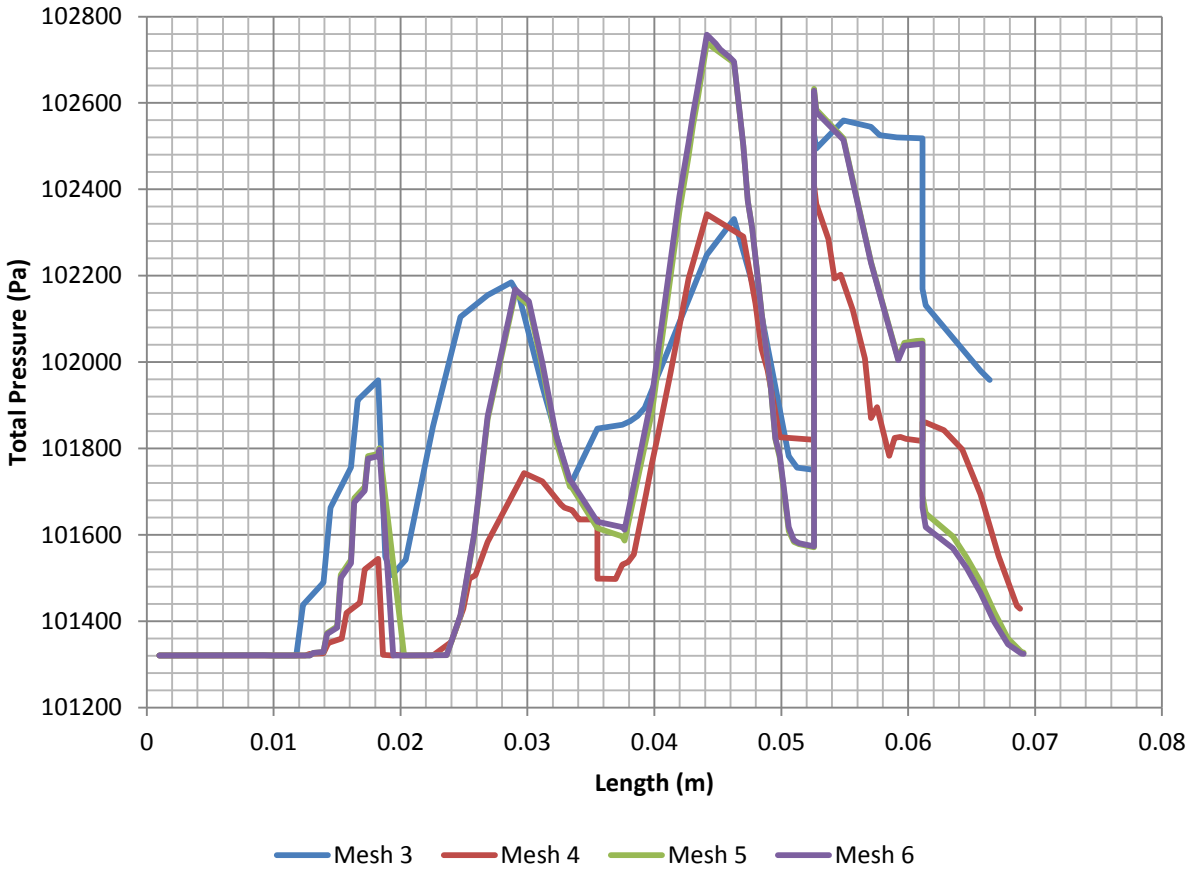

Figure 52 - SolidWorks Flow Simulation Grid Independence using Total Pressure Distribution at Diffuser Exit along Y Mid-Plane for 3.5 + Flat + Conical – Small Scale

ANSYS FLUENT Grid Independence Results

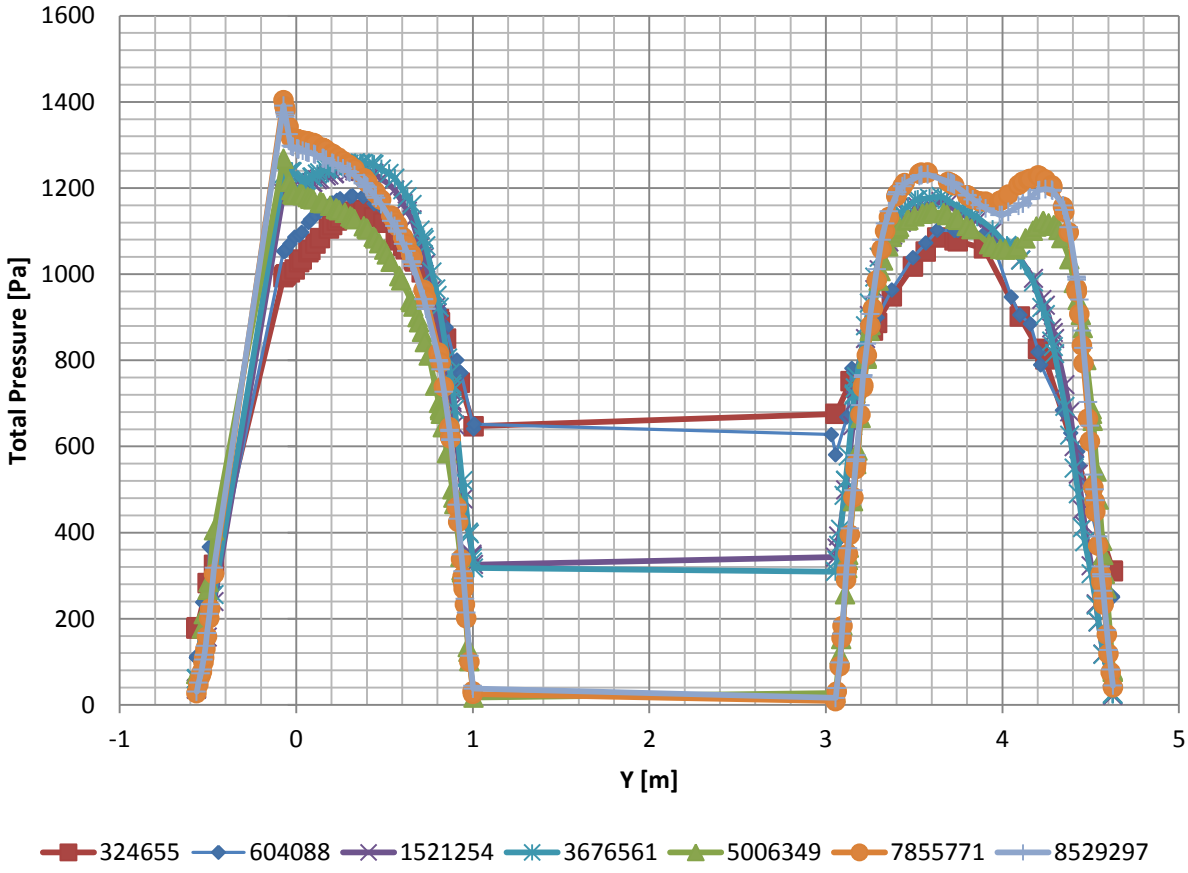

Figure 53 - ANSYS FLUENT Grid Independence Study using Total Pressure Distribution at Diffuser Exit along Y Mid-Plane for 7.5 Base Tunnel - Full Size

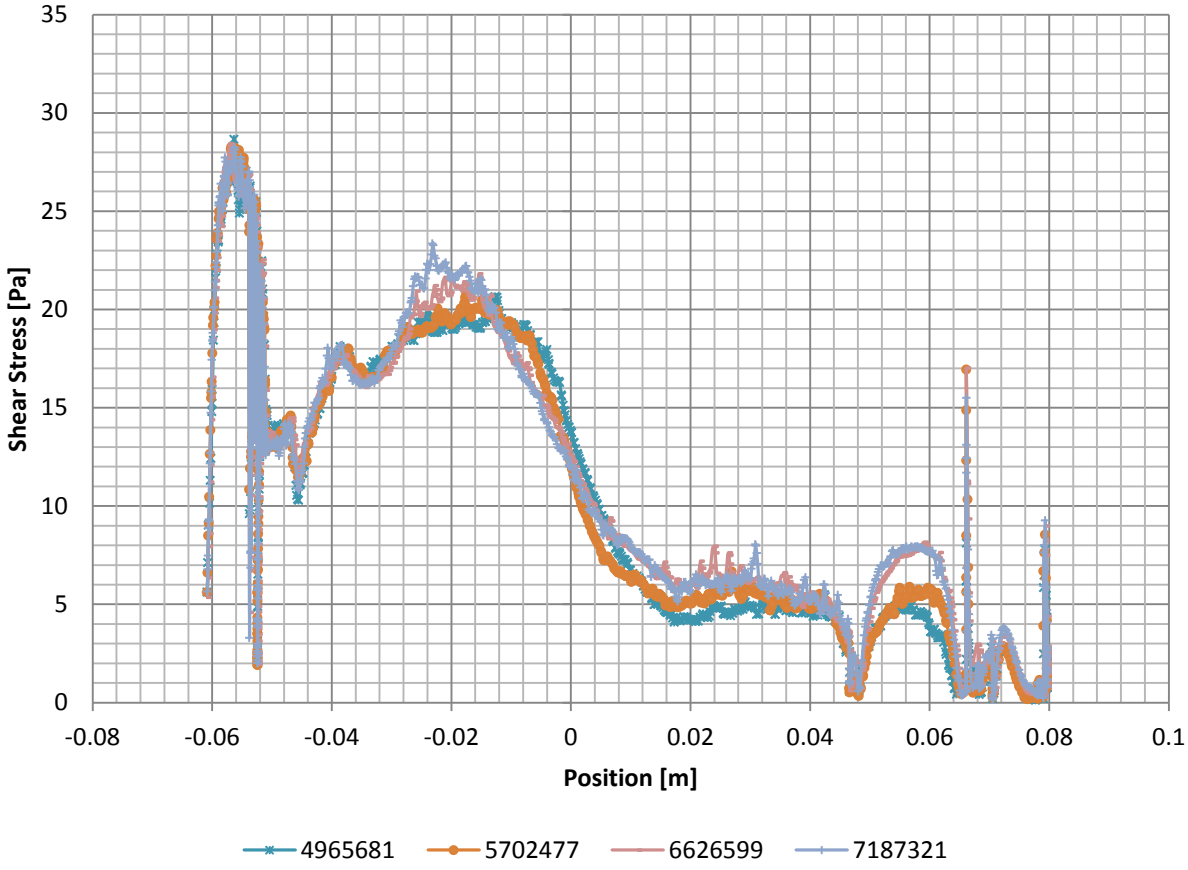

Figure 54 - ANSYS FLUENT Grid Independence Study Using Shear Stress along Engine Nacelle Top Surface for 7.5 Base Tunnel - Small Scale

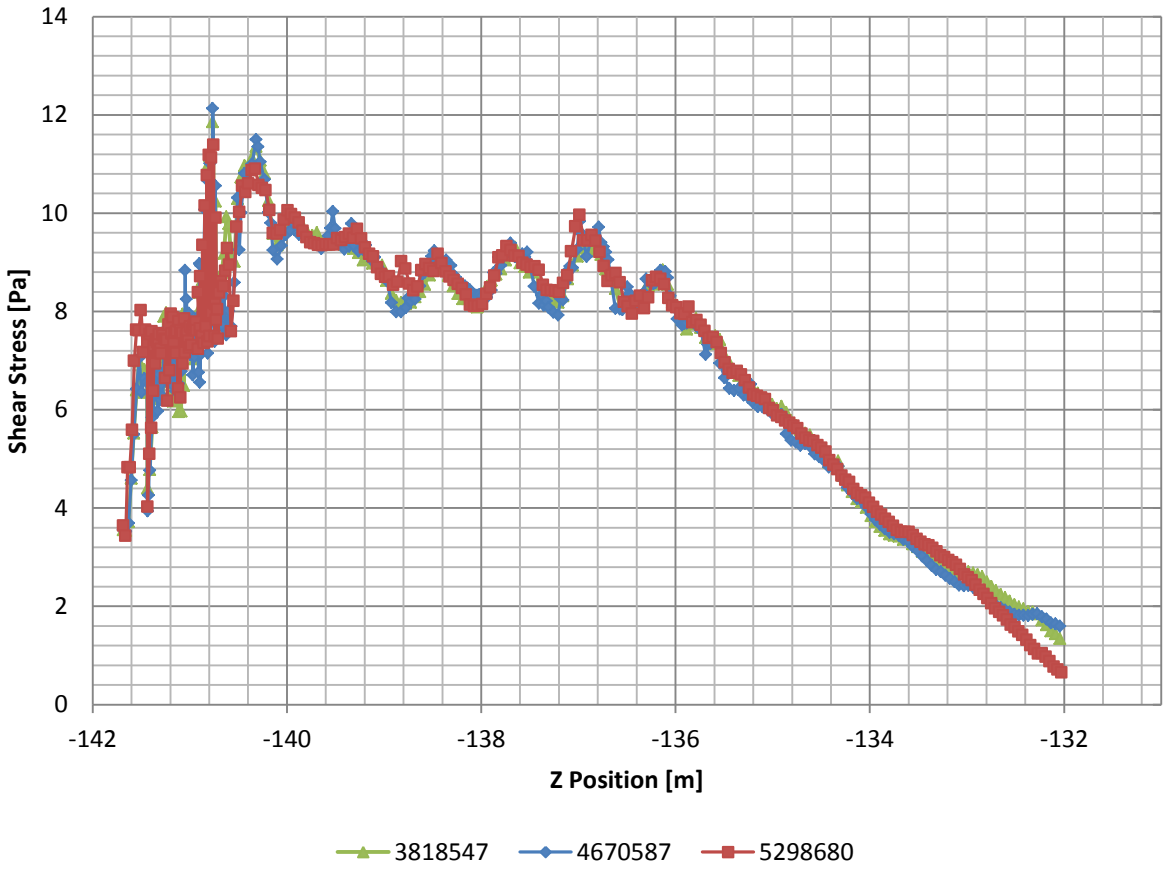

Figure 55 – ANSYS FLUENT Grid Independence Studying using Shear Stress along Top of Engine Nacelle for 3.5 + Flat + Conical - Full Size

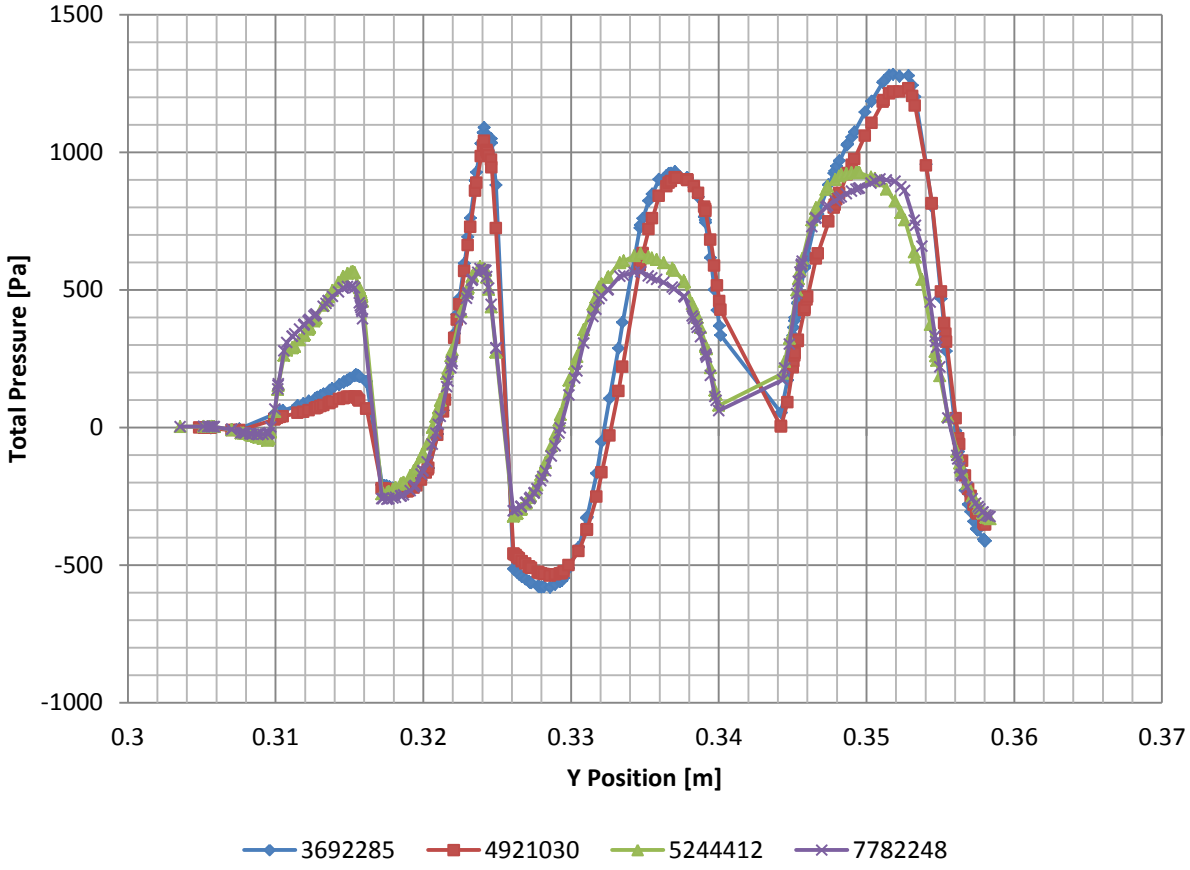

Figure 56 - ANSYS FLUENT Grid Independence Study using Total Pressure Distribution at Exit of Diffuser along Y Mid-Plane for 3.5 + Flat + Conical - Small Scale

APPENDIX B

SOLIDWORKS FLOW FIELD DISTRIBUTIONS

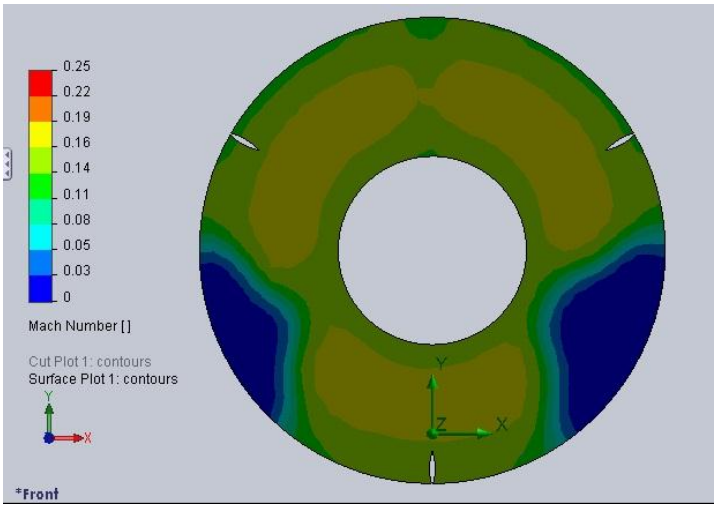

Figure 57 – SolidWorks Flow Simulation Mach Number Distribution at Exit of 7.5 Base Tunnel - Full Size - Uniform Flow

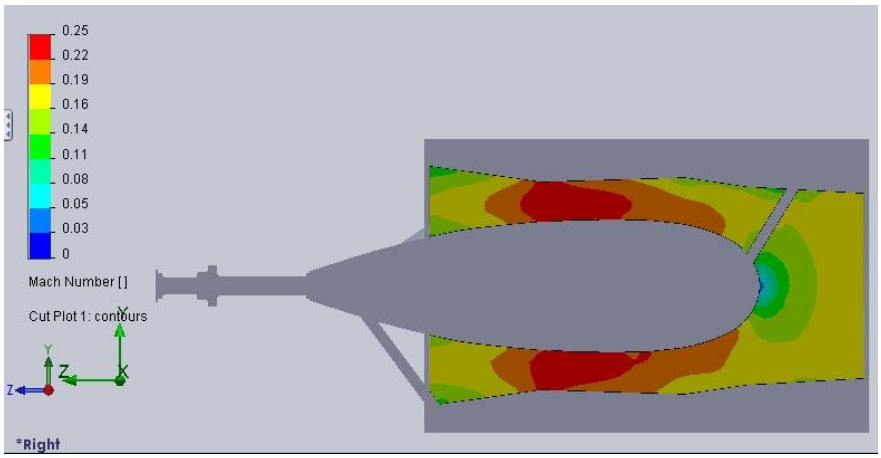

Figure 58 – SolidWorks Flow Simulation Mach Number Distribution along 7.5 Base Tunnel Cross-Section - Full Size – Uniform

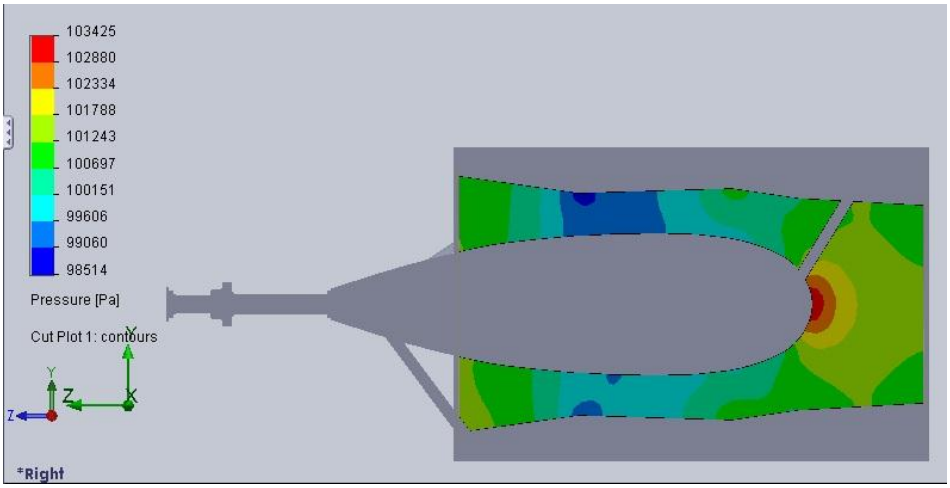

Figure 59 – SolidWorks Flow Simulation Static Pressure Distribution along 7.5 Base Tunnel Cross-Section - Full Size - Uniform Flow

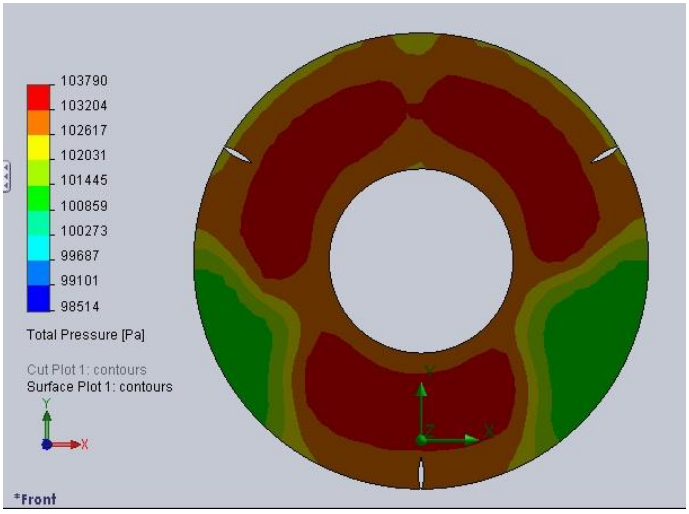

Figure 60 – SolidWorks Flow Simulation Total Pressure Distribution at Exit of 7.5 Base Tunnel – Full Size – Uniform Flow

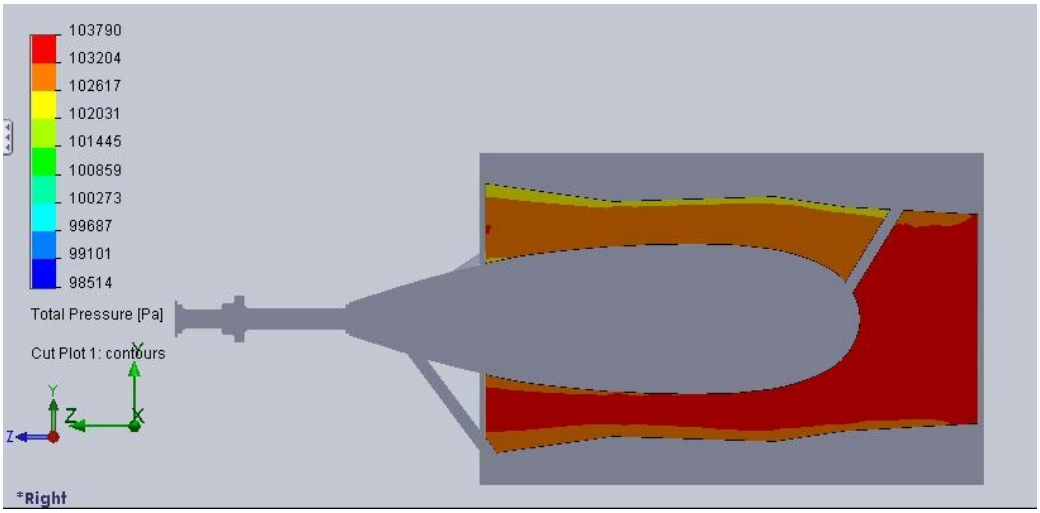

Figure 61 – SolidWorks Flow Simulation Total Pressure Distribution along Cross-Section of Tunnel of 7.5 Base Tunnel – Full Size – Uniform Flow

7.5 BASE TUNNEL – FULL SIZE – FULLY DEVELOPED FLOW

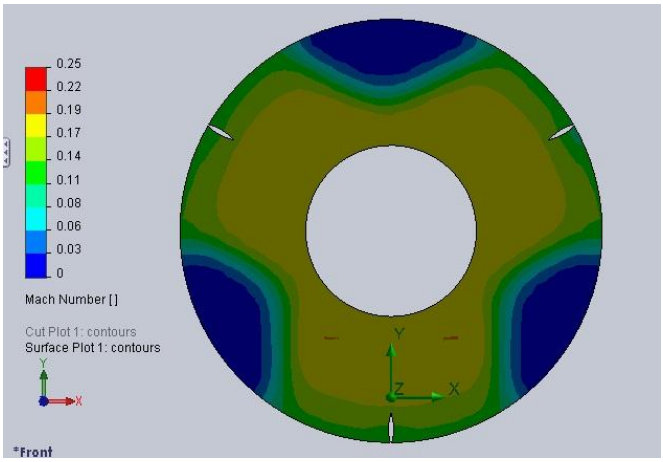

Figure 62 – SolidWorks Flow Simulation Mach Number Distribution at Exit of 7.5 Base Tunnel – Full Size – Fully Developed Flow

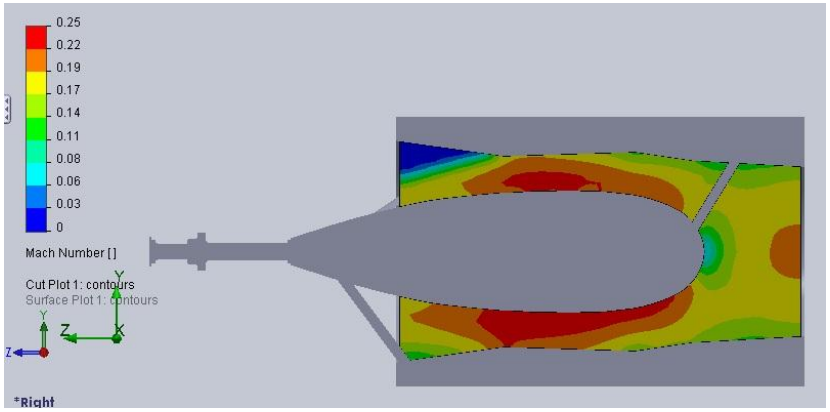

Figure 63 – SolidWorks Flow Simulation Mach Number Distribution along 7.5 Base Tunnel Cross-Section – Full Size – Fully Developed Flow

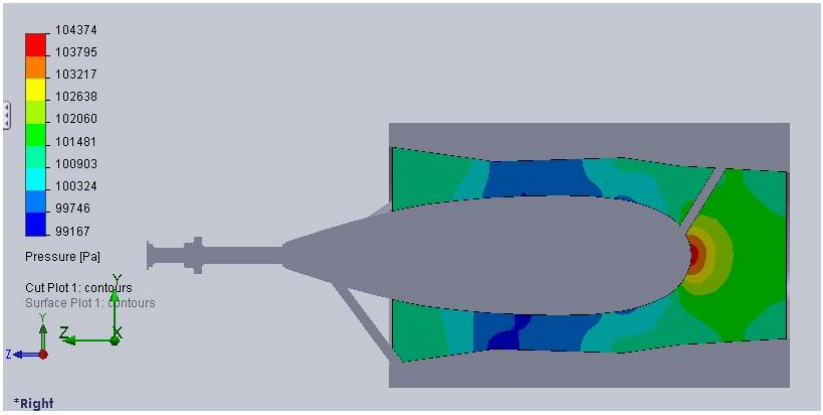

Figure 64 – SolidWorks Flow Simulation Static Pressure Distribution along 7.5 Base Tunnel Cross-Section – Full Size – Fully Developed Flow

3.5 BASE TUNNEL – FULL SIZE – UNIFORM FLOW

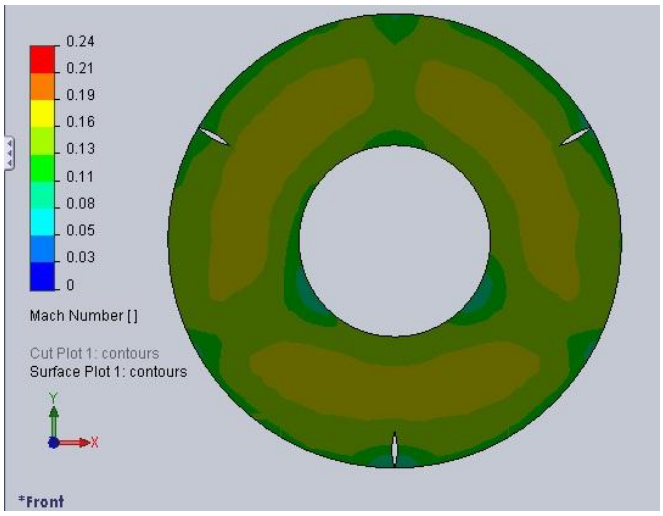

Figure 65 – SolidWorks Flow Simulation Mach Number Distribution at Exit of 3.5 Base Tunnel – Full Size – Uniform Flow

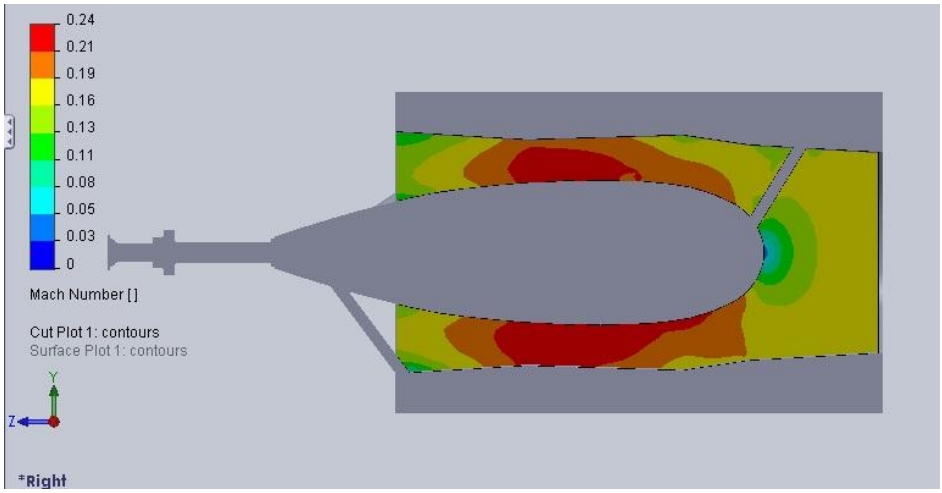

Figure 66 – SolidWorks Flow Simulation Mach Number Distribution along 3.5 Base Tunnel Cross-Section – Full Size – Uniform Flow

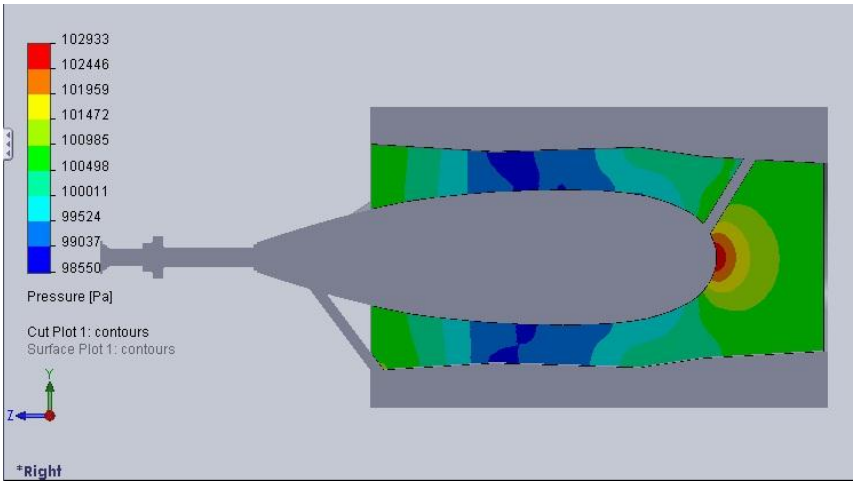

Figure 67 – SolidWorks Flow Simulation Static Pressure Distribution along 3.5 Base Tunnel Cross-Section – Full Size – Uniform Flow

Figure 68 – SolidWorks Flow Simulation Total Pressure Distribution at Exit of 3.5 Base Tunnel – Full Size – Uniform Flow

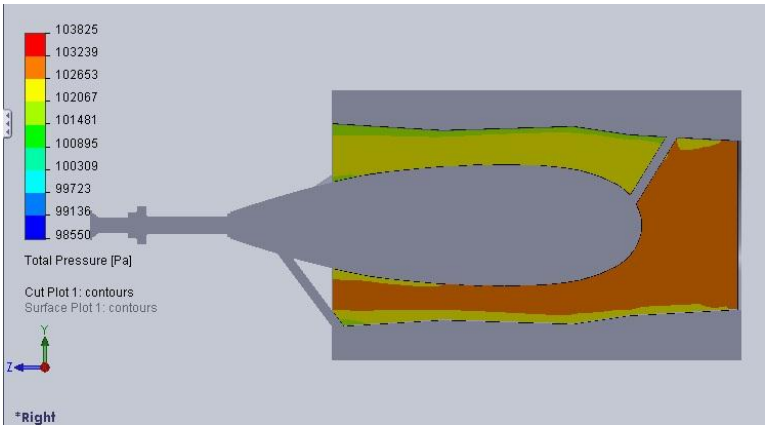

Figure 69 – SolidWorks Flow Simulation Total Pressure Distribution along 3.5 Base Tunnel Cross-Section – Full Size – Uniform Flow

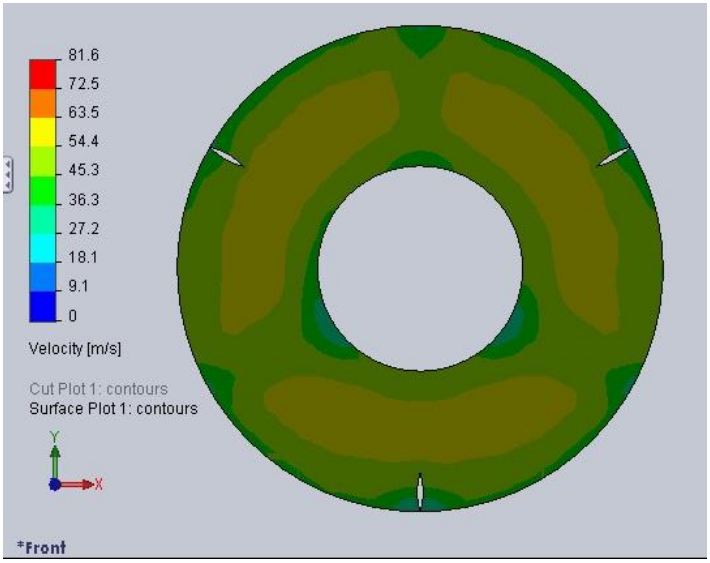

Figure 70 – SolidWorks Flow Simulation Velocity Distribution at Exit of 3.5 Base Tunnel – Full Size – Uniform Flow

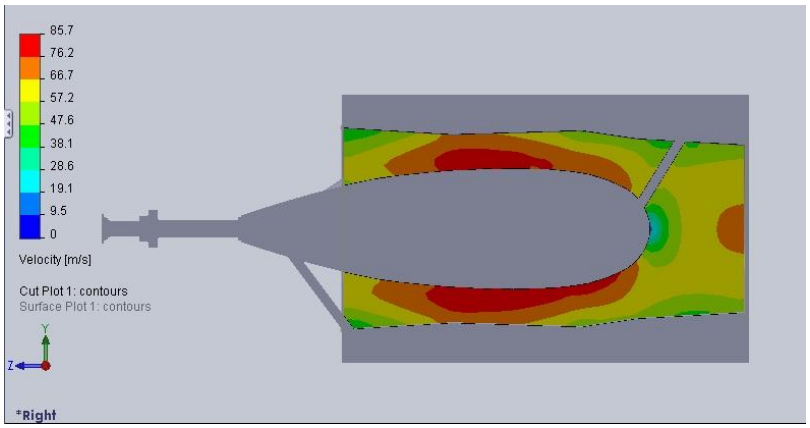

Figure 71 – SolidWorks Flow Simulation Velocity Distribution along 3.5 Base Tunnel Cross-Section – Full Size – Uniform Flow

3.5 BASE TUNNEL – FULL SIZE – FULLY DEVELOPED FLOW

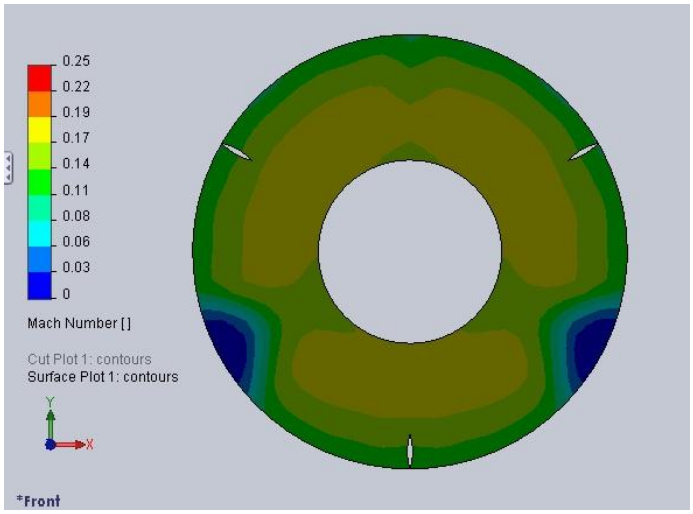

Figure 72 – SolidWorks Flow Simulation Mach Number Distribution at Exit of 3.5 Base Tunnel - Full Size - Fully Developed Flow

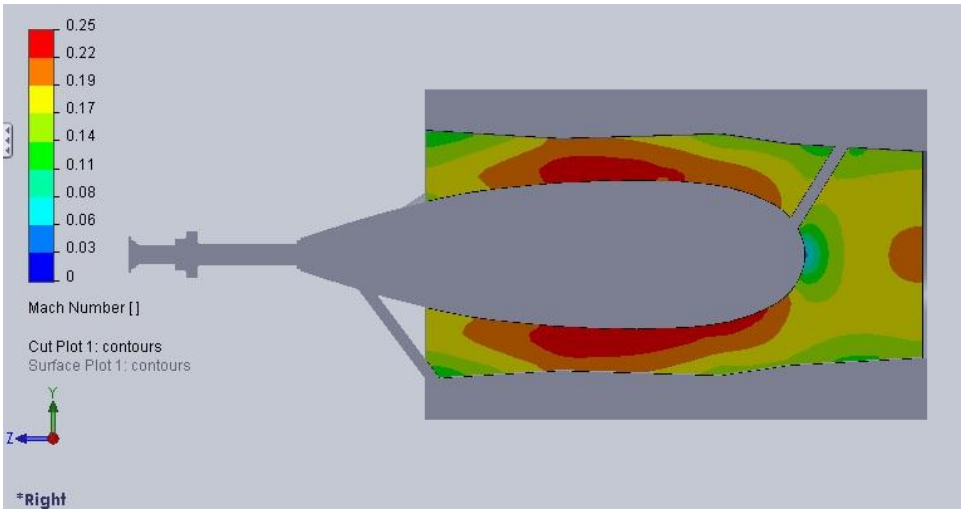

Figure 73 – SolidWorks Flow Simulation Mach Number Distribution through Cross-Section of 3.5 Base Tunnel - Full Size - Fully Developed Flow

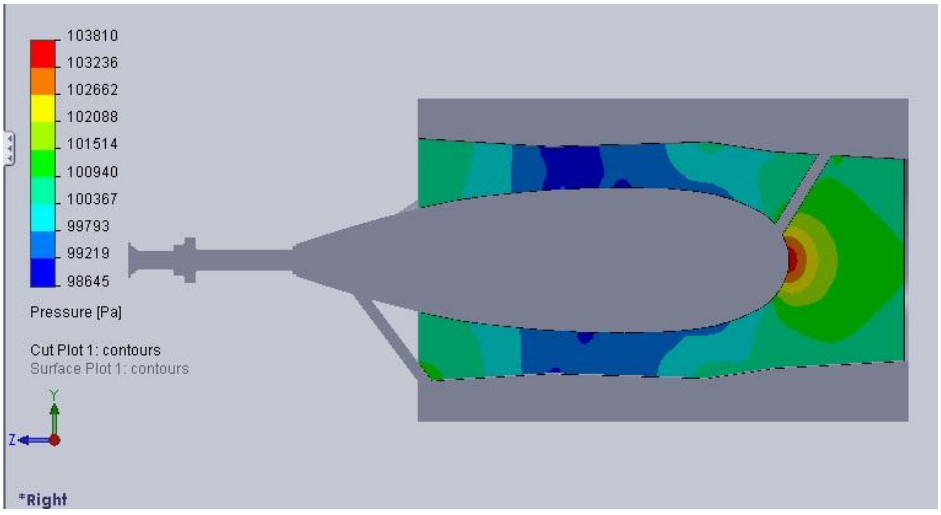

Figure 74 – SolidWorks Flow Simulation Static Pressure Distribution through Cross-Section of 3.5 Base Tunnel - Full Size - Fully Developed Flow

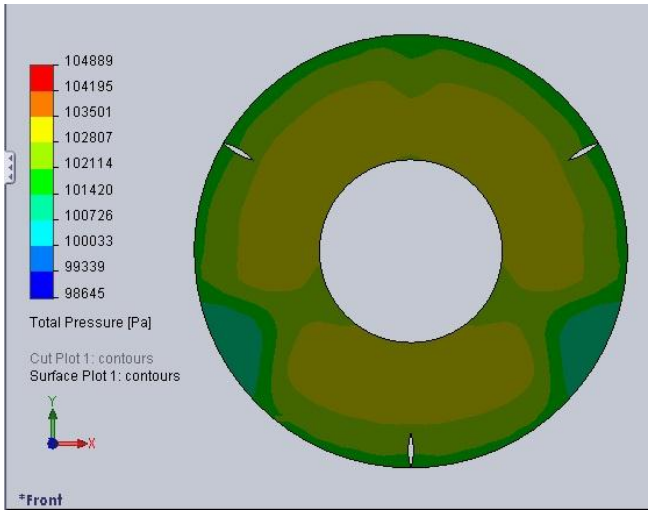

Figure 75 – SolidWorks Flow Simulation Total Pressure Distribution at Exit of 3.5 Base Tunnel - Full Size - Fully Developed Flow

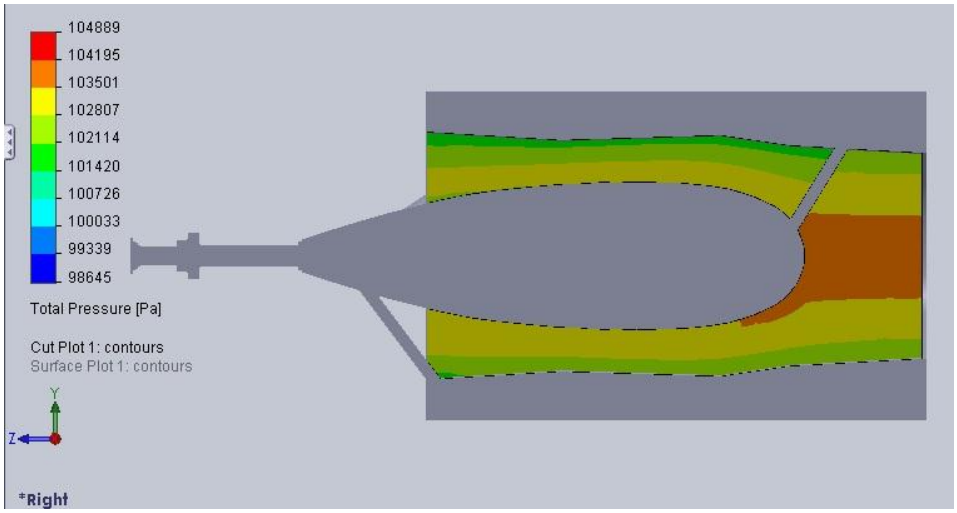

Figure 76 - SolidWorks Flow Simulation Total Pressure Distribution through Cross-Section of 3.5 Base Tunnel - Full Size - Fully Developed Flow

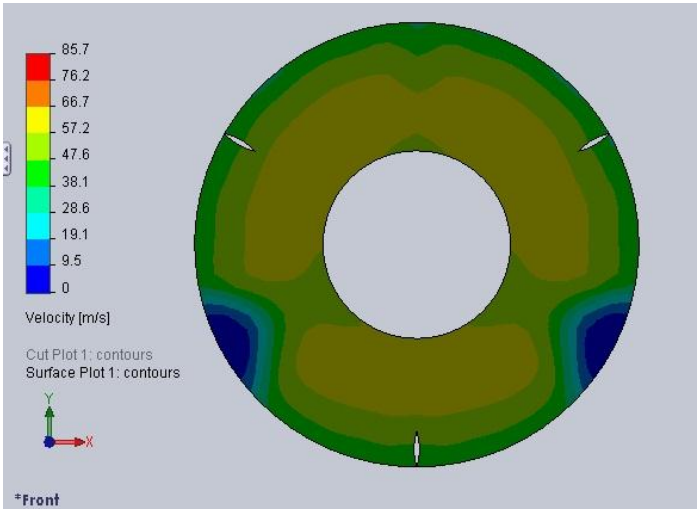

Figure 77 - SolidWorks Flow Simulation Velocity Distribution at Exit of 3.5 Base Tunnel - Full Size - Fully Developed Flow

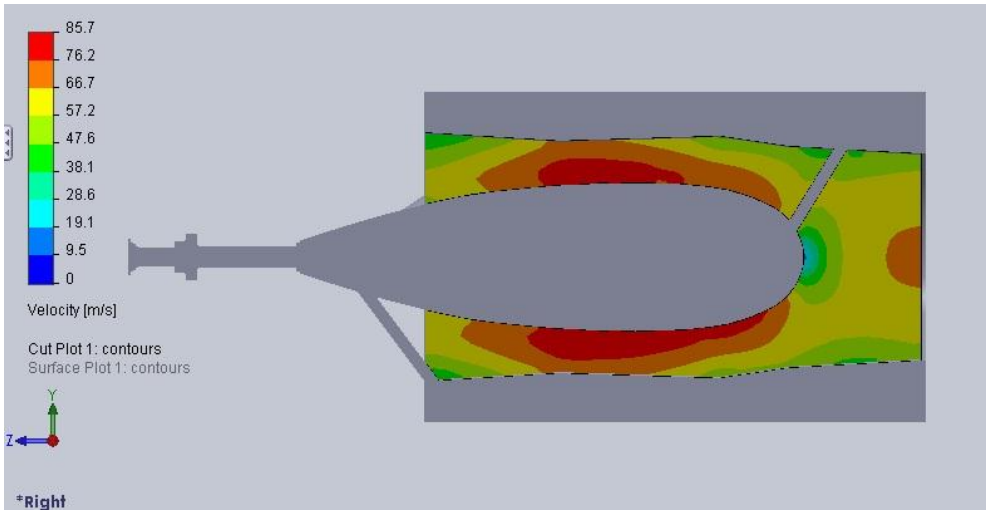

Figure 78 - SolidWorks Flow Simulation Velocity Distribution through Cross-Section of 3.5 Base Tunnel - Full Size - Fully Developed Flow

3.5 + FLAT – FULL SIZE – UNIFORM FLOW

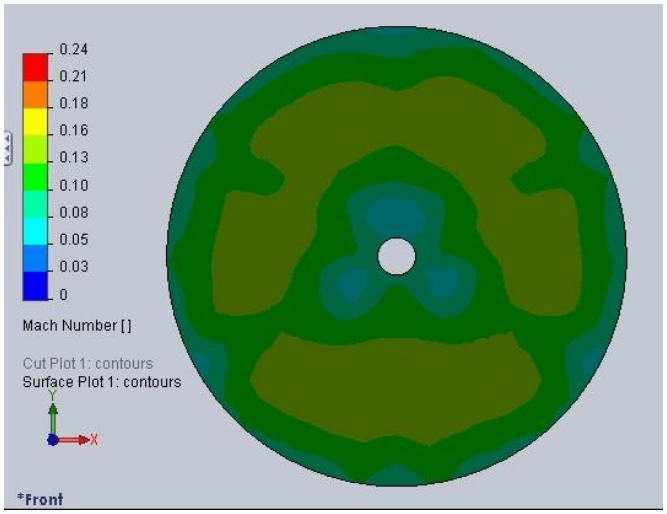

Figure 79 - SolidWorks Flow Simulation Mach Number Distribution at Exit of 3.5 + Flat Tunnel - Full Size - Uniform Flow

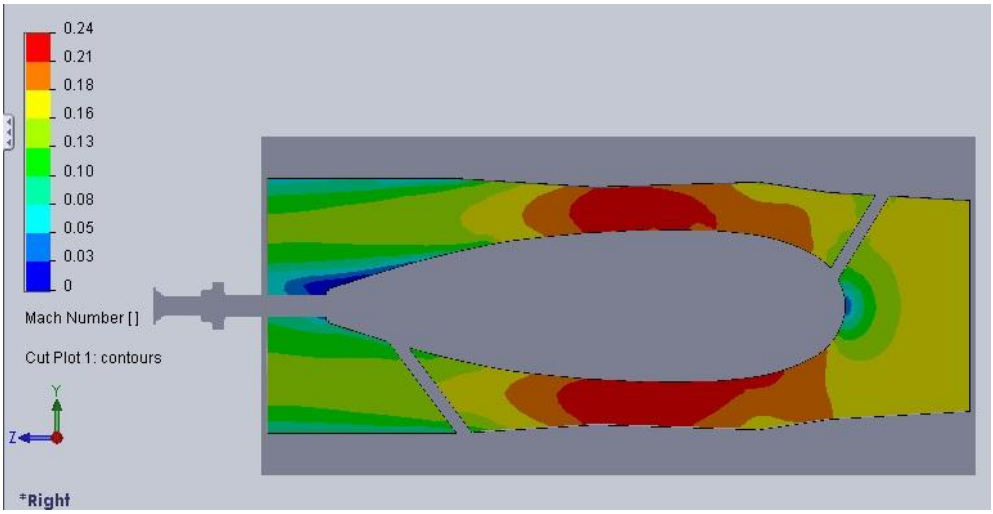

Figure 80 - SolidWorks Flow Simulation Mach Number Distribution through Cross-Section of 3.5 + Flat - Full Size - Uniform Flow

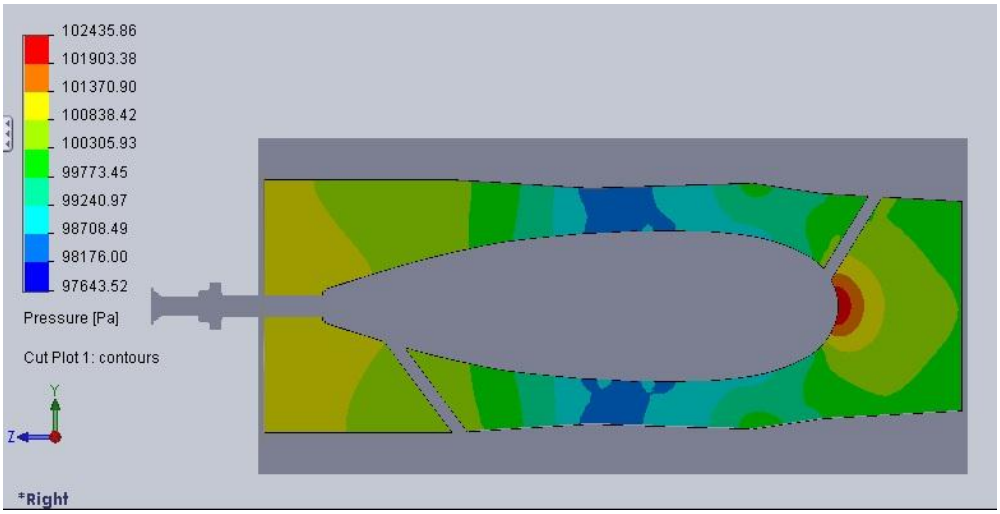

Figure 81 - SolidWorks Flow Simulation Static Pressure Distribution through Cross-Section of 3.5 + Flat - Full Size - Uniform Flow

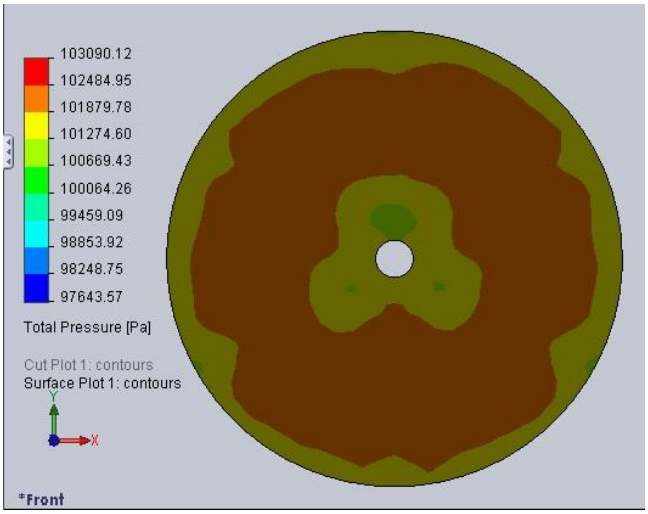

Figure 82 - SolidWorks Flow Simulation Total Pressure Distribution at Exit of 3.5 + Flat - Full Size - Uniform Flow

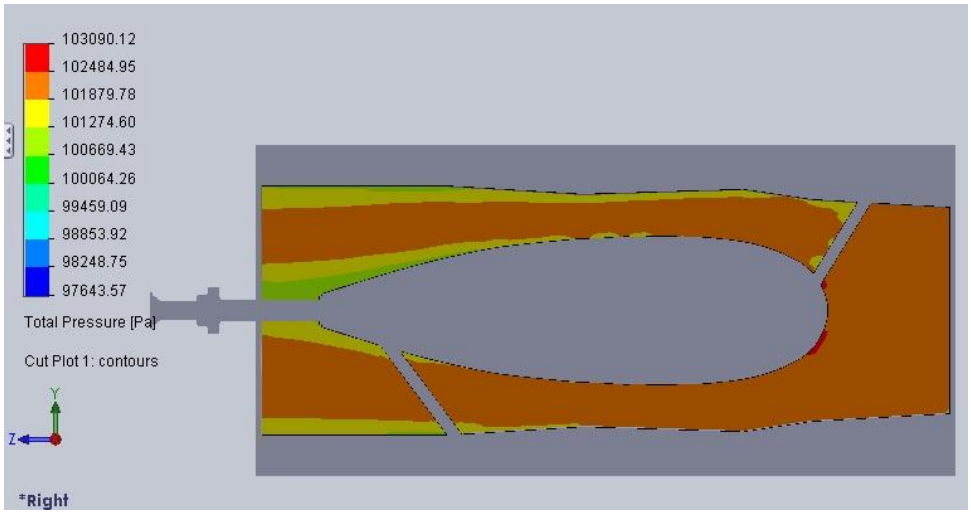

Figure 83 - SolidWorks Flow Simulation Total Pressure Distribution through Cross-Section of 3.5 + Flat - Full Size - Uniform Flow

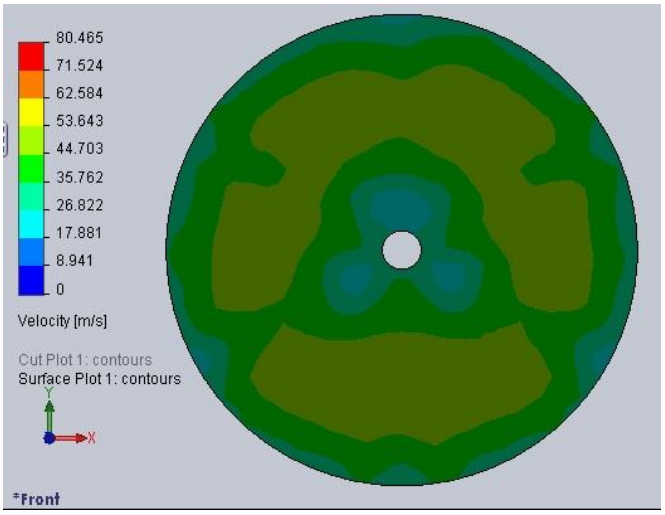

Figure 84 - SolidWorks Flow Simulation Velocity Distribution at Exit of 3.5 + Flat - Full Size - Uniform Flow

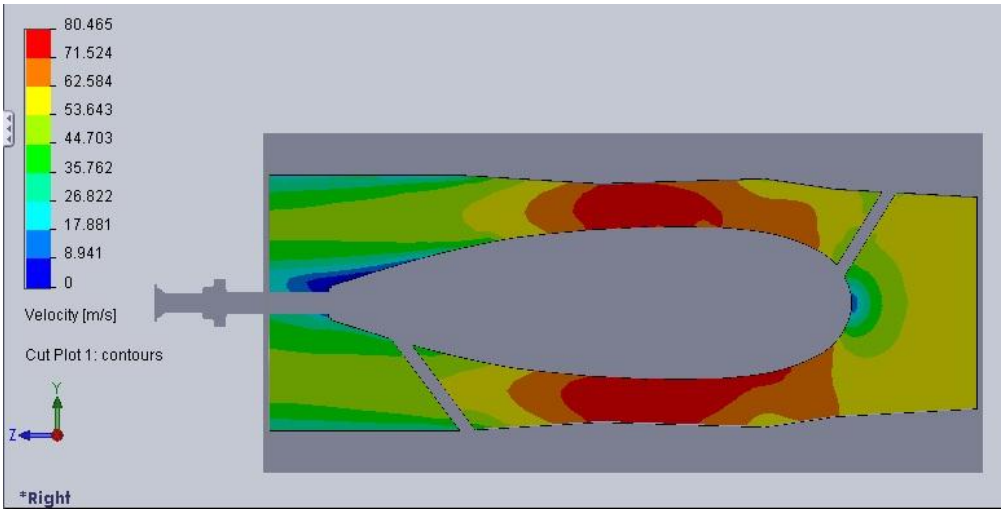

Figure 85 - SolidWorks Flow Simulation Velocity Distribution through Cross-Section of 3.5 + Flat - Full Size - Uniform Flow

3.5 + FLAT – FULL SIZE – FULLY DEVELOPED FLOW

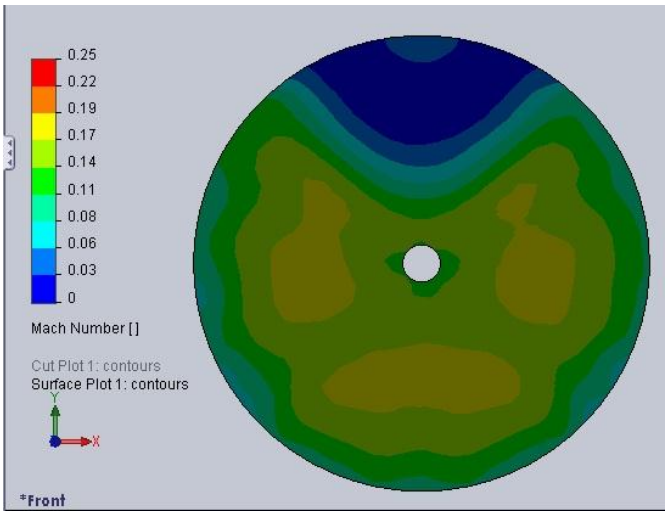

Figure 86 - SolidWorks Flow Simulation Mach Number Distribution at Exit of 3.5 + Flat - Full Size - Fully Developed Flow

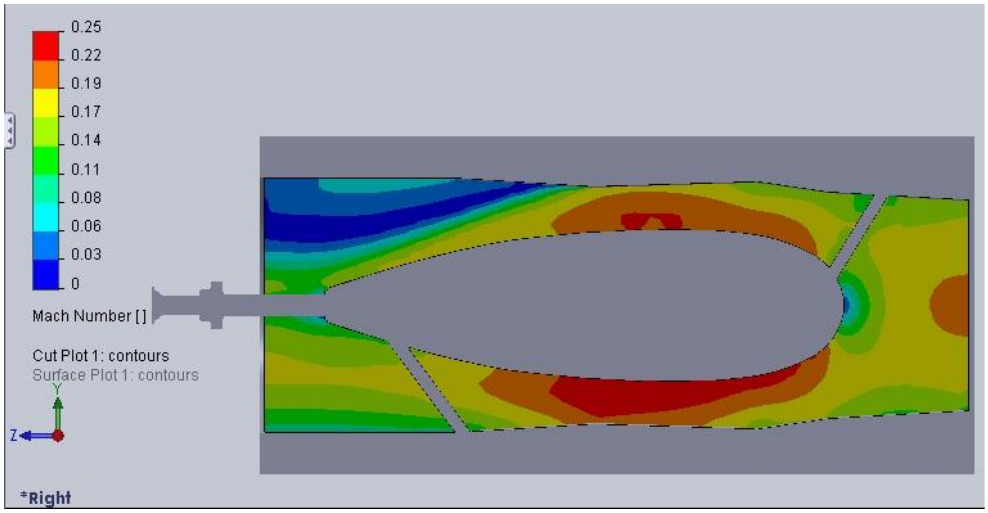

Figure 87 - SolidWorks Flow Simulation Mach Number Distribution through Cross-Section of 3.5 + Flat - Full Size – Fully Developed Flow

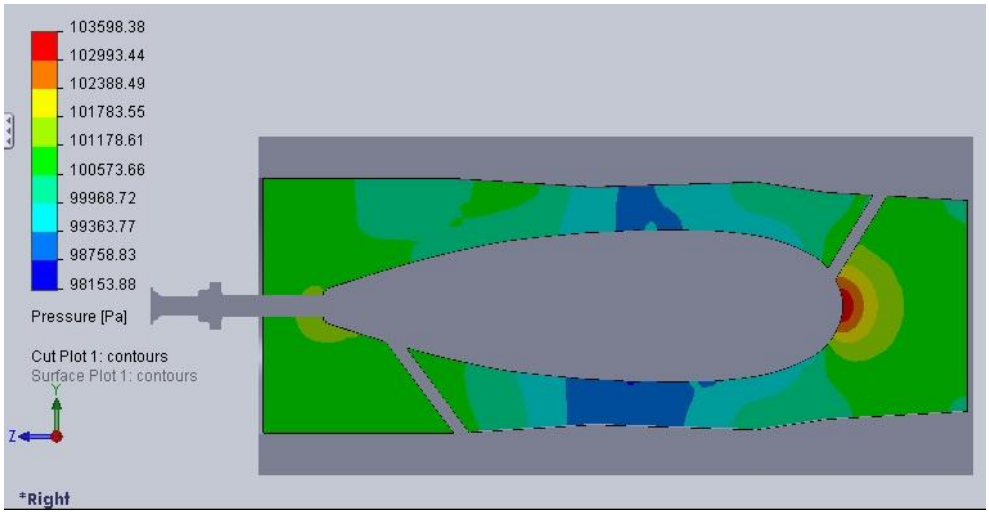

Figure 88 - SolidWorks Flow Simulation Static Pressure Distribution through Cross-Section of 3.5 + Flat - Full Size - Fully Developed Flow

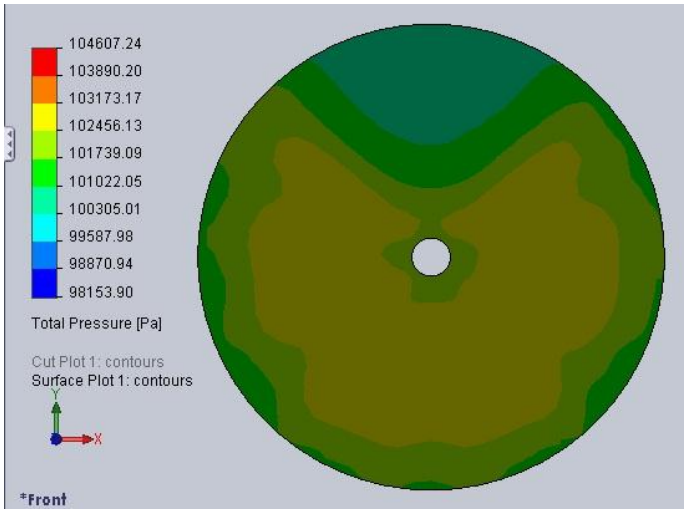

Figure 89 - SolidWorks Flow Simulation Total Pressure Distribution at Exit of 3.5 + Flat - Full Size - Fully Developed Flow

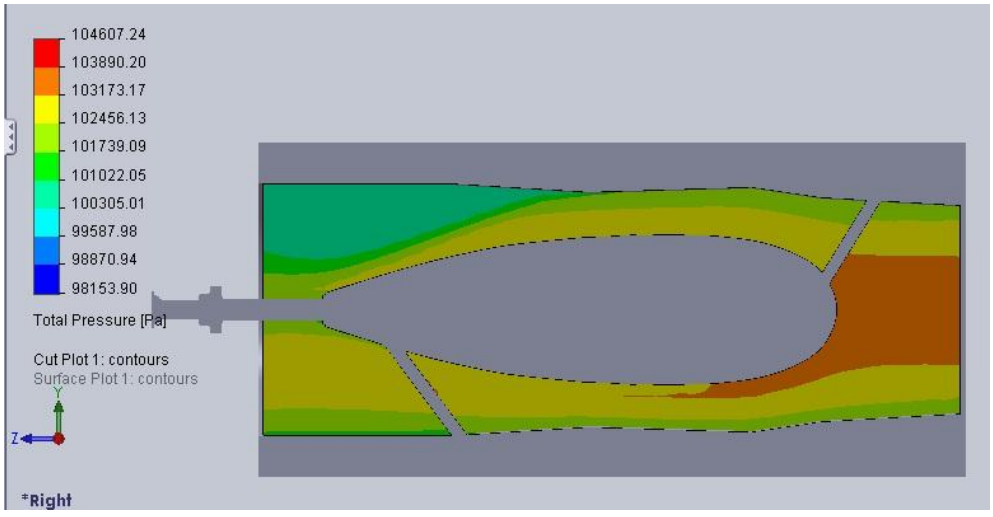

Figure 90 - SolidWorks Flow Simulation Total Pressure Distribution through Cross-Section of 3.5 + Flat - Full Size - Fully Developed Flow

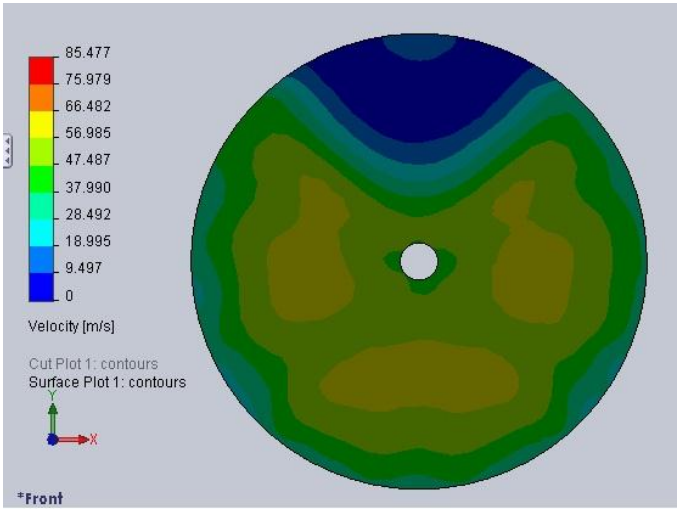

Figure 91 - SolidWorks Flow Simulation Velocity Distribution at Exit of 3.5 + Flat - Full Size - Fully Developed Flow

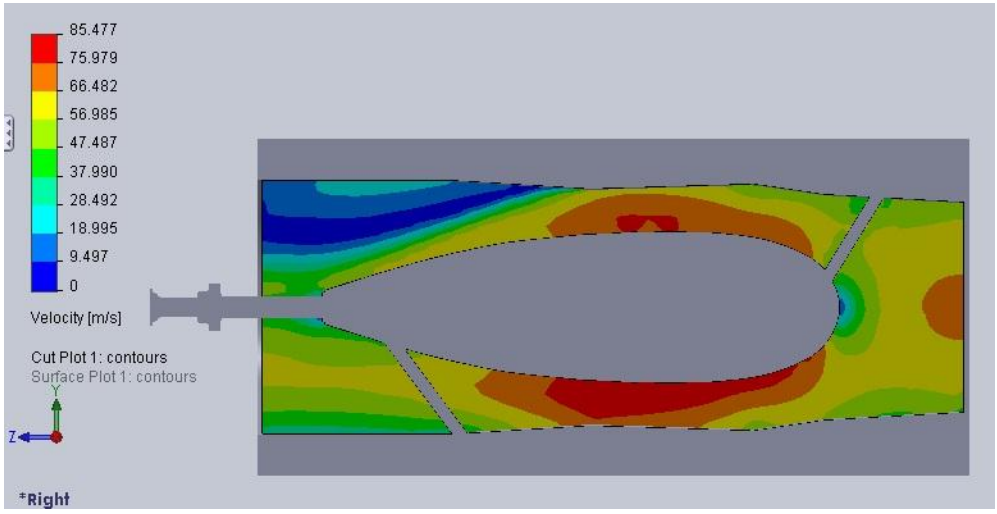

Figure 92 - SolidWorks Flow Simulation Velocity Distribution through Cross-Section of 3.5 + Flat - Full Size - Fully Developed Flow

3.5 + FLAT + CONICAL – FULL SIZE – UNIFORM FLOW

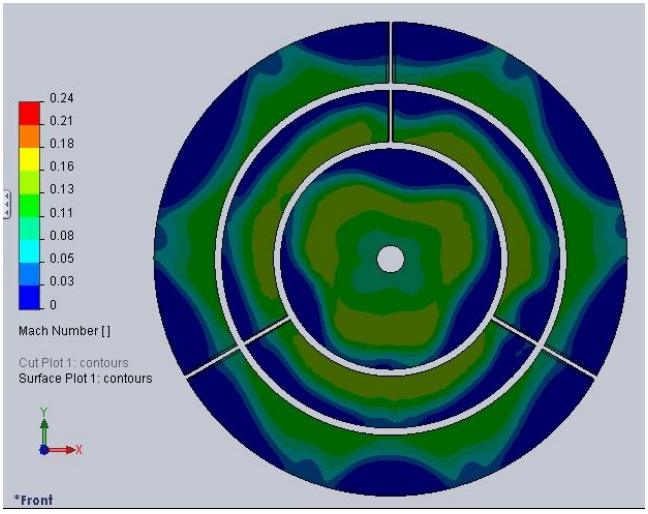

Figure 93 - SolidWorks Flow Simulation Mach Number Distribution at Exit of 3.5 + Flat + Conical - Full Size - Uniform Flow

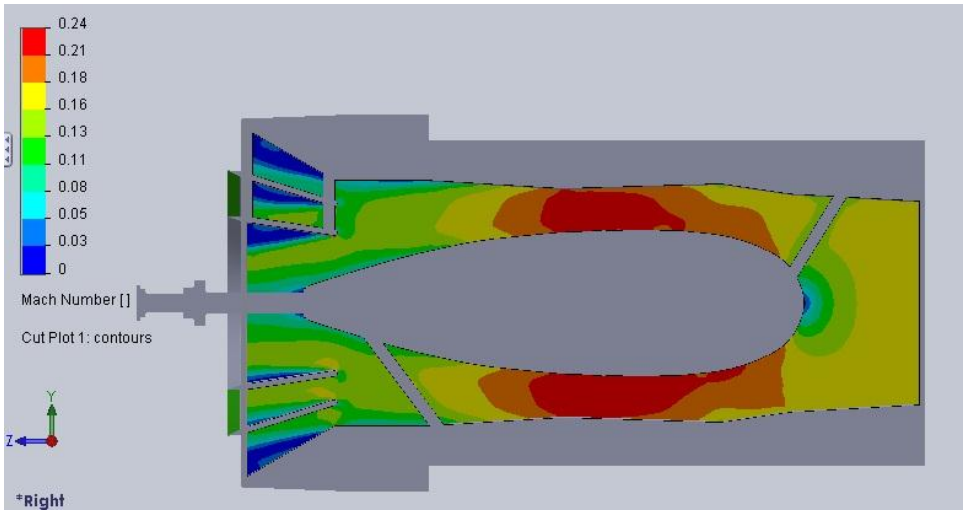

Figure 94 - SolidWorks Flow Simulation Mach Number Distribution through Cross-Section of 3.5 + Flat + Conical - Full Size - Uniform Flow

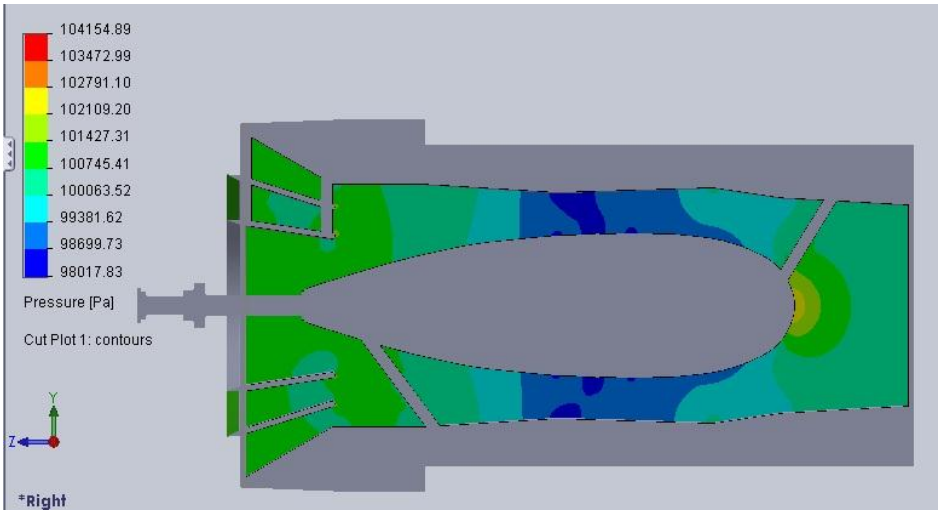

Figure 95 - SolidWorks Flow Simulation Static Pressure Distribution through Cross-Section of 3.5 + Flat + Conical - Full Size - Uniform Flow

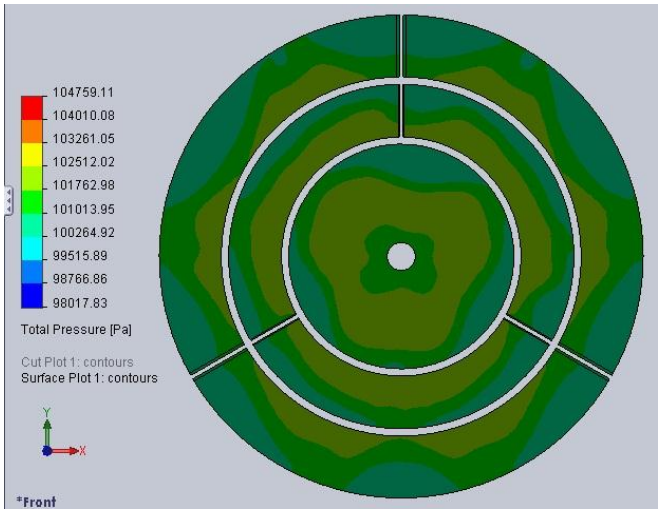

Figure 96 - SolidWorks Flow Simulation Total Pressure Distribution at Exit of 3.5 + Flat + Conical - Full Size - Uniform Flow

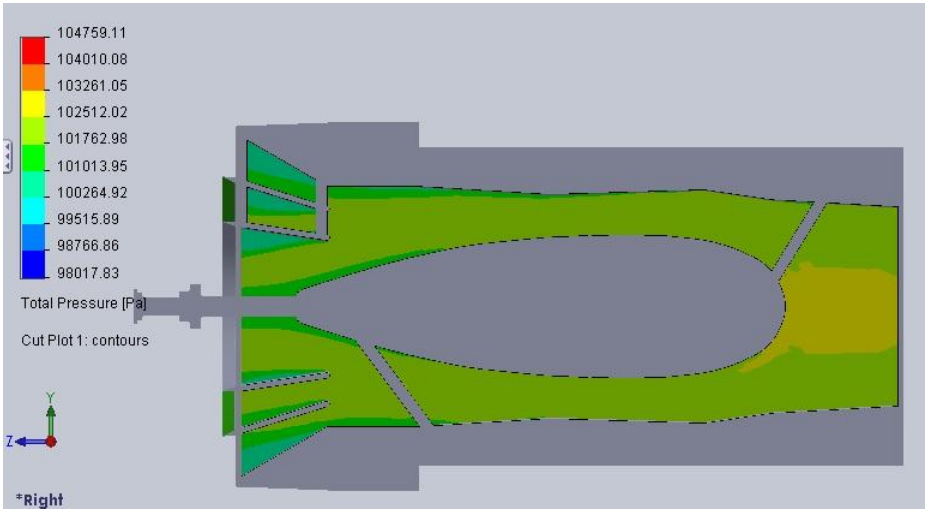

Figure 97 - SolidWorks Flow Simulation Total Pressure Distribution through Cross-Section of 3.5 + Flat + Conical - Full Size - Uniform Flow

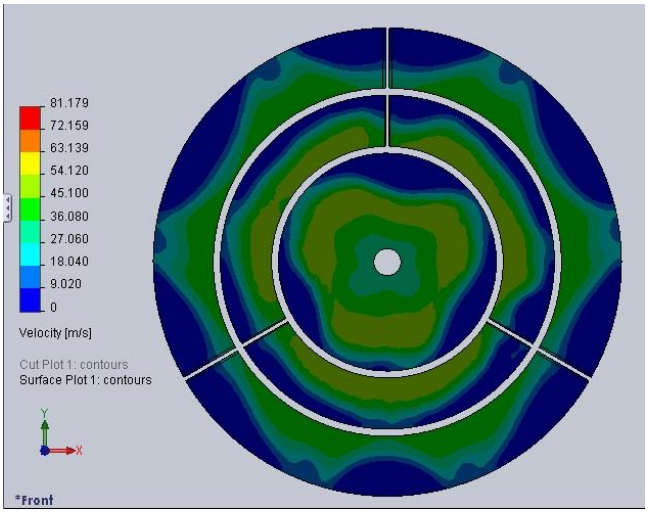

Figure 98 - SolidWorks Flow Simulation Velocity Distribution at Exit of 3.5 + Flat + Conical - Full Size - Uniform Flow

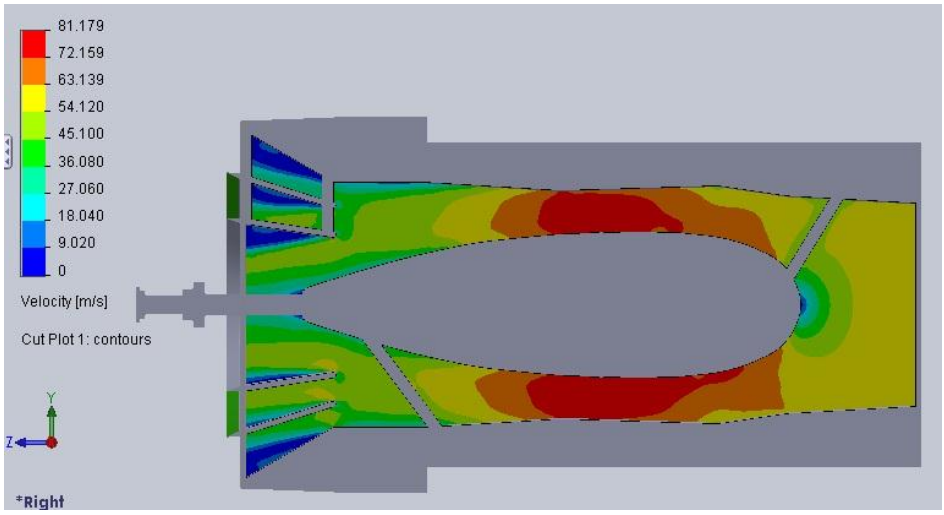

Figure 99 - SolidWorks Flow Simulation Velocity Distribution through Cross-Section of 3.5 + Flat + Conical - Full Size - Uniform Flow

3.5 + FLAT + CONICAL – FULL SIZE – FULLY DEVELOPED FLOW

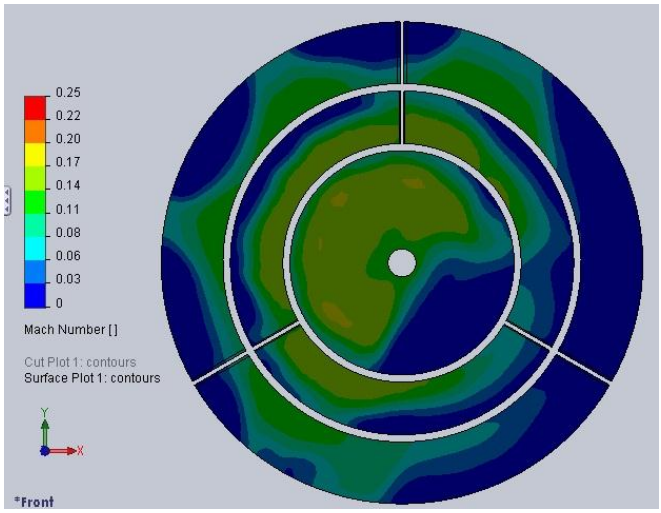

Figure 100 - SolidWorks Flow Simulation Mach Number Distribution at Exit of 3.5 + Flat + Conical - Full Size - Fully Developed Flow

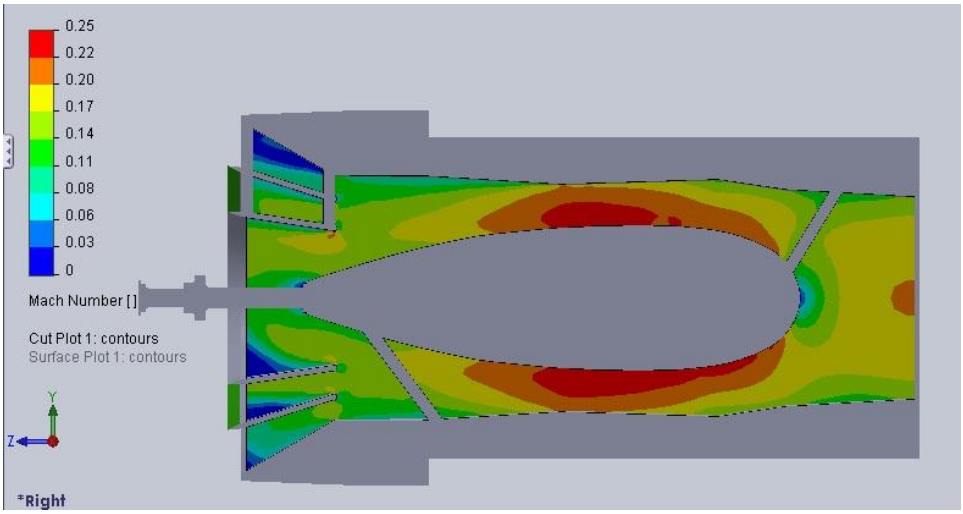

Figure 101 - SolidWorks Flow Simulation Mach Number Distribution through Cross-Section of 3.5 + Flat + Conical - Full Size - Fully Developed Flow

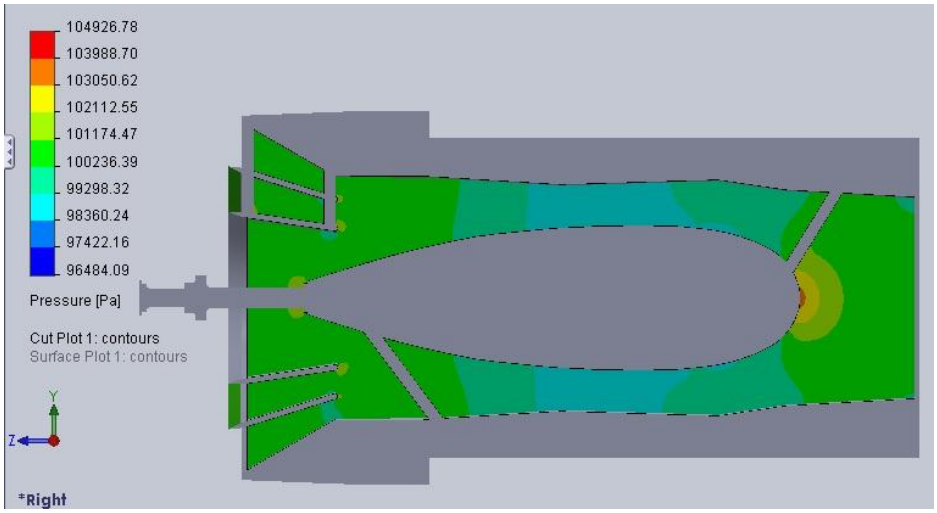

Figure 102 - SolidWorks Flow Simulation Static Pressure Distribution through Cross-Section of 3.5 + Flat + Conical - Full Size - Fully Developed Flow

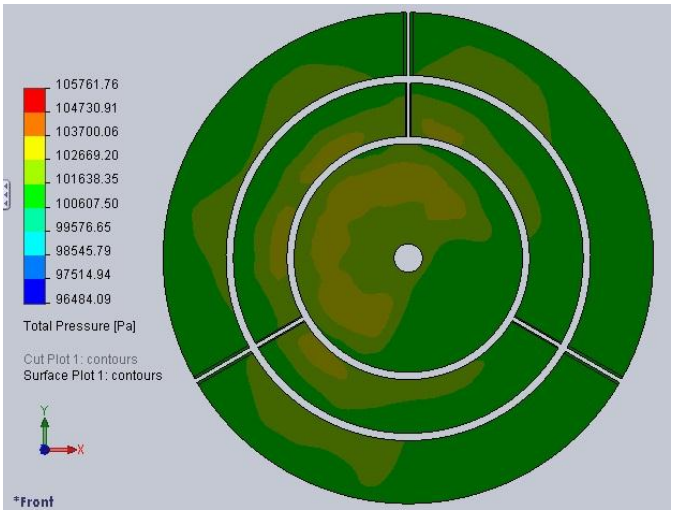

Figure 103 - SolidWorks Flow Simulation Total Pressure Distribution at Exit of 3.5 + Flat + Conical - Full Size - Fully Developed Flow

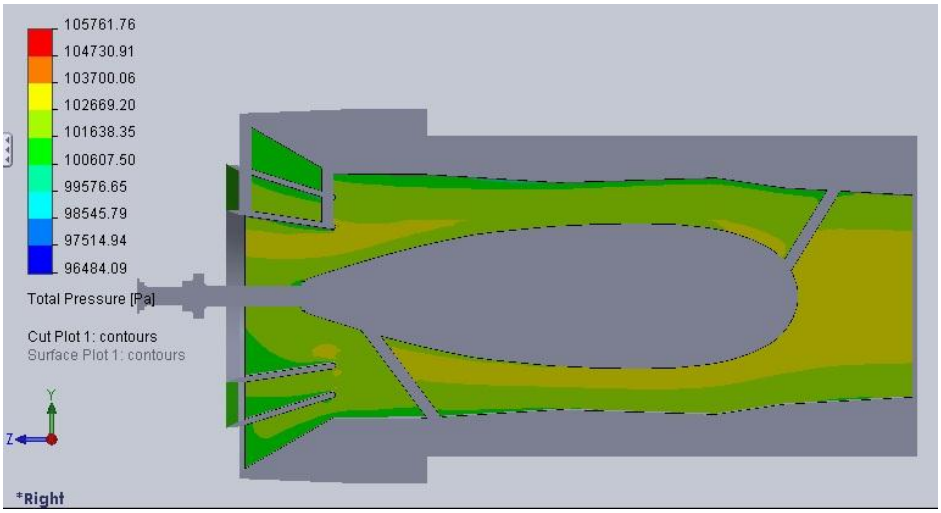

Figure 104 - SolidWorks Flow Simulation Total Pressure Distribution through Cross-Section of 3.5 + Flat + Conical - Full Size - Fully Developed Flow

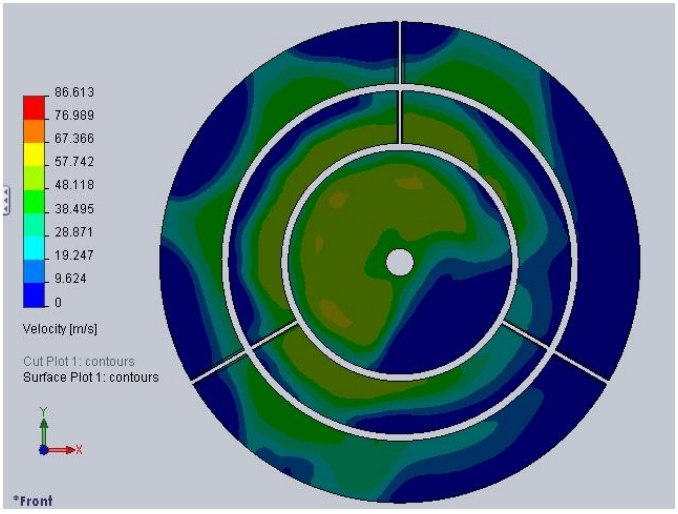

Figure 105 - SolidWorks Flow Simulation Velocity Distribution at Exit of 3.5 + Flat + Conical - Full Size - Fully Developed Flow

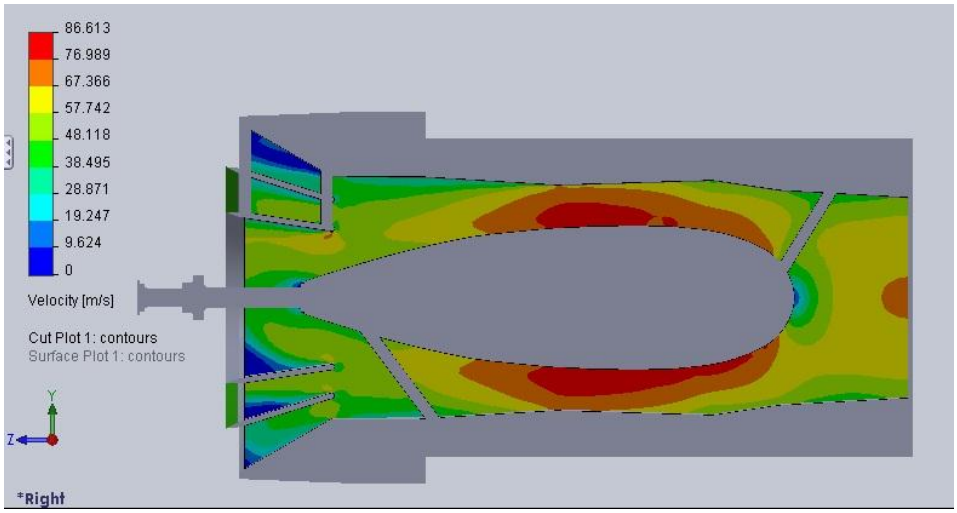

Figure 106 - SolidWorks Flow Simulation Velocity Distribution through Cross-Section of 3.5 + Flat + Conical - Full Size - Fully Developed Flow

7.5 BASE TUNNEL – SMALL SCALE – UNIFORM FLOW

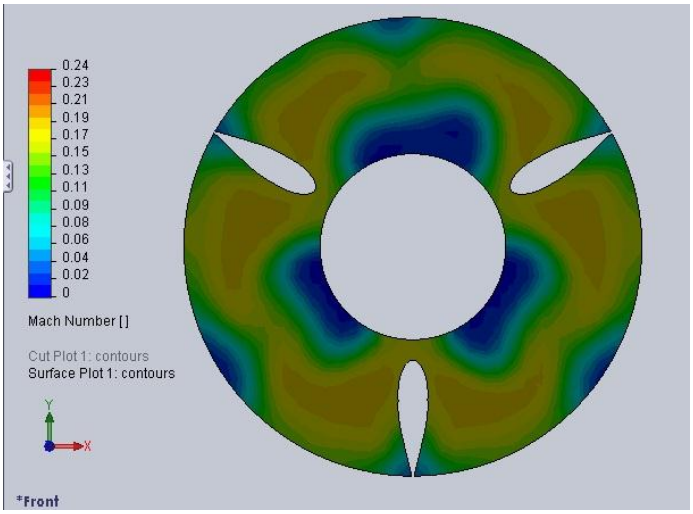

Figure 107 - SolidWorks Flow Simulation Mach Number Distribution at Exit of 7.5 Base Tunnel - Small Scale - Uniform Flow

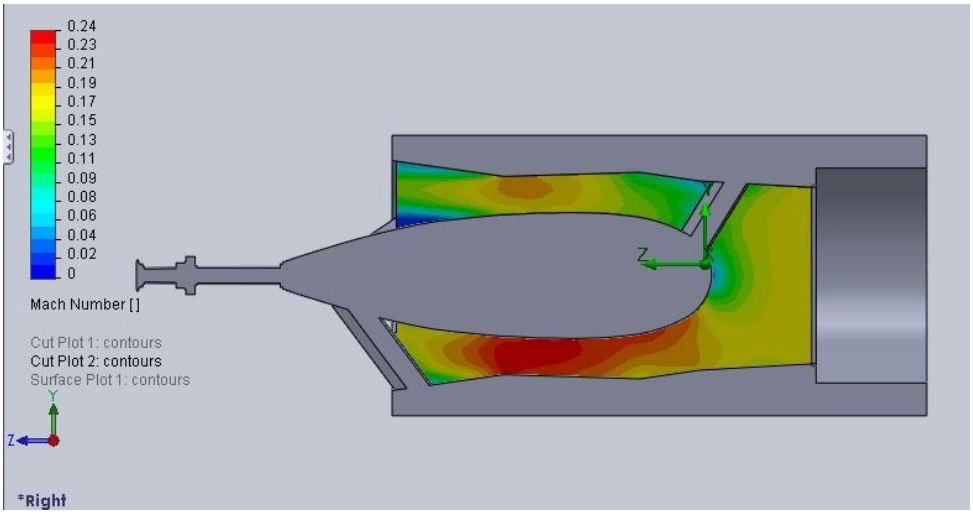

Figure 108 - SolidWorks Flow Simulation Mach Number Distribution through Cross-Section of 7.5 Base Tunnel - Small Scale - Uniform Flow

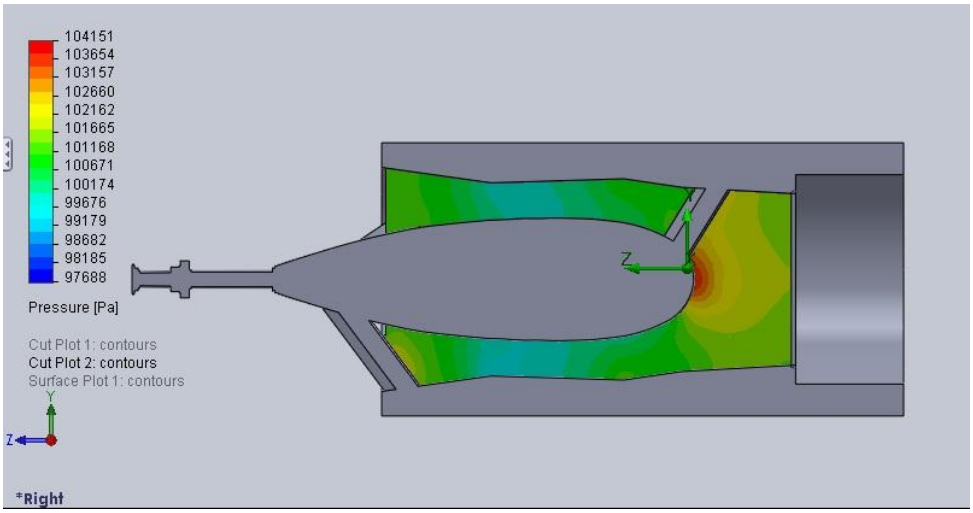

Figure 109 - SolidWorks Flow Simulation Static Pressure Distribution through Cross-Section of 7.5 Base Tunnel - Small Scale - Uniform Flow

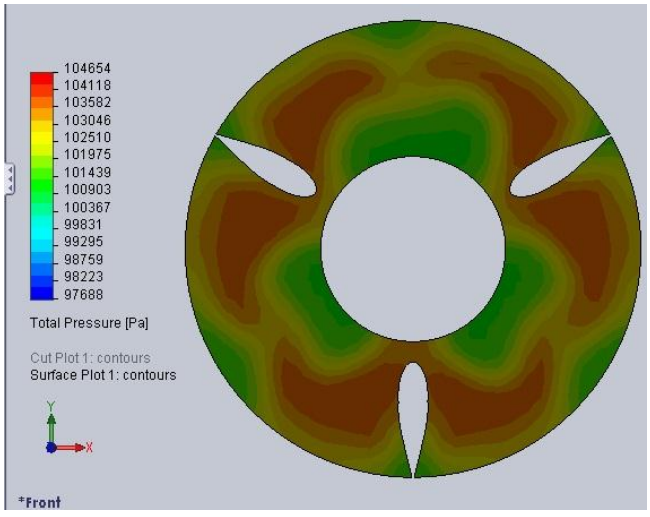

Figure 110 - SolidWorks Flow Simulation Total Pressure Distribution at Exit of 7.5 Base Tunnel - Small Scale - Uniform Flow

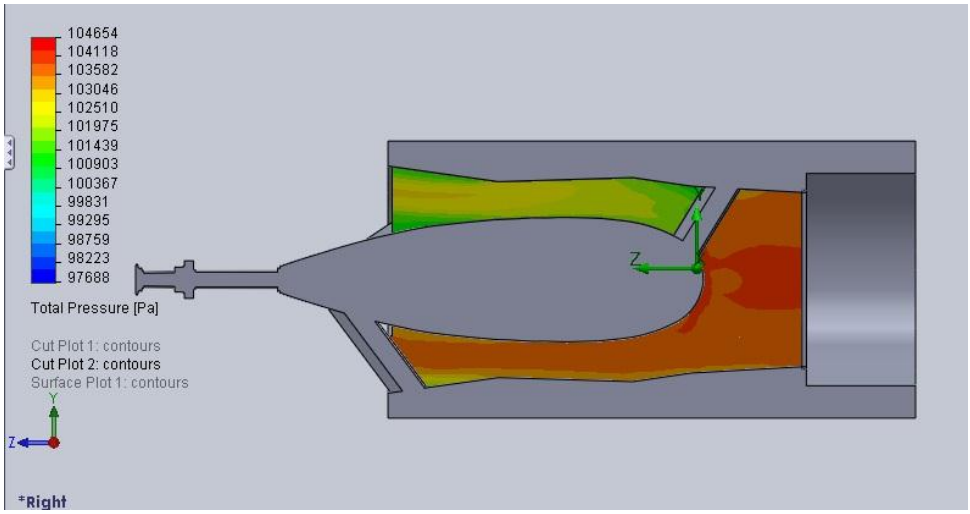

Figure 111 - SolidWorks Flow Simulation Total Pressure Distribution through Cross-Section of 7.5 Base Tunnel - Small Scale - Uniform Flow

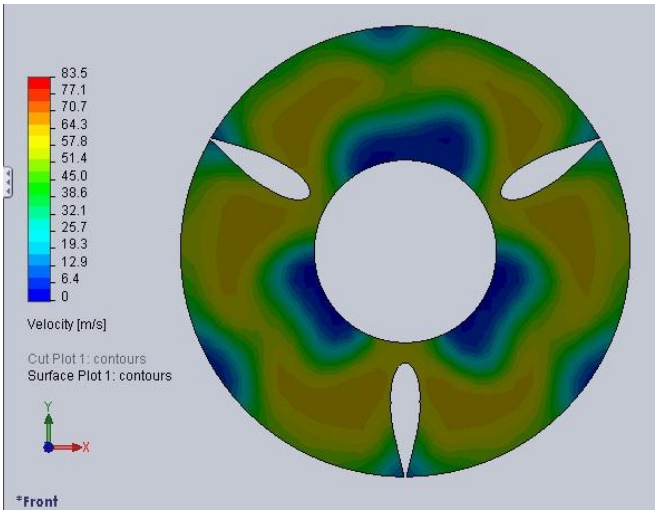

Figure 112 - SolidWorks Flow Simulation Velocity Distribution at Exit of 7.5 Base Tunnel - Small Scale - Uniform Flow

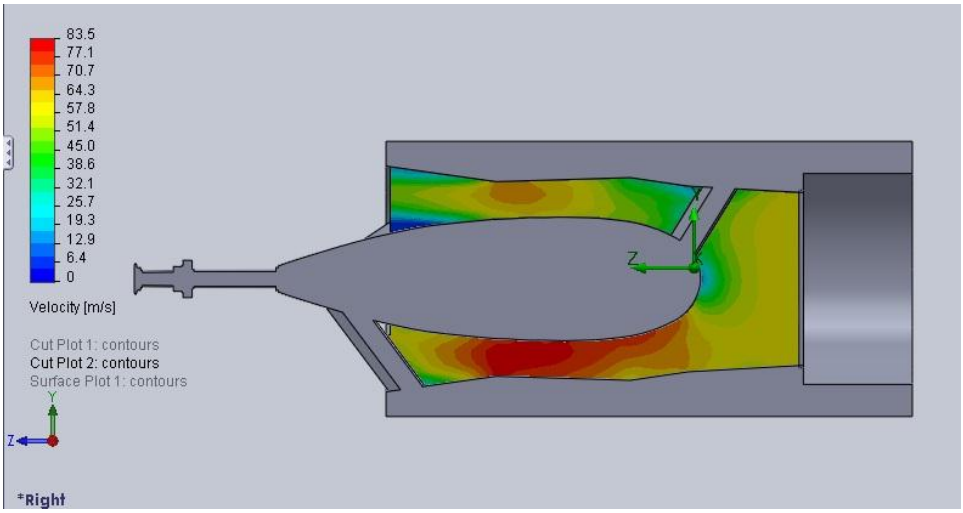

Figure 113 - SolidWorks Flow Simulation Velocity Distribution through Cross-Section of 7.5 Base Tunnel - Small Scale - Uniform Flow

7.5 BASE TUNNEL – SMALL SCALE – FULLY DEVELOPED FLOW

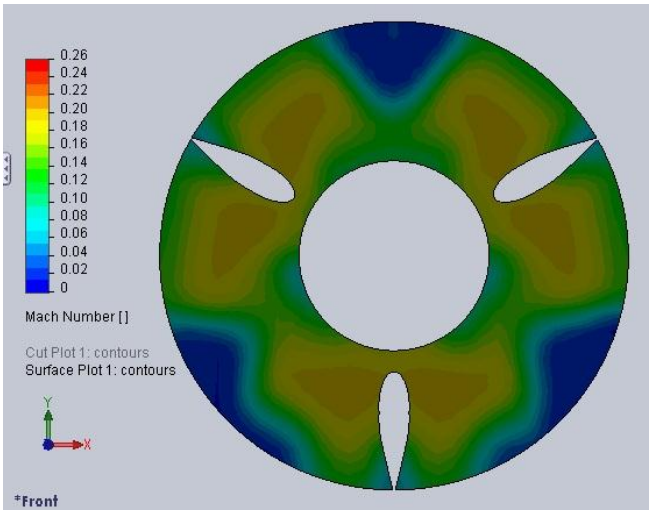

Figure 114 - SolidWorks Flow Simulation Mach Number Distribution at Exit of 7.5 Base Tunnel - Small Scale - Fully Developed Flow

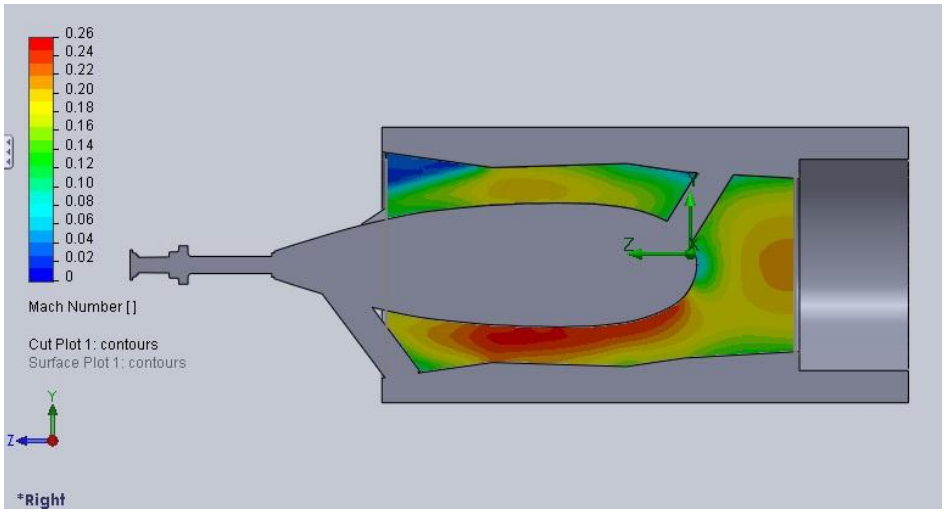

Figure 115 - SolidWorks Flow Simulation Mach Number Distribution through Cross-Section of 7.5 Base Tunnel - Small Scale - Fully Developed Flow

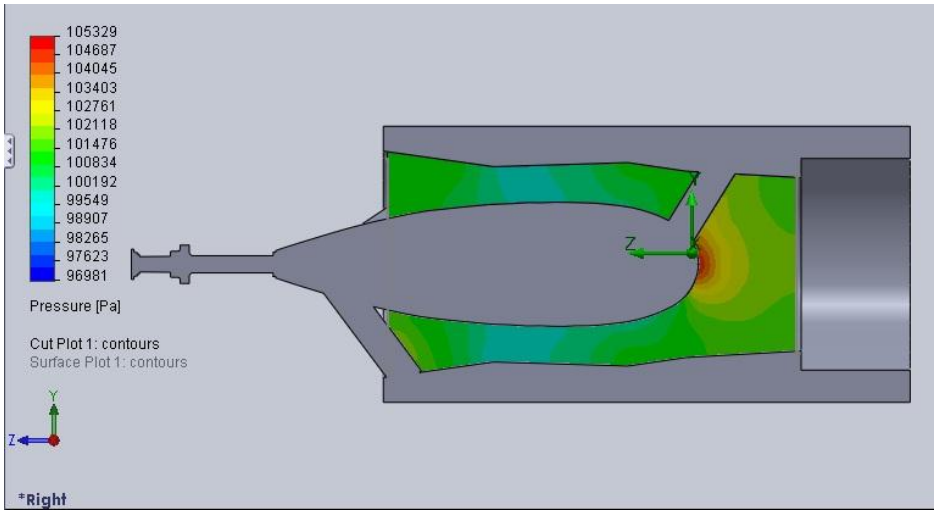

Figure 116 - SolidWorks Flow Simulation Static Pressure Distribution through Cross-Section of 7.5 Base Tunnel – Small Scale – Fully Developed Flow

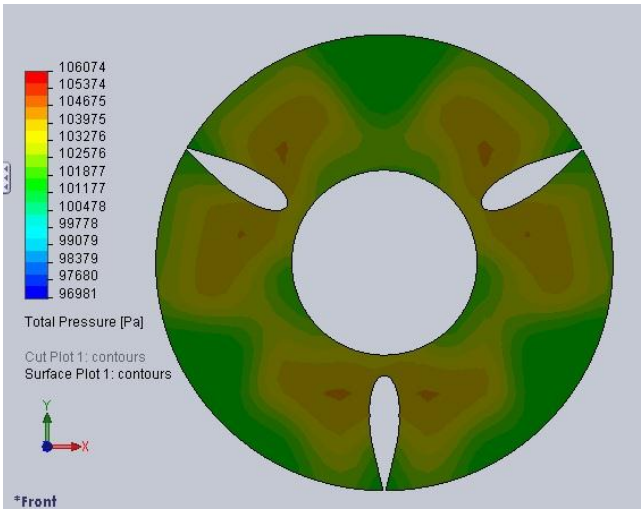

Figure 117 - SolidWorks Flow Simulation Total Pressure Distribution at Exit of 7.5 Base Tunnel - Small Scale - Fully Developed Flow

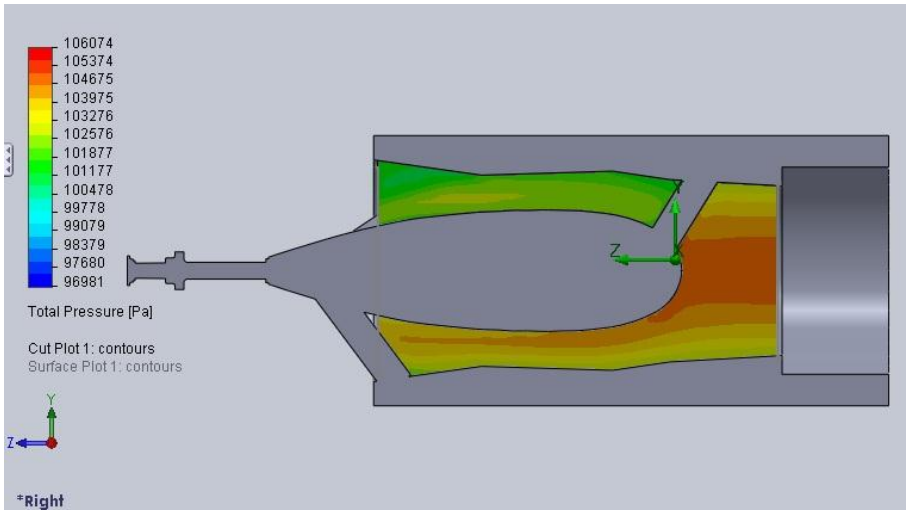

Figure 118 - SolidWorks Flow Simulation Total Pressure Distribution through Cross-Section of 7.5 Base Tunnel - Small Scale - Fully Developed Flow

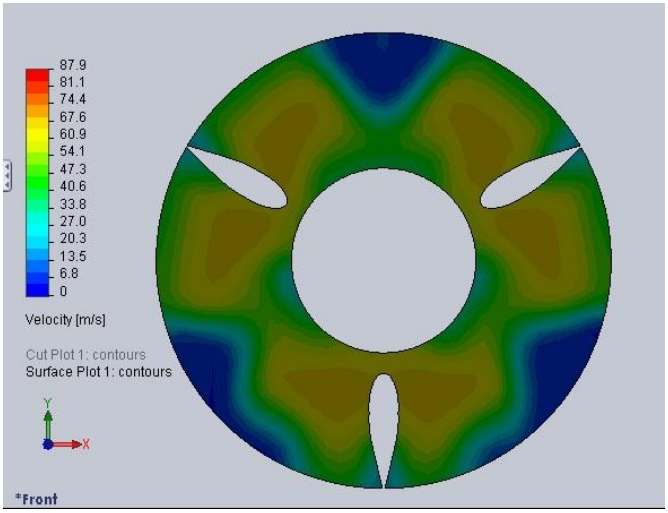

Figure 119 - SolidWorks Flow Simulation Velocity Distribution at Exit of 7.5 Base Tunnel - Small Scale - Fully Developed Flow

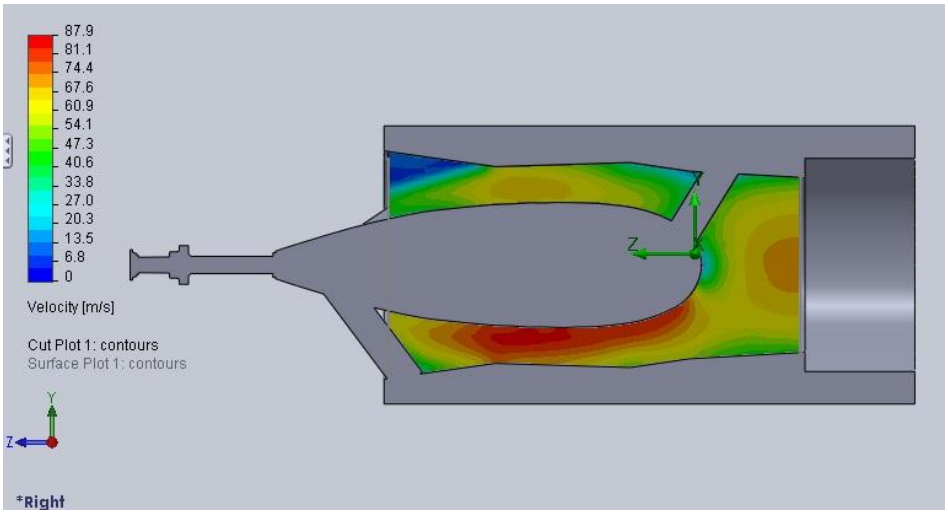

Figure 120 - SolidWorks Flow Simulation Velocity Distribution through Cross-Section of 7.5 Base Tunnel - Small Scale - Fully Developed Flow

3.5 BASE TUNNEL – SMALL SCALE – UNIFORM FLOW

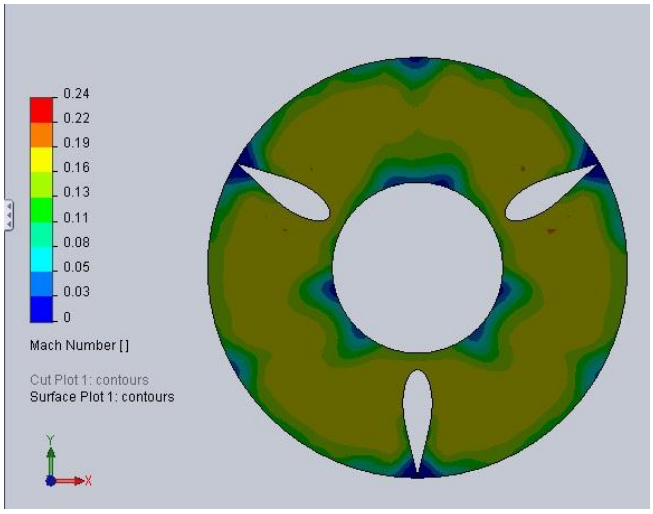

Figure 121 - SolidWorks Flow Simulation Mach Number Distribution at Exit of 3.5 Base Tunnel - Small Scale - Uniform Flow

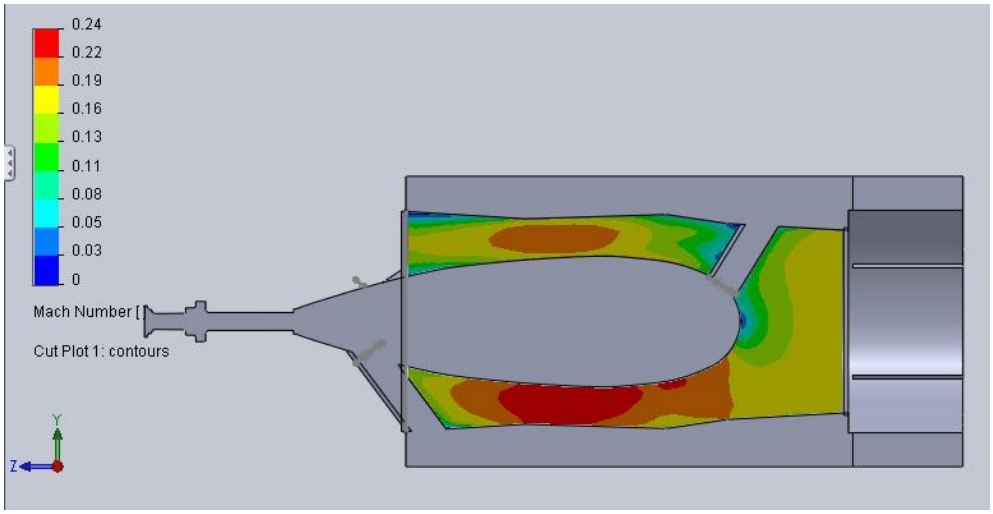

Figure 122 - SolidWorks Flow Simulation Mach Number Distribution through Cross-Section of 3.5 Base Tunnel - Small Scale - Uniform Flow

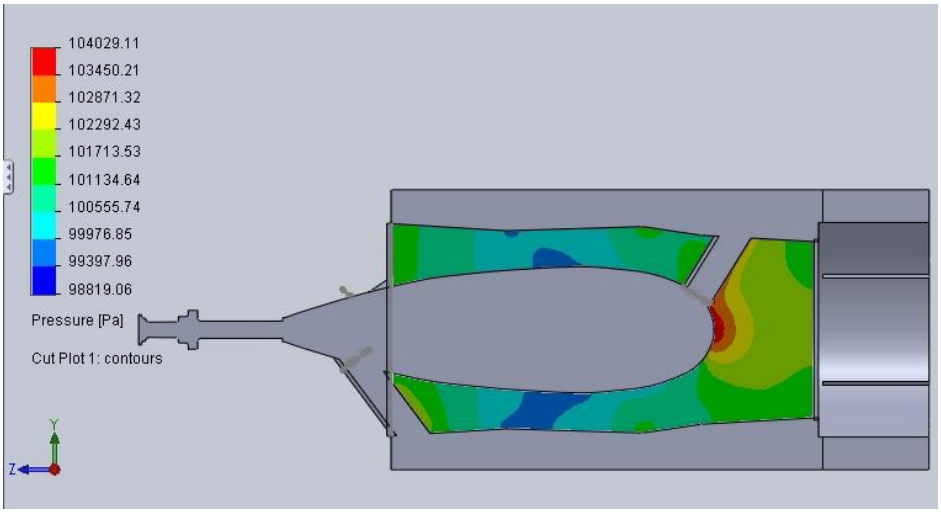

Figure 123 - SolidWorks Flow Simulation Static Pressure Distribution through Cross-Section of 3.5 Base Tunnel - Small Scale - Uniform Flow

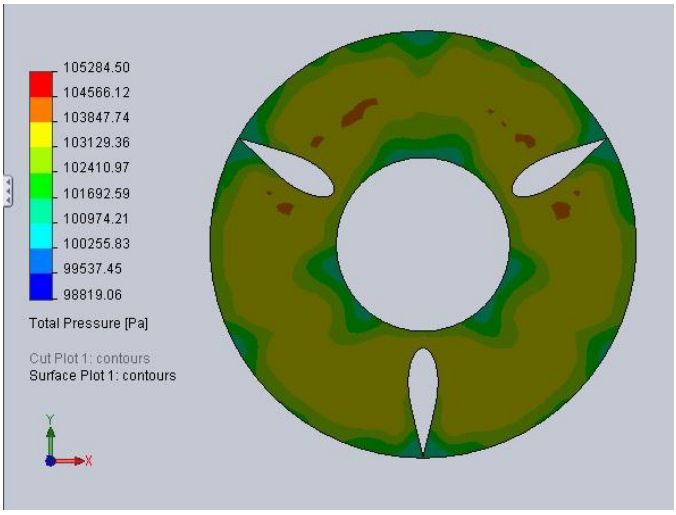

Figure 124 - SolidWorks Flow Simulation Total Pressure Distribution at Exit of 3.5 Base Tunnel - Small Scale - Uniform Flow

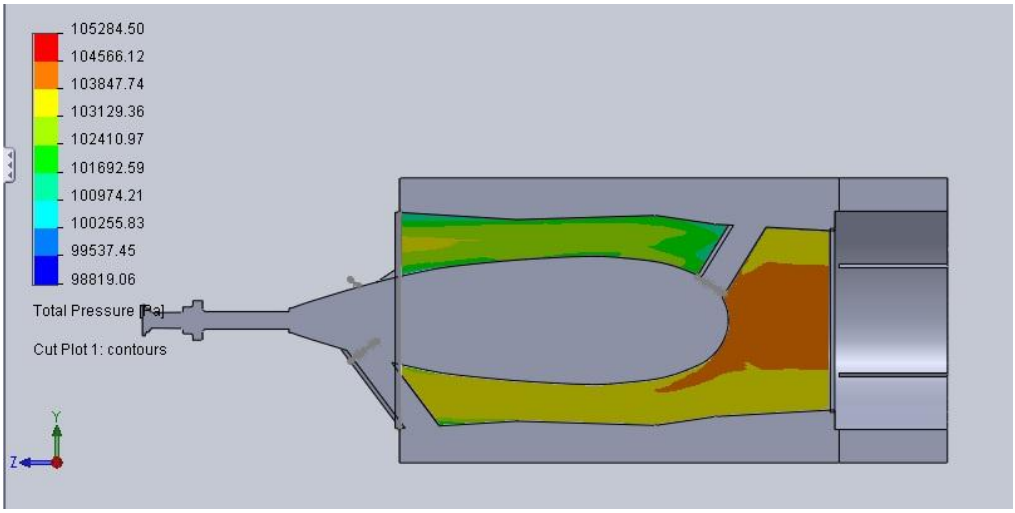

Figure 125 - SolidWorks Flow Simulation Total Pressure Distribution through Cross-Section of 3.5 Base Tunnel - Small Scale - Uniform Flow

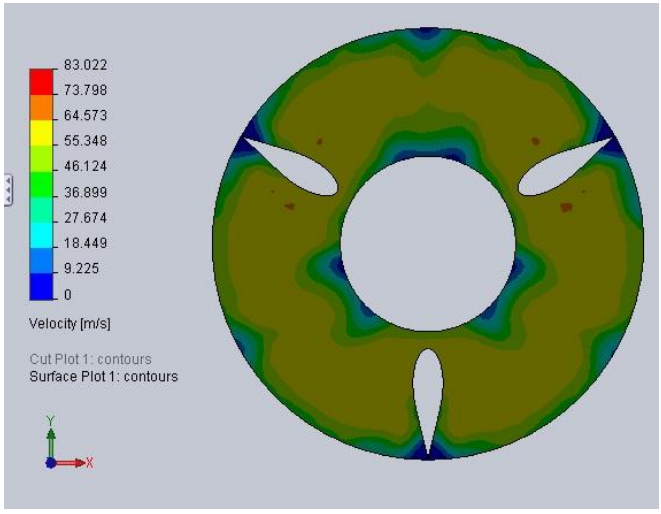

Figure 126 - SolidWorks Flow Simulation Velocity Distribution at Exit of 3.5 Base Tunnel - Small Scale – Uniform Flow

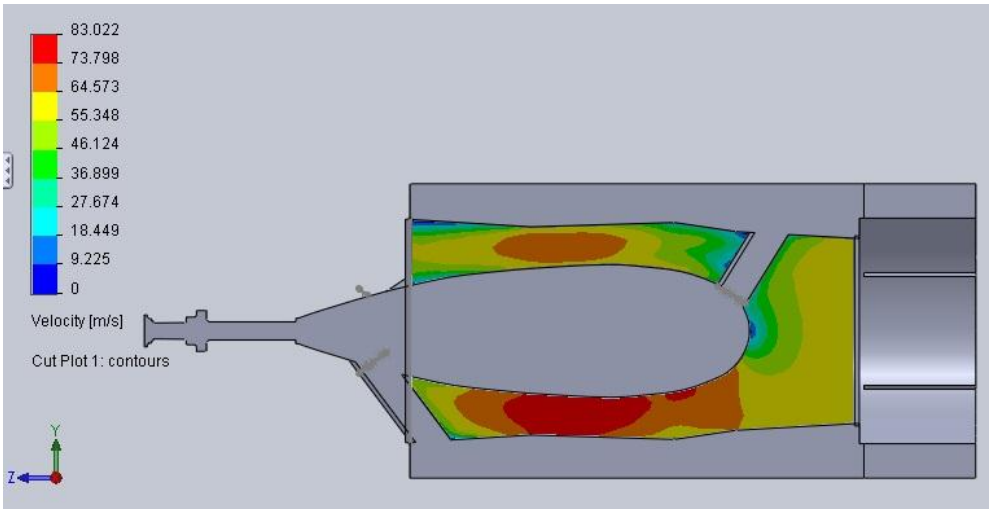

Figure 127 - SolidWorks Flow Simulation Velocity Distribution through Cross-Section of 3.5 Base Tunnel - Small Scale – Uniform Flow

3.5 BASE TUNNEL – SMALL SCALE – FULLY DEVELOPED FLOW

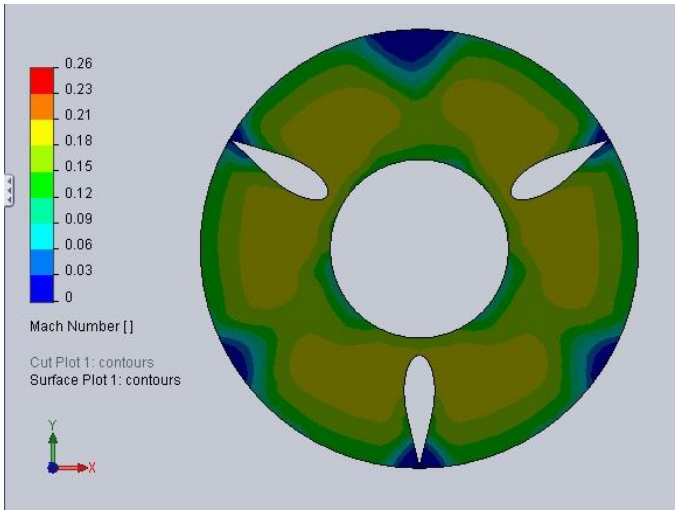

Figure 128 - SolidWorks Flow Simulation Mach Number Distribution at Exit of 3.5 Base Tunnel - Small Scale - Fully Developed Flow

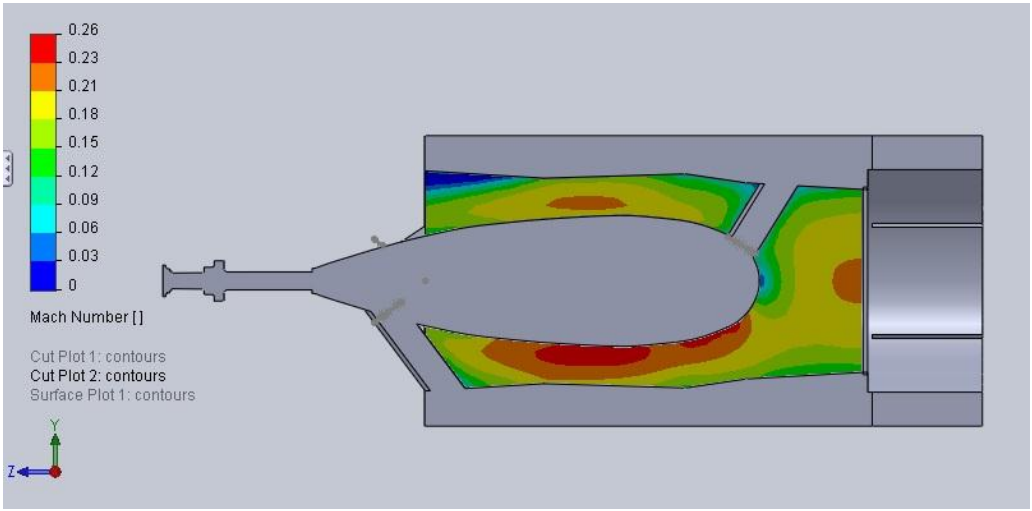

Figure 129 - SolidWorks Flow Simulation Mach Number Distribution through Cross-Section of 3.5 Base Tunnel - Small Scale - Fully Developed Flow

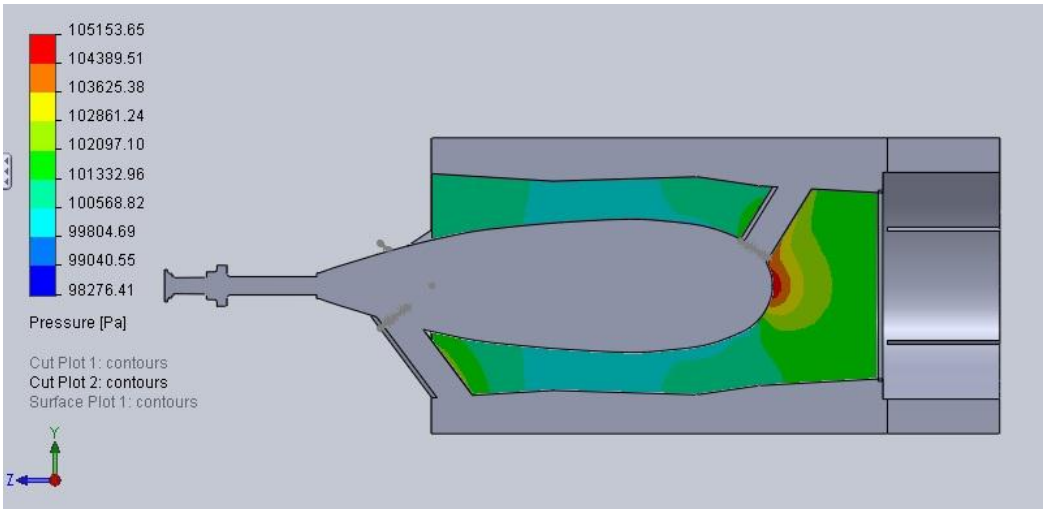

Figure 130 - SolidWorks Flow Simulation Static Pressure Distribution through Cross-Section of 3.5 Base Tunnel - Small Scale - Fully Developed Flow

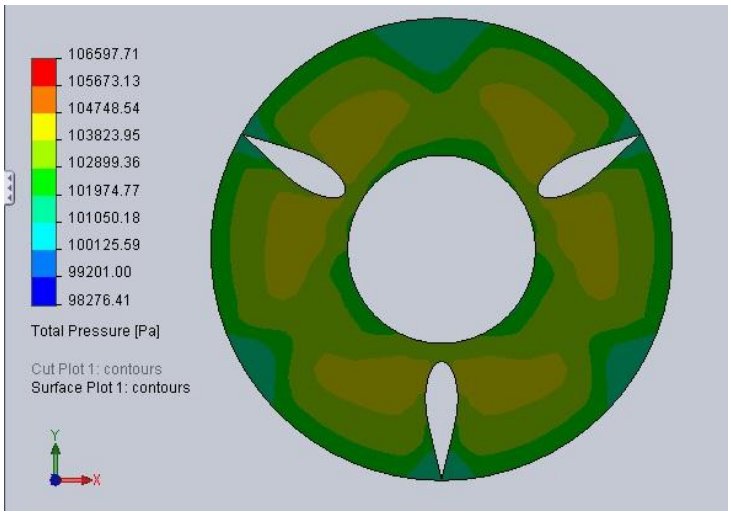

Figure 131 - SolidWorks Flow Simulation Total Pressure Distribution at Exit of 3.5 Base Tunnel - Small Scale - Fully Developed Flow

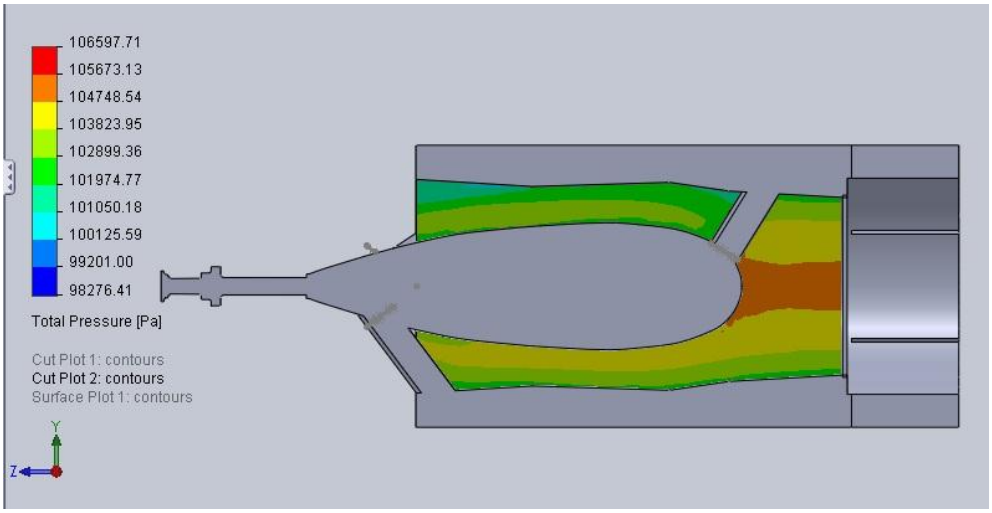

Figure 132 - SolidWorks Flow Simulation Total Pressure Distribution through Cross-Section of 3.5 Base Tunnel - Small Scale - Fully Developed Flow

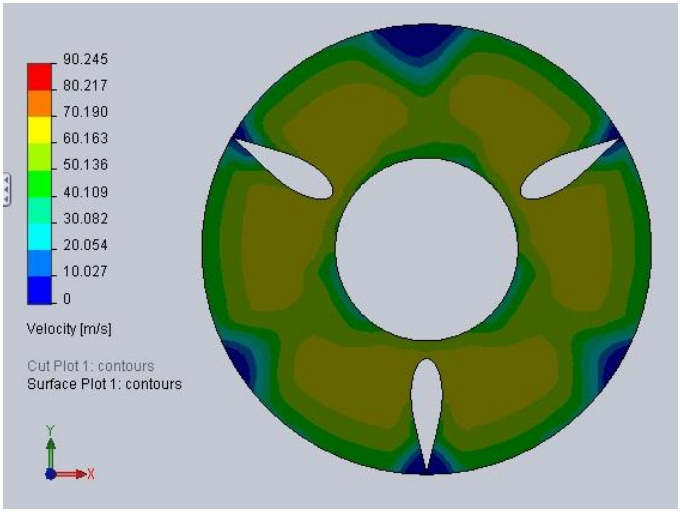

Figure 133 - SolidWorks Flow Simulation Velocity Distribution at Exit of 3.5 Base Tunnel - Small Scale - Fully Developed Flow

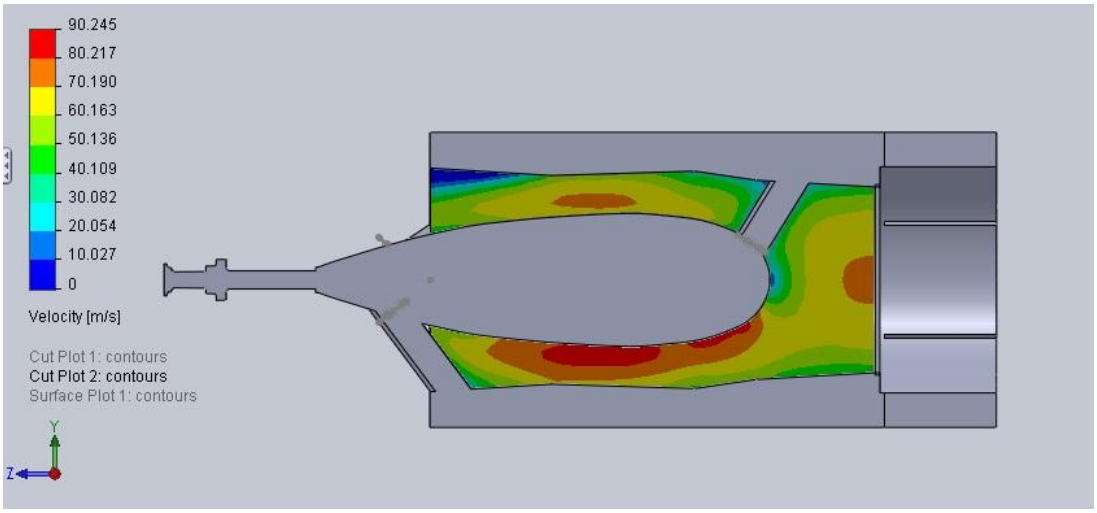

Figure 134 - SolidWorks Flow Simulation Velocity Distribution through Cross-Section of 3.5 Base Tunnel - Small Scale - Fully Developed Flow

3.5 + FLAT – SMALL SCALE – UNIFORM FLOW

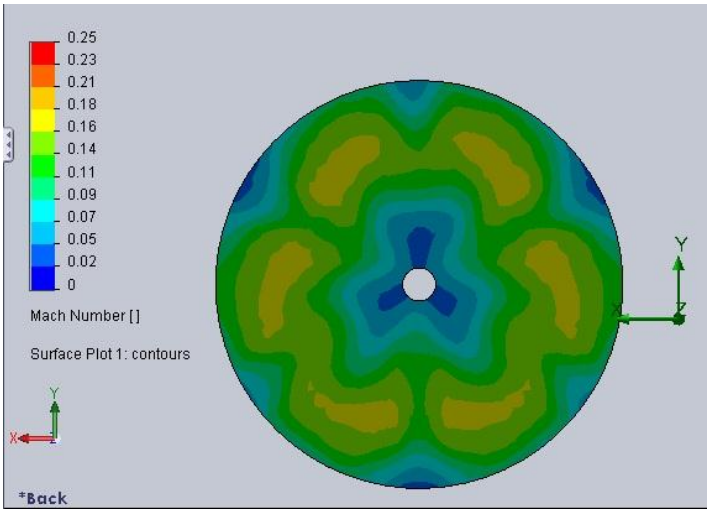

Figure 135 - SolidWorks Flow Simulation Mach Number Distribution at Exit of 3.5 + Flat - Small Scale - Uniform Flow

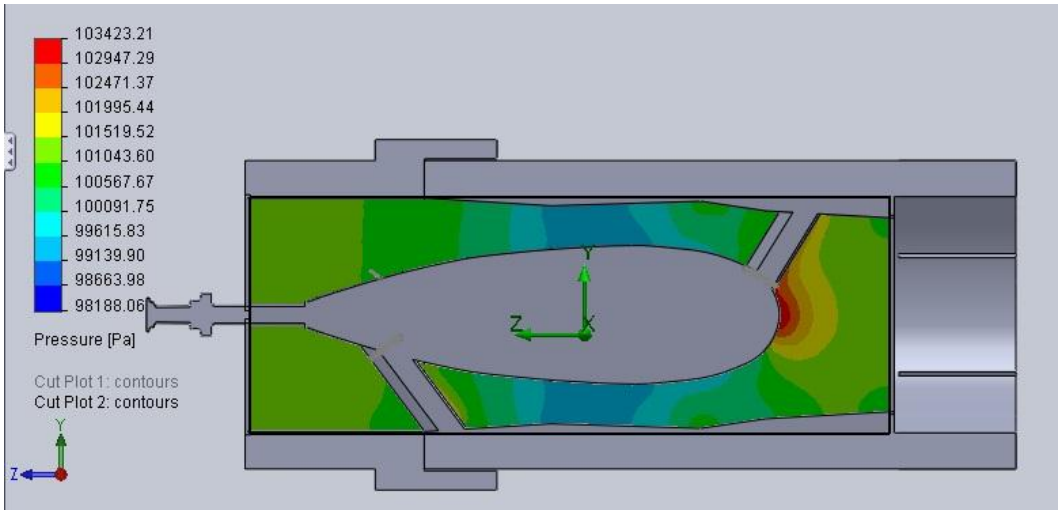

Figure 136 - SolidWorks Flow Simulation Static Pressure Distribution through Cross-Section of 3.5 + Flat - Small Scale - Uniform Flow

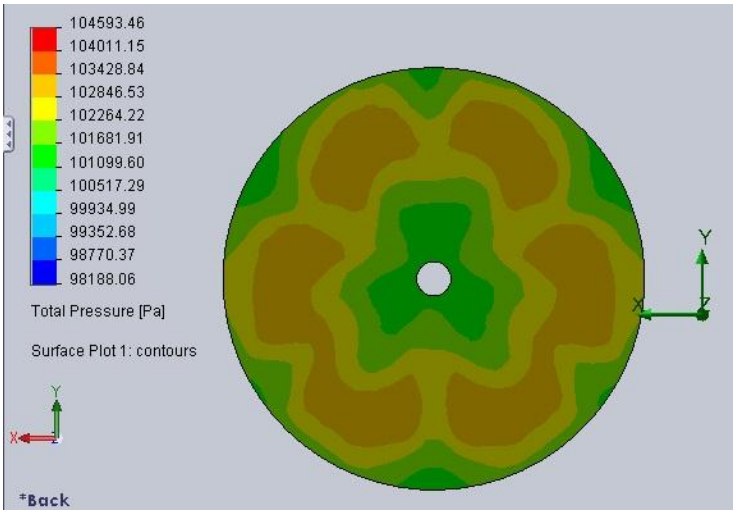

Figure 137 - SolidWorks Flow Simulation Total Pressure Distribution at Exit of 3.5 + Flat - Small Scale - Uniform Flow

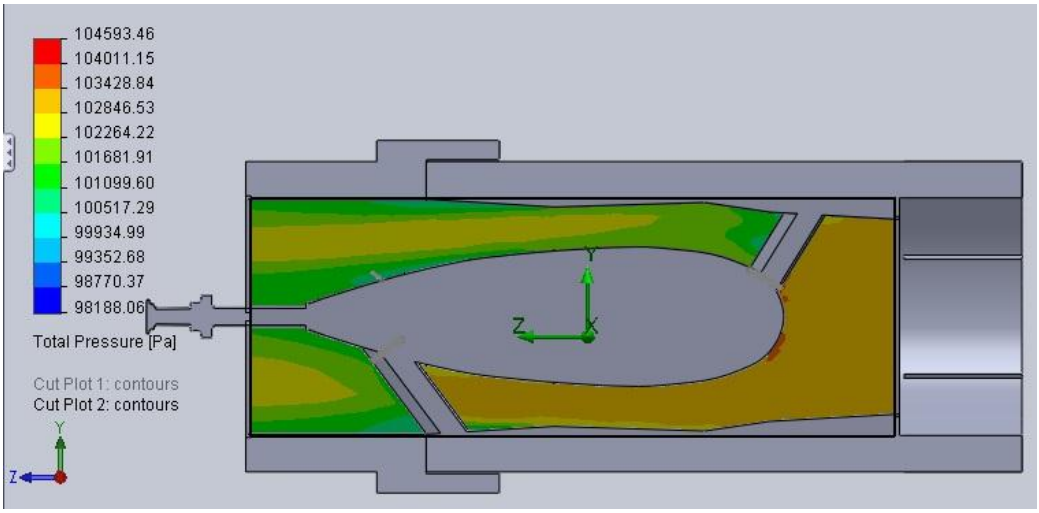

Figure 138 - SolidWorks Flow Simulation Total Pressure Distribution through Cross-Section of 3.5 + Flat - Small Scale - Uniform Flow

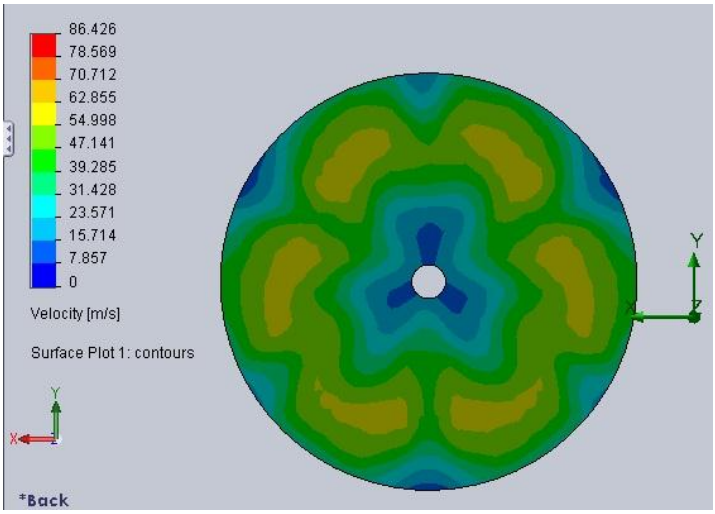

Figure 139 - SolidWorks Flow Simulation Velocity Distribution at Exit of 3.5 + Flat - Small Scale - Uniform Flow

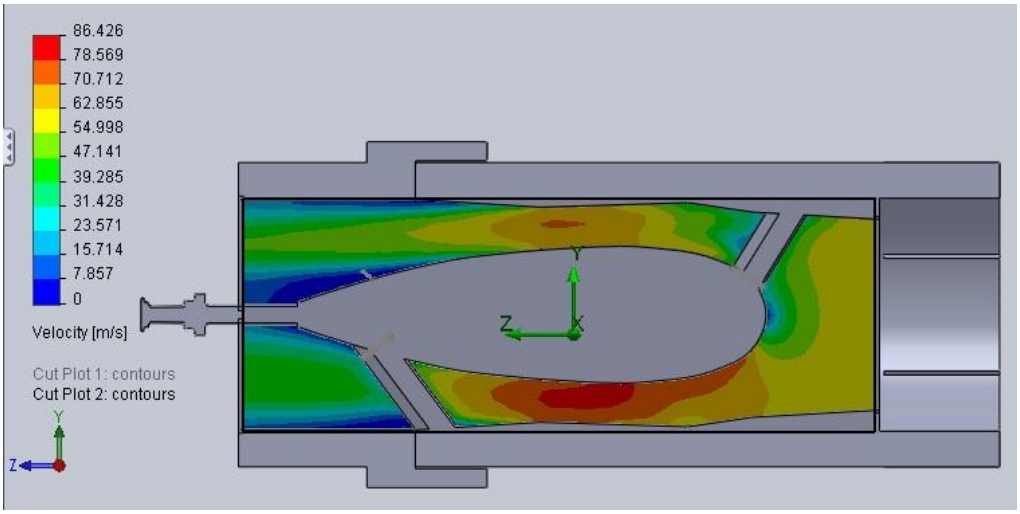

Figure 140 - SolidWorks Flow Simulation Velocity Distribution through Cross-Section of 3.5 + Flat - Small Scale - Uniform Flow

3.5 + FLAT – SMALL SCALE – FULLY DEVELOPED FLOW

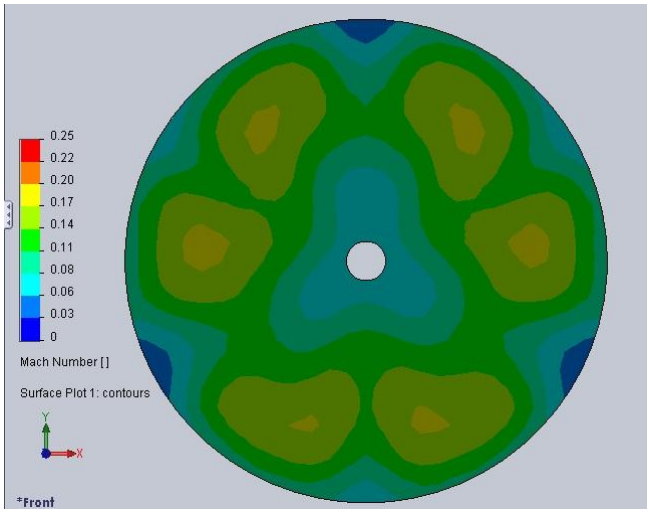

Figure 141 - SolidWorks Flow Simulation Mach Number Distribution at Exit of 3.5 + Flat - Small Scale - Fully Developed Flow

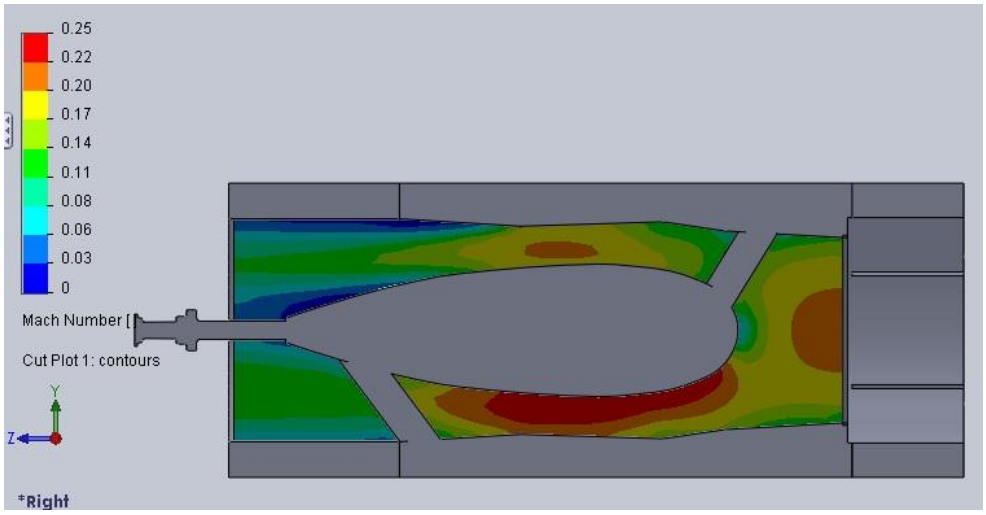

Figure 142 - SolidWorks Flow Simulation Mach Number Distribution through Cross-Section of 3.5 + Flat - Small Scale - Fully Developed Flow

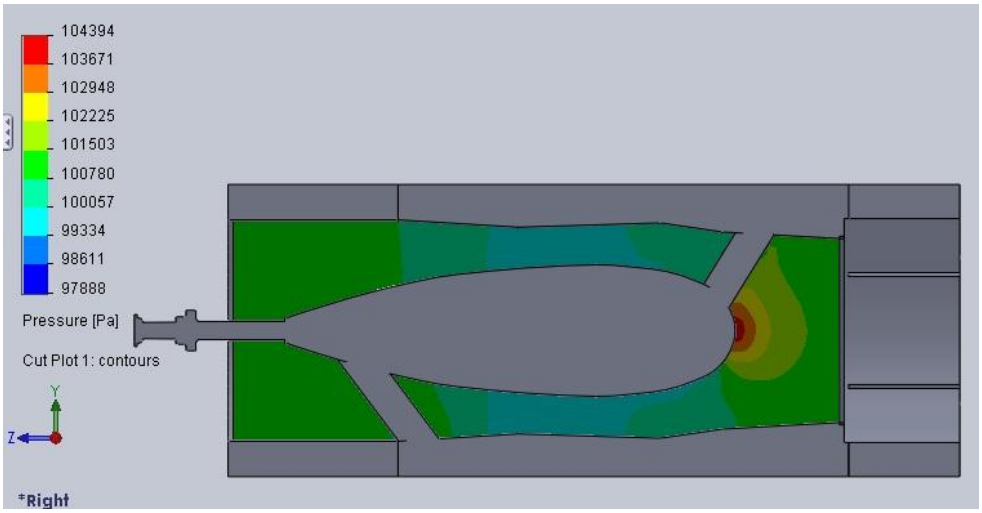

Figure 143 - SolidWorks Flow Simulation Static Pressure Distribution through Cross-Section of 3.5 + Flat - Small Scale - Fully Developed Flow

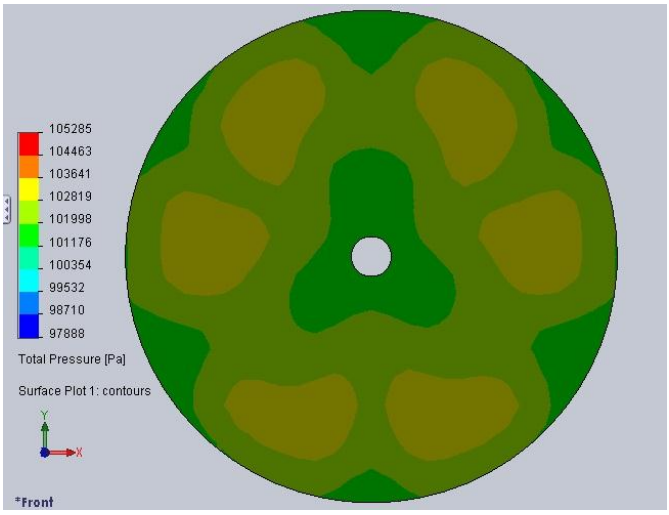

Figure 144 - SolidWorks Flow Simulation Total Pressure Distribution at Exit of 3.5 + Flat - Small Scale - Fully Developed Flow

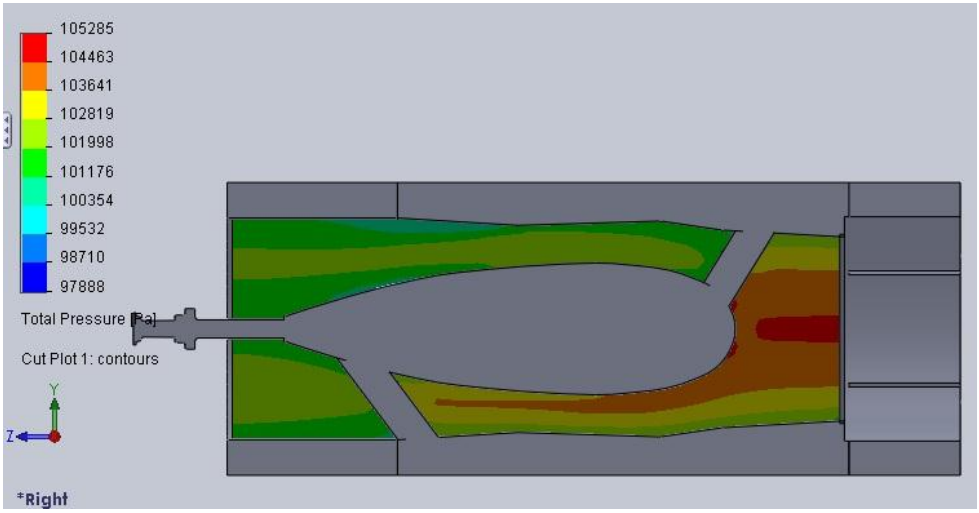

Figure 145 - SolidWorks Flow Simulation Total Pressure Distribution through Cross-Section of 3.5 + Flat - Small Scale - Fully Developed Flow

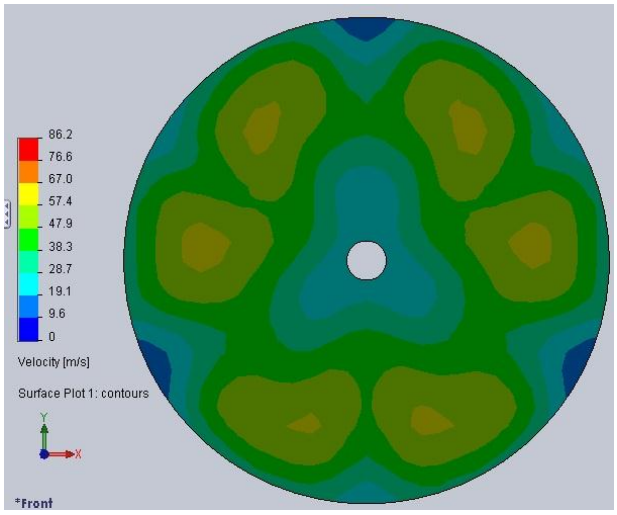

Figure 146 - SolidWorks Flow Simulation Velocity Distribution at Exit of 3.5 + Flat - Small Scale - Fully Developed Flow

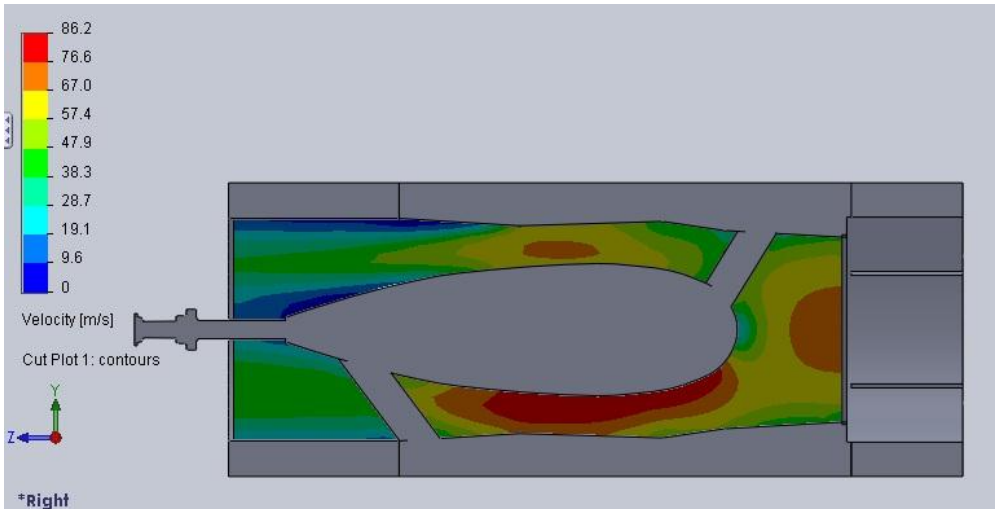

Figure 147 - SolidWorks Flow Simulation Velocity Distribution through Cross-Section of 3.5 + Flat - Small Scale - Fully Developed Flow

3.5 + FLAT + CONICAL – SMALL SCALE – UNIFORM FLOW

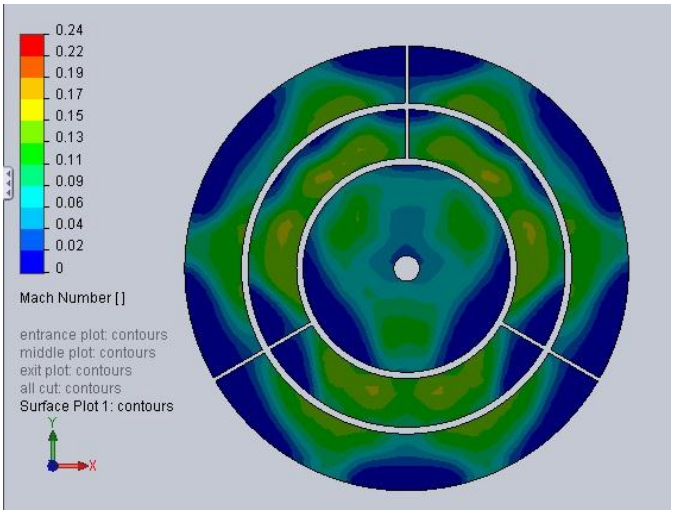

Figure 148 - SolidWorks Flow Simulation Mach Number Distribution at Exit of 3.5 + Flat + Conical - Small Scale - Uniform Flow

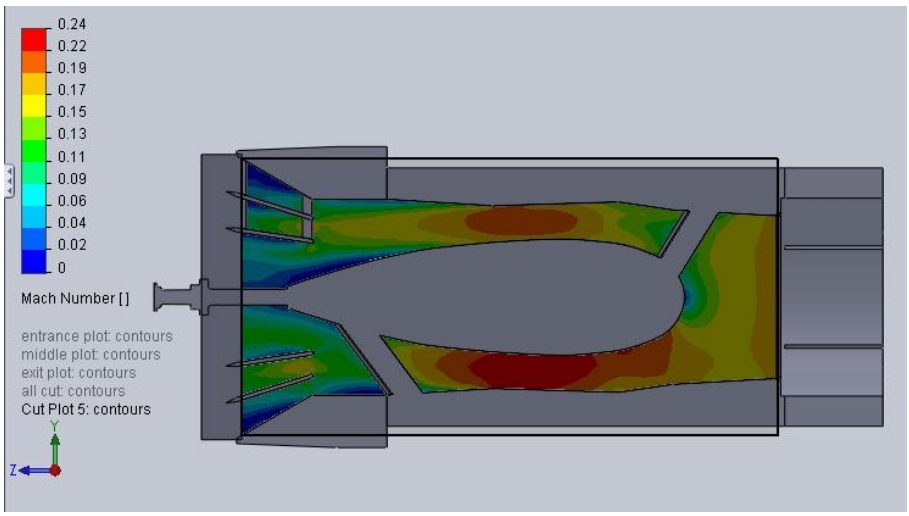

Figure 149 - SolidWorks Flow Simulation Mach Number Distribution through Cross-Section of 3.5 + Flat + Conical - Small Scale - Fully Developed Flow

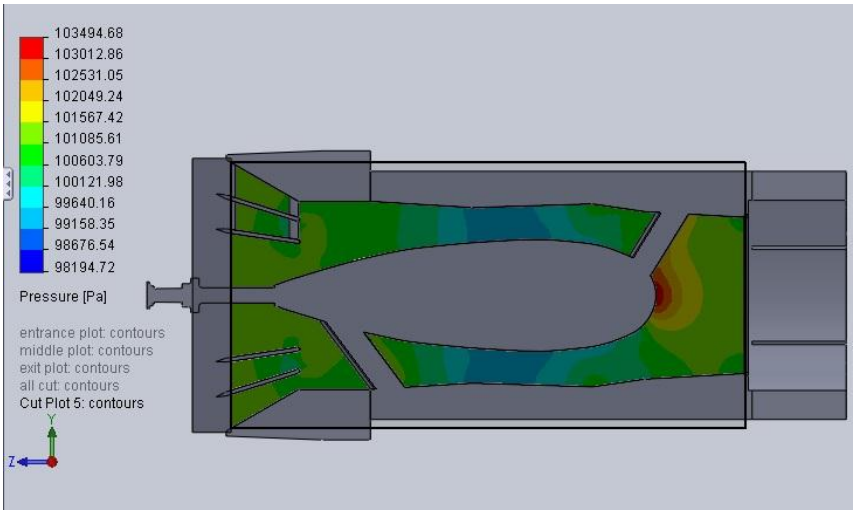

Figure 150 - SolidWorks Flow Simulation Static Pressure Distribution through Cross-Section of 3.5 + Flat + Conical - Small Scale - Fully Developed Flow

Figure 151 - SolidWorks Flow Simulation Total Pressure Distribution at Exit of 3.5 + Flat + Conical - Small Scale - Uniform Flow

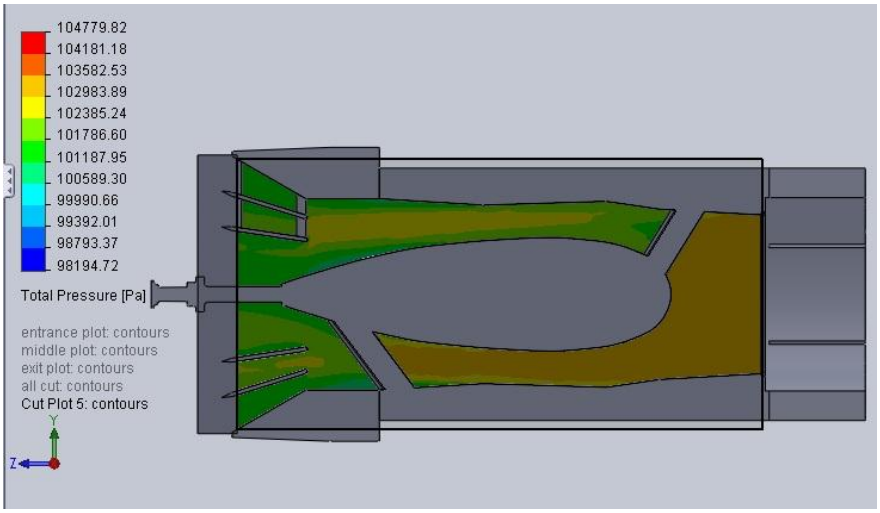

Figure 152 - SolidWorks Flow Simulation Total Pressure Distribution through Cross-Section of 3.5 + Flat + Conical - Small Scale - Uniform Flow

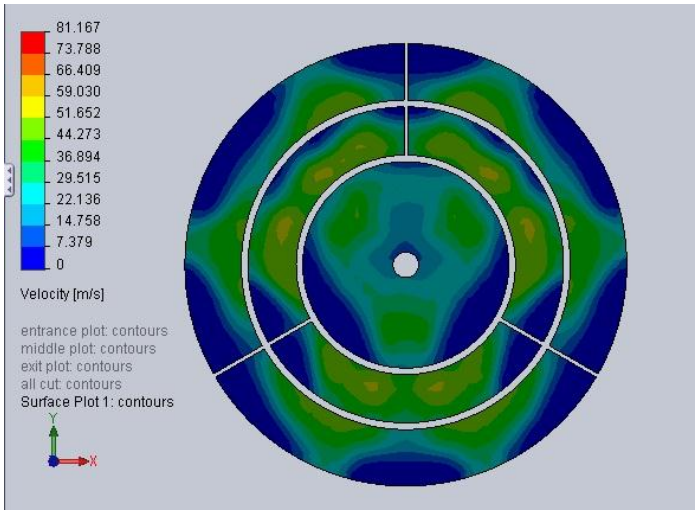

Figure 153 - SolidWorks Flow Simulation Velocity Distribution at Exit of 3.5 + Flat + Conical - Small Scale - Uniform Flow

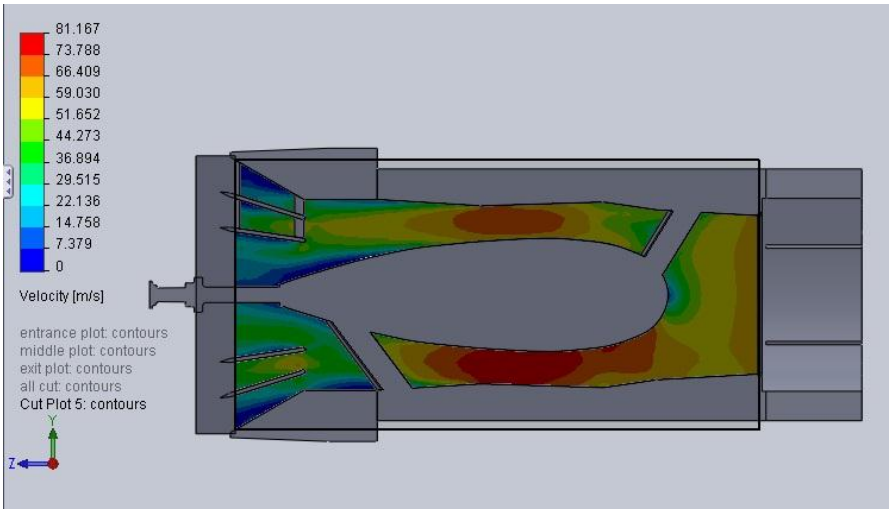

Figure 154 - SolidWorks Flow Simulation Velocity Distribution through Cross-Section of 3.5 + Flat + Conical - Small Scale - Uniform Flow

3.5 + FLAT + CONICAL – SMALL SCALE – FULLY DEVELOPED FLOW

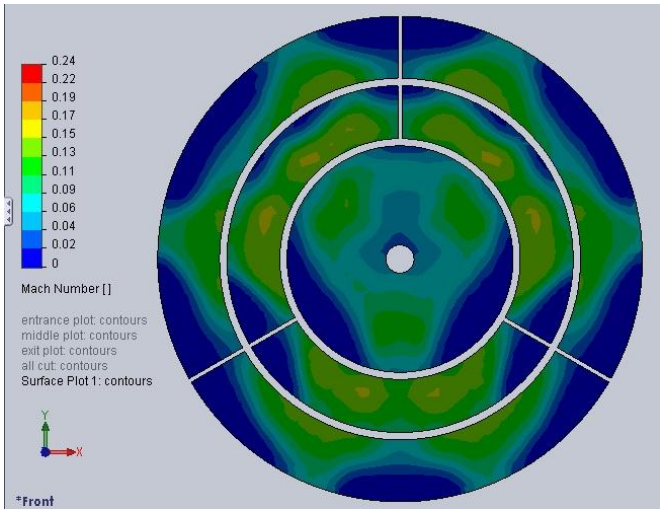

Figure 155 - SolidWorks Flow Simulation Mach Number Distribution at Exit of 3.5 + Flat + Conical - Small Scale - Fully Developed Flow

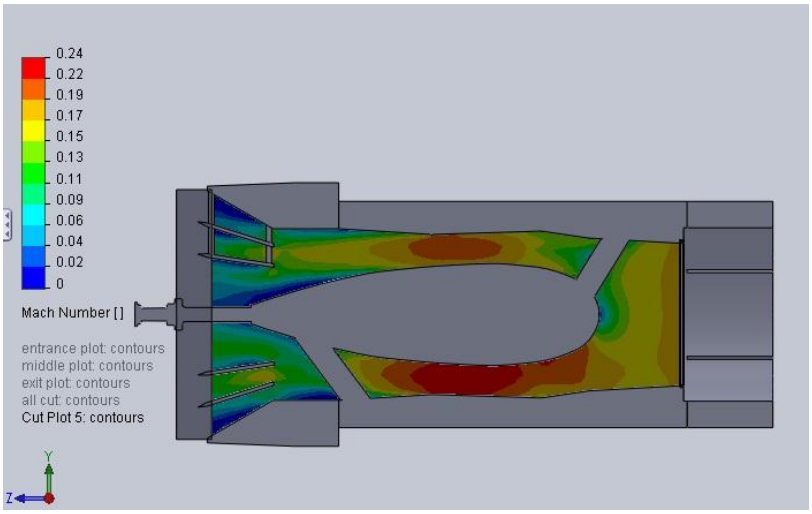

Figure 156 - SolidWorks Flow Simulation Mach Number Distribution through Cross-Section of 3.5 + Flat + Conical - Small Scale - Fully Developed Flow

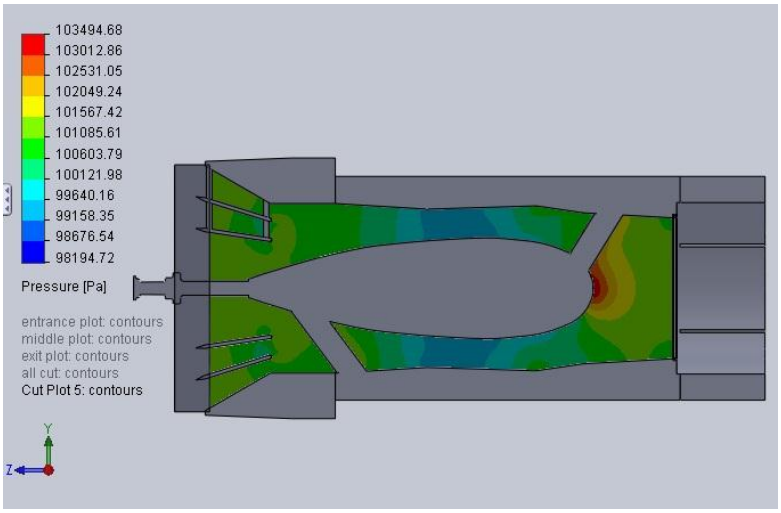

Figure 157 - SolidWorks Flow Simulation Static Pressure Distribution through Cross-Section of 3.5 + Flat + Conical - Small Scale - Fully Developed Flow

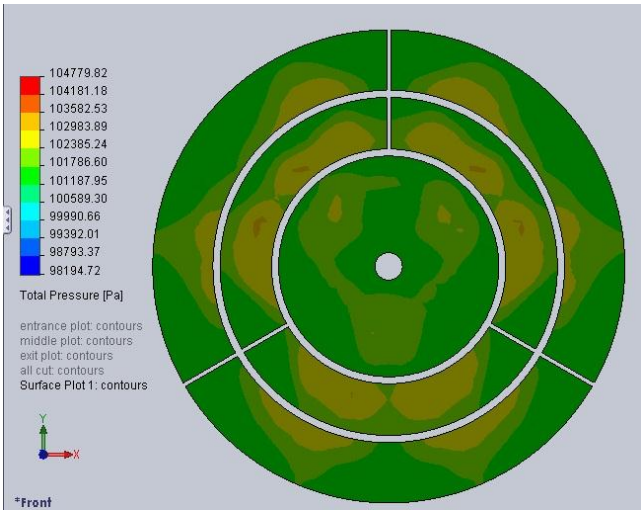

Figure 158 - SolidWorks Flow Simulation Total Pressure Distribution at Exit of 3.5 + Flat + Conical - Small Scale - Fully Developed Flow

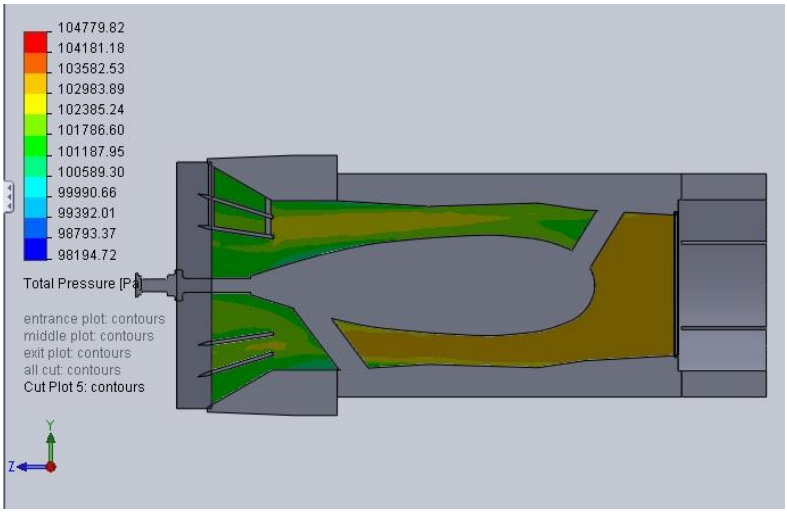

Figure 159 - SolidWorks Flow Simulation Total Pressure Distribution through Cross-Section of 3.5 + Flat + Conical - Small Scale - Fully Developed Flow

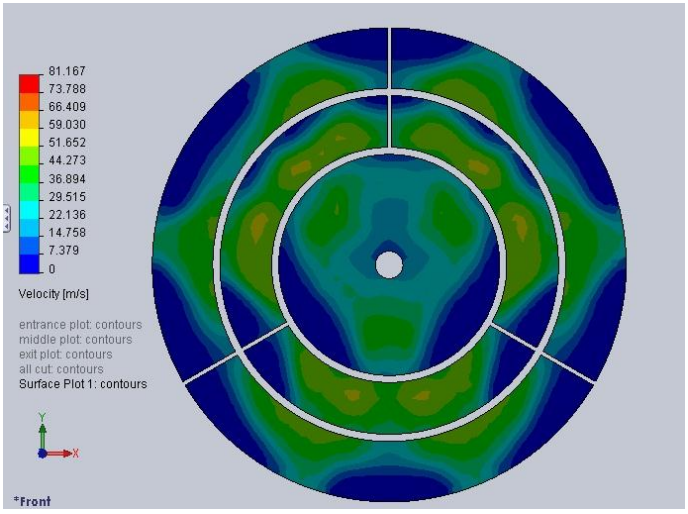

Figure 160 - SolidWorks Flow Simulation Velocity Distribution at Exit of 3.5 + Flat + Conical - Small Scale - Fully Developed Flow

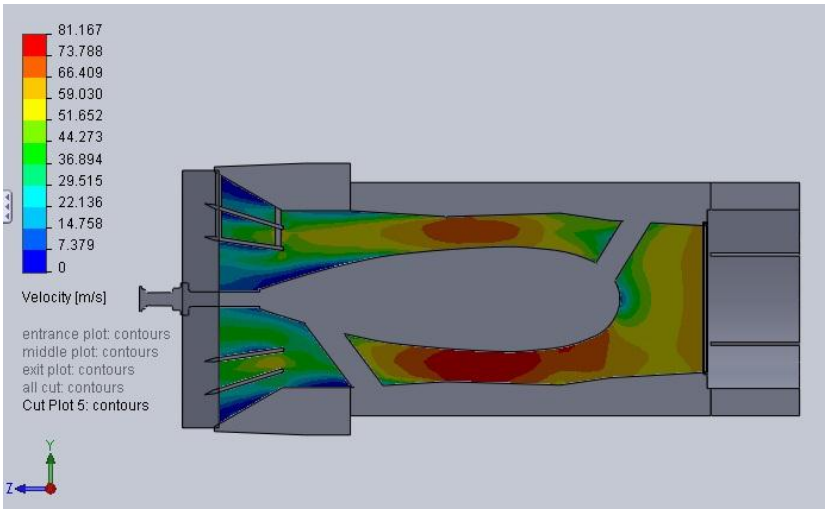

Figure 161 - SolidWorks Flow Simulation Velocity Distribution through Cross-Section of 3.5 + Flat + Conical - Small Scale - Fully Developed Flow

APPENDIX C

ANSYS FLUENT FLOW FIELD DISTRIBUTIONS

7.5 BASE TUNNEL – FULL SIZE – UNIFORM FLOW

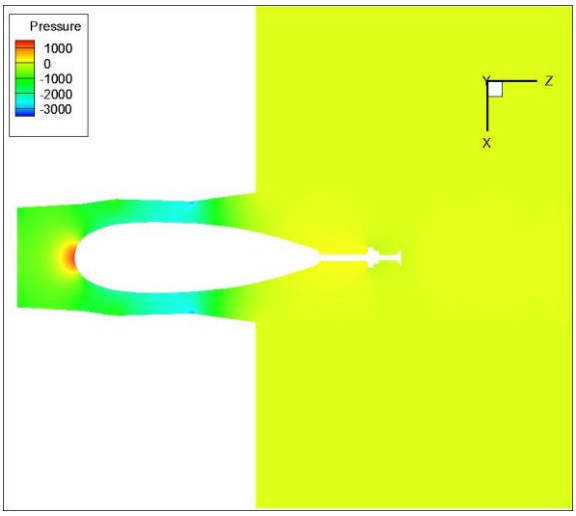

Figure 162 - ANSYS FLUENT Static Pressure Distribution through Cross-Section of 7.5 Base Tunnel - Full Size - Uniform Flow

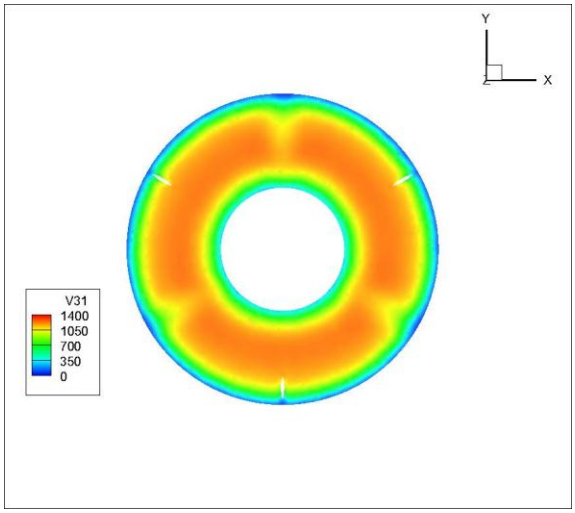

Figure 163 - ANSYS FLUENT Total Pressure Distribution at Exit of 7.5 Base Tunnel - Full Size - Uniform Flow

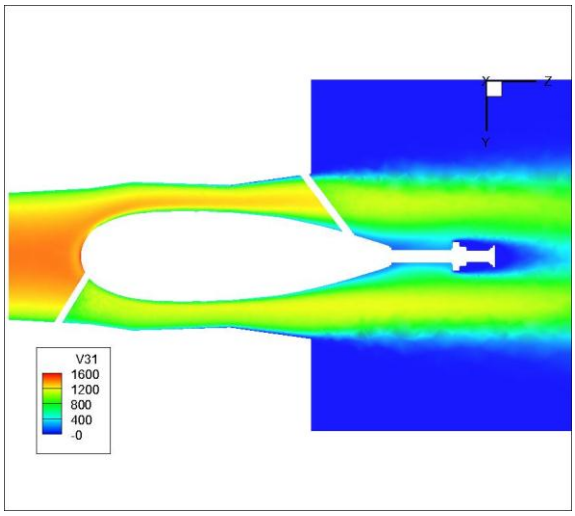

Figure 164 - ANSYS FLUENT Total Pressure Distribution through Cross-Section of 7.5 Base Tunnel - Full Size - Uniform Flow

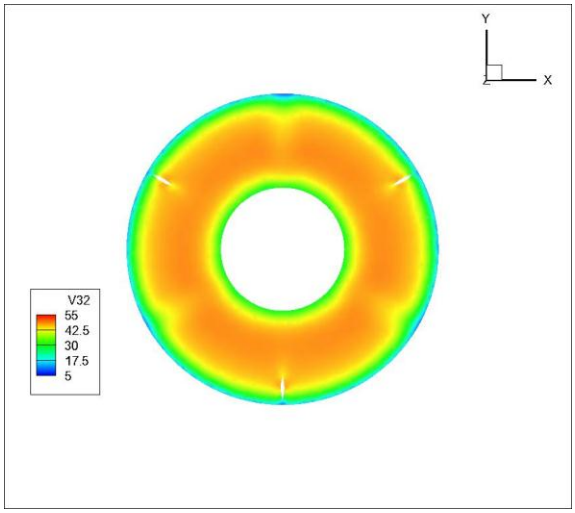

Figure 165 - ANSYS FLUENT Velocity Distribution at Exit of 7.5 Base Tunnel - Full Size - Uniform Flow

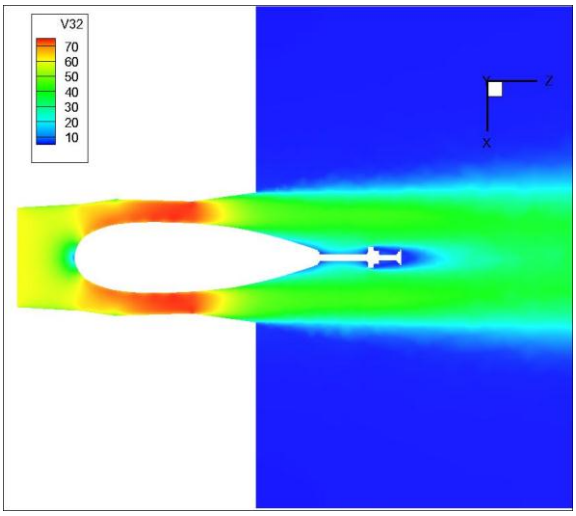

Figure 166 - ANSYS FLUENT Velocity Distribution through Cross-Section of 7.5 Base Tunnel - Full Size - Uniform Flow

7.5 BASE TUNNEL – FULL SIZE – FULLY DEVELOPED FLOW

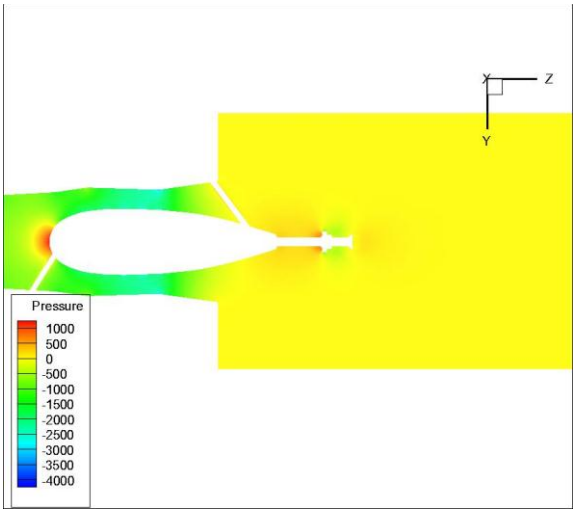

Figure 167 - ANSYS FLUENT Static Pressure Distribution through Cross-Section of 7.5 Base Tunnel - Full Size - Fully Developed Flow

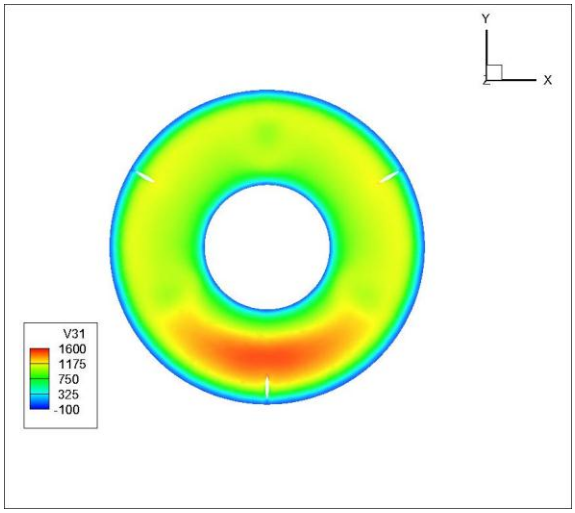

Figure 168 - ANSYS FLUENT Total Pressure Distribution at Exit of 7.5 Base Tunnel - Full Size - Fully Developed Flow

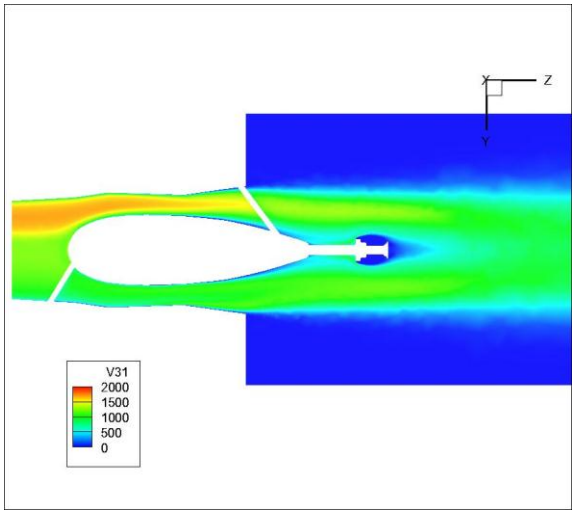

Figure 169 - ANSYS FLUENT Total Pressure Distribution through Cross-Section of 7.5 Base Tunnel - Full Size - Fully Developed Flow

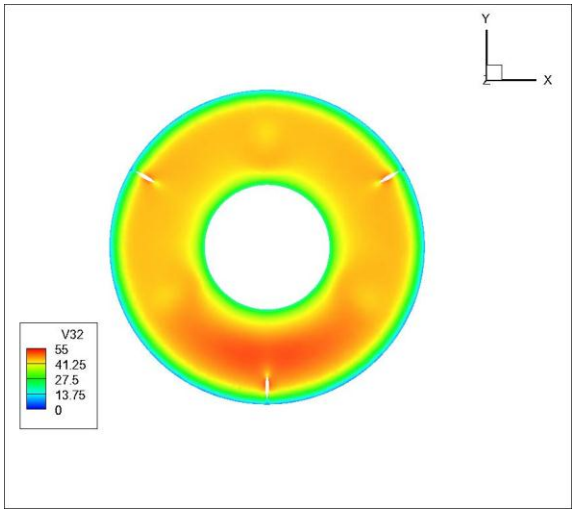

Figure 170 - ANSYS FLUENT Velocity Distribution at Exit of 7.5 Base Tunnel - Full Size - Fully Developed Flow

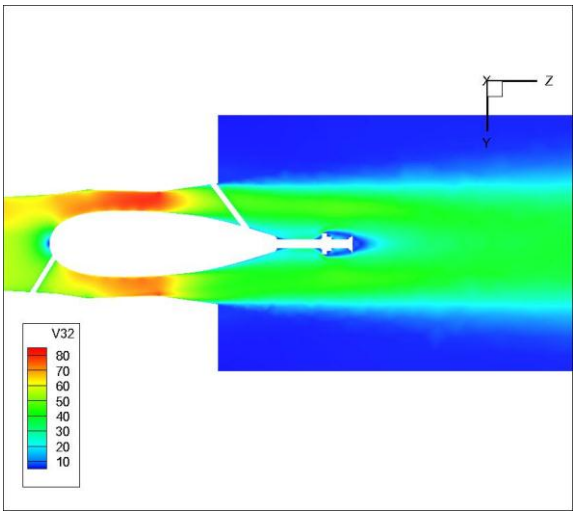

Figure 171 - ANSYS FLUENT Velocity Distribution through Cross-Section of 7.5 Base Tunnel - Full Size - Fully Developed Flow

3.5 BASE TUNNEL – FULL SIZE – UNIFORM FLOW

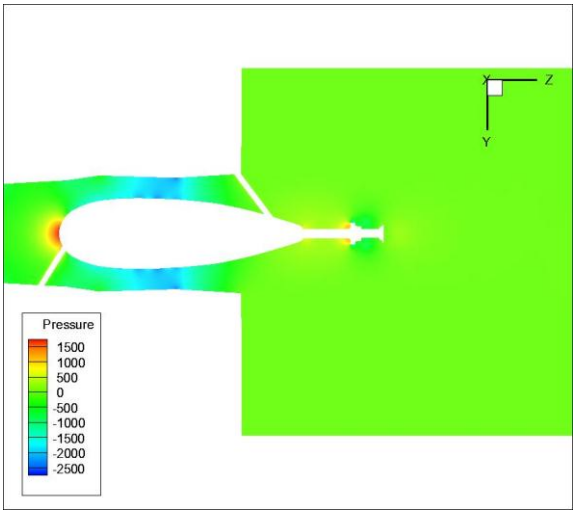

Figure 172 - ANSYS FLUENT Static Pressure Distribution through Cross-Section of 3.5 Base Tunnel - Full Size - Uniform Flow

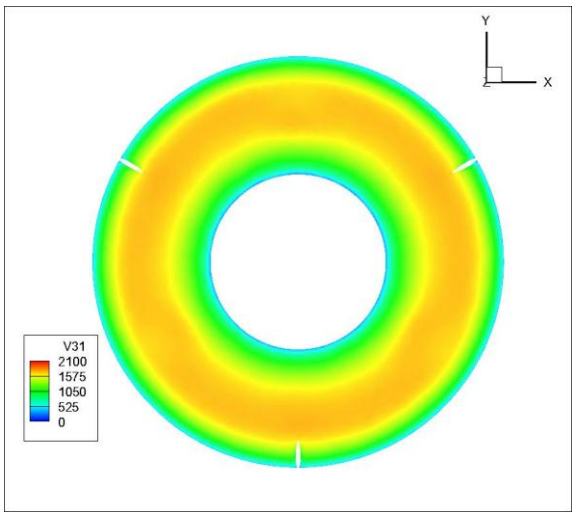

Figure 173 - ANSYS FLUENT Total Pressure Distribution at Exit of 3.5 Base Tunnel - Full Size - Uniform Flow

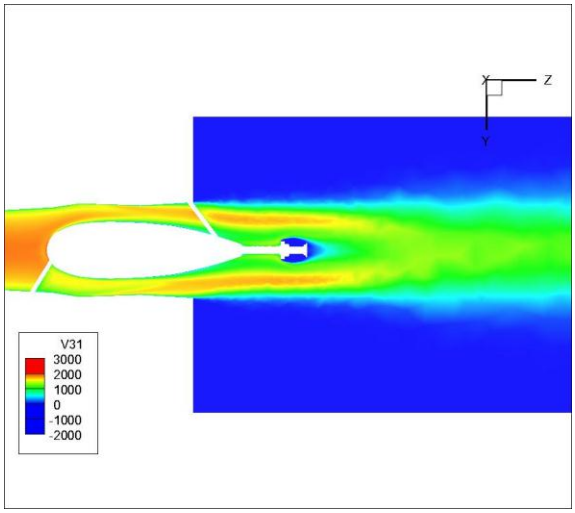

Figure 174 - ANSYS FLUENT Total Pressure Distribution through Cross-Section of 3.5 Base Tunnel - Full Size - Uniform Flow

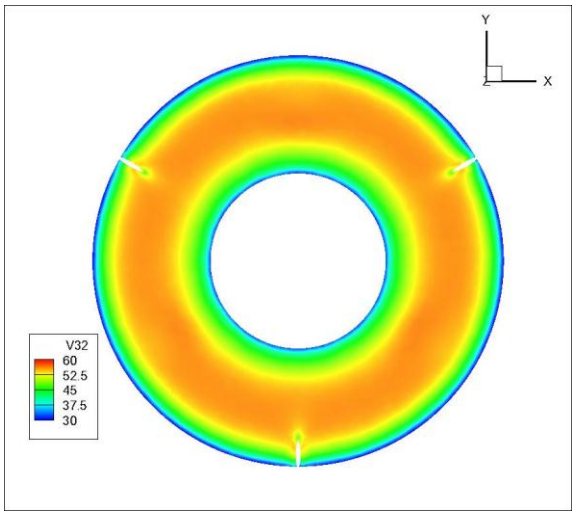

Figure 175 - ANSYS FLUENT Velocity Distribution at Exit of 3.5 Base Tunnel - Full Size - Uniform Flow

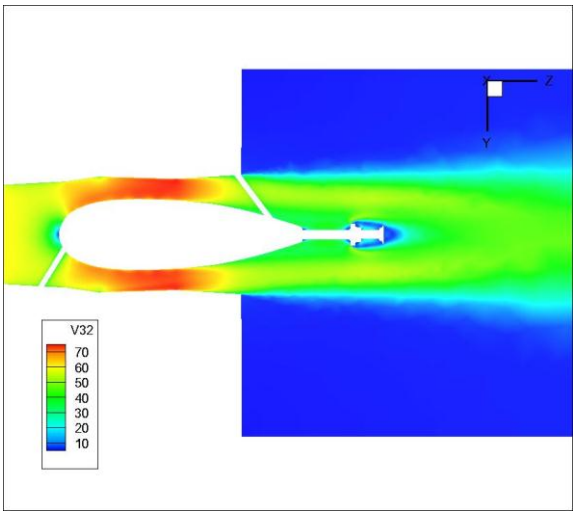

Figure 176 - ANSYS FLUENT Velocity Distribution through Cross-Section of 3.5 Base Tunnel - Full Size - Uniform Flow

3.5 BASE TUNNEL – FULL SIZE – FULLY DEVELOPED FLOW

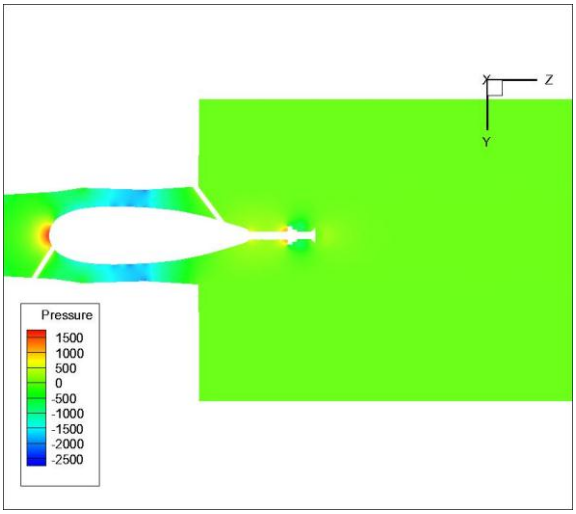

Figure 177 - ANSYS FLUENT Static Pressure Distribution through Cross-Section of 3.5 Base Tunnel - Full Size - Fully Developed Flow

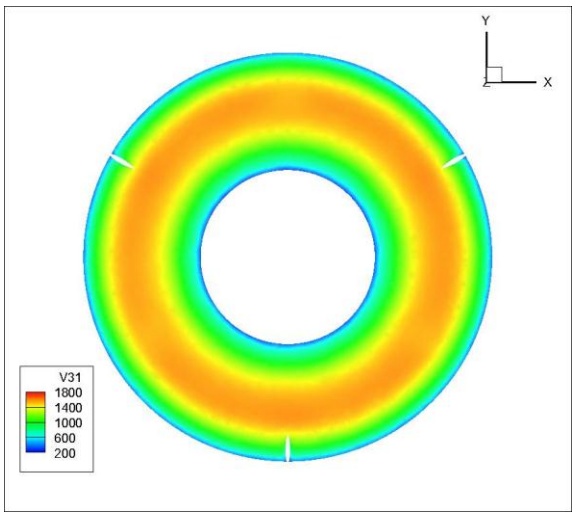

Figure 178 - ANSYS FLUENT Total Pressure Distribution at Exit of 3.5 Base Tunnel - Full Size - Fully Developed Flow

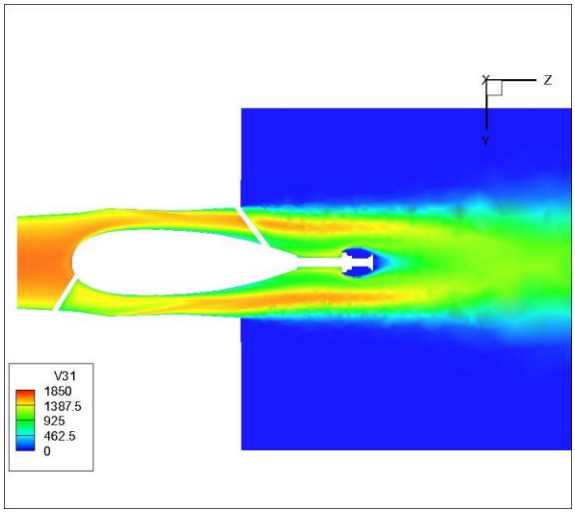

Figure 179 - ANSYS FLUENT Total Pressure Distribution through Cross-Section of 3.5 Base Tunnel - Full Size - Fully Developed Flow

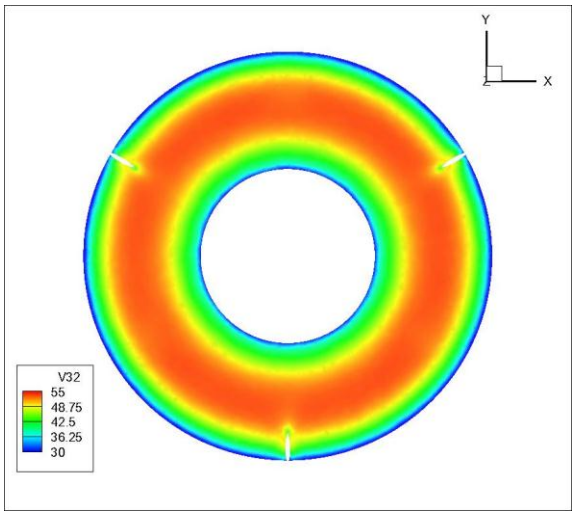

Figure 180 - ANSYS FLUENT Velocity Distribution at Exit of 3.5 Base Tunnel - Full Size - Fully Developed Flow

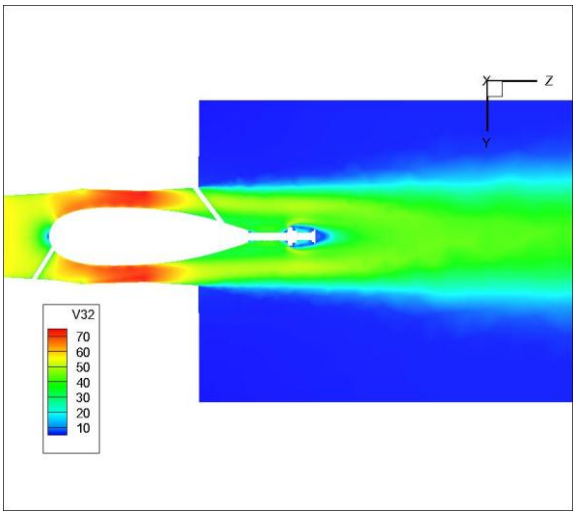

Figure 181 - ANSYS FLUENT Velocity Distribution through Cross-Section of 3.5 Base Tunnel - Full Size - Fully Developed Flow

3.5 + FLAT – FULL SIZE – UNIFORM FLOW

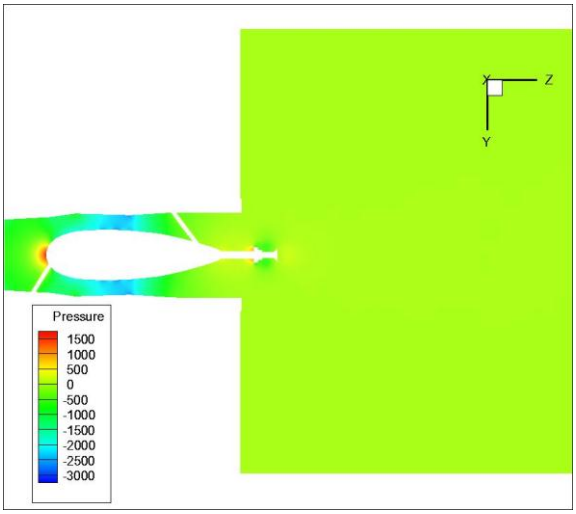

Figure 182 - ANSYS FLUENT Static Pressure Distribution through 3.5 + Flat - Full Size - Uniform Flow

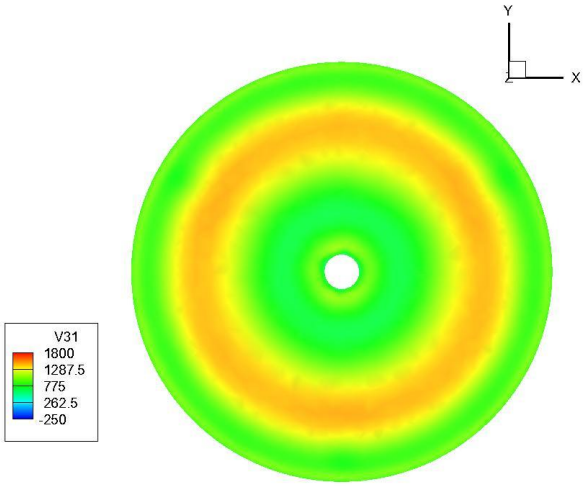

Figure 183 - ANSYS FLUENT Total Pressure Distribution at Exit of 3.5 + Flat - Full Size - Uniform Flow

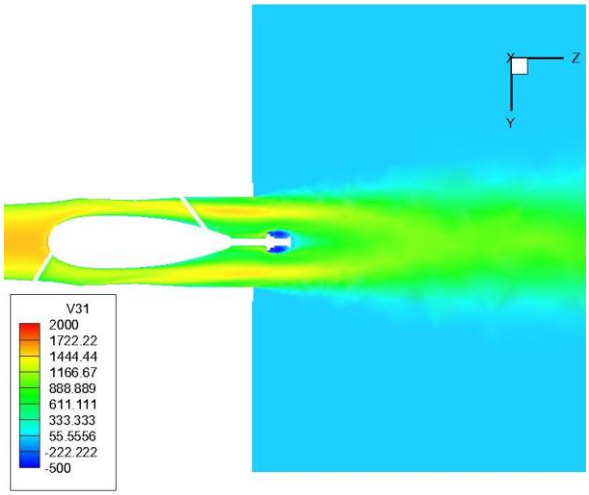

Figure 184 - ANSYS FLUENT Total Pressure Distribution through Cross-Section of 3.5 + Flat - Full Size - Uniform Flow

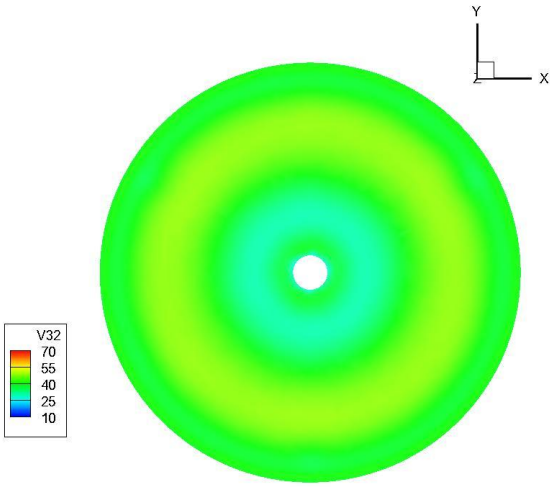

Figure 185 - ANSYS FLUENT Velocity Distribution at Exit of 3.5 + Flat - Full Size - Uniform Flow

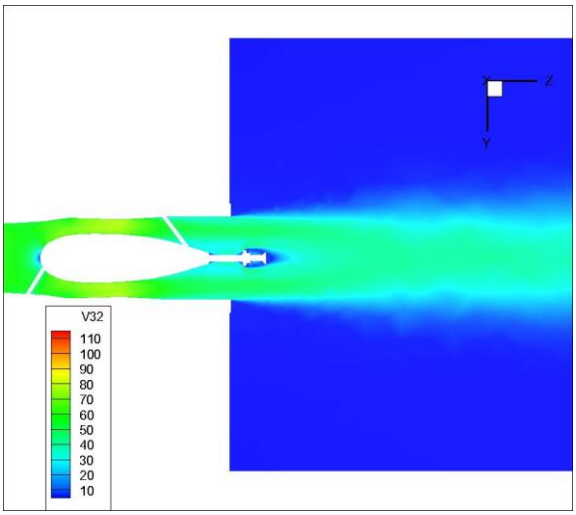

Figure 186 - ANSYS FLUENT Velocity Distribution through Cross-Section of 3.5 + Flat - Full Size - Uniform Flow

3.5 + FLAT – FULL SIZE – FULLY DEVELOPED FLOW

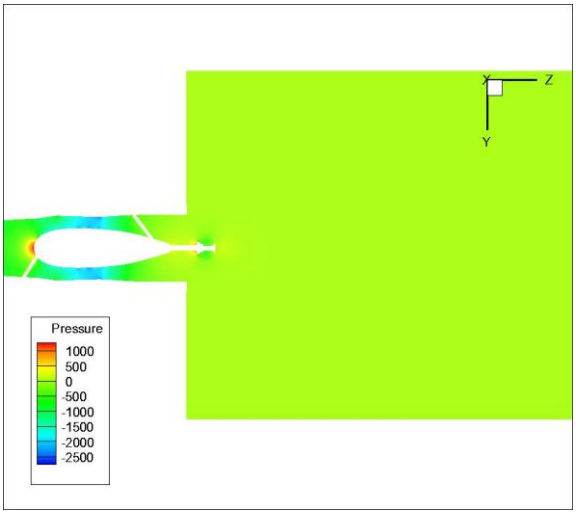

Figure 187 - ANSYS FLUENT Static Pressure Distribution through Cross-Section of 3.5 + Flat - Full Size - Fully Developed Flow

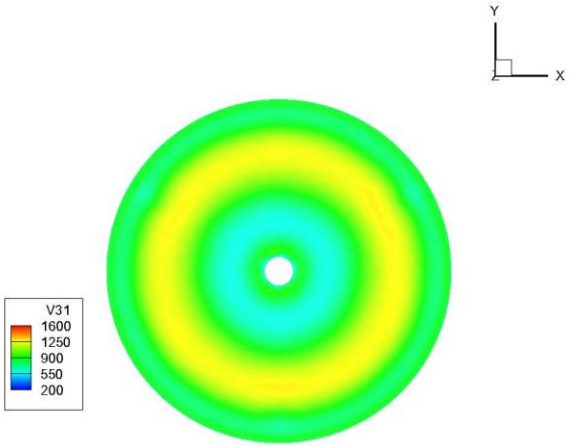

Figure 188 - ANSYS FLUENT Total Pressure Distribution at Exit of 3.5 + Flat - Full Size - Fully Developed Flow

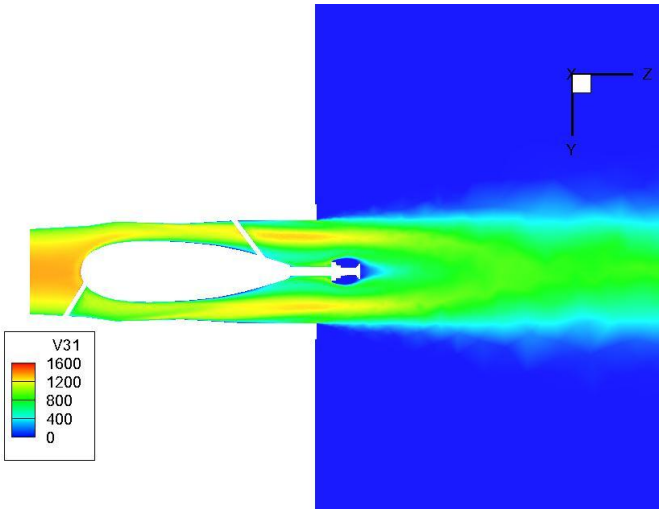

Figure 189 - ANSYS FLUENT Total Pressure Distribution through Cross-Section of 3.5 + Flat - Full Size - Fully Developed Flow

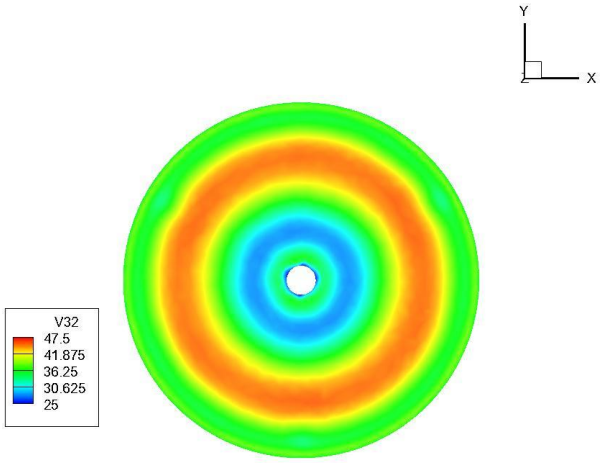

Figure 190 - ANSYS FLUENT Velocity Distribution at Exit of 3.5 + Flat - Full Size - Fully Developed Flow

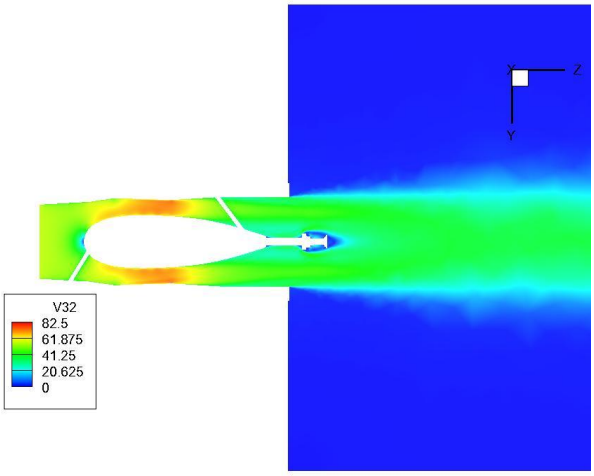

Figure 191 - ANSYS FLUENT Velocity Distribution across Cross-Section of 3.5 + Flat - Full Size - Fully Developed Flow

3.5 + FLAT + CONICAL – FULL SIZE – UNIFORM FLOW

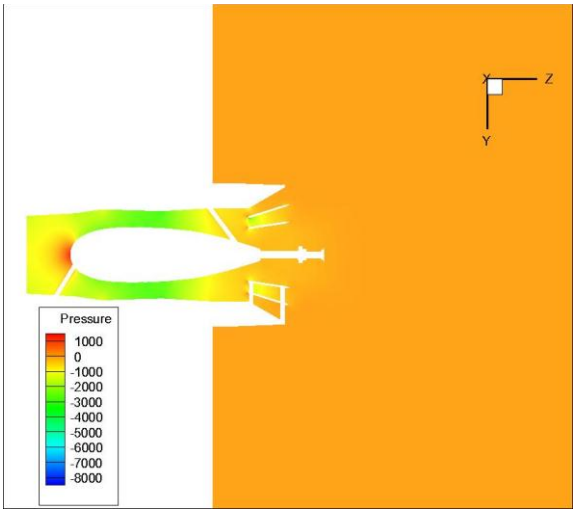

Figure 192 - ANSYS FLUENT Static Pressure Distribution through Cross-Section of 3.5 + Flat + Conical - Full Size - Uniform Flow

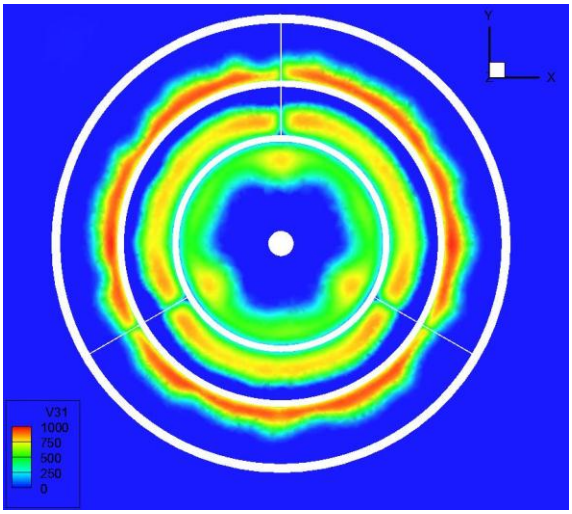

Figure 193 - ANSYS FLUENT Total Pressure Distribution at Exit of 3.5 + Flat + Conical - Full Size - Uniform Flow

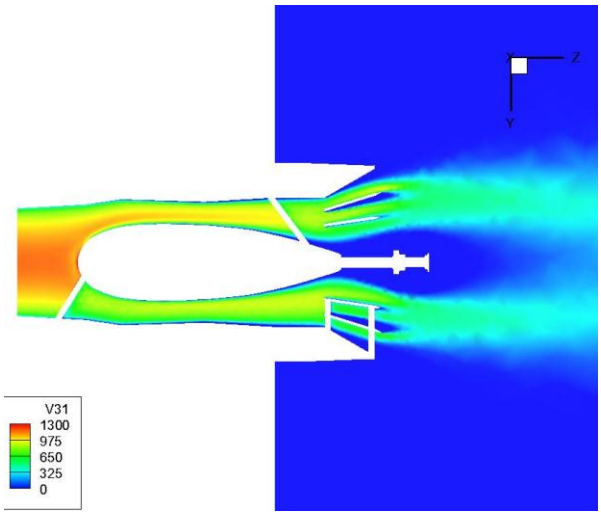

Figure 194 - ANSYS FLUENT Total Pressure Distribution through Cross-Section of 3.5 + Flat + Conical - Full Size - Uniform Flow

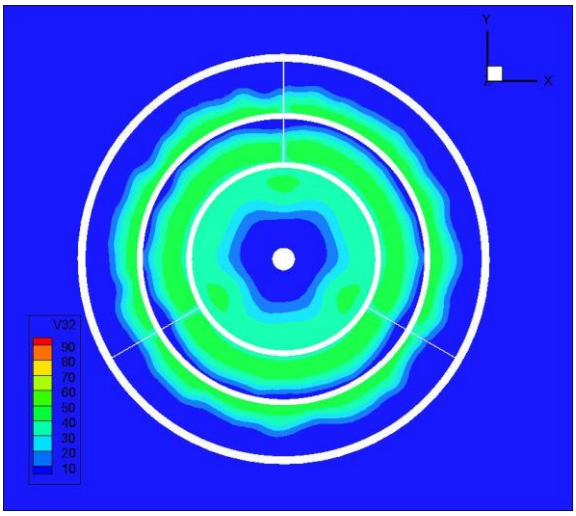

Figure 195 - ANSYS FLUENT Velocity Distribution at Exit of 3.5 + Flat + Conical - Full Size - Uniform Flow

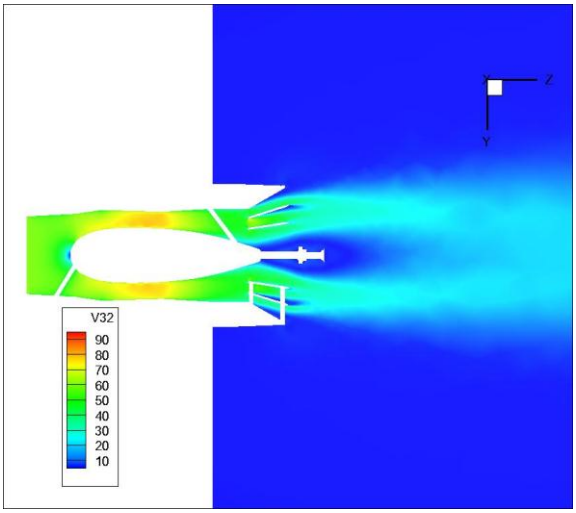

Figure 196 - ANSYS FLUENT Velocity Distribution through Cross-Section of 3.5 + Flat + Conical - Full Size - Uniform Flow

3.5 + FLAT + CONICAL – FULL SIZE – FULLY DEVELOPED FLOW

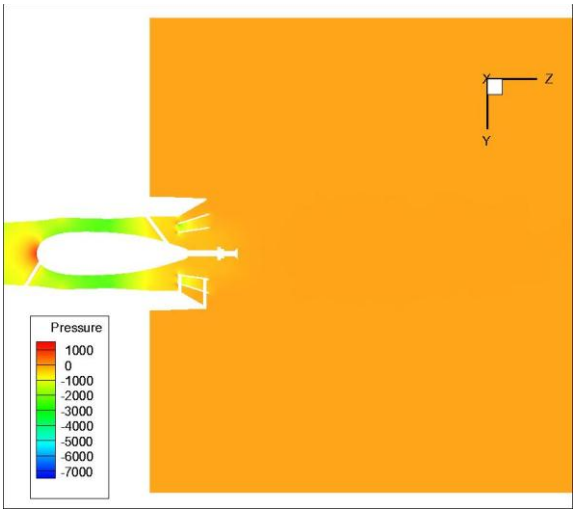

Figure 197 - ANSYS FLUENT Static Pressure Distribution through Cross-Section of 3.5 + Flat + Conical - Full Size - Fully Developed Flow

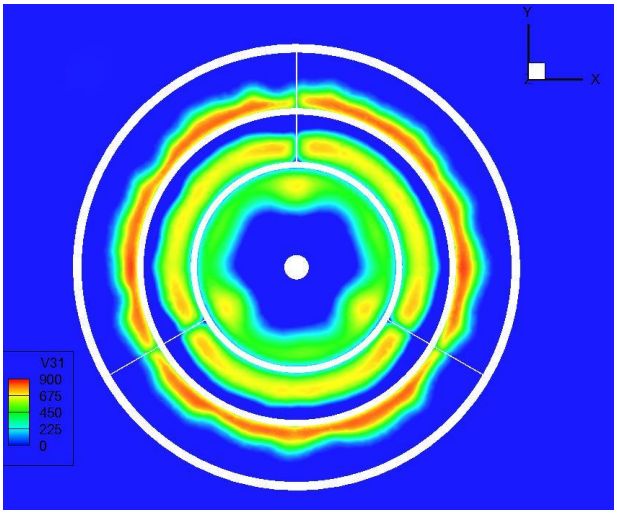

Figure 198 - ANSYS FLUENT Total Pressure Distribution at Exit of 3.5 + Flat + Conical - Full Size - Fully Developed Flow

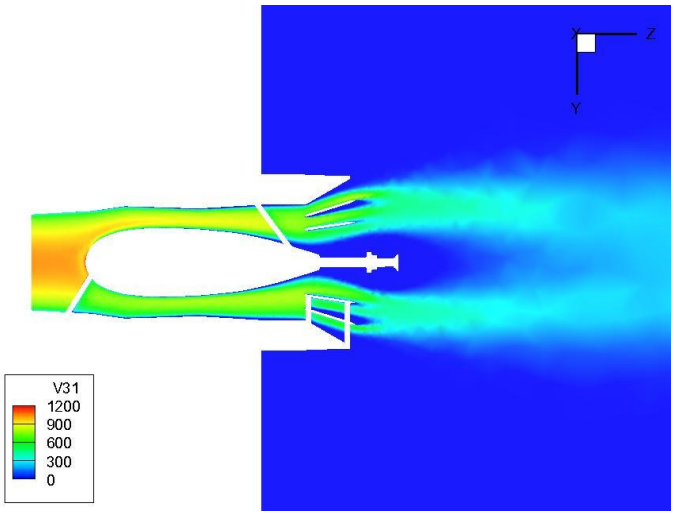

Figure 199 - ANSYS FLUENT Total Pressure Distribution through Cross-Section of 3.5 + Flat + Conical - Full Size - Fully Developed Flow

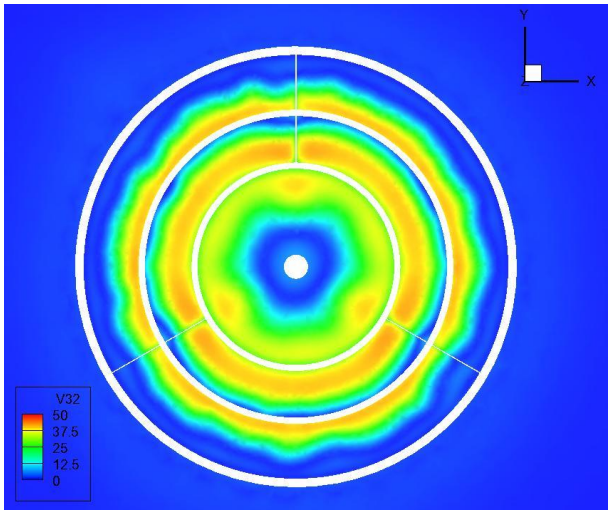

Figure 200 - ANSYS FLUENT Velocity Distribution at Exit of 3.5 + Flat + Conical - Full Size - Fully Developed Flow

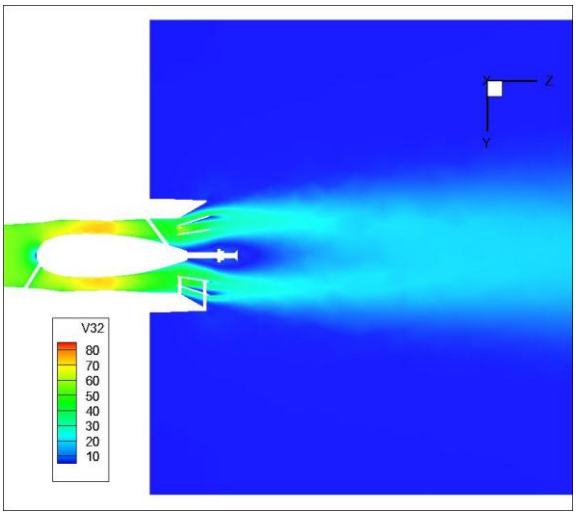

Figure 201 - ANSYS FLUENT Velocity Distribution through Cross-Section of 3.5 + Flat + Conical - Full Size - Fully Developed Flow

7.5 BASE TUNNEL – SMALL SCALE – UNIFORM FLOW

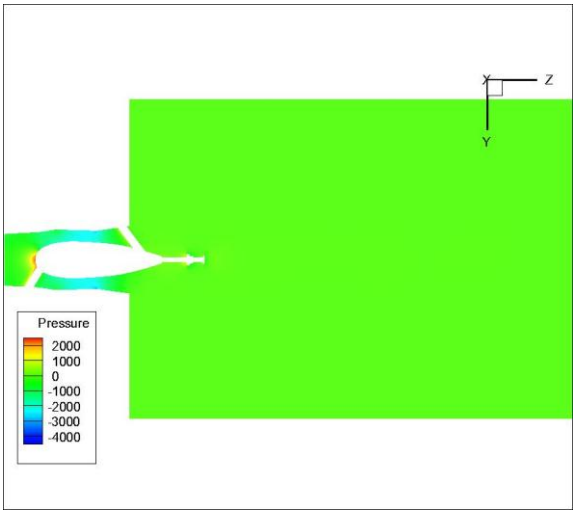

Figure 202 - ANSYS FLUENT Static Pressure Distribution through Cross-Section of 7.5 Base Tunnel - Small Scale - Uniform Flow

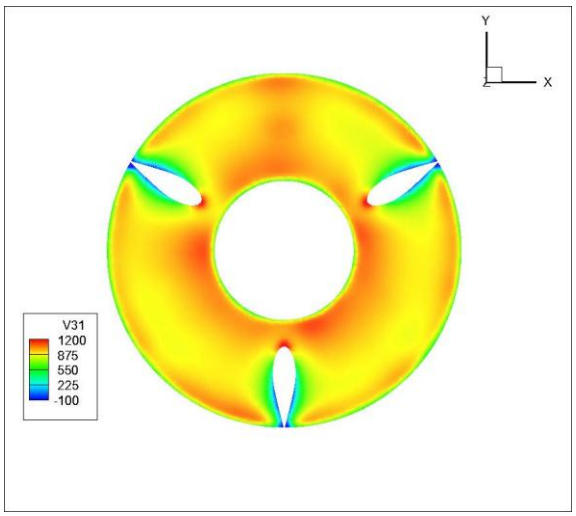

Figure 203 - ANSYS FLUENT Total Pressure Distribution at Exit of 7.5 Base Tunnel - Small Scale - Uniform Flow

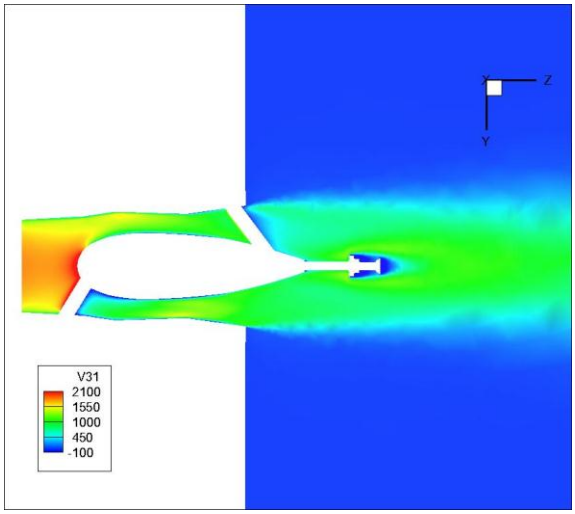

Figure 204 - ANSYS FLUENT Total Pressure Distribution through Cross-Section of 7.5 Base Tunnel - Small Scale - Uniform Flow

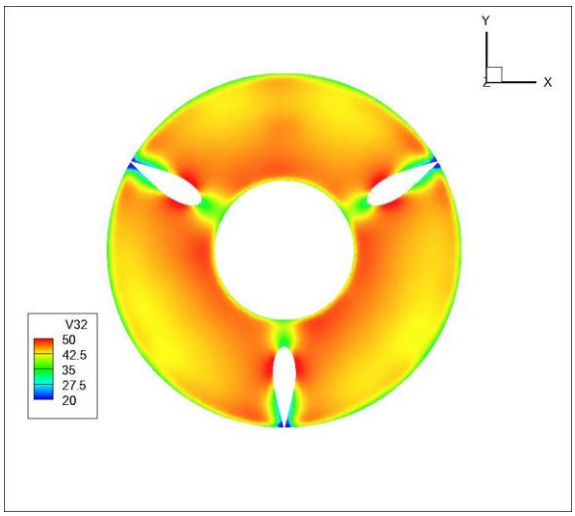

Figure 205 - ANSYS FLUENT Velocity Distribution at Exit of 7.5 Base Tunnel - Small Scale - Uniform Flow

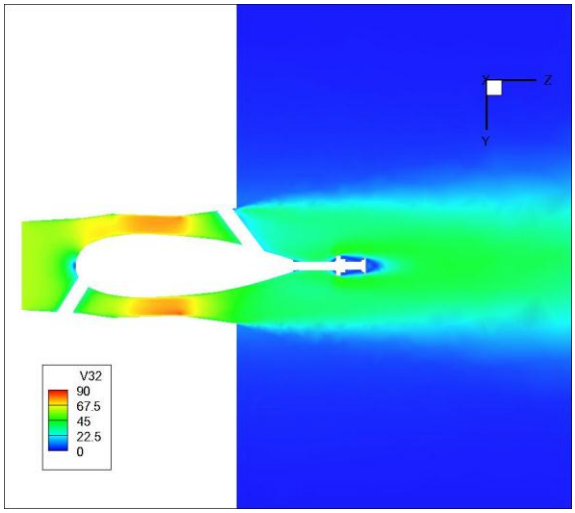

Figure 206 - ANSYS FLUENT Velocity Distribution through Cross-Section of 7.5 Base Tunnel - Small Scale - Uniform Flow

7.5 BASE TUNNEL – SMALL SCALE – FULLY DEVELOPED FLOW

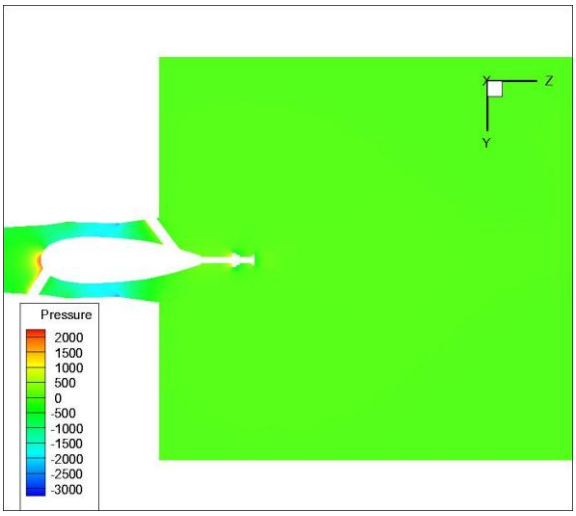

Figure 207 - ANSYS FLUENT Static Pressure Distribution through Cross-Section of 7.5 Base Tunnel - Small Scale - Fully Developed Flow

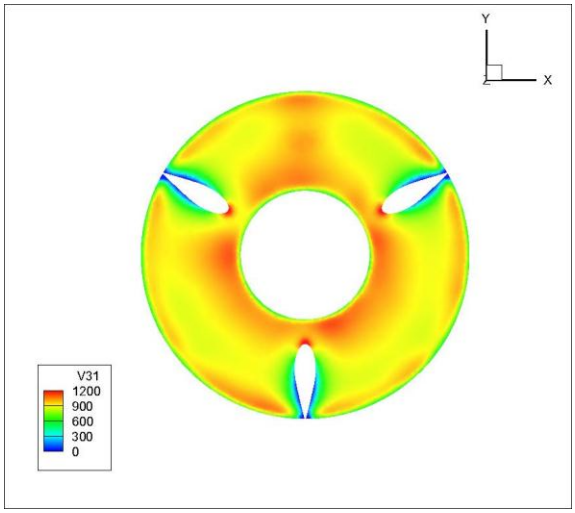

Figure 208 - ANSYS FLUENT Total Pressure Distribution at Exit of 7.5 Base Tunnel - Small Scale - Fully Developed Flow

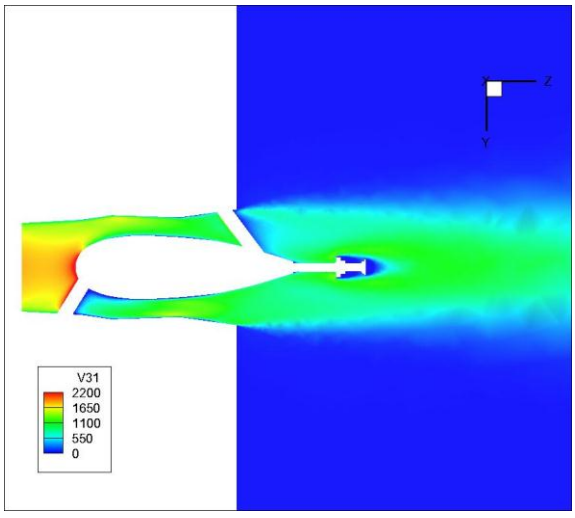

Figure 209 - ANSYS FLUENT Total Pressure Distribution through Cross-Section of 7.5 Base Tunnel - Small Scale - Fully Developed Flow

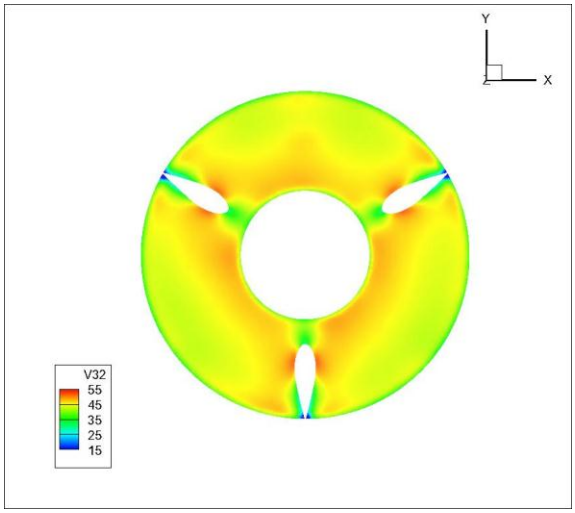

Figure 210 - ANSYS FLUENT Velocity Distribution at Exit of 7.5 Base Tunnel - Small Scale - Uniform Flow

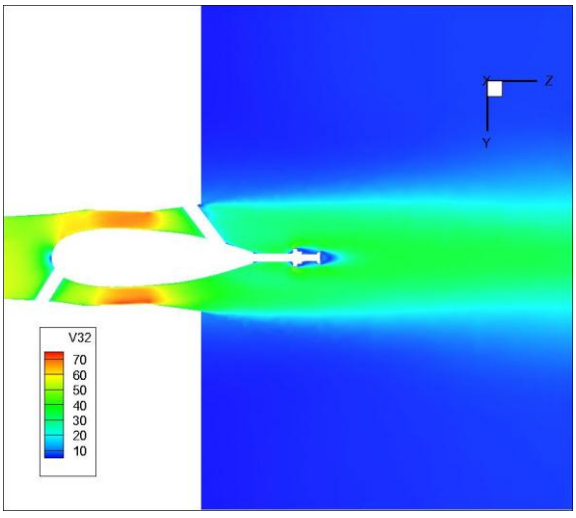

Figure 211 - ANSYS FLUENT Velocity Distribution through Cross-Section of 7.5 Base Tunnel - Small Scale - Fully Developed Flow

3.5 BASE TUNNEL – SMALL SCALE – UNIFORM FLOW

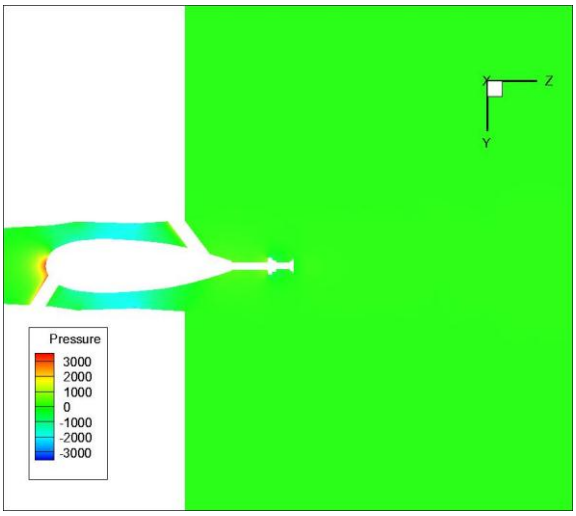

Figure 212 - ANSYS FLUENT Static Pressure Distribution through Cross-Section of 3.5 Base Tunnel - Small Scale - Uniform Flow

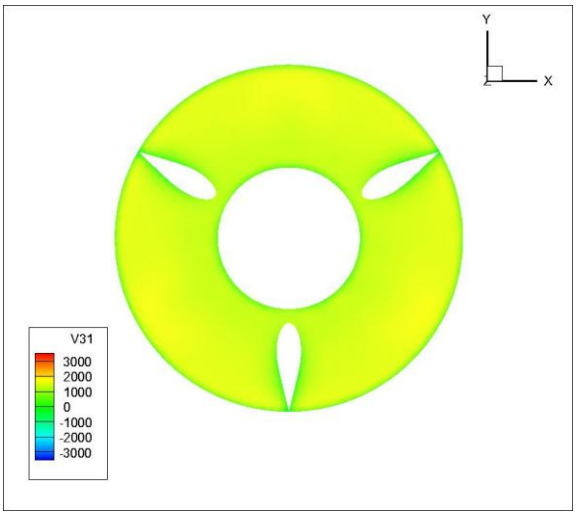

Figure 213 - ANSYS FLUENT Total Pressure Distribution at Exit of 3.5 Base Tunnel - Small Scale - Uniform Flow

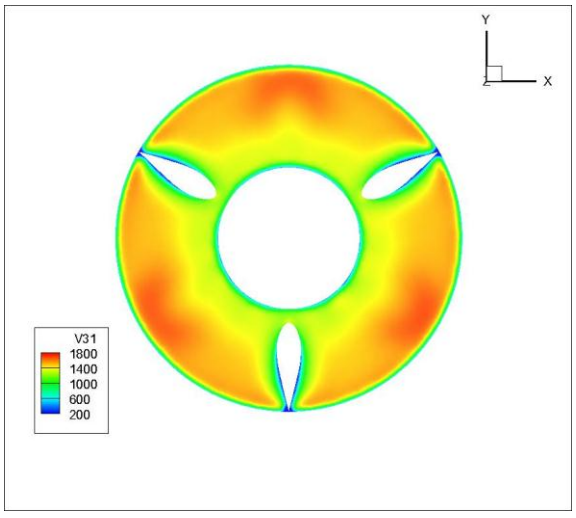

Figure 214 - ANSYS FLUENT Total Pressure Distribution at Exit of 3.5 Base Tunnel - Small Scale - Uniform Flow

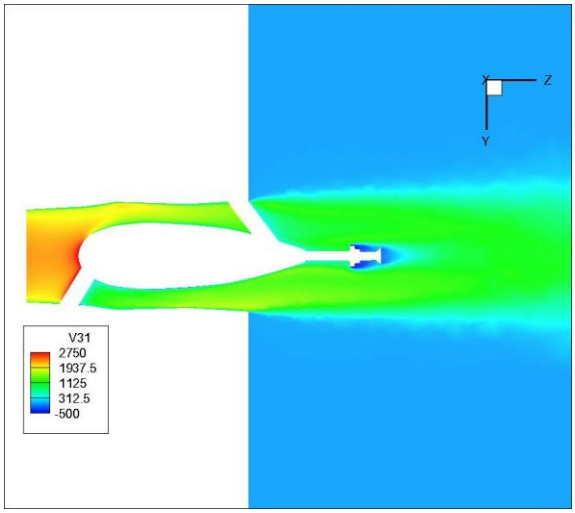

Figure 215 - ANSYS FLUENT Total Pressure Distribution through Cross-Section of 3.5 Base Tunnel - Small Scale - Uniform Flow

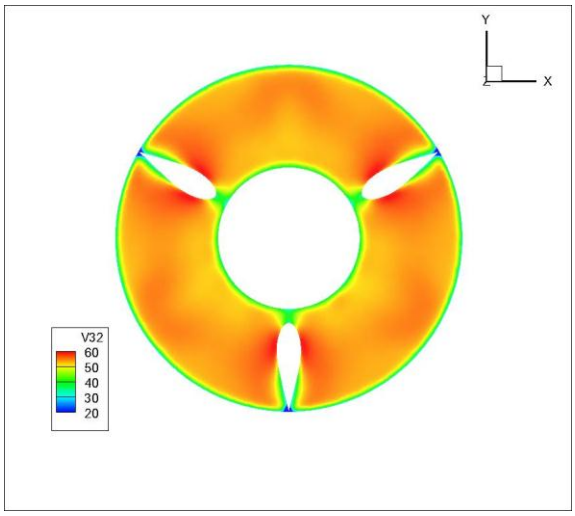

Figure 216 - ANSYS FLUENT Velocity Distribution at Exit of 3.5 Base Tunnel - Small Scale - Uniform Flow

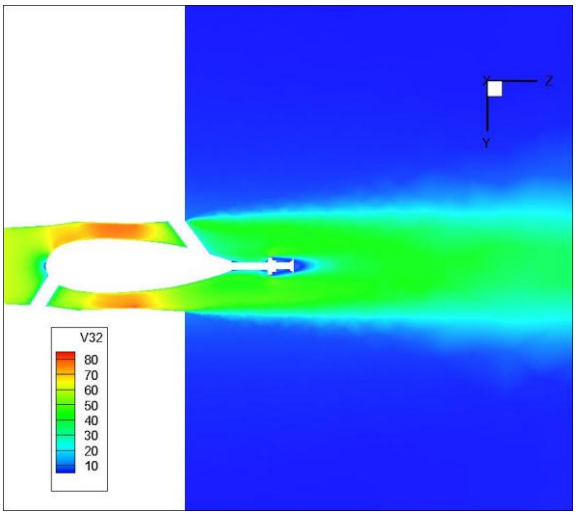

Figure 217 - ANSYS FLUENT Velocity Distribution through Cross-Section of 3.5 Base Tunnel - Small Scale - Uniform Flow

3.5 BASE TUNNEL – SMALL SCALE – FULLY DEVELOPED FLOW

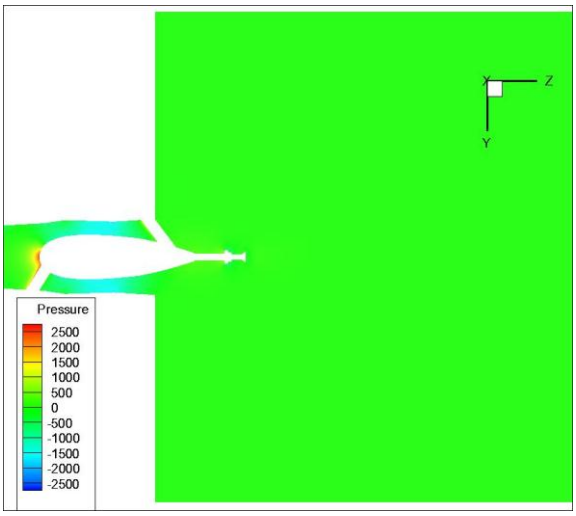

Figure 218 - ANSYS FLUENT Static Pressure Distribution through Cross-Section of 3.5 Base Tunnel - Small Scale - Fully Developed Flow

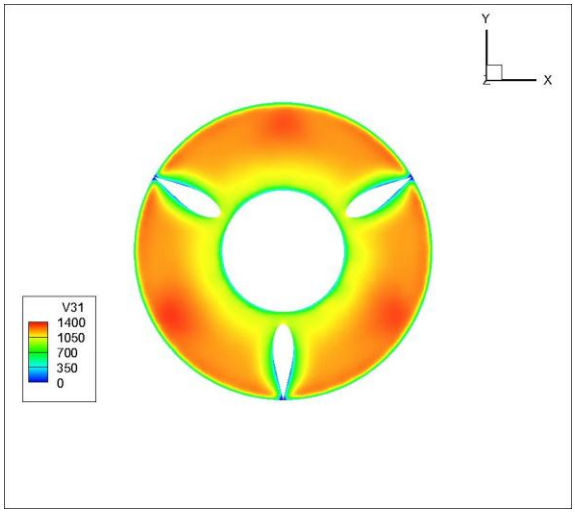

Figure 219 - ANSYS FLUENT Total Pressure Distribution at Exit of 3.5 Base Tunnel - Small Scale - Fully Developed Flow

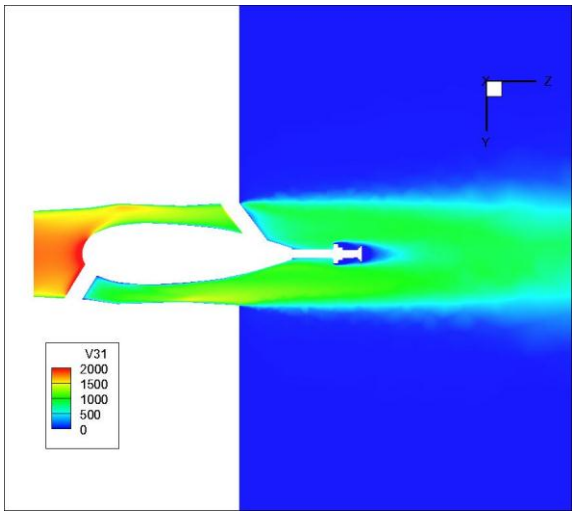

Figure 220 - ANSYS FLUENT Total Pressure Distribution through Cross-Section of 3.5 Base Tunnel - Small Scale - Fully Developed Flow

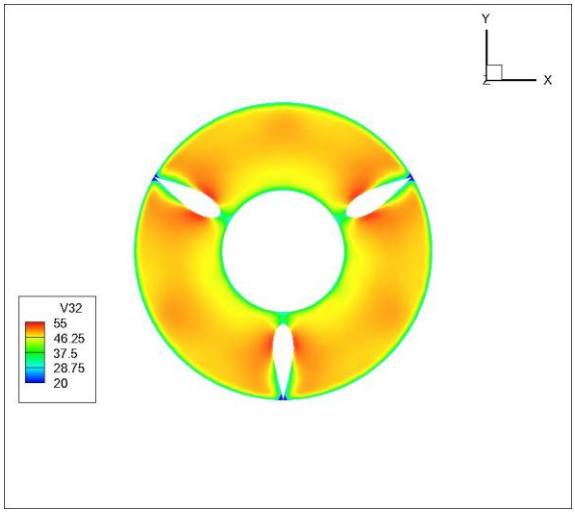

Figure 221 - ANSYS FLUENT Velocity Distribution at Exit of 3.5 Base Tunnel - Small Scale - Fully Developed Flow

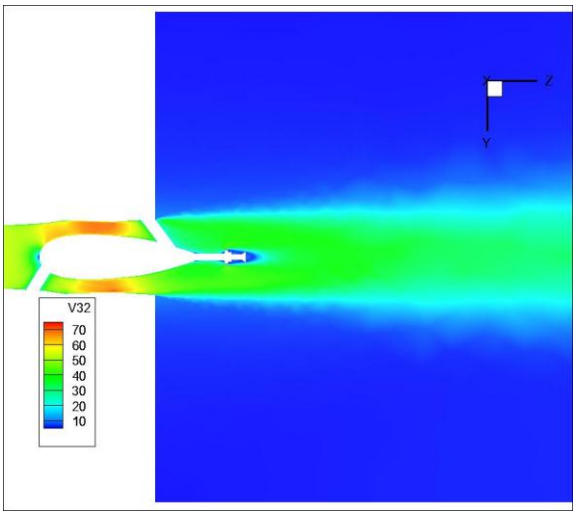

Figure 222 - ANSYS FLUENT Velocity Distribution through Cross-Section of 3.5 Base Tunnel - Small Scale - Fully Developed Flow

3.5 + FLAT – SMALL SCALE – UNIFORM FLOW

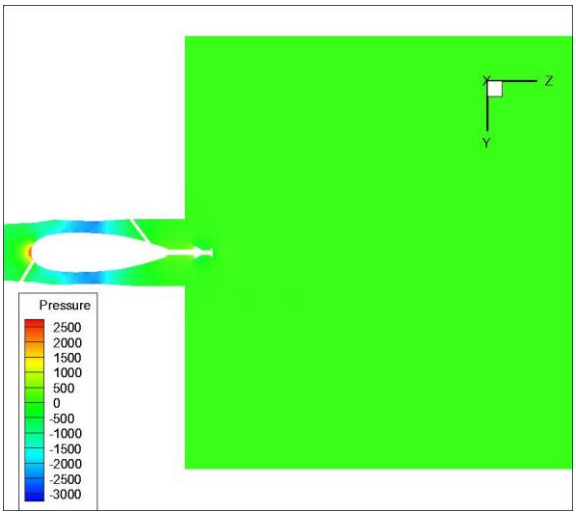

Figure 223 - ANSYS FLUENT Static Pressure Distribution through Cross-Section of 3.5 + Flat - Small Scale - Uniform Flow

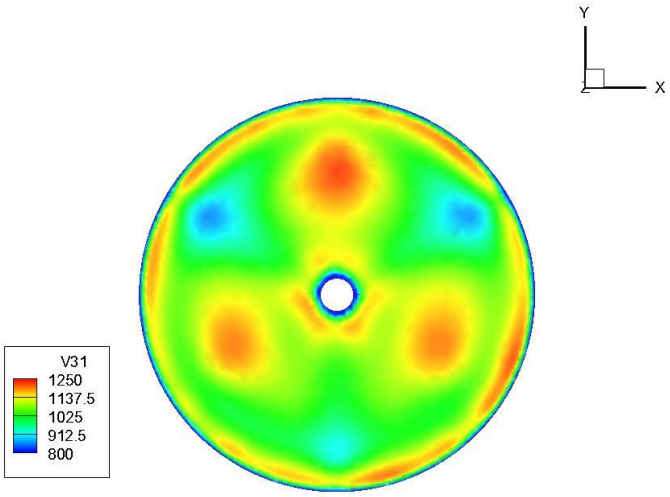

Figure 224 - ANSYS FLUENT Total Pressure Distribution at Exit of 3.5 + Flat - Small Scale - Uniform Flow

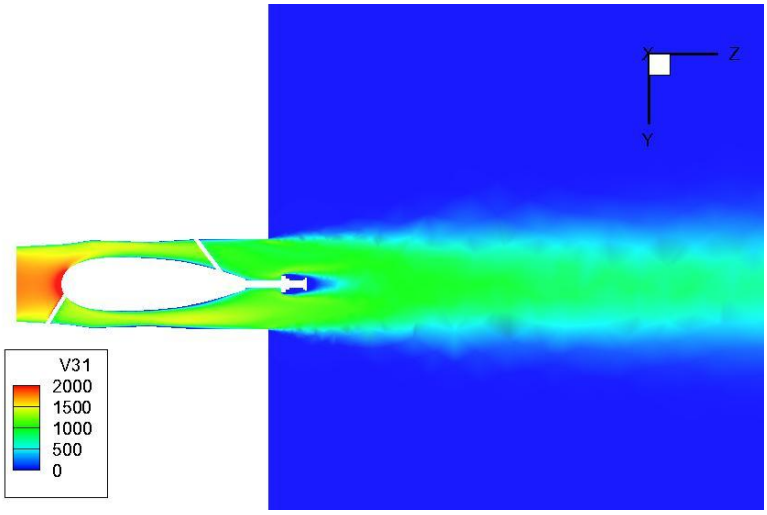

Figure 225 - ANSYS FLUENT Total Pressure Distribution through Cross-Section of 3.5 + Flat - Small Scale - Uniform Flow

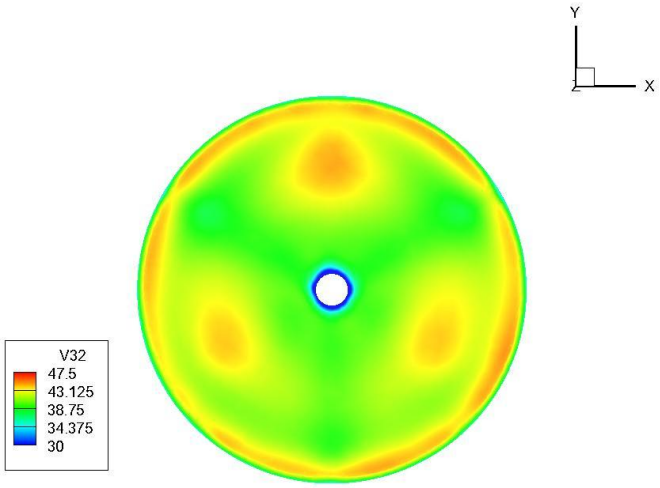

Figure 226 - ANSYS FLUENT Velocity Distribution at Exit of 3.5 + Flat - Small Scale - Uniform Flow

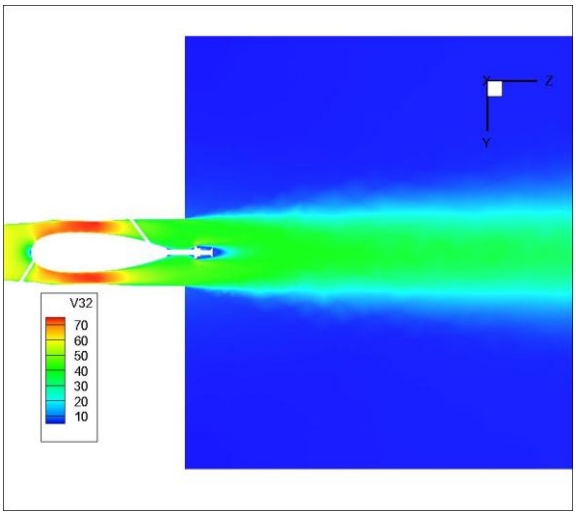

Figure 227 - ANSYS FLUENT Velocity Distribution through Cross-Section of 3.5 + Flat - Small Scale - Uniform Flow

3.5 + FLAT – SMALL SCALE – FULLY DEVELOPED FLOW

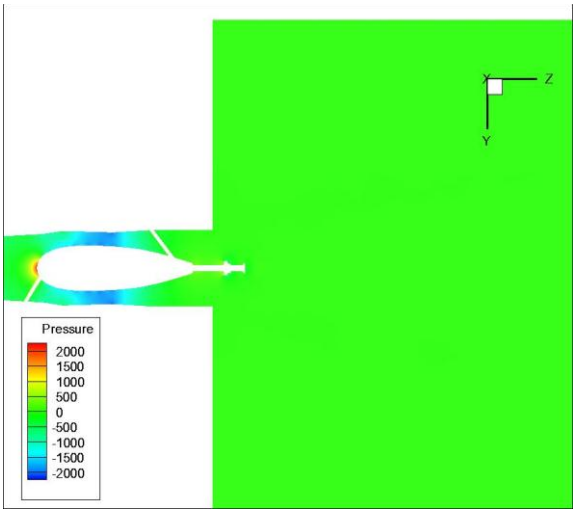

Figure 228 - ANSYS FLUENT Static Pressure Distribution through Cross-Section of 3.5 + Flat - Small Scale - Fully Developed Flow

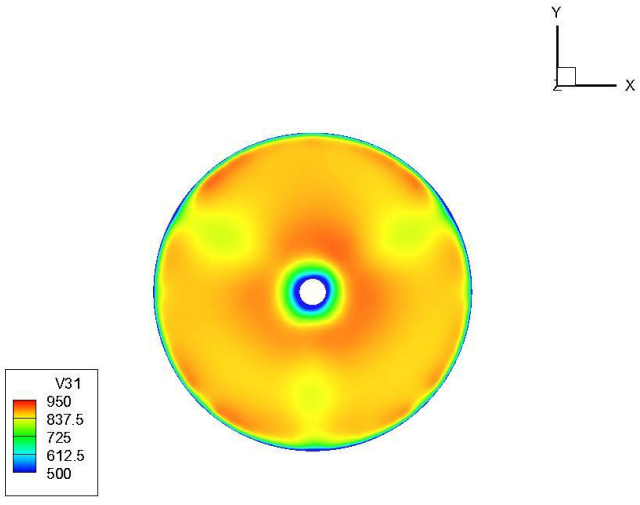

Figure 229 - ANSYS FLUENT Total Pressure Distribution at Exit of 3.5 + Flat - Small Scale - Fully Developed Flow

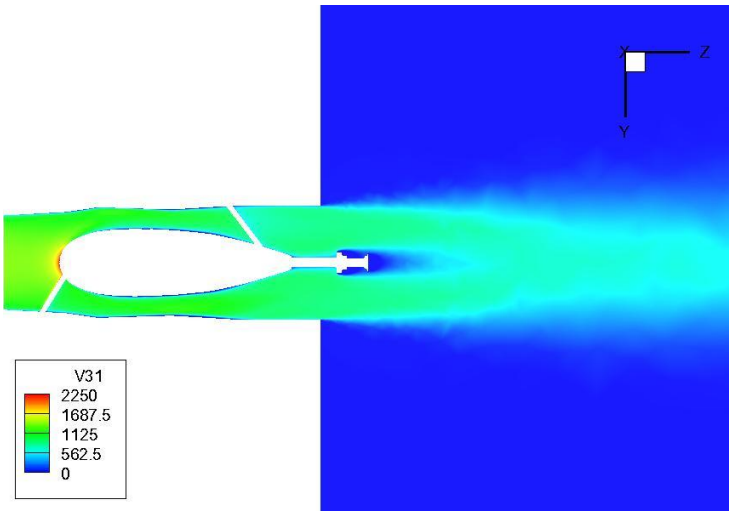

Figure 230 - ANSYS FLUENT Total Pressure Distribution through Cross-Section of 3.5 + Flat - Small Scale - Fully Developed Flow

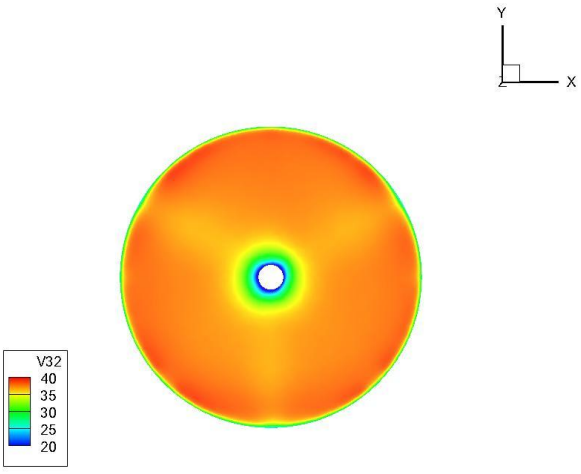

Figure 231 - ANSYS FLUENT Velocity Distribution at Exit of 3.5 + Flat - Small Scale - Fully Developed Flow

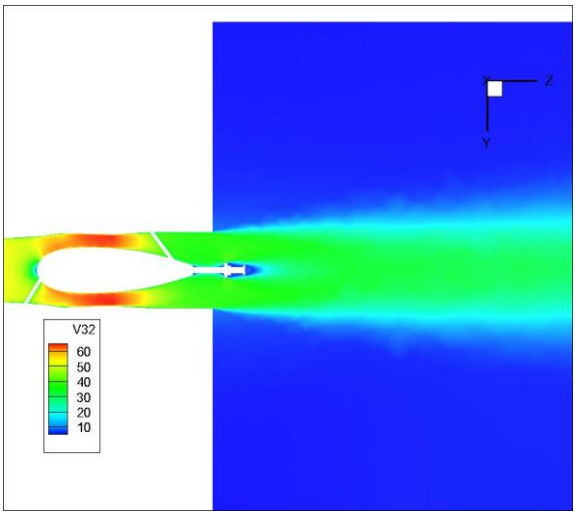

Figure 232 - ANSYS FLUENT Total Pressure Distribution through Cross-Section of 3.5 + Flat - Small Scale - Fully Developed Flow

3.5 + FLAT + CONICAL – SMALL SCALE – UNIFORM FLOW

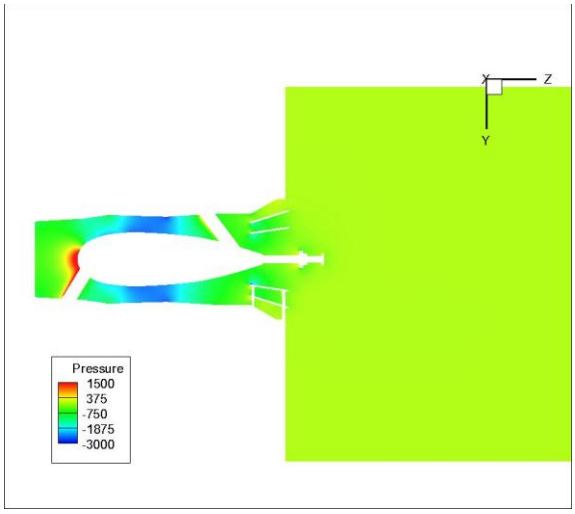

Figure 233 - ANSYS FLUENT Static Pressure Distribution through Cross-Section of 3.5 + Flat + Conical - Small Scale - Uniform Flow

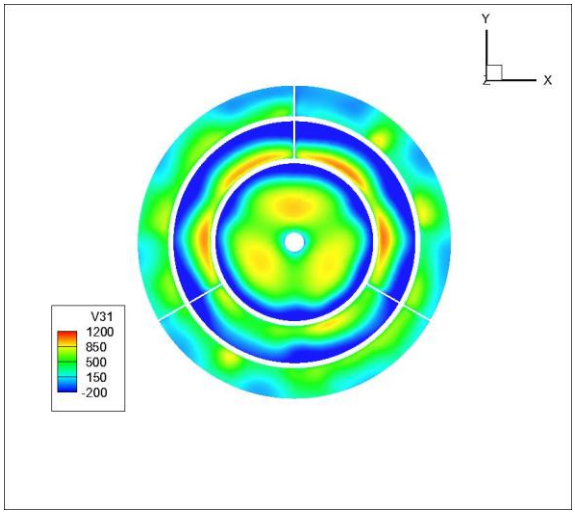

Figure 234 - ANSYS FLUENT Total Pressure Distribution at Exit of 3.5 + Flat + Conical - Small Scale - Uniform Flow

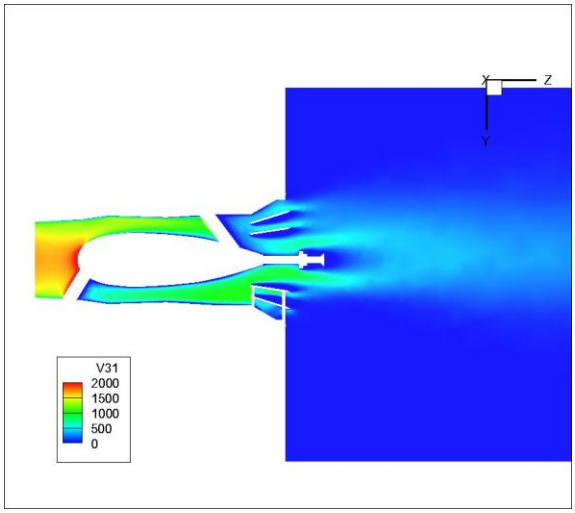

Figure 235 - ANSYS FLUENT Total Pressure Distribution through Cross-Section of 3.5 + Flat + Conical - Small Scale - Uniform Flow

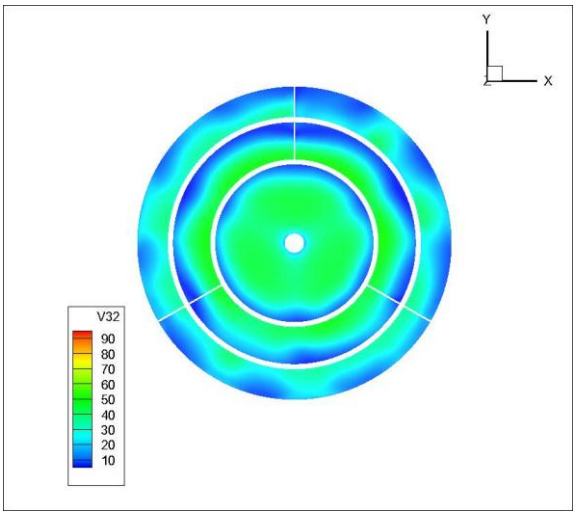

Figure 236 - ANSYS FLUENT Velocity Distribution at Exit of 3.5 + Flat + Conical - Small Scale - Uniform Flow

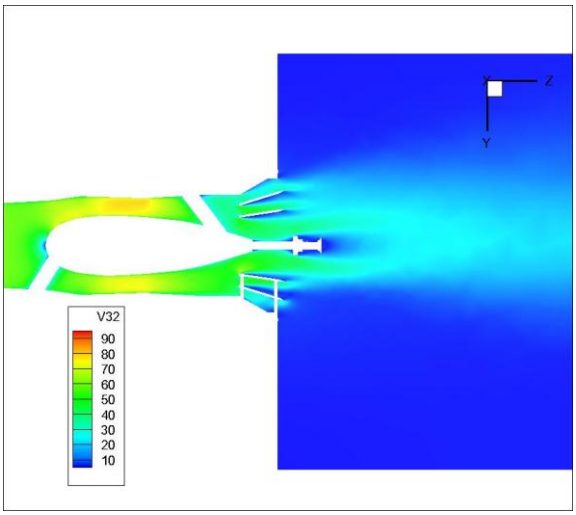

Figure 237 - ANSYS FLUENT Velocity Distribution through Cross-Section of 3.5 + Flat + Conical - Small Scale - Uniform Flow

3.5 + FLAT + CONICAL – SMALL SCALE – FULLY DEVELOPED FLOW

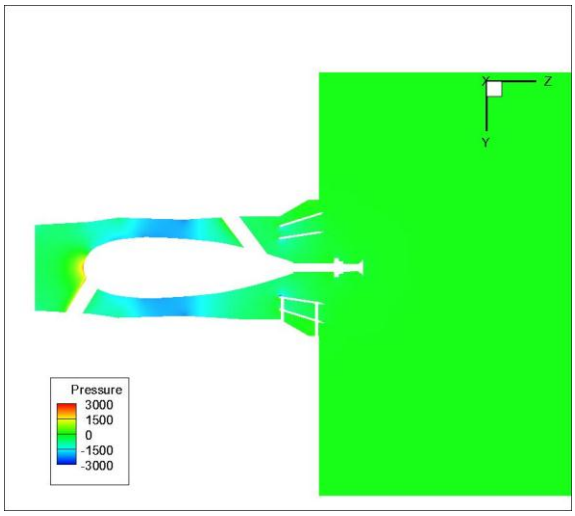

Figure 238 - ANSYS FLUENT Static Pressure Distribution through Cross-Section of 3.5 + Flat + Conical - Small Scale - Fully Developed Flow

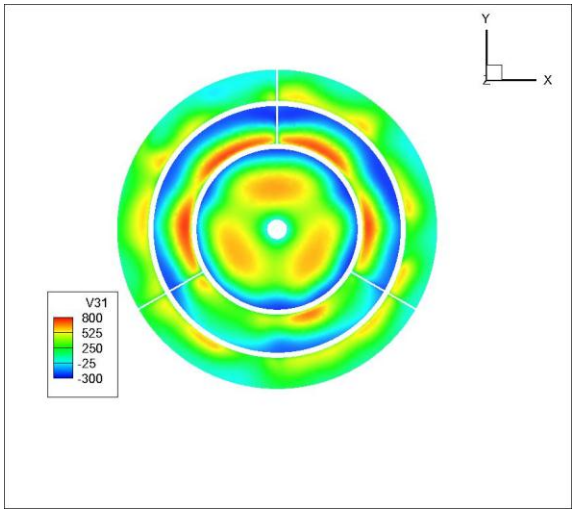

Figure 239 - ANSYS FLUENT Total Pressure Distribution at Exit of 3.5 + Flat + Conical - Small Scale - Fully Developed Flow

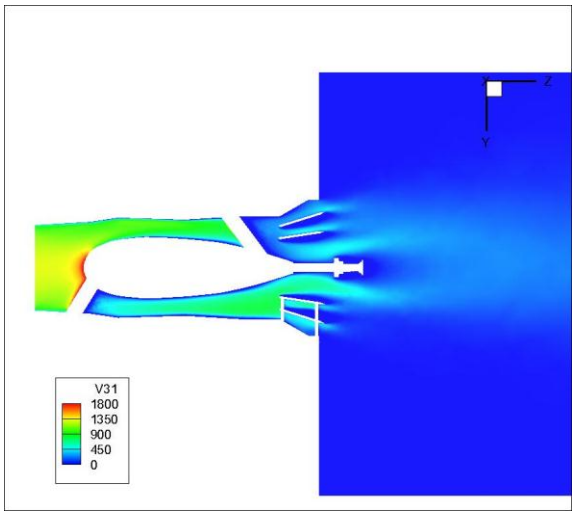

Figure 240 - ANSYS FLUENT Total Pressure Distribution through Cross-Section of 3.5 + Flat + Conical - Small Scale - Fully Developed Flow

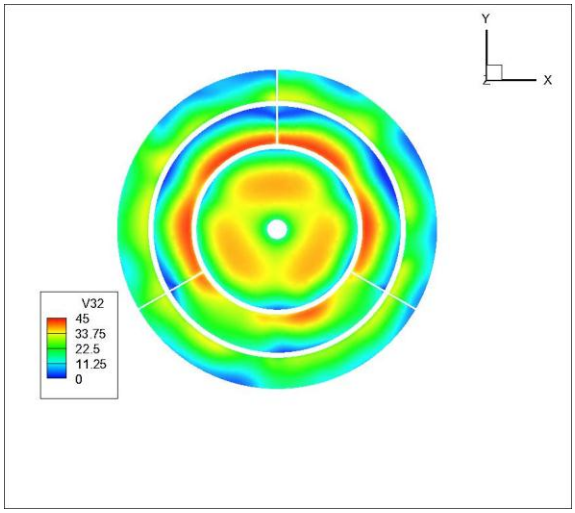

Figure 241 - ANSYS FLUENT Velocity Distribution at Exit of 3.5 + Flat + Conical - Small Scale - Fully Developed Flow

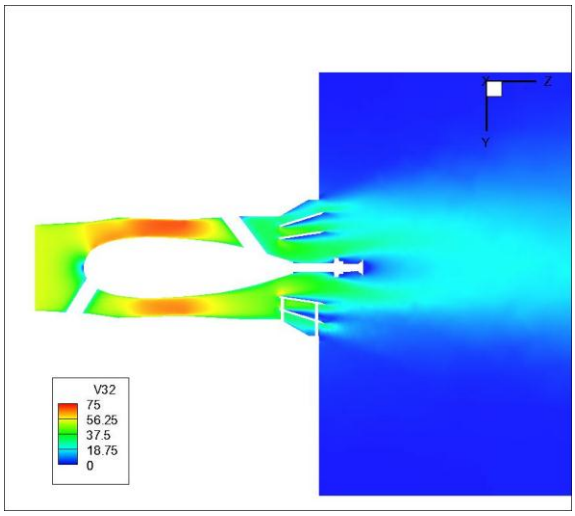

Figure 242 - ANSYS FLUENT Velocity Distribution through Cross-Section of 3.5 + Flat + Conical - Small Scale - Fully Developed Flow

APPENDIX D

DIFFUSER MODEL DRAWINGS

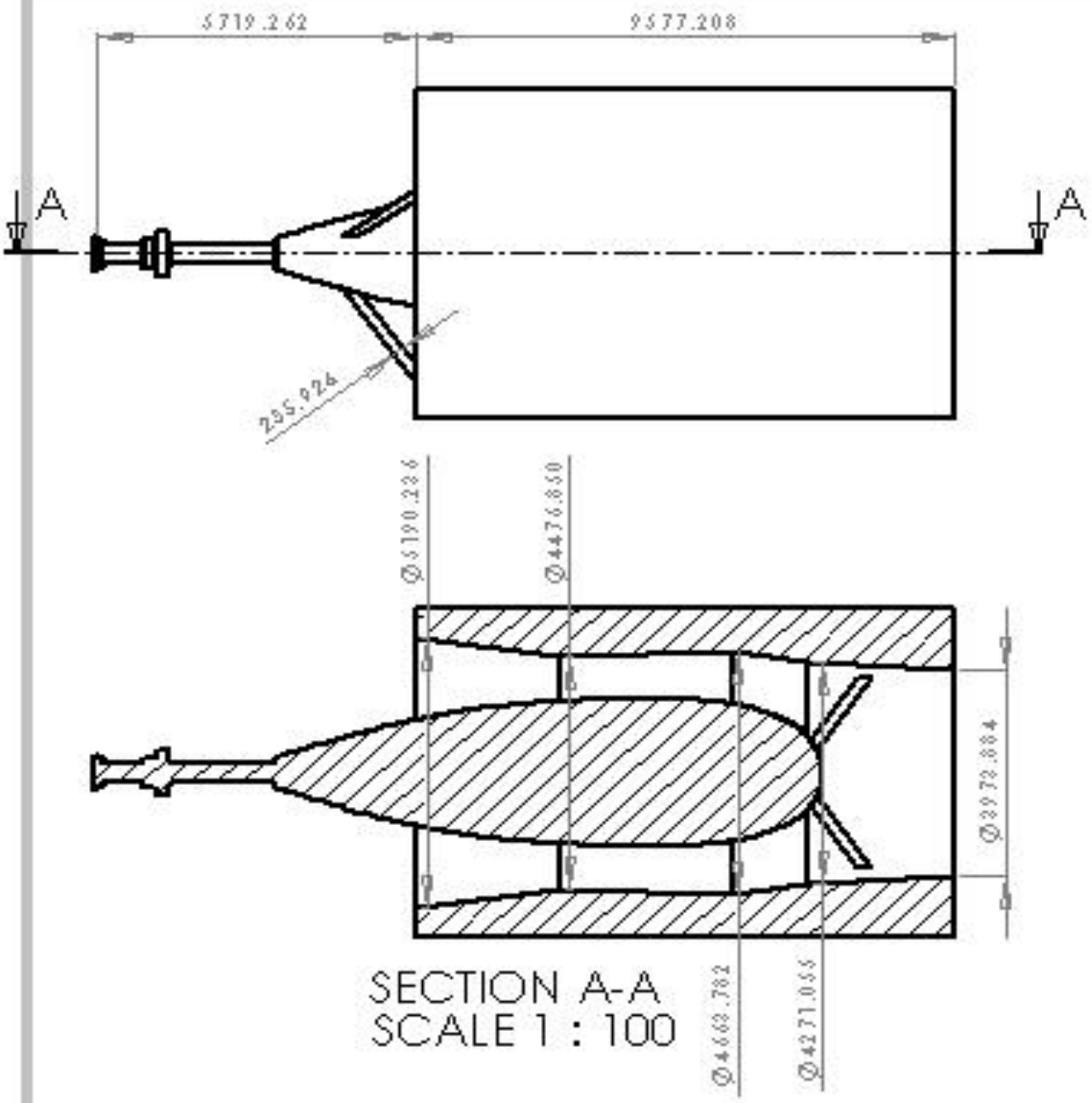

SECTION A-A
SCALE 1 : 100

Base Tunnel 7.5 - Full Size

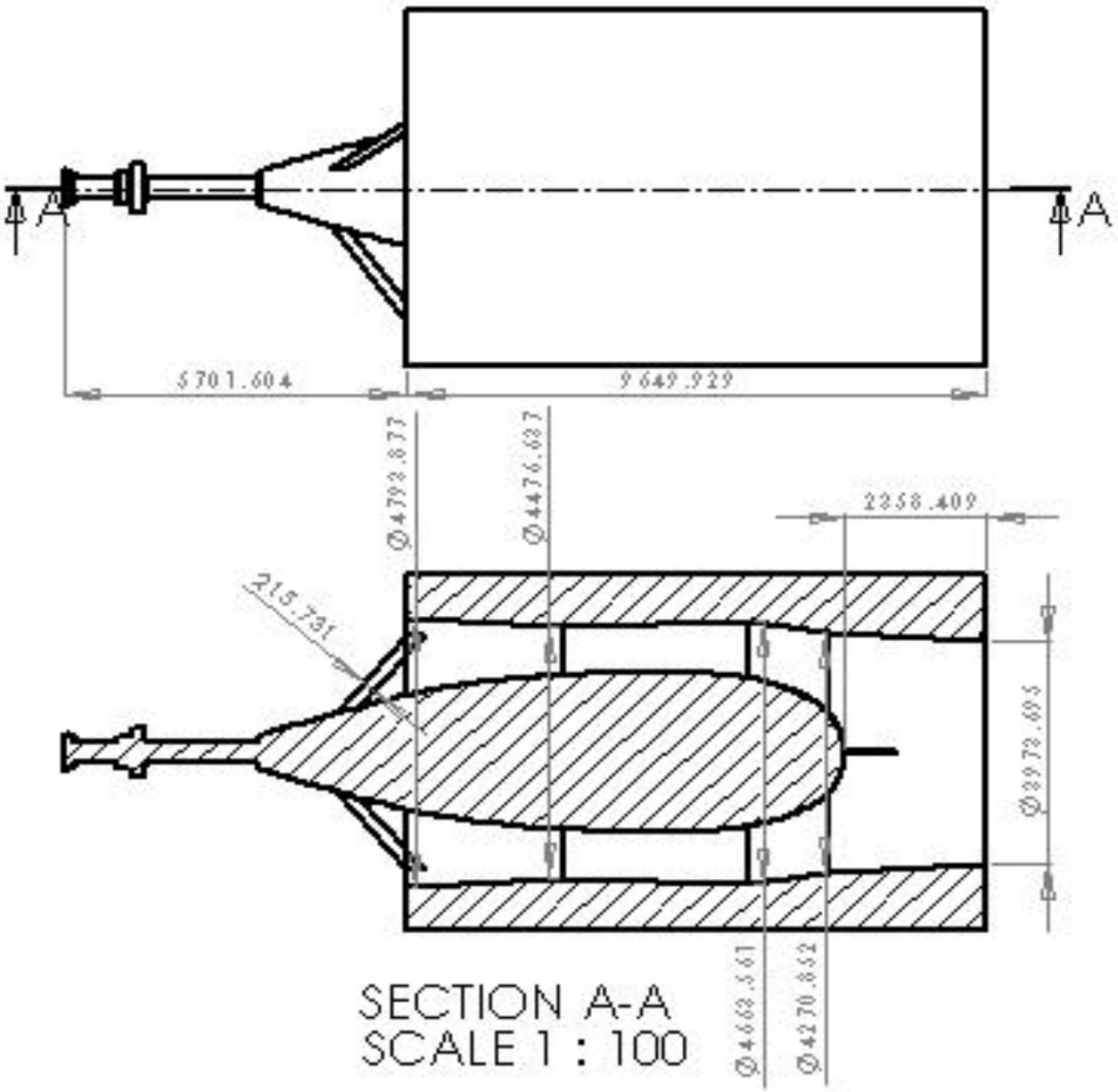

SECTION A-A
SCALE 1 : 100

Base Tunnel 3.5 - Full Size .rp

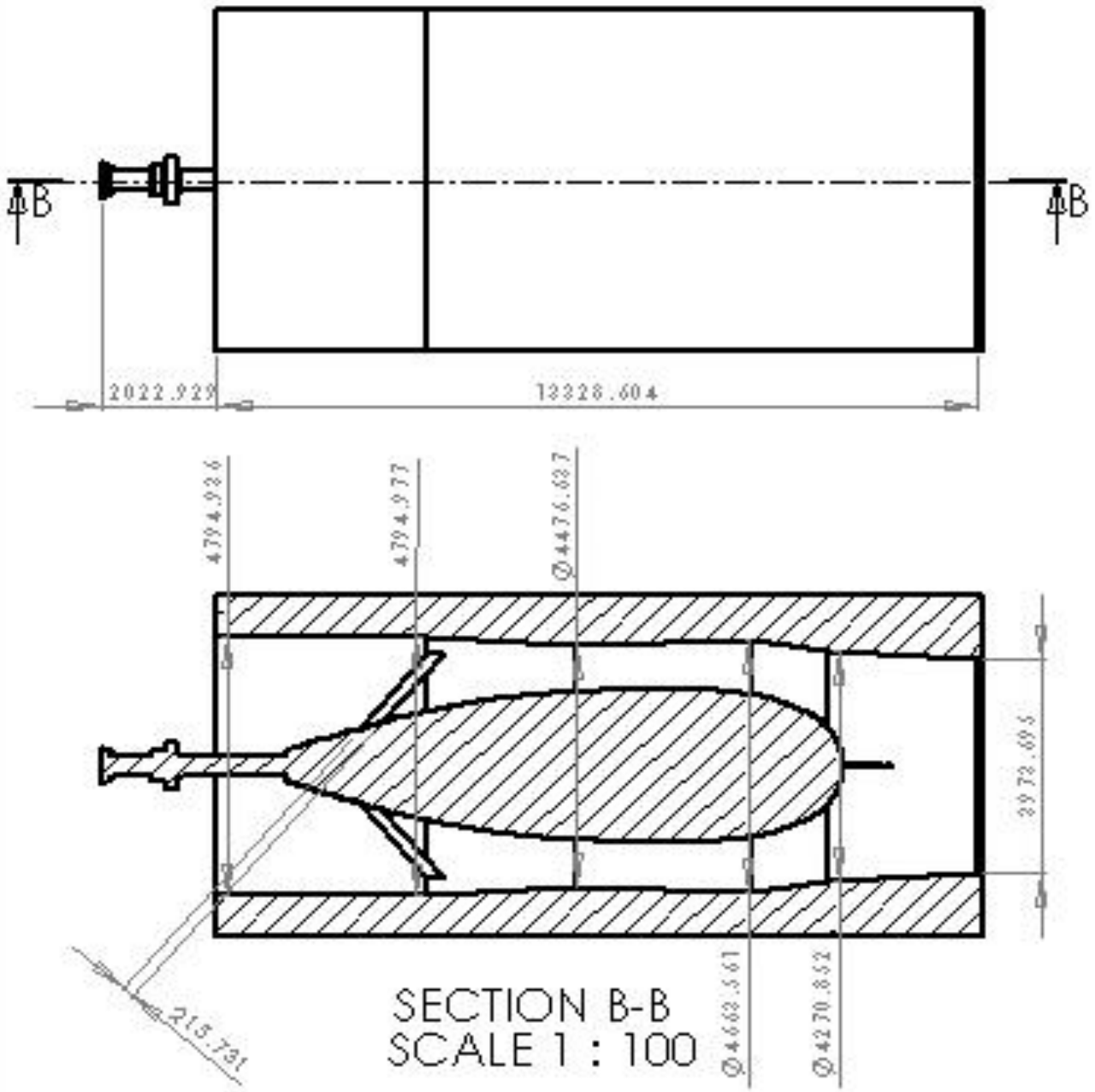

3.5 - Flat - Full Size

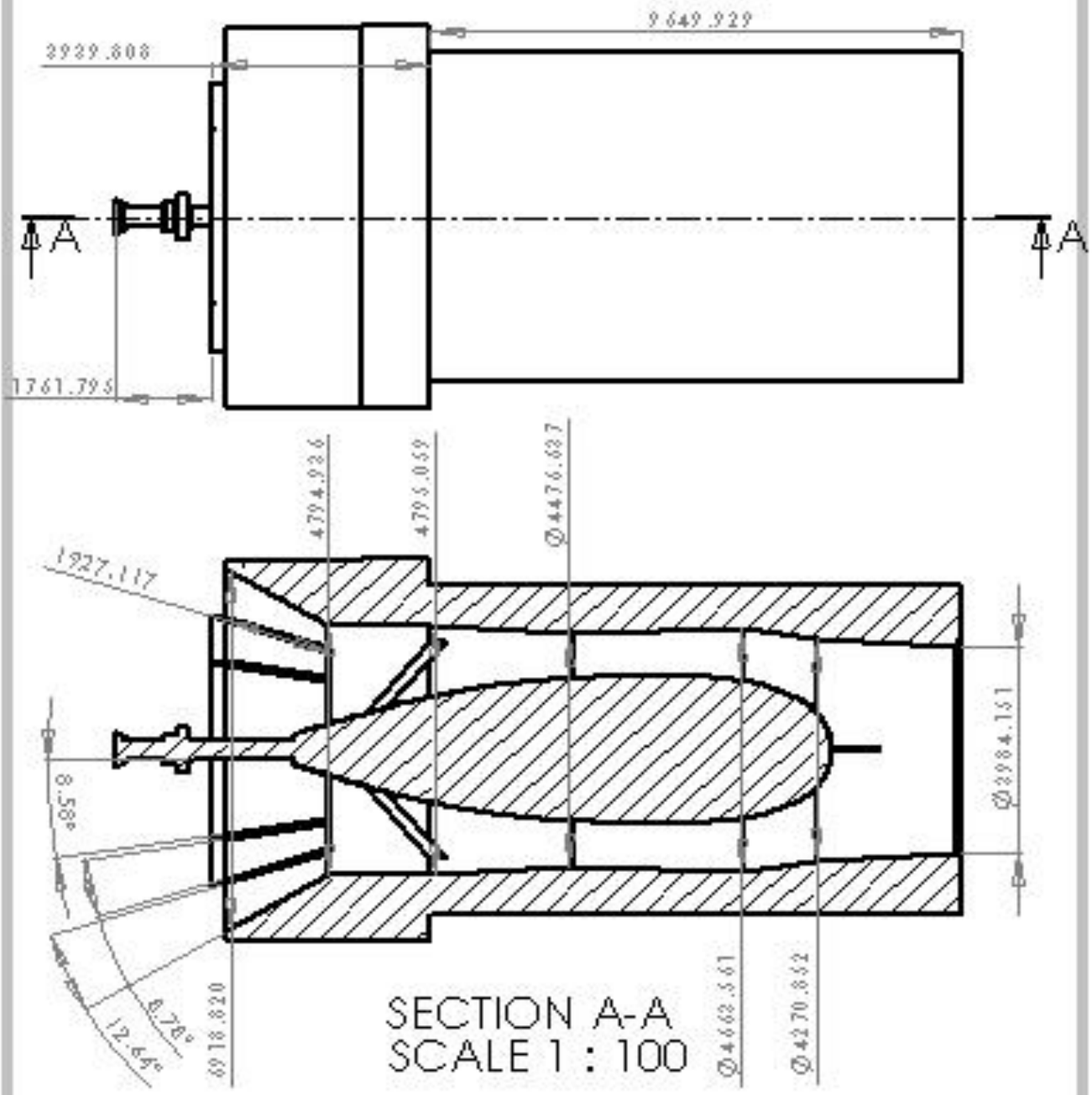

3.5" + Flat + Conical - Full Size

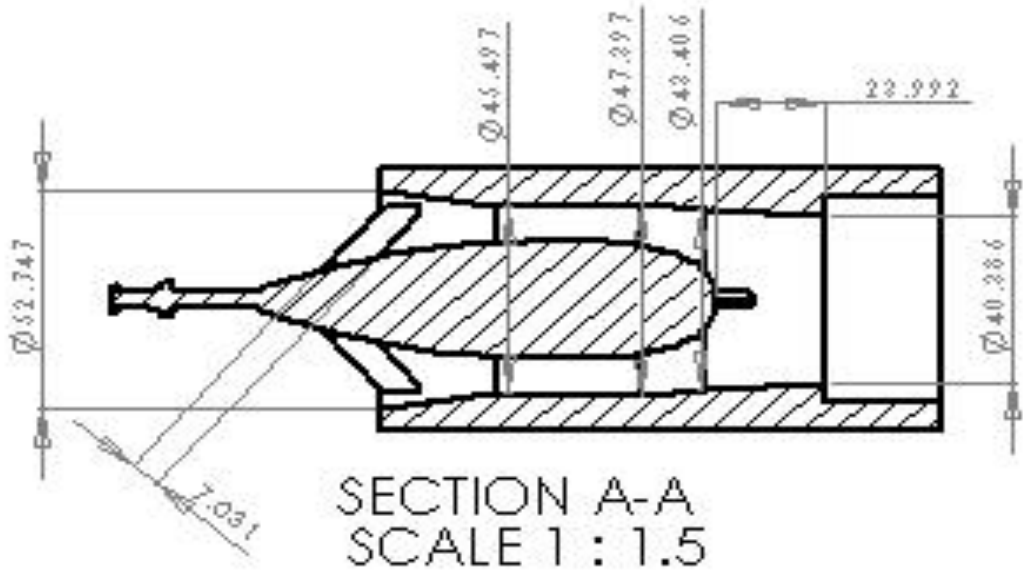

SECTION A-A
SCALE 1 : 1.5

Base Tunnel 7.5 - Small Scale

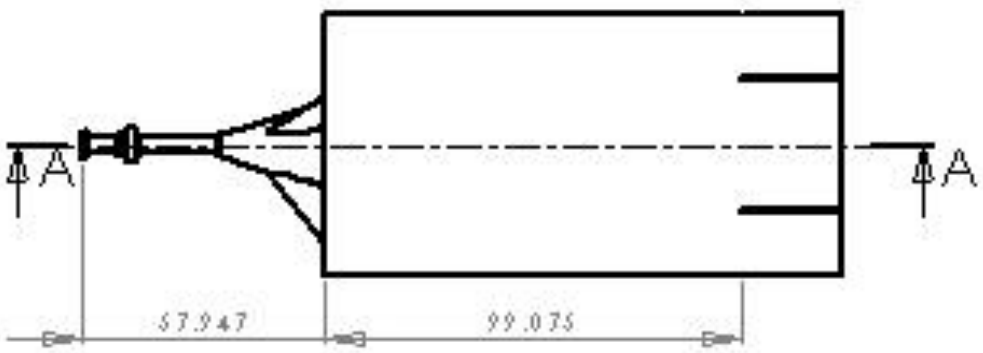

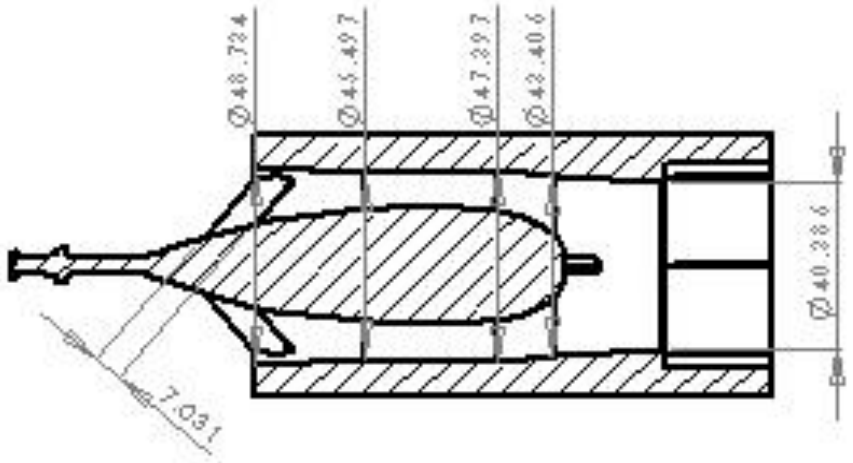

SECTION A-A
SCALE 1 : 1.5

3.5" Base Tunnel - Small Scale

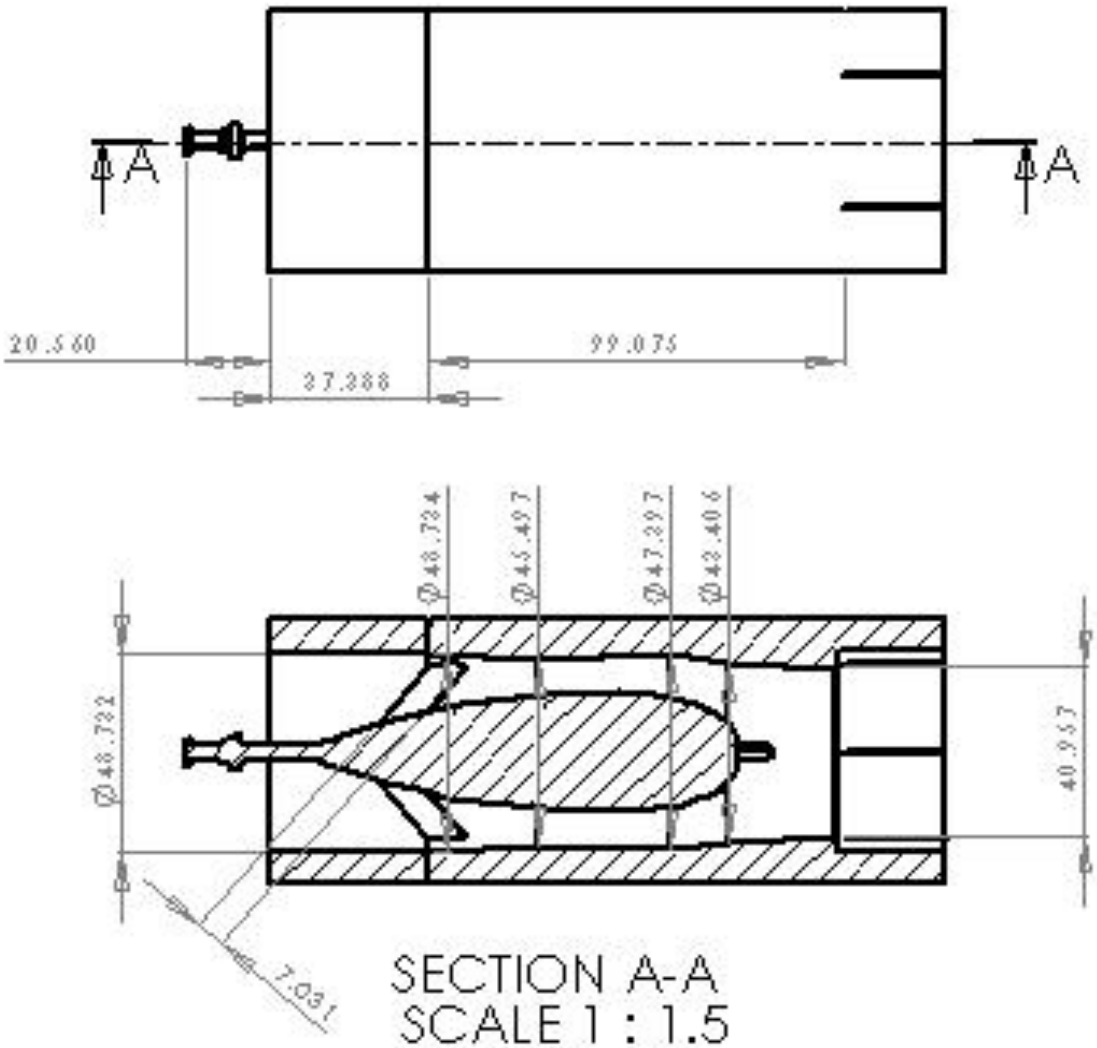

SECTION A-A
SCALE 1 : 1.5

3.5" Base Tunnel - Small Scale

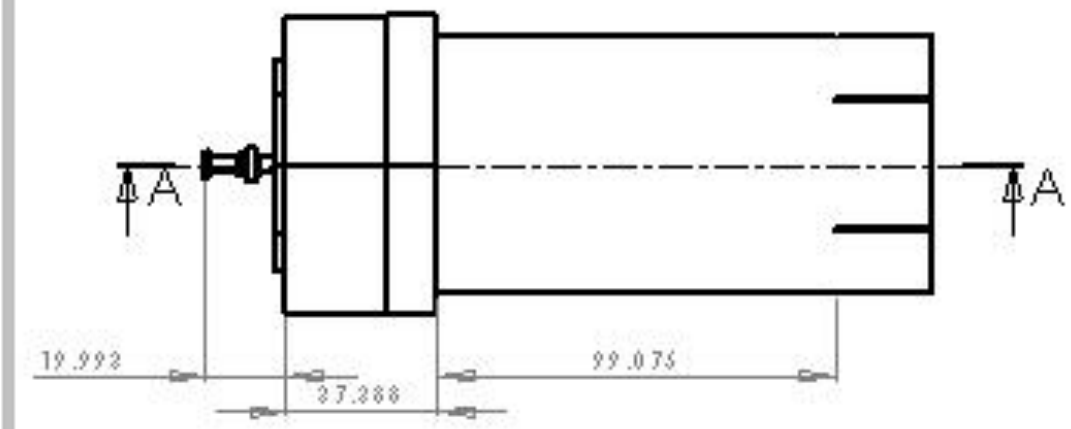

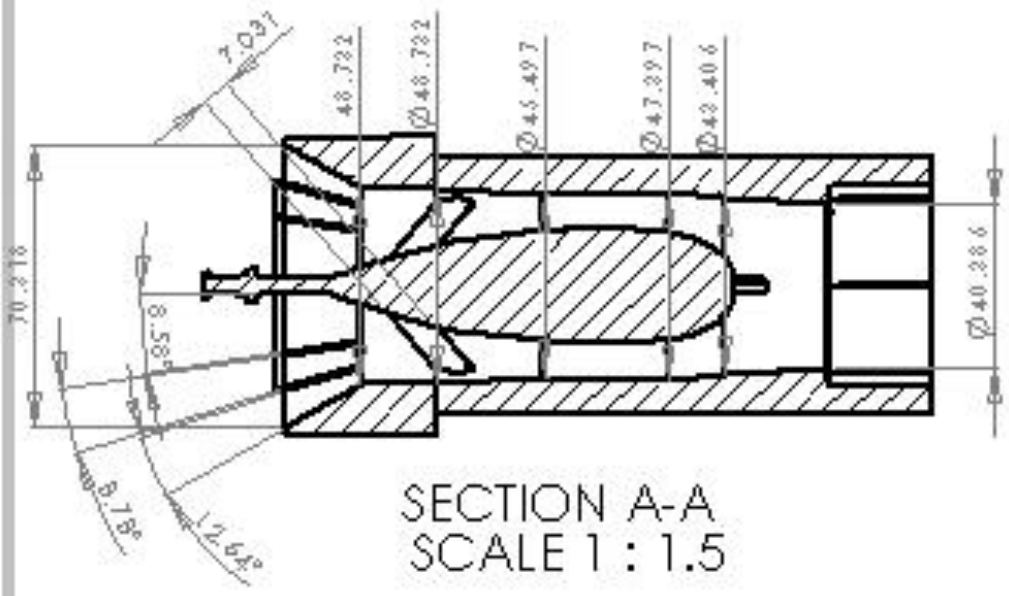

SECTION A-A
SCALE 1 : 1.5

3.5 " Flat + Conical - Small Scale